Multifunctional hybrid alginate-based hydrogels for cell immobilization

Luca SZABÓ

École
polytechnique
fédérale
de Lausanne

2020

Acknowledgement

Abstract

Cell therapy could be a solution for many diseases that currently pose a huge health burden on patients. Especially, cell therapies based on cell microencapsulation are of great interest. Immunoprotection of cells would allow to avoid the need for immunosuppression and the need for human donors, as the use of xenogeneic cell sources could be feasible. An optimal biomaterial for the microencapsulation of cells must be tailored for the type of cells and the intended application. Hydrogels are great candidates for cell immobilization, due to their high biocompatibility and extracellular matrix-like properties. Amongst them, alginate has outstanding potential with its favorable gelling properties, high biocompatibility, and relatively easy availability. However, in many aspects, it cannot fulfill the requirements of an optimal biomaterial for cell immobilization and transplantation. It lacks good mechanical properties, long-term durability and stability, and has poor shape recovery ability. In addition, severe immune reactions of the host system to the transplanted microcapsules can happen, which eventually result in cell death and early graft failure. Hence, the main focus of the present project was functionalization of alginate to develop new hydrogel materials with improved properties for cell microencapsulation.

First, the thesis presents a robust, straightforward strategy and its optimization for the functionalization of alginate on the hydroxyl groups with poly(ethylene)glycol (PEG) via stable carbamate bond. The end-functionality of the heterobifunctional PEG provides a reactive group for covalent crosslinking. Hence, dual ionic-covalent microsphere preparation is achieved by extrusion of the aqueous polymer solution into a gelation bath containing ionic cross-linker and followed by concomitant covalent cross-linking.

The possibility of using a variety of covalent cross-linkers was explored. Depending on the end-functionality of the heterobifunctional PEG, the chemical structure of the cross-linker is adjustable. This thesis presents thiol-thiol, thiol-acrylate, thiol-maleimide and thiol-acrylamide interactions, and compares the mechanical properties of the resulted microspheres to those of Ca-alginate. Both the mechanical resistance and the shape recovery performance of microspheres stabilized by an additional chemical cross-linking was improved. In addition, the stability of these microspheres towards non gellifying solutions was significantly enhanced.

Still, biomaterials are exposed to the risk of immune responses when transplanted, such as inflammation and fibrosis. Introduction of the anti-inflammatory drug ketoprofen to alginate backbone through a PEG linker and consecutive microsphere formation provides controlled ketoprofen release. Based on this strategy, development of new types of anti-fibrotic derivatives of pirfenidone were realized. Conjugation of the most potential derivative to PEG followed by grafting on alginate resulted in a polymer capable of forming microspheres. Covalent conjugation of the drug was further compared to co-encapsulation of the drug with Ca-alginate.

Eventually, the thesis presents the development of multicomponent hybrid hydrogel microspheres, combining the introduction of covalent cross-linking and anti-inflammatory compounds within the hydrogel network. The feasibility of using the newly developed biomaterials are confirmed by *in vitro* and *in vivo* assays.

Keywords: hydrogel, alginate, cross-reactive functionalities, cell microencapsulation, microspheres, poly(ethylene)glycol, diabetes.

Résumé

La thérapie cellulaire pourrait être une solution pour de nombreuses maladies qui représentent actuellement un fardeau important pour la santé des patients. En particulier, les thérapies cellulaires basées sur la microencapsulation cellulaire suscitent aujourd'hui un grand intérêt. L'immunoprotection des cellules permettrait d'éviter d'avoir recours à des traitements immunosuppressifs et à des donneurs humains car l'utilisation de sources de cellules xénogéniques est alors réalisable. Dans cette perspective, un biomatériau utilisé à des fins de microencapsulation cellulaire doit être adapté au type de cellules et à l'application envisagée. Les hydrogels sont d'excellents candidats pour l'immobilisation des cellules, en raison de leur remarquable biocompatibilité et de leurs propriétés de type matrice extracellulaire. Parmi eux, l'alginate a un potentiel immense car ce dernier est doté de propriétés gélifiantes avantageuses, une haute biocompatibilité et une disponibilité relativement aisée. Cependant, à bien des égards, l'alginate ne peut remplir les conditions d'un biomatériau destiné à l'immobilisation et la transplantation de cellules. En effet, ce matériau est dépourvu de bonnes propriétés mécaniques, de durabilité et de stabilité à long terme ne possède qu'une faible capacité de récupération de forme. De plus, de sévères réactions immunitaires provenant de l'hôte peuvent se produire lors de la transplantation de microcapsules, pouvant entrainer la mort cellulaire et l'échec précoce de la greffe. Cette thèse a pour objectif d'améliorer les propriétés physicochimiques susmentionnées de l'alginate en fonctionnalisant l'alginate afin de développer de nouveaux types de matériaux hydrogels dotés de propriétés supérieures et optimales pour la microencapsulation cellulaire.

Dans un premier temps, la thèse présente une stratégie robuste et simple pour la fonctionnalisation de l'alginate sur les groupes hydroxyles avec du poly (éthylène) glycol (PEG) via une liaison carbamate stable, ainsi que l'optimisation de la synthèse. La fonctionnalité finale de ce PEG hétérobifonctionnel permet de présenter un groupe réactif utilisé pour la réticulation covalente. Une préparation de microsphères à caractère doublement ioniques et covalentes est obtenue par extrusion de la solution aqueuse de polymère dans un bain de gélification contenant un agent de réticulation ionique et suivie d'une réticulation covalente concomitante.

La possibilité d'utiliser une variété de réticulants covalents a ensuite été explorée. La structure chimique du réticulant est ajustable selon la fonctionnalité finale du PEG hétérobifonctionnel (thiol, acrylate, acrylamide or maléimide). Cette thèse présente alors les interactions thiol-thiol, thiol-acrylate, thiol-maléimide et thiol-acrylamide, et compare les propriétés mécaniques des

microsphères obtenues à celles du calcium-alginate (Ca-alginate). Les résultats montrent que la résistance mécanique et les performances de récupération de forme des microsphères renforcées par une réticulation chimique ont été améliorées. De plus, la stabilité de ces microsphères au contact des solutions non gélifiantes a été considérablement augmentée.

Cependant, les biomatériaux sont sujet au risque de réponses immunitaires lors de leur transplantation, tels que l'inflammation et la fibrose. L'introduction d'un médicament anti-inflammatoire comme le kétoprofène dans le squelette de l'alginate via un linker PEG et la formation de microsphères correspondantes permet d'assurer une libération contrôlée du kétoprofène. En s'inspirant de cette stratégie, de nouveaux types de dérivés anti-fibrotiques de pirfenidone ont été développés. La conjugaison du dérivé le plus potentiel au PEG suivie d'un greffage sur l'alginate a permis de développer un polymère capable de former des microsphères. La conjugaison du médicament par liaison covalente a été également comparée à la co-encapsulation du médicament avec du Ca-alginate.

En résumé, cette thèse présente le développement de microsphères d'hydrogel hybrides à plusieurs composants (alginate et PEG), combinant l'introduction de composés réticulants covalents (thiol, acrylamide, acrylate et maléimide) et anti-inflammatoires (pirfenidone) au sein du réseau hydrogel. La faisabilité de l'utilisation de ces biomatériaux nouvellement développés est confirmée par des essais *in vitro* et *in vivo*.

Mots-clés: hydrogel, alginate, fonctionnalités de réactivité croisée, microencapsulation cellulaire, microsphères, poly(éthylène) glycol, diabète.

Abbreviations

A

Alg	Alginate
Aq.	Aqueous
Ar	Aromatic

B

Ba-alg	Barium-alginate
BrBn	Benzyl bromide
Boc	Di-tert-butyl dicarbonate

C

CAR	Chimerin antigen receptor
Ca-alg	Calcium-alginate
CDMT	2-chloro-4,6-dimethoxy-1,3,5-triazine
°C	Celsius degree
CDI	Carbonyldiimidazole
CEA	Commissariat à l'Ènergie atomique
$CaCl_2$	Calcium chloride
CuI	Copper(I) iodide
$CHCl_3$	Chloroform
calcd.	Calculated
CO_2	Carbon dioxide

D

DM	Diabetes mellitus
DMSO	Dimethyl sulfoxide
DOSY	Diffusion ordered spectroscopy
DCC	N,N'-Dicyclohexyl-carbodiimide
DMAP	4-Dimethylamino-pyridine
DCM	Dichloromethane
DMF	Dimethylformamide
DMEM	Dulbecco Modified Eagle's Medium
3D	3-Dimensional

E

EDTA	Ethylenediamine-tetraacetic acid
EDCI	1-Ethyl-3-(3-dimethylaminopropyl) carbodiimide
EtOH	Ethanol
Et_3N	Triethyl amine

F

FDA	Food and Drug Administration/ Fluorescein diacetate
FITC	Fluorescein Isothiocyanate
FCC	Flash column chromatography

equiv	Equivalent		**H**	
EtOAc	Ethyl acetate		hESC	Human embryonic stem cell
ESI	Electrospray ionization		HRP	Horseradish peroxidase
			hMSC	Human mesenchymal stem cell
G			HCl	Hydrochloric acid
g	gram		HCOOH	Formic acid
			h	Hour
I			Huh7	Human hepatocellular carcinoma cells
iPSC	Induced pluripotent stem cell		H_2SO_4	
IR	Infrared		HRMS	High resolution mass spectrometry
IEQ	Islet equivalents		HBSS	Hank's Balanced Salt Solution
K			**M**	
KO^{t}Bu	Potassium tert-butoxide		MS	Microsphere
K_2CO_3	Potassium carbonate		MSC	Mesenchymal stem cell
KOH	Potassium hydroxyde		MIN6	Mouse Insulinoma cells
			MWCO	Molecular weight cut off
L			MOPS	3-(N-morpholino) propanesulfonic acid
LC-MS	Liquid chromatography-Mass spectrometry		mL	Milliliter Human hepatocellular carcinoma cells
			MeOH	Methanol
N			MTT	3-(4,5-Dimethylthiazol-2-yl)-2,5-diphenyltetrazolium bromide
NPI	Neonatal pig islet		MFFD	Micro-flow focusing droplet
Na-alg	Sodium-alginate		$MgSO_4$	Magnesium sulfate
NHS	*N*-hydrosuccinimide		min	Minutes
NMM	*N*-methylmorpholine			

NaOH	Sodium hydroxyde
NMR	Nuclear magnetic resonance
NaCl	Sodium chloride
NaH	Sodium hydride
NaHCO$_3$	Sodium bicarbonate
NH$_4$Cl	Ammonium chloride

R

rt	Room temperature

P

PEG	Poly(ethylene)glycol
PERV	Porcine endogeneous retroviruses
PFO	Pericapsular fibrotic overgrowth
PLL	Poly-L-lysine
PLO	Poly-L-ornithine
PLA	Poly-L-arginin
PSS	Propylene glycol alginate sodium sulfate
PI	Propidium iodide
PFD	Pirfenidone
pMSC	Pig pancreatic-derived Mesenchymal Stromal Cells
PE	Petroleum ether
ppm	Parts per million

S

α-SMA	α-smooth muscle actin
sat.	saturated

T

T1D	Type 1 diabetes mellitus
T2D	Type 2 diabetes mellitus
TBA	Tetrabutyl ammonium
TEG	tetra(ethylene glycol)
TsCl	Tosyl chloride
THF	Tetrahydrofuran
TGFβ1	Transforming growth factor beta 1
TLC	Thin layer chromatography

U

UV	Ultraviolet
UF	Ultrafiltration

W

Wt%	Weight percent

Table of contents

1. Introduction

1.1. Cell therapy

Somatic cell therapy, as defined by the FDA in 1993, is the "prevention, treatment, cure, diagnosis, or mitigation of disease or injuries in humans by the administration of autologous, allogeneic, or xenogeneic cells that have been manipulated or altered ex vivo".[1] Cell-based therapy is an emerging field in the pharmaceutical field, which had been long dominated by small molecule drugs, and recently biologics (i.e. antibody-based drugs, recombinant hormones).[2] However, the idea of using live-cells as therapeutic agents was already established decades ago for bone marrow regeneration by human hematopoietic stem cell transplantation.[3] Cell-based therapy offers the potential of not only treat, but also cure certain diseases. This is due to numerous special features of cells: they are able to sense their environment, react to it, produce and deliver therapeutic agents. In addition, cell behaviors could be engineered to perform special tasks.[4] Therefore, cell-based therapy could represent a promising new treatment in a variety of medical fields including oncology, cardiology, immunology, neurology, rheumatology, hematology, diabetes, hepatic and vascular diseases, amongst others.[5] Some of the main potential applications of cell therapy are illustrated in Figure 1.1.
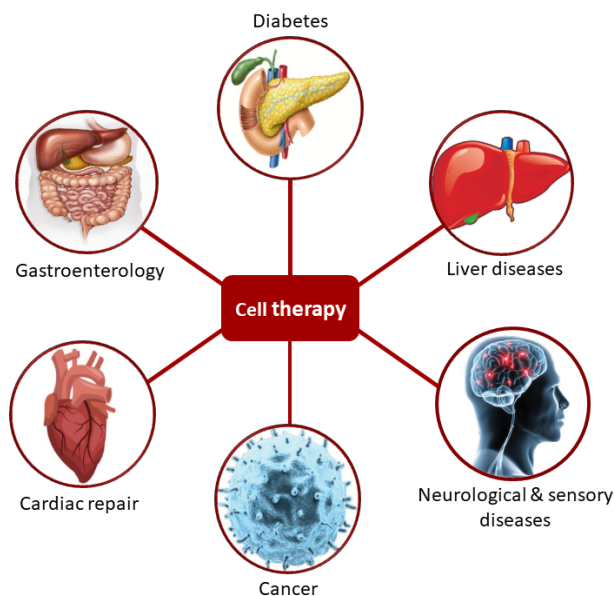
Figure 1.1. Main potential applications of cell therapy.

The promise of cell-based therapies is supported by several FDA approved cell-therapy products. *Provenge,* an immunotherapy product developed for the treatment of metastatic, symptomatic

and hormone-refractory prostate cancer, was approved in 2010 by the FDA. The therapy is based on *ex vivo* incubation of the patient's harvested dendritic cells and antigen presenting cells with a recombinant antigen protein for activation. Once matured, the activated cells are infused back into the patient to fight cancerous prostate cells.[6] In 2016, *Strimvelis*, the first stem-cell based gene therapy product was approved for the treatment of the rare disease adenosine deaminasine-deficient severe combined immunodeficiency.[7] These were followed by the approval in 2017 of two chimeric antigen receptors (CAR) T-cell products, manufactured by Novartis (*Kymriah*) and Gilead (*Yescarta*), for the treatment of certain types of leukemia and lymphoma.[8] In fact, in the development of cell therapies, T-cell mediated cancer therapy represents the area of the most intense research efforts.[9–11] The patient's T-cells are collected, and modified with a CAR gene able to recognize and attack cancer cells once infused back.

Stem-cell based therapies hold great promise due to their theoretical ability to differentiate into any types of cells, replacing dysfunctional or damaged cells and potentially serving as an inexhaustible cell source.[12] In 1998, the first stem cell isolation was performed on developing human embryos,[13] which then brought up extensive ethical concerns, but also an intense research interest for this field. The applications of cell products derived from pluripotent stem cell could cover almost all areas of medicine: i) retinal repair for ocular diseases,[14] ii) heart tissue repair for coronary artery diseases,[15] iii) diabetes treatment by stem cell derived insulin producing pancreatic cells,[16,17] iv) alveolar cells for lung diseases,[18,19] v) derivatization of blood cells for hematological diseases,[20,21] vi) treatment of Crohn disease[22] and other intestinal disorders with intestinal organoids,[23,24] vii) neurological diseases such as Parkinson or Alzheimer,[25] viii) skin grafts and hair loss repair.[26] Despite significant progress in the field, the development of stem cell-based therapies is still considered a controversial research area that raises serious ethical and safety concerns.[27–29] The main ethical issue regarding the destruction of human embryo in the case of hESCs (human embryonic stem cell) has been solved by the appearance of iPSCs (induced pluripotent stem cell). However, undesired cell differentiation and malignant transformations still remain a valid risk.

1.1.1.   Cell therapy for the treatment of diabetes

Diabetes mellitus (DM) is a severe metabolic disorder, characterized by high blood glucose levels. Figure 1.2 represents the extremely large burden diabetes places on our society worldwide. The number of people suffering from diabetes in 2017 was more than 400 million, and this number is expected to rise above 600 million by 2045. Unregulated high blood glucose level caused the death

of 4 million people in 2017. The ratio of Type 1 diabetes mellitus (T1D) to Type 2 (T2D) is around 10 %.
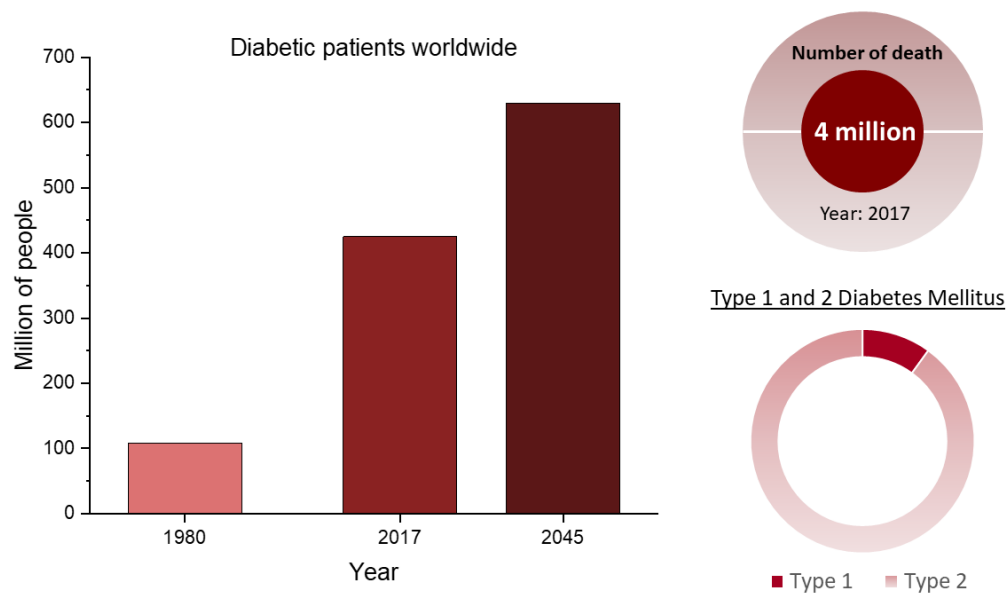
Figure 1.2. Diabetes in numbers worldwide (Data from the webpage of the International Diabetes Federation https://idf.org).

In T1D, the insulin producing islet cells–responsible for optimal blood glucose level regulation–are completely destroyed due to autoimmune processes.[30]

While there is currently no cure for T1D, the most common treatment relies on intensive exogenous insulin supply, which requires a constant awareness of the blood glucose levels from patients. Despite insulin therapy, many patients do not achieve recommended therapeutic goals in terms of blood glucose control, leading to severe hypo- or hyperglycemia episodes. Up to 40% of this population remains at high risk of cardio-vascular complications and morbidity.[31,32] Cell therapy in diabetes treatment can create a continuous insulin delivery system, by replacing the dysfunctional β-cells by other insulin producing cells. Nowadays, allogeneic islet transplantation is recognized as a minimally invasive and efficient treatment option for selected T1D patients suffering from severe uncontrolled hypoglycemia episodes, resulting in the restoration of optimal glycemic control in 60% of the recipients.[33,34] The evolution of islet transplantation from the time of insulin discovery in 1921 is shown in Figure 1.3.

| 1921 | 1966 | 1972 | 1990 | 2000 | 2005 |

Banting & Best
Insulin
discovery

Kelly et al.
First whole
pancreas
transplantation

Ballinger & Lacy
Established
islet isolation
method from
rodents

Scharp et al.
First case of
clinical insulin
independence

Shapiro et al.
New protocol: 7
patients achieved
and maintained
insulin
independence

Hering et al.
Improved
immuno-
suppression
method

Figure 1.3. Milestones in the evolution of islet transplantation (references: 1966,[35] 1972,[36] 1990,[37] 2000,[38] 2005[39]).

Results from clinical trials suggest that the main realistic goals of islet transplantation, for the moment, are long-term improvements in metabolic control, decrease in the hypoglycemic events, delayed diabetic complications (such as chronic microvascular problems) and a general improvement in the quality of life. However, several factors are restricting the access of a larger number of patients to adult islet allotransplantation, including: i) the shortage of suitable pancreases from deceased organ donors, ii) low and variable islet preparation quality, iii) the loss of islet functionality over time and iv) the need for lifelong immunosuppression to prevent rejection-mediated loss of the transplant. In addition, to reach the final goal of long-term insulin independence is still far away. Future possible directions to improve the outcomes of islet transplantations include finding alternative cell sources, better transplantation sites and improved immunosuppression.[40]

1.1.2. Current limitations and challenges

Despite their huge potential, most cell-based therapies are still far from becoming standard, widespread procedures. The main requirements that every medical treatment must meet are safety and efficacy. In the case of cell based therapies, it is extremely challenging to obtain sufficient data on these two aspects, mainly due to the limited number of patients involved in the studies and the lack of standardized clinical trials.[41] In addition, to promote the translation of cell therapy products from clinical studies to future commercial use, there is an indispensable need for the development of robust cell production methods. To ensure a continuous, satisfactory cell supply, sufficient amount of cells with a reproducible quality needs to be produced, at a reasonable cost.[5,42]

For many applications in cell-based therapies, the shortage of human donors constitutes a huge limitation for making more significant progress. Considerable efforts are made to improve the isolation and purification methods for maximizing the number of viable cells available for therapeutic purposes.[43,44] Further serious drawback of cell transplantation is the need for lifelong immunosuppressive treatment,[45–48] placing a huge burden on patients. Immunosuppression is essential to avoid graft rejection, but it comes with several side effects and also increases the risk of infectious complications, which could potentially lead to premature death.[46] Possible side effects include diarrhea, nausea, vomiting, hypertension, abdominal pain but also more serious neuro- and hepatotoxicity, osteoporosis, renal failure or leukopenia, depending on the type of immunosuppressive regimen.[47]

To overcome the issue of limited allogeneic cell sources and the need for lifelong immunosuppressive treatment, encapsulation of effector cells within an adequate three-dimensional (3D) semipermeable membrane appears as a viable alternative. The existing encapsulation techniques and biomaterials for cell transplantation will be further discussed in Section 1.3.

1.2.   Xenotransplantation

The waiting list for organ transplantation, only in the USA, currently exceeds 113 000 patients, while the transplants realized in 2018 only reached 36 000. As illustrated in Figure 1.4, the number of patients on the transplant waiting list has been increasing since 2000, while the number of transplants did not follow at the same rate.
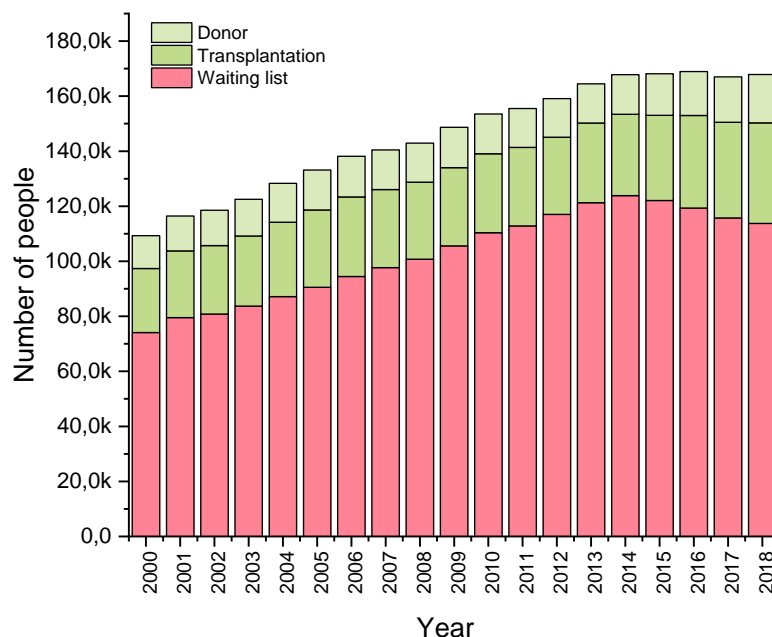
Figure 1.4. Data from the U.S. Government Information on Organ Donation and Transplantation (https://www.organdonor.gov/statistics-stories/statistics.html).

Xenotransplantation, which is the transplantation of organs or cells derived from other than human species, aims at bridging the gap between the number of patients waiting for transplantation and the actual procedures carried out. Pigs are considered the main alternative source to replace human organ and cell donors, owing to their similarity to humans in organ size and physiology, the ease of pig breeding and possibility for genetic modification to become better donor candidates.[49] The genome editing technologies developed over the last 10 years, in particular CRISPR/Cas9, allowed the production of genetically modified pigs with incorporation of human genes regulating the immune response and free from several porcine antigens (GalT/CMAH/b4GalNT2 triple gene KO).[50] Using the same CRISPR technology it was demonstrated that the zoonotic risk of porcine endogenous retroviruses (PERV) could be inhibited by the generation of a porcine line which is devoid of PERV genes.[51] In addition, in the case of diabetes treatment, the porcine insulin only differs in one amino acid of the peptide sequence structure compared to human insulin, and shows no difference in metabolic control or in the frequency of hypoglycemic episodes.[52]

For islet xenotransplantation, there is no debate about the porcine islets being the best alternative to human cells. However, there are some controversies in the optimum age of donor pigs.[53–55]
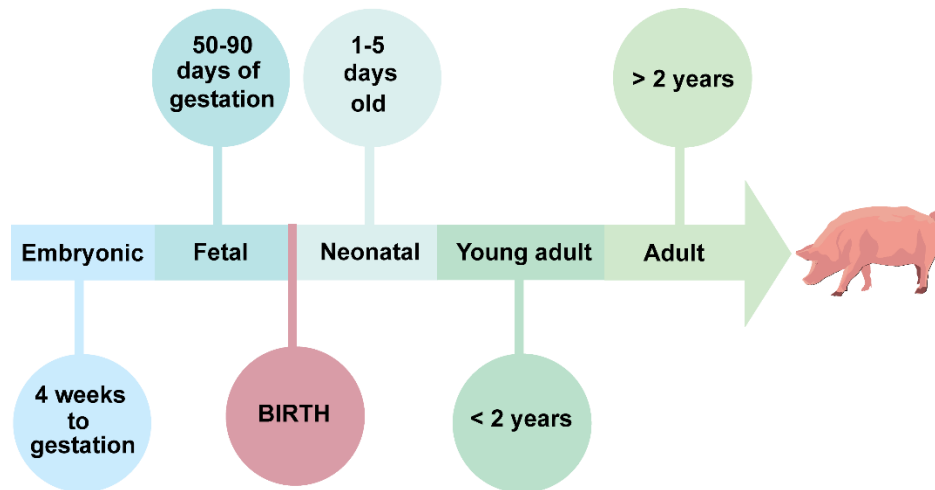
Figure 1.5. Different pig ages for the harvesting of cells for transplantation.

The earliest when insulin producing cells can be recovered is at the embryonic state. While pig gestation lasts around 115 days, a moderate production of insulin is observed after 4 weeks of gestation. The harvesting of these embryonic cells does not require isolation and purification steps, but results in low isolation yields. Embryonic precursor tissue has a significant growth potential and was shown to induce vascularization in the transplant recipient.[56] The major drawback of using embryonic cells is the significant delay (4 to 6 months) in graft function and cell functionality after transplantation. However, the tissue after transplantation is mainly endocrine, composed of insulin positive β cells primarily.[57]

At around 50-90 days of gestation, fetal insulin producing cells can be obtained. Up to one month after birth, neonatal islet-like cells can be harvested. These two cell types are quite similar in terms of their growth potential. Cell isolation and purification is relatively easy, but a few days of *in vitro* culture is required for the formation of selective endocrine cell clusters. Both cell types are characterized by delayed *in vivo* functionality after transplantation (around 8 weeks for fetal cells and 4 weeks for neonatal cells), but show ability to proliferate post-transplantation.[58,59] The exact amount of islet-producing cells derived from fetal or neonatal sources required to induce normoglycemia is yet to be precisely determined, but estimates are around 100 fetal and 70 neonatal pig donors per patient. A major advantage of neonatal pig islets is their resistance against hypoxia,[60] which is a serious concern in islet transplantation.

Young adult and adult pig islets are mature in structure, which makes their isolation and purification more demanding and expensive. The highest islet yield/pancreas is obtained from adult pigs followed by young adults. However, especially in pigs younger than two years old, the islets are very fragile and difficult to culture.[54] The high economic burden of maintaining pigs in

clean and isolated breeding structures for a long time constitutes the main motivation for looking into alternatives such as neonatal, fetal or even embryonic derived insulin-producing cells.

The safe use of xenogeneic cells in transplantation procedures requires strict immune protection, that avoids exposure of the xenograft to the host immune system and therefore lowers the risk of a detrimental immune reaction. In the context of T1D treatment, the microencapsulation of insulin-producing cells into 3D semi-permeable hydrogels holds the potential to achieve such protection and to maintain cell functionality without the requirement of an immunosuppressive regimen. This approach is detailed in the following section.

1.3. Microencapsulation

Microencapsulation is the technique of entrapping a gas, liquid or solid core within a coating material, forming capsules that fall into the micrometer range. Successful microencapsulation requires the knowledge of choosing the adapted coating material for a given core, as well as the suitable encapsulation method depending on the application.
Microencapsulation has been widely used in many industries, such as food, agrochemical, cosmetic, energy and pharmaceutical industries. However, microencapsulation of living cells is one of the most challenging, clinically relevant and actively researched application area.[61–64]

The first example of entrapping living cells within a membrane dates back to 1933, when Bisceglie et al. encapsulated mouse tumor cells and implanted them in the abdominal cavity of pigs (Figure 1.6).[65] The aim was to examine the lack of vascularization on the tumor cells by immunoisolation. The cells showed viability long enough to conclude to the efficient immune protective effect of the applied membrane. However, the development of this concept for disease treatment started in the 1950's. Algire et al. developed diffusion chambers made of cellulose ester that could allow the diffusion of metabolites while protecting the homografts from the host immune system.[66] A few years later, Chang introduced the concept of artificial cells.[67,68] He used an emulsion method for enveloping hemoglobin and red blood cell enzymes. In 1980, Lim presented the first rat islet encapsulation in alginate-based material that achieved normoglycemia for 20 days in a rodent model.[69] A few years later, in 1994, the first clinical trial of microencapsulated islet allotransplatation was carried out in a 38-year-old diabetic man. Insulin independence was reported up to nine months post-transplantation. In addition, the patient reported significant improvement in his quality of life after the treatment.[70]

1933	1950	1957	1980	1994

Bisceglie et al.

First encapsulation of tumor cells

Algire et al.

Concept of immuno-isolation

Chang

Introduction of the concept of artificial cells

Lim et al.

First islet encapsulation in alginate

Soon-Shiong et al.

First human trial of islet allo-transplantation
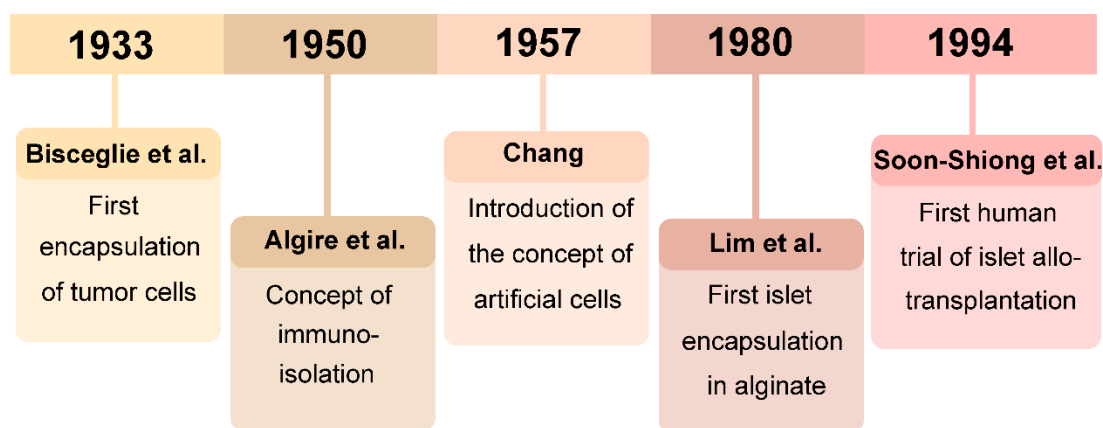
Figure 1.6. Chronology of cell microencapsulation for clinical use.

The immobilization of cells is possible using both macro- or microdevices. Several geometries of macrodevices were reported for the entrapment of islets, including toroidal capsules,[71] flat disks,[72] or planar slab with gas chambers,[73] amongst others. From a safety point-of-view, macrodevices can be easily retrieved after transplantation. However, these devices are characterized by a low surface area, which impedes the fast diffusion of metabolites and leads to low oxygen supply. Microcapsules allow a better mass transfer due to their higher surface area, but can be more complicated to retrieve *in vivo*.

The process of cell microencapsulation involves two main steps: droplet formation with the living cells distributed within the biomaterial, followed by gelation of the droplet or membrane formation on the surface of the droplet.[74] The droplet formation can be accomplished by emulsification,[75–77] droplet-based technologies,[78] or microfluidic methods.[79–81] In droplet-based technologies, the liquid is extruded through a nozzle or a needle. As illustrated in Figure 1.7, this can happen under simple gravity, or with the aid of a coaxial air-flow,[82,83] electrostatic potential,[82,84,85] vibration,[86] rotation[87,88] or jet-cutting.[87,89] More recently, 3D printing technology was also reported for cell-laden sphere formation.[90–92] When choosing the most suitable encapsulation method for a certain application, one should take into consideration the desired sphere main diameter, the acceptable size distribution, the production scale and the tolerance of the cell being encapsulated.[78]
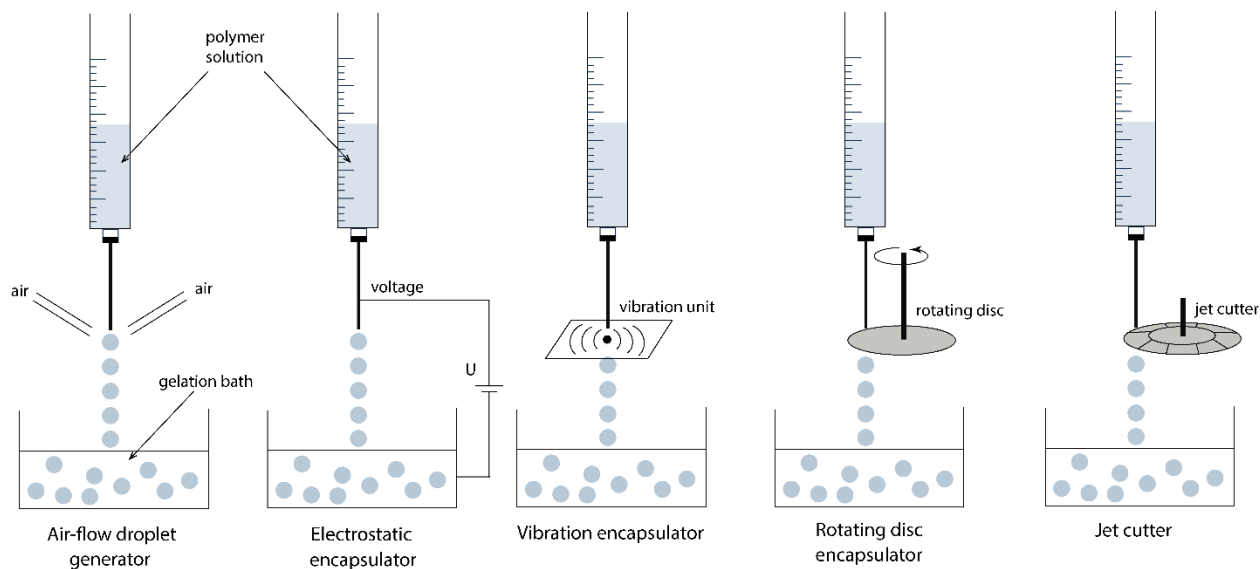
Figure 1.7. Principle of droplet formation using different techniques.

Microfluidic-based droplet formation and encapsulation has been reported as a promising technique to obtain homogeneous, monodisperse droplets of desired size.[93,94] The aqueous polymer solution is being pushed through micro-sized channels, and an immiscible oil phase helps droplet formation (Figure 1.8). Microfluidic chips can be designed and fine-tuned to fit the intended applications, so that droplets of different sizes and shapes can be generated. In order to avoid clogging of the channels caused by too early gelation, droplet formation and gelation must be kept well-separated.[79] Microfluidic technology offers a precise control over the size, shape and morphology of the formed spheres. However, the risk of clogging, and the presence of oil present potential drawbacks. Microfluidic encapsulation in all-aqueous-phase was also realized for porcine adipose-derived stem cells.[95]
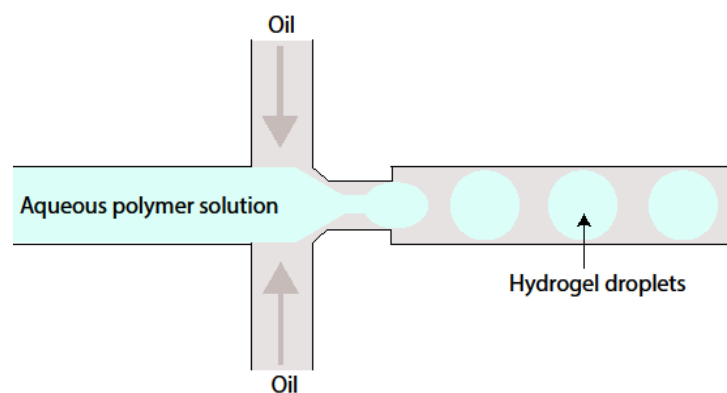
Figure 1.8. Microfluidic droplet formation. The channel of the continuous phase contains the aqueous polymer solution, and the dispersed oil phase is used to shear the polymer solution and form the droplet.

1.3.1.   Encapsulation biomaterials

The importance of adequate materials chosen for specific cell applications is undeniable. However, there are certain requirements that all types of encapsulation biomaterials must fulfil in order to provide optimal protection and maximize cell survival. The desired maximal cell survival is dependent on the targeted application; for liver regeneration a one-month period could be enough, while for T1D 1–3 years would be a good target. One of the main encapsulation biomaterial requirements is presented in Figure 1.9. The encapsulation material should serve as a semi-permeable membrane, allowing the selective diffusion of small oxygen, nutrients, metabolic waste and therapeutic compounds (such as insulin), while excluding antibodies, T cells and immunoglobulins, thus providing satisfactory immune protection for encapsulated cells.[96]
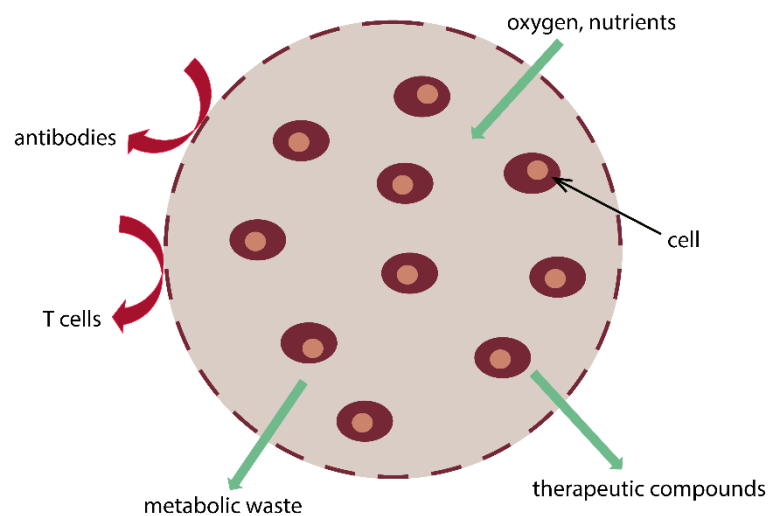
Figure 1.9. Concept of selective permeability for cell microencapsulation.

Furthermore, basic requirements include high biocompatibility and low immunogenicity that induce minimum host tissue response. From a mechanical point of view, encapsulation materials must exhibit high durability and good *in vivo* stability to provide long term protection for the cells. Shape recovery performance (elasticity) is also essential in order to avoid any microsphere (MS) deformation or breakage during the transplantation procedure or when exposed to any mechanical compression post-transplantation. If all these requirements are completed, the protocols to produce the MS should involve mild preparation techniques ensuring minimal damage to cells, and must be reproducible as well as up-scalable, to ease the translation to clinical trials and applications.[96]

Some of the main challenges in realizing the translation to clinical applications include the lack of biomaterials fulfilling all requirements, as well as poor cell survival, aggregation and migration.[97] Indeed, encapsulation materials are not only serving as a membrane, but they also interact with cells. To improve the material properties to offer a more favorable environment for cell survival and functionality, mimicking the extracellular matrix, introducing growth factors or special cell receptor binding motifs can be realized.[98]

1.3.2.   Hydrogels

Hydrogels consist of a 3D network made of natural or synthetic polymer chains, presenting high water content. The first use of hydrogels was reported by Wichterle et al. in 1960, who proposed hydrophilic cross-linked poly-2-(hydroxyethyl methacrylate) for medical applications–such as contact lens–instead of the previously used hard solid polymers, impermeable to metabolites, often causing irritation.[99] Hydrogels make perfect candidates as bioencapsulation materials due to their ability to absorb high amounts of water and their mechanical properties resembling those of native tissues and extracellular matrix.[100–102] Hydrogels are composed of cross-linked hydrophilic polymers which properties can be tuned to match the requirements of intended applications. More advanced gels can also be prepared by controlling the degradation kinetics, cross-linking density, hydrophilicity and stiffness or by adding biological cues.

Hydrogels can be derived from natural sources, or can also be chemically synthesized. Depending on the type of cross-linking forming the hydrogel network, we can differentiate between physical or chemical hydrogels.

1.3.2.1. Physical hydrogels

Physical hydrogels, also referred to as reversible hydrogels, are generally formed by reversible, non-covalent interactions. These involve metal ion-ligand interactions, chain entanglements, and/or secondary forces, such as hydrogen bonding or hydrophobic interactions.[103–105] Preference for the use of physical hydrogels might be desired when straightforward, one-step preparation process and fast gelation kinetics are needed. However, the interactions forming physical hydrogels can be easily weakened or damaged by changes in the ionic media, temperature or pH.

While physical hydrogels obtained via ionic bonding will be mostly discussed herein, hydrogen bonding,[106,107] and hydrophobic interactions[108,109] are common cross-linking methods used for the generation of physical self-healing hydrogels.

Amongst the polymers which are used for the preparation of ionically cross-linked hydrogels, sodium alginate (Na-alg) is by far the most reported material for cell encapsulation applications.[110]

1.3.2.2. Alginate

Alginate (alg) is a nature-derived linear polysaccharide, widely used in many industries. It is the most frequent choice for tissue engineering and cell encapsulation applications.[111] Alg can be found mainly in brown algae, but is also produced by certain bacteria.[112] Commercially available alg are exclusively extracted from algal sources, typically in the form of Na-alg as a result of the alkali treatment used for the extraction.[113] Na-alg is water soluble, and mainly used in its 3D cross-linked form as a hydrogel.

The structure of alg is constructed of block units of 1,4-linked α-L-guluronic acid (G units) and 1,4-β-D-mannuronic acid (M units) (Figure 1.10).[114] The ratio and length of homogeneous (MM, GG) and heterogeneous (MG) blocks depend on the extraction source, and have a significant influence on the physico-chemical properties of the alg.[115] Alg G units give more strength and rigidity, while M units provide more flexibility and softness to the resulting hydrogels.[116,117]
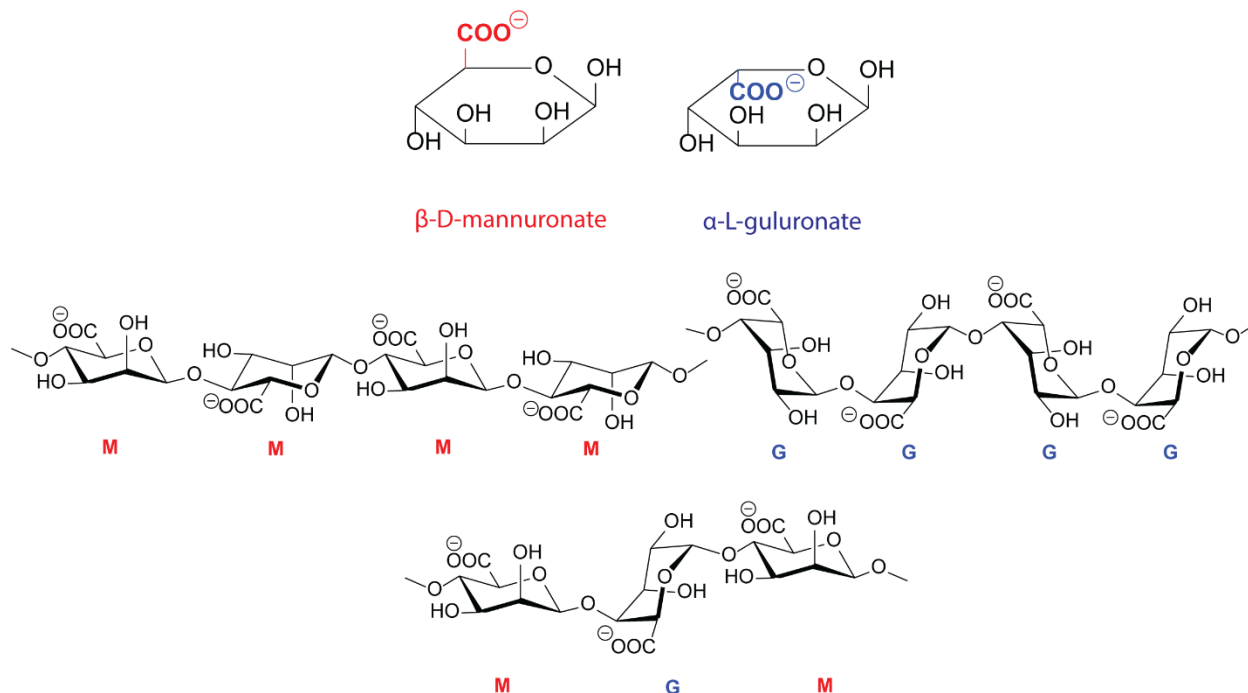
Figure 1.10. Alginate structure.

The popularity of alg in biomedical applications is the result of many beneficial features, such as biocompatibility, minimal toxicity, commercial availability at an affordable price, and excellent gelling properties under mild conditions.[118] Alg is decorated with carboxylic and hydroxyl functionalities on its backbone, however, it is only the carboxylate moieties that participate in the gelation process. In the presence of divalent cations (Ca^{2+}, Ba^{2+}, Sr^{2+}, Mg^{2+}), alg GG units ionically bind to the cations, creating junction zones and a rigid hydrogel network. A widely accepted model for the gelation of alg is the egg-box model, in which the divalent cation binds to two G units of two different polymer chains, creating a "zigzag" shape (Figure 1.11).[119,120]
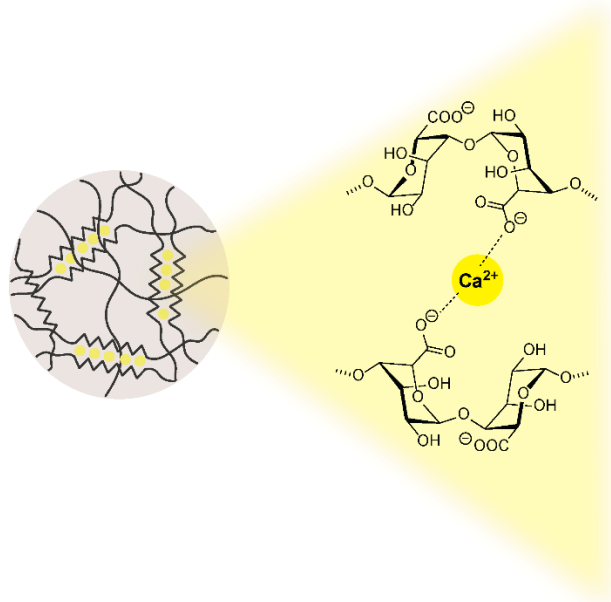
Figure 1.11. Ionic binding in physical alg-based hydrogels, "egg-box" model.

Despite favorable properties, alg-based physical hydrogels suffer from several drawbacks for biomedical applications such as limited mechanical stability and durability *in vivo*, insufficient shape recovery performance and permeability issues. Several *in vivo* studies in small and large animal models presented that physically cross-linked alg provides immunoprotection for encapsulated cells, however, without the limited life-time of the graft reported. In addition, to obtain more stable alg microspheres, in most cases a certain concentration of Ba^{2+} ions is used, which raises the concern of potential toxicity for further clinical applications.[121–123] Intense research efforts have thus been dedicated to engineer polymeric hydrogels which maintain the advantageous properties of alg while overcoming its main shortcomings. These aspects will be discussed in the next sections.

1.3.2.3. Chemical hydrogels

In chemical hydrogels, the network junctions are constructed by irreversible covalent bonds. While covalent cross-linking processes take extended time in comparison with ionic interactions, chemical hydrogels are generally used when high mechanical resistance and long-term durability are needed. When designing a chemical hydrogel for cell immobilization, one has to take into account that the chemical reaction and conditions applied should not be detrimental to cells which are suspended in the precursor polymer solution prior to the encapsulation process.[124] In addition,

the most challenging issue is a suitable technology to produce spherical hydrogels because chemical cross-linking does not occur as fast as physical cross-linking.

One of the most straightforward route toward chemical hydrogel relies on the use of cross-linking agents which react with functional groups of different polymeric chains to create a network of covalent junctions. However, the possible cytotoxicity of such cross-linkers significantly limits the applicability of this method when hydrogels are intended for cell microencapsulation.

Light-induced free-radical polymerization presents relatively fast gelation kinetics, but formation of spheres is extremely challenging. Further drawback includes the low availability of cytocompatible photo initiators, which combined with the required exposure time for complete polymerization significantly compromises the use of photopolymerization.[125] Examples of successful cell encapsulation with PEG-,[126] chitosan-[127] or dextran-based[128] hydrogels were reported, but these attempts did not lead to spherical hydrogel formations.
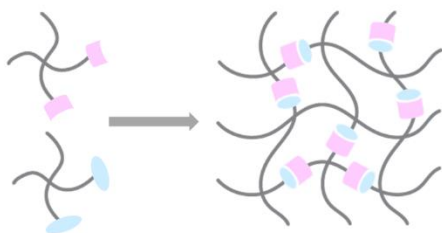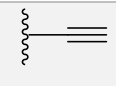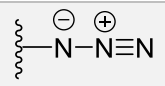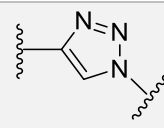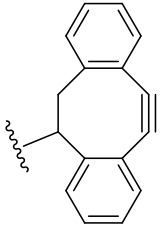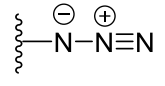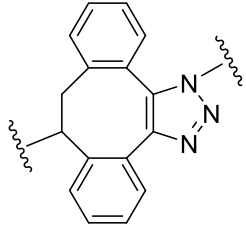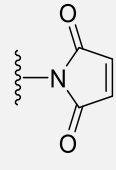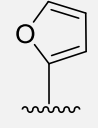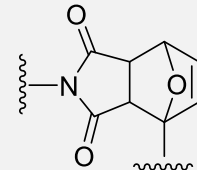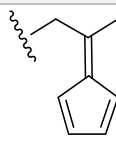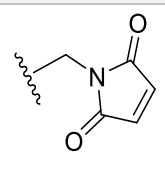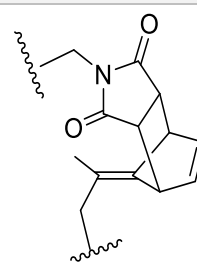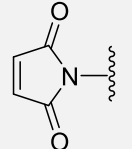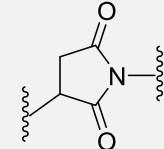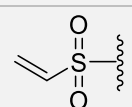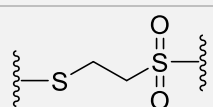
A relatively new type of covalent cross-linking is the enzyme-mediated gelation. Its advantages include rapid gelation kinetics under mild conditions, high substrate specificity and cell compatibility. Transglutaminase and horseradish peroxidases (HRP) are the most frequently used enzyme catalysts. The unsatisfactory stability and limited availability of certain enzymes still pose a challenge in this specific field of cross-linking.[129] HRP-catalysed oxidative coupling of alg with phenol moiety (alg-Ph) was presented to develop cross-linked microcapsules for mammalian cell entrapment. Cell viability higher than 90% with cell proliferation was maintained for more than two months of the study.[130] HRP cross-linked microcapsules of hollow core were also developed, by first enveloping human hepatoma cell line (HepG2) cells in a carboxymethylcellulose-phenol (CMC-Ph) core. It was further coated with HRP cross-linked alg-Ph, and finally CMC-Ph core was degraded by cellulose addition. Cells were allowed to grow and form spherical tissues in the hollow core before also degrading the alg-Ph shell by alg lyase addition.[131]
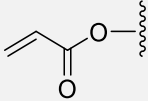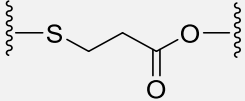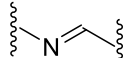
Click chemistry is an extremely important tool in the preparation of biomaterials.[132–135] The term "click chemistry" was introduced by Sharpless and co-workers in 2001, together with defined requirements for a reaction to fall into this category.[136] Click reactions are modular, fast, and spontaneously happening processes under mild conditions. Starting from easily available materials, using simple reagents, they afford the products with high yields, without the formation of toxic by-products. Given all these advantageous features, click chemistry is the most appealing

type of chemical cross-linking for biomaterial synthesis. The main types of click reactions used for hydrogel formation are summarized in Table 1.1. The copper-catalyzed azide-alkyne click reaction was presented as a covalent cross-linking method for hydrogel preparation.[137,138] It was also successfully used for the formation of spherical alg microbeads.[139] However, its applicability in the presence of cells is very limited due to the high toxicity of copper. Therefore, copper-free strain-promoted azide-alkyne cross-linking was suggested as an alternative. This type of cross-linking is well tolerated by living cells, as reported in many studies with high cell viability post encapsulation within the hydrogel matrix. However, these examples did not yield spherical hydrogel geometries. Examples include encapsulation of human mesenchymal stem cells (hMSC) within PEG-based hydrogel cross-linked by strain-promoted cycloaddition.[140] A combination of gelatin and PEG, both derivatized to undergo copper-free cycloaddition, were successfully used for mouse fibroblast encapsulation and presented good viability up to 14 days.[141] Chondrocyte cell survival was well tolerated in a hyaluronic acid based hydrogel, cross-linked with a 4-arm PEG via the same mechanism.[142]

Classic Diels-Alder reaction between furan and maleimide can lead to covalently cross-linked hydrogels suitable for cell encapsulation. Gelation of one-hour length between furan modified hyaluronic acid and bismaleimide-PEG was found to be suitable for encapsulated ATDC-5 cell viability and proliferation.[143] Due to the slow gelation kinetics between furan and maleimide, Diels-Alder reaction between fulvene and maleimide was also proposed for faster gelation.[144] Michael addition between thiol-maleimide,[145] thiol-vinylsulfone[146,147] or thiol-acrylate[148] led to formation of covalently cross-linked hydrogels, and was well tolerated by a variety of cells. However, formation of spherical cell entrapped hydrogels is highly challenging by this type of cross-linking. Schiff-base reaction between an amine and aldehyde generates a dynamic covalent bond, widely used in biomedical applications.[149,150]

Table 1.1. Examples of chemical cross-linking with click chemistry.

Name of the reaction			
Cu-catalyzed azide-alkyne cycloaddition			
Strain promoted azide-alkyne cycloaddition			
Diels-Alder reaction			
Fulvene-Maleimide Diels-Alder reaction			
Michael addition			

	—SH	(acrylate structure)	(thioether ester structure)
Schiff-base reaction	—NH₂	(aldehyde structure)	(imine structure)

In conclusion, chemically cross-linked hydrogels can provide long stability, but due to the slow kinetics of the covalent bond formation in many cases, the generation of spherical MS can be altered.

1.3.2.4. Hybrid hydrogels

Taking advantage of the properties of both chemical and physical hydrogels, novel hybrid materials which combine electrostatic interaction with covalent cross-linking display very promising properties for cell microencapsulation. The physical interactions provide fast gelation and the formation of spherical beads, while the biocompatible covalent linkage reinforces the hydrogel network, and allows for tunable permeability and gel stiffness. Thus, they are very propitious for therapeutic delivery by combining injectability and mechanical durability.

Alg is a very prosperous polymer for the generation of hybrid hydrogels, due to its natural ability to form physical gels by exposure to divalent cations, and the presence of both carboxylic and hydroxyl groups amenable to chemical derivatization. Thus, chemical cross-linking of alg can be achieved by derivatization to obtain a functionality susceptible to covalently cross-link. One approach to form hybrid hydrogels is based on the involvement of methacrylate functionality for chemical photo cross-linking which is combined with the ionic cross-linking of alg. Dual covalent-ionic cross-linked hydrogel beads were developed by equipping alg with photo cross-linkable 2-aminoethyl methacrylate (Figure 1.12/a). Alg derivative was extruded into Ca^{2+} containing gelation bath, and the resulted physically cross-linked droplets were exposed to UV for 15 min for chemical photo cross-linking. The generated dual cross-linked beads exhibited high stability compared to unmodified alg beads.[151] Triple cross-linked alg hydrogel was developed by combining alg-aldehyde (obtained by oxidation of alg) with methacrylated gelatin (Figure 1.12/b). Alg was first exposed to Ca^{2+} ions for physical cross-linking, followed by photo cross-linking of methacrylate functionalities of gelatin. This double network hydrogel was further cross-linked over time by imine formation between aldehyde groups of alg and amine groups of gelatin. The

resulted triple-network hydrogel network displayed high elasticity, and was found to be an ideal platform for long-term hMSC survival. [152]
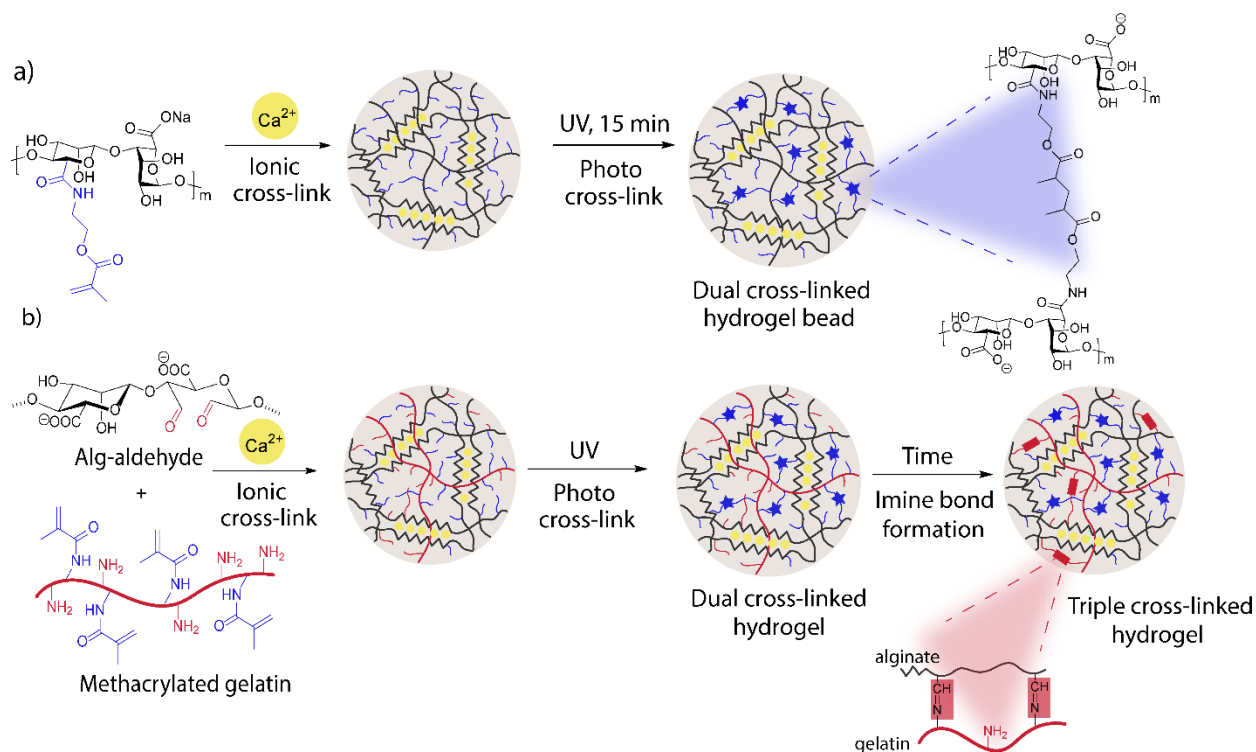
Figure 1.12. Use of methacrylate functionality to introduce photo cross-linking. a) Formation of dual cross-linked hydrogel bead b) Formation of triple cross-linked hydrogel network.

Introduction of PEG to the hydrogel network is another widely used method for the design of hybrid hydrogels. Hybrid alg-based MS was prepared by functionalizing Na-alg with azide-terminated PEG chains.[153] Hybrid MS are formed by chemical cross-linking of the azide group with phosphine-functionalized agents present in the gelation bath via Staudinger ligation (Scheme 1.1/a). Microbeads with enhanced stability were formed as confirmed by exposure to strong chelating EDTA solution. Encapsulation of rat and human islet cells within the hybrid hydrogel resulted in similar viability and functionality results as within the control alg.[154]

Similarly, Na-alg functionalized with PEG-thiol or with cysteamine was prepared to obtain hybrid hydrogel MS (Scheme 1.1/b). The modified Na-alg maintained its gelling ability in the presence of Ca²⁺ ions, while thiol end groups underwent disulfide bridge formation to provide chemical cross-linking.[155]
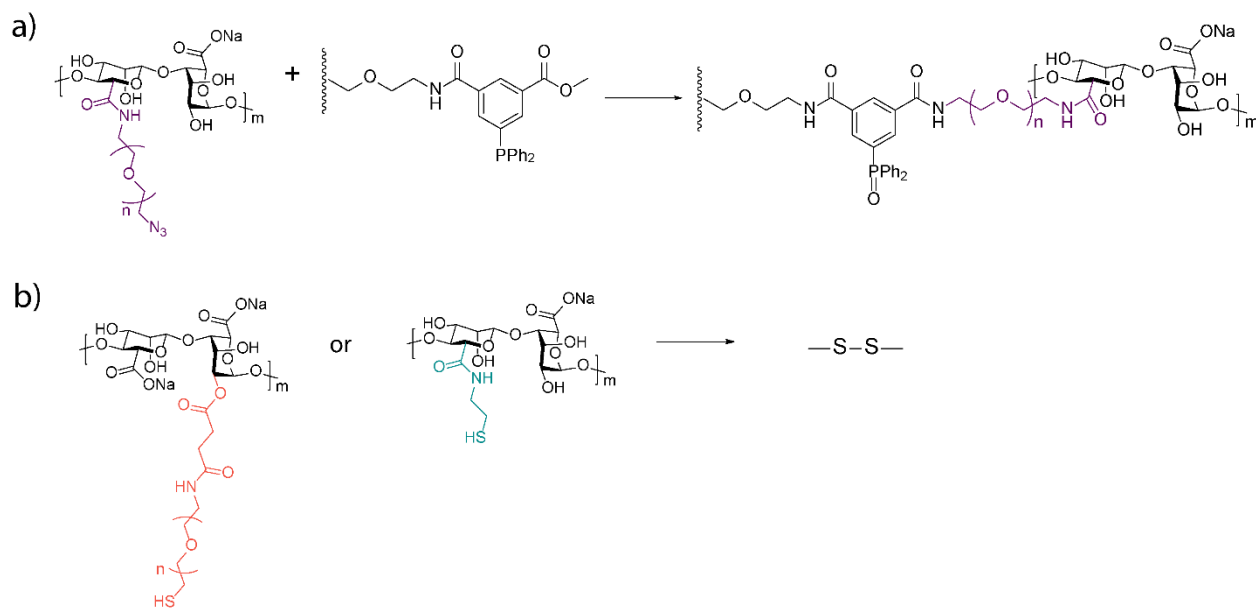
Scheme 1.1. PEGylated alg derivatives for the formation of hybrid hydrogels. a) Chemical cross-linking via Staudinger ligation b) Chemical cross-linking via disulfide bridge formation.

1.3.3. Limitations of current hydrogels and possible solutions

Despite the high potential of microencapsulated cell transplantation for the treatment of many human diseases, the translation to standard medical care is still hindered by serious unsolved issues. Among the factors that need to be addressed, one can cite biocompatibility towards both the encapsulated cells and the host recipient, long-term integrity of the capsules to ensure uninterrupted immune protection, long-term cell survival and functionality, and biosafety.[61] In addition, there is an unmet medical need for standardized sources of cells, of suitable quantity and reproducible quality for transplantation. In order to achieve long-term graft survival and functionality, two main challenges should be tackled. First, mechanical durability and chemical stability of the hydrogel MS should be enhanced. Second, efficient immunoprotection and mitigation of adverse pericapsular fibrotic overgrowth (PFO) should be reduced. These aspects are discussed in the upcoming paragraphs.

1.3.3.1. Microcapsule stability

Microcapsules formed by the ionic interactions of Na-alg with divalent cations (mostly Ca-alg MS) are known to perform poorly in terms of elasticity[156] and stability in physiological environment.[157] Destabilization of the MS can occur either in the presence of non-gelling ions (Na^+, K^+) by ion exchange, or in the presence of strong chelating agents (citrate, lactate, phosphate), which have a high affinity towards divalent gelling ions (Ca^{2+}, Ba^{2+}, Mg^{2+}).[158] If the integrity of the transplanted capsules is damaged, the cells are exposed to the host immune system. In addition, the inadequate physical properties of the capsules can enhance fibrotic reactions.[159]

Improvement of the stability of Ca-alg microcapsules has been a topic of intensive research since the eighties within the field of alg research.[160–162] Stabilization of alg-derived hydrogels was achieved by polyelectrolyte complexation with polycations. This technique, initially reported by Lim and Sun in 1980,[163] implies subsequent coating of the initially formed hydrogels with polycations such as poly-L-lysine (PLL), poly-L-ornithine (PLO), poly-L-arginin (PLA) and chitosan. A final layer of Na-alg is added to neutralize the excess of positive charges, resulting in alginate-polycation-alginate (APA) microcapsules. A few of these formulations have even reached human clinical trials, but with limited success.[164] Human islets were encapsulated in alg-PLO-alg MS and transplanted to diabetic patients. While improved mean daily blood glucose levels, decreased exogenous insulin necessity, and good safety were demonstrated, long-term graft functionality was not achieved.[165,166] Alg-PLL-alg encapsulated fetal porcine islets transplanted into a diabetic patient reached a reduction of 30% in his insulin dose, but only for a short period (less than one year). Encouragingly though, some viable and functional islets could be retrieved after ten years.[167] In addition, the use of polycation layers caused biocompatibility issues; in many cases, the activation of pro-inflammatory cytokines and growth factor was reported.[168–171]

Another way of achieving further stabilization of Ca-alg microcapsules is by introducing covalent cross-linking within the alg ionic network. In this case, a critical factor that one should take into consideration, is the non-toxicity, cell-compatibility and harmlessness of the chemical reaction, reagents and catalysts used. Many examples can be found in the literature for photo cross-linking of methacrylated alg derivatives.[172–175] Exposure to UV light, however, might be detrimental to certain cell types.

To avoid the use of any toxic reagents, click chemistry is a preferred way of covalent cross-linking (Figure 1.13). Diels-Alder click chemistry was proposed by García-Astrain and Avérous to cross-link a furan-modified alg with a bismaleimide derivative.[176] The same concept can be applied using maleimide modified 4-arm PEG.[177] Tetrazine-norbornene reaction was also presented as a cross-linking for alg-based cell encapsulation.[178] However, these were not used to form spherical microcapsules. Azide-alkyne [3+2] cycloaddition between an azide and an alkyne functionalized alg lead to spherical click microcapsules presenting improved stability in EDTA solution compared to Ca^{2+} cross-linked capsules.[139] In addition, disulfide bridge formation was shown to reinforce microcapsule stability, and led to successful encapsulation of human hepatocellular carcinoma (Huh7) cells.[179] Click cross-linked alg hydrogels are very attractive materials for cell encapsulation, however, in most cases introduction of the click cross-reactive functions involves the modification on the carboxylate groups. Therefore, the benefit from the chemical cross-linking is only achieved at the price of losing available sites for ionic cross-linking.
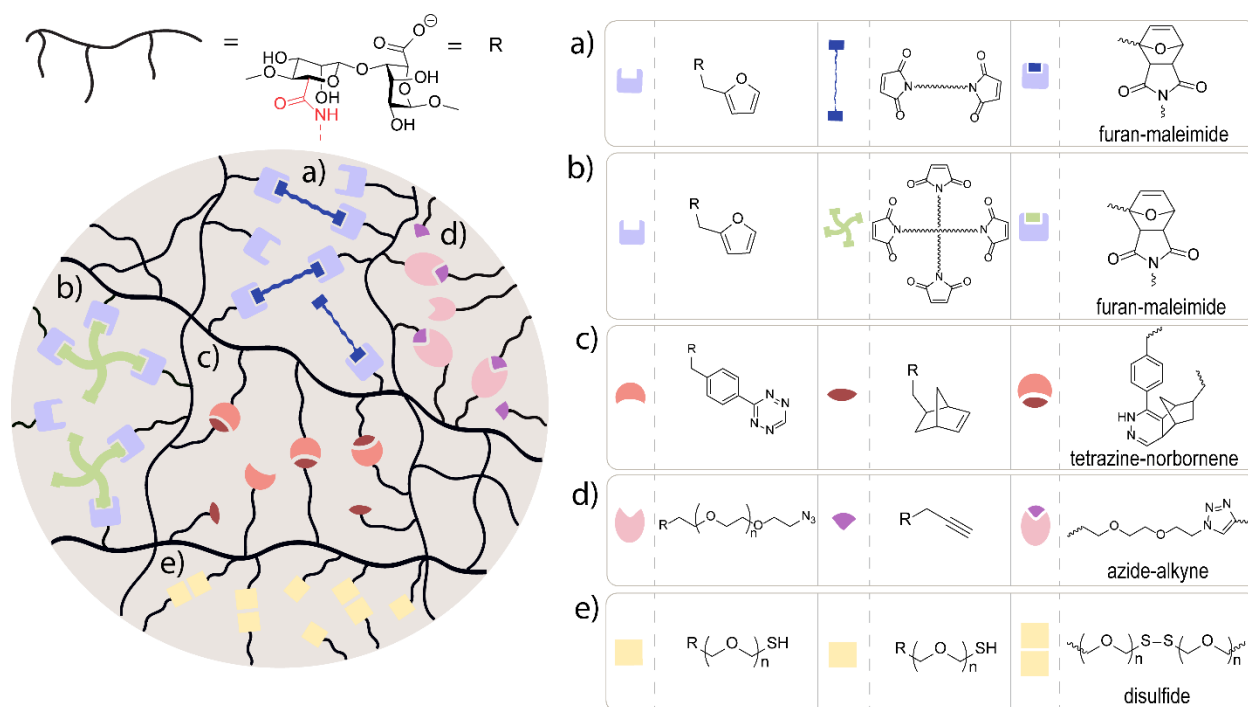
Figure 1.13. Mechanical stability improvement of alg hydrogels by click chemistry. Na-alg is functionalized on the carboxyl moiety.

1.3.3.2. Microcapsule immunoprotection

While many factors might contribute to the early loss of graft functionality, fibrotic overgrowth

around the transplanted capsules is without doubt one of the most common reasons.[180,181] Biomaterials used to entrap living cells must be biocompatible, without exception. Still, the requirement of biocompatibility is a very complex issue, therefore, the more simple definition of *biotolerability* has been introduced.[182] Biotolerability of a material is its ability to "reside in the body for long periods of time with only low degrees of inflammatory reactions".[183] An additional difficulty in developing biomaterials which trigger minimum foreign body response, is the obstacle to translate *in vitro* results to *in vivo*, and small animal study results to human outcomes.

The mechanism of inflammation and fibrotic tissue formation is a very complex process, consisting of three main phases: 1) acute inflammation 2) chronic inflammation and 3) granulation tissue development.[184] These processes result in microcapsules covered by fibrotic tissue, which then impedes the free diffusion of essential nutrients, oxygen and metabolites. Even the slightest decrease in the oxygen levels can lead to detrimental drop in functionality performance or cell death. This is of particular importance in the context of islet transplantation as these cells are highly sensitive to the available oxygen levels in their environment.[185,186]

Numerous attempts have been presented in pursuance of reducing fibrotic reactions to the transplanted microspheres. Most of the studies relate to alg-derived hydrogels. One of the main approaches targets the MS surface. Macrophages and proteins tend to attach to the surface of implanted materials. Surface modification to reduce adhesive properties was reported. Ba-alg microcapsules coated with chitosan achieved reduced pericapsular fibrosis compared to bare Ba-alg formulations.[187] Addition of PEG has been shown to further decrease protein absorption in many cases.[188,189] Vegas and co-workers developed a combinatorial library of modified alg with the aim of finding the best candidates for improving the biocompatibility of alg-based encapsulation materials. Out of the 774 synthesized candidates, a triazole-containing polymer performed the best, and showed reduced inflammatory reactions in both rodent and non-human primate models for up to six months.[190] A more recent approach proposed the use of polymer brushes for surface modification of alg MS.[191–193]

The diameter of alg MS was shown to affect the severity of foreign body response to microencapsulated cells, however, the optimal MS size is still under debate. A general view is that smaller MS induce weaker foreign body response than larger geometries.[194,195] More recently, though, Veiseh et al. encapsulated rat islets in 1.5 mm or 0.5 mm diameter Ba-alg, and found that larger geometry spheres exhibited better biocompatibility features implanted in rodents and non-human primates.[196] Moreover, efficient purification of alg has a crucial influence on the outcome of the engraftment.[197] Even low amounts of proteins, endotoxins and polyphenols present in the

alg material can trigger fibrotic reactions.[198,199]

Other approaches target the cell content within the MS, instead of their surfaces. The cellular content of the capsules plays a huge role in the inflammatory responses as well, by producing danger-associated molecular patterns.[200] Co-encapsulation of mesenchymal stem cells (MSCs) was demonstrated to reduce fibrosis in both xeno- and allotransplantation models, improve graft survival, and even enhancing angiogenesis when co-encapsulated with islet cells.[201–204] Similarly, using regulatory T cells in the presence of islets presented delays in graft rejection, due to the reduced amount of effector T-lymphocytes present in close proximity of the transplanted islets.[205,206]

Another strategy to enhance cell functionality and reduce fibrotic reactions is the co-encapsulation of small drugs with anti-inflammatory, anti-fibrotic or immunosuppressive drugs. *In vivo* screening of a variety of anti-inflammatory drugs suggested the superior effectiveness of curcumin and dexamethasone over the rest of the investigated drugs. Further co-encapsulation of curcumin with rat islets and transplantation into diabetic mice revealed diminished PFO around the capsules and improved glycaemic control.[207] An *in vitro* study of rat islets co-encapsulated with pentoxifylline showed a decreased likelihood of lymphocyte attack towards the drug containing MS.[208] Inclusion of rapamycin in the PEG coating around porcine islet loaded alg MS was found to be efficient for mitigating PFO and reduce macrophage proliferation around the capsules.[209] Reduced fibrotic overgrowth was observed *in vivo* for MS containing rat islets co-encapsulated with ketoprofen anti-inflammatory drug.[210] However, a major shortcoming for this co-encapsulation strategy is the fast burst release of the drugs from the network, typically within the first 24 hours. This implies that the drug content might delays severe immune reaction in the initial phase of acute inflammation, but might not be efficient at further stages of the inflammation process due to incapability to maintain a long-term drug release.

1.4. Alginate functionalization

This section is based on the review paper: Luca Szabó, Sandrine Gerber-Lemaire* and Christine Wandrey *"Strategies to functionalize the anionic biopolymer Na-alginate without restricting its polyelectrolyte properties" (Under preparation).*

The backbone of alg displays carboxyl and hydroxyl functional groups, allowing the modification and fine-tuning of the polymer properties by chemical functionalization. Carboxyl groups offer a straightforward modification sites thanks to the many existing activating agents that can be

applied under mild conditions. The carboxyl groups, however, are responsible for the ability of alg to interact with divalent cations. Therefore, modifications on these functional groups can interfere with the fast ionic gelation of alg and the stability of the resulting hydrogels. In order to preserve the ionic cross-linking abilities of alg, functionalization of the hydroxyl groups is favored. A schematic illustration of the possible alg derivatization routes is depicted in Figure 1.14.
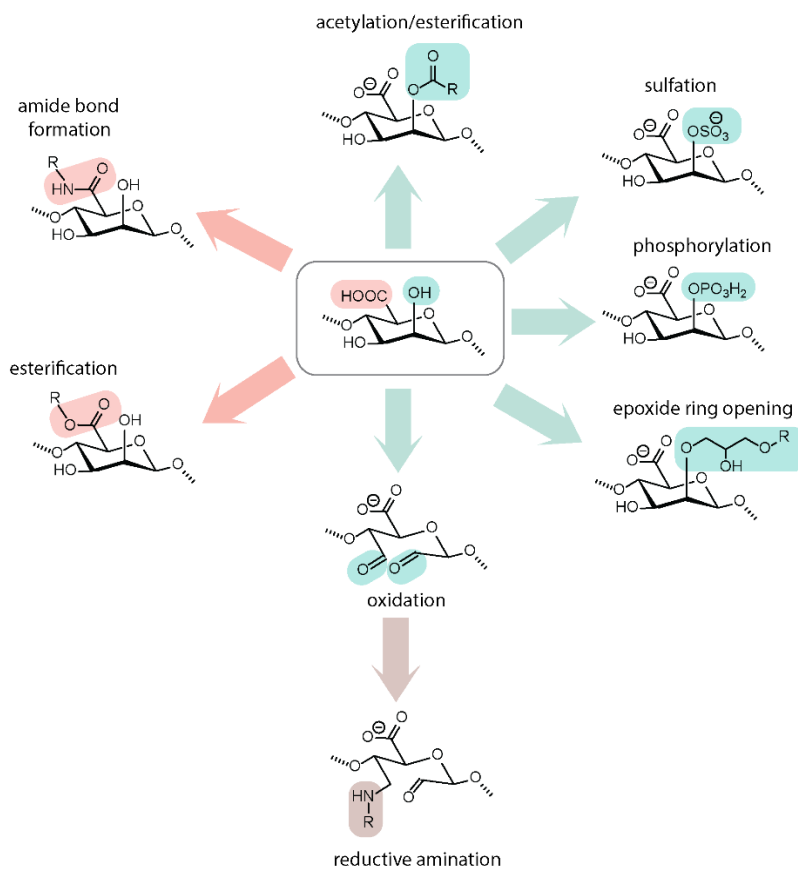
Figure 1.14. Alg modification routes.

1.4.1.   Modifications involving the carboxyl groups

Alg carboxyl groups are most commonly activated with a combination of 1-ethyl-3-(3-dimethylaminopropyl)carbodiimide and *N*-hydrosuccinimide (EDC/NHS), to form a new amide or ester bond. This type of carbodiimide chemistry was used for the functionalization of alg with tyramine, to obtain bioactive alg surfaces, suitable for cell culture platforms.[211] A linear perfluorinated (PEG) linker was introduced within the alg backbone through amide bond formation using the same coupling agents. The modified polymer was then further used to

ionically cross-link into 3D MS and encapsulate mouse insulinoma (MIN6) cells. Enhanced proliferation of the cells within this polymer was observed, compared to control Ba-alg beads.[212] As mentioned in previous sections, click-reaction is a valuable route for covalent cross-linking of alg derivatives. To introduce the functionalities amenable for click reactions, the most common way is to apply the carbodiimide chemistry on the alg carboxylate group. Following this pathway, Breger et al. prepared azide and alkyne functionalized alg, which underwent copper-catalyzed cycloaddition and resulted in highly stable MS in EDTA solution.[139] Ghanian and co-workers presented a furan substituted alg following the activation of the carboxylate groups with EDC/NHS, and subsequently cross-linked it with 4-arm PEG containing maleimide end-functionalities.[177] Vegas et al. prepared a large combinatorial alg hydrogel library, in order to find derivatives of alg that could potentially decrease the fibrotic response of the transplanted microcapsules. They presented the conversion of alg into ester or amide derivatives using 2-chloro-4,6-dimethoxy-1,3,5-triazine/*N*-methylmorpholine (CDMT/NMM).[190] Esterification of the alg carboxylate could also be achieved using the EDC/NHS coupling agent pair, for the introduction of catechol within the alg backbone. While the resulted hydrogel exhibited excellent mechanical and chemical stability properties, catechol was found to have a detrimental effect on the insulin secretion ability of encapsulated murine islet cells.[213]

1.4.2. Modifications involving the hydroxyl groups

Modification of the alg preserving its ionic crosslinking abilities is feasible by alteration of the hydroxyl groups. The first reported transformation dates back to 1946, when successful acetylation of approximately one hydroxyl group of alginic acid, Na-alg and Ca-alg was performed using ketene.[214,215] Later on, diacetlyation reactions were reported, using acetic acid or acetic anhydride.[216–220] Acetylation of alg did not result in significant modification of its properties. However, these reactions allowed a better understanding of some of the alg reactivity and features.

Other esterification reactions were commonly applied for various reasons,[221–223] such as for increasing the density of the carboxylate groups on the alg network. Alg presenting high carboxylate density was successfully used for the immobilization of lactic acid bacteria.[224] Esterification of the alg hydroxyl groups was also achieved using succinic anhydride, for further conjugation to thiol-equipped PEG derivatives. Formation of hydrogel MS was achieved by ionic gelation in the presence of Ca^{2+} ions and complementary cross-linking resulting from disulfide

bridge formation when exposed to air. These dual ionic-covalent hydrogels supported the good viability of primary human foreskin fibroblasts up to four weeks after microencapsulation.[155]

Sulfation of alg is a commonly used procedure to obtain characteristics similar to those of heparin. Heparin, a widely used anticoagulant glycosaminoglycan, contains carboxyl and sulfate functional groups. Hence, conversion of the alg hydroxyl groups to sulfate groups results in a high degree of similarity to heparin. The sulfation is usually performed using chlorosulfonic acid in formamide.[225–229] However, $N(SO_3Na)_3$ was also proposed as a milder, less pollutant sulfation reagent.[230] A clinically relevant sulfated alg derivative is the propylene glycol alg sodium sulfate (PSS), that was used in China for many years as a heparinoid drug for the treatment of cardiovascular diseases.[231] PSS is prepared by sulfation of the hydroxyl groups and esterification of the carboxyl groups of alg.[229]

Phosphorylation has also been successfully performed, however, not many examples can be find in the literature. Phosphorylation of alg was achieved by a phosphoric acid and urea generated adduct. The resulted phosphorylated alg polymer was used to induce hydroxyapatite nucleation and growth.[232] In addition, alg treated with a mixture of $H_3PO_4/P_2O_5/Et_3PO_4$/hexanol also resulted in O-phosphorylated derivatives, as a potential encapsulation materials.[233]

Alg are hydrophilic materials by nature, yet, certain applications might require to have an additional hydrophobic domain. The alg hydroxyl groups were reported to perform epoxide ring opening reactions leading to the introduction of long alkyl chains. The resulted alg derivative is capable of self-assemble into polymeric micelles in solution. The hydrophobic alkyl chains form a hydrophobic core, while alg constitutes a hydrophilic shell. These micelles are able to deliver water-insoluble drugs, by entrapment within the hydrophobic core.[234–236] Epoxide ring opening was also used to introduce methacrylate groups, amenable for further covalent cross-linking, while preserving the carboxylate sites for water treatment goals.[237]

One of the most frequently followed pathway for the modification of the hydroxyl group involves the oxidation of alg. This results in the opening of the polysaccharide backbone between two vicinal alcohols, and the emergence of two highly reactive aldehyde groups, which are generally further functionalized by reductive amination reactions. However, oxidation was also performed to modulate the degradability properties of alg.[238–242] Optimization and timing of polymer degradation rates is especially important in the field of tissue engineering.

Many opt for functionalization of the aldehyde groups obtained after oxidation, as a way of preserving the carboxylate functionalities. However, a major consideration to keep in mind is that oxidation is accompanied with substantial polymer degradation.[243–246] Depending on the type of amine being used in the reductive amination step, alg can be altered to have hydrophobic character,[247,248] deliver drugs,[249,250] or remove heavy metals from water.[251,252]

Alternatively, oxidized alg can also be used to further cross-link with the addition of an external cross-linker. The typical cross-linking reaction used is imine formation with amines by Schiff base reaction. Gelatin cross-linked alg are widely used in biomedical applications, as addition of gelatin enhances cell adhesion and cell proliferation properties of the hydrogel.[253–257] Other types of cross-linkers have also been presented, such as adipic dihydrazide,[258] oxime, semicarbazone or hydrazine.[259]

2. Thesis objectives

Encapsulation and transplantation of cells to treat or cure serious diseases could alleviate the life of many patients. To reach the final goal of using encapsulated cell-based therapy as a routine clinical procedure requires the collaboration of researchers from several fields, and the improvement of many aspects of the encapsulation and transplantation processes. Amongst all, improvement of the bioencapsulation material is extremely important to provide the most favorable environment for long-term survival and functionality of the entrapped cells.

The main goal of the present thesis work was to develop new alg-based hydrogel materials that could provide a beneficial 3D surrounding for microencapsulated cells. To overcome the shortcomings of the currently existing materials, the two main objectives were to 1) increase the mechanical and chemical stability, and to 2) reduce the fibrotic response against transplanted microcapsules. A third objective was to optimize the synthetic procedures for the functionalization of alg in order to obtain reproducible polymer batches with minimal degradation, as well as tunable properties to match the requirements of different encapsulation processes.
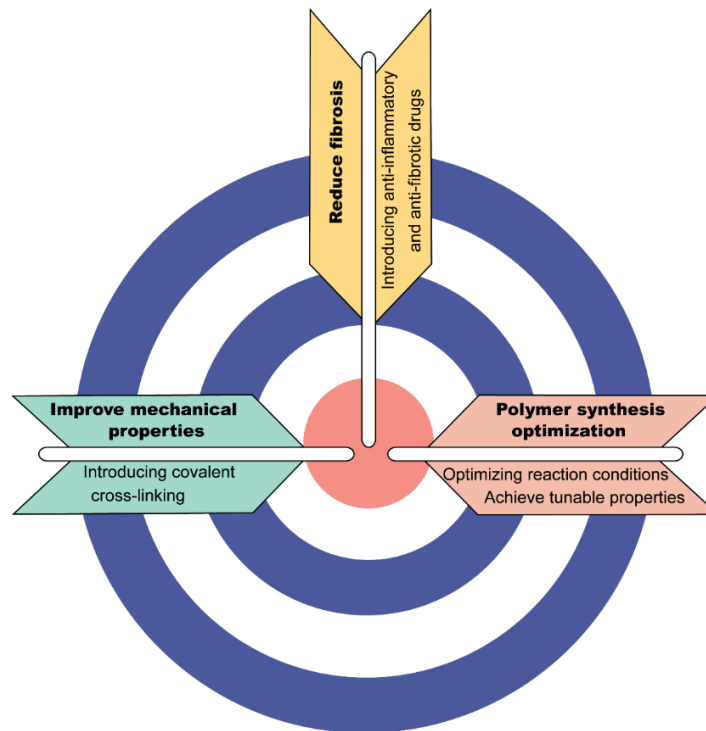
Figure 2.1. Main goals of the thesis.

Na-alg is an excellent candidate for cell encapsulation purposes, due to its biocompatibility and advantageous gelling properties. The gelation requires very mild conditions, and happens spontaneously in the presence of divalent cations. However, it generates only reversible physical cross-links, which are susceptible to destabilization even under physiological conditions. Functionalization of alg by introducing linear PEG chains, capable of covalently cross-link results in dual cross-linked, highly stable microcapsules. Furthermore, the addition of PEG also increases the otherwise very poor shape recovery performance of Ca-alg beads.

Table 2.1 highlights some of the essential properties that the hydrogel MS for transplantation should fulfill. The advantages and limitations of the unmodified Ca-alg MS, and our targeted improvements of its properties by using multifunctional MS are presented.

Table 2.1. Properties of unmodified Ca-alg MS, and targeted improvements of certain properties with multifunctional MS composed of PEGylated alg polymers.

	Ca-alg MS	Multifunctional MS
Elasticity Ability to recover shape after several compressions	*Needs improvement*	*~50% shape recovery performance*
Durability Mechanical and chemical stability over time *in vivo*	*Needs improvement*	*Higher concentration of non-gelling ions tolerated*
Fibrosis Formation of fibrotic tissue around MS due to immune reactions	*Fibrotic overgrowth of encapsulated cells*	*Reduction by addition of anti-inflammatory drugs*
Biocompatibility of the material Properties of the material compatible with the host system	*Good*	*Retained*
Gelling conditions Easy gel formation under mild conditions	*Good*	*Retained*

The thesis also focuses on the development and optimization of a robust synthetic strategy to covalently graft PEG derivatives on the hydroxyl groups of alg. Many parameters can be controlled in order to minimize the polymer chain degradation during chemical transformations, and obtain fine-tunable and reproducible viscosity values of the final polymer solutions, which will be presented in the current work.

One of the main causes of microencapsulated cell graft failure is the immune reaction of the host system to the transplanted MS. Inflammation and PFO around the microcapsules result in hindered diffusion of essential oxygen and nutrients, eventually leading to cell death and loss of the graft. To reduce PFO, we envisaged the covalent conjugation of anti-inflammatory and anti-fibrotic drugs to the hydrogel network. Covalent conjugation was feasible by coupling the drugs to PEG derivatives, before conjugation to the alg backbone. This strategy has the advantage of sustained, controlled drug release over the widely used drug co-encapsulation, which results in a very fast, burst release of the drug.

Eventually, by combining the two strategies of improving mechanical properties and reducing PFO, novel multifunctional alg-based hydrogel system was emerged. These multifunctional microcapsules have the potential to prevent premature loss of cell functionality due to host immune system reaction and fibrotic overgrowth, while displaying excellent elasticity and stability under physiological conditions.
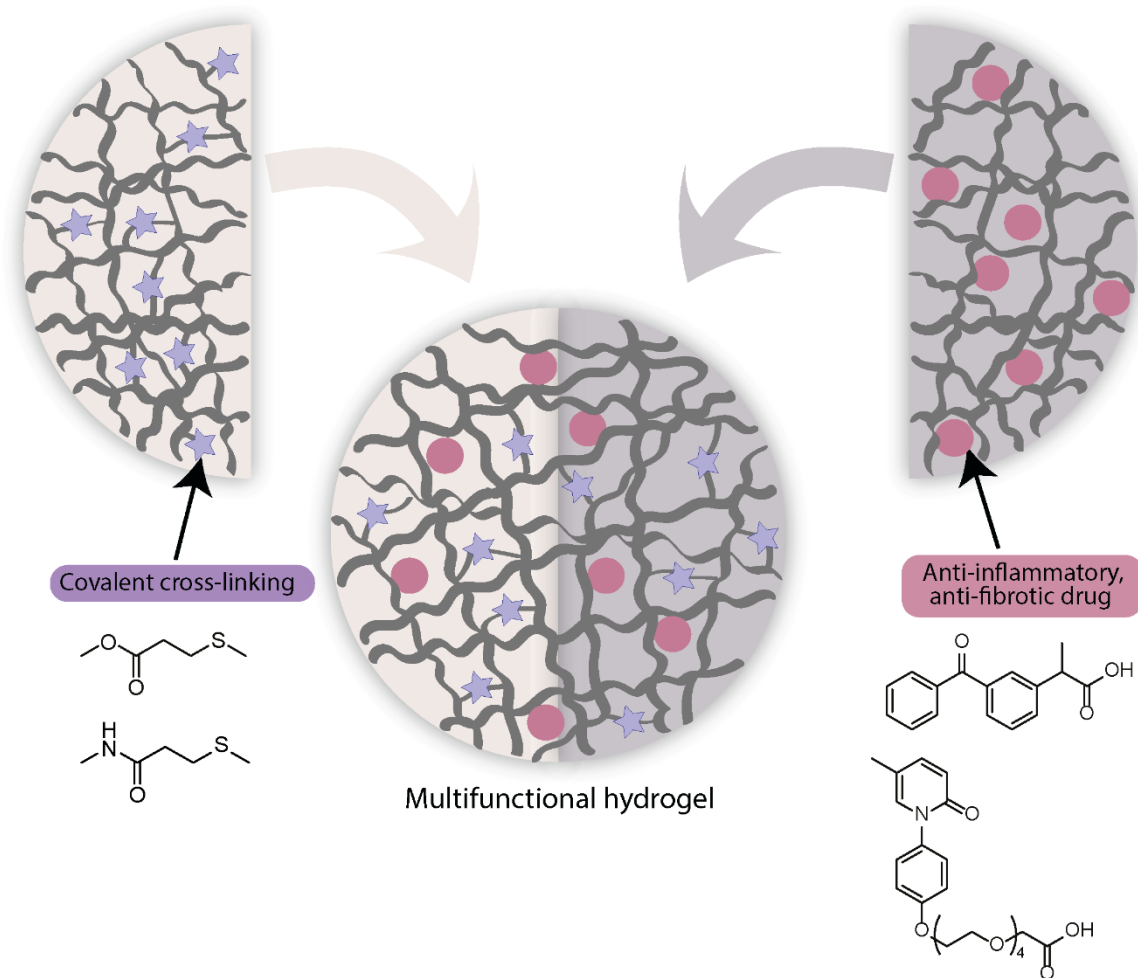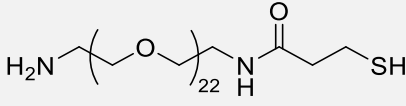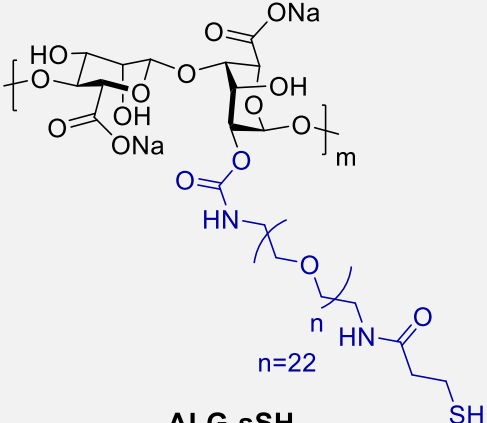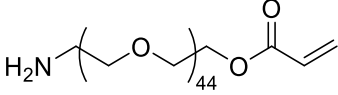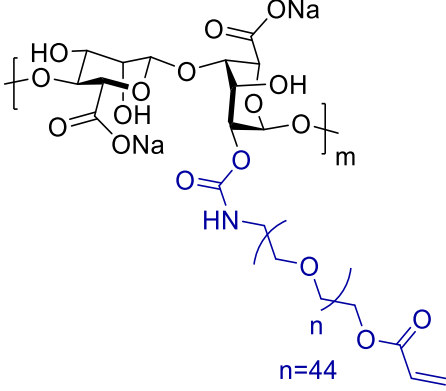
Figure 2.2. Formation of multifunctional hydrogel MS by combining the benefits of different strategies.

3. Results and Discussion

In order to follow easily the types of PEG derivatives and PEGylated alg derivatives throughout the thesis, Table 3.1 provides a nomenclature with the corresponding chemical structures of the compounds used within the frame of this study. The PEG derivatives were either synthesized (PEG-sSH, PEG-KET(ester) and PEG-PFD), or obtained from commercial sources (PEG-ACR, PEG-MAL, PEG-SH, PEG-ACA).

Table 3.1. Structure and nomenclature of PEG and PEGylated alg polymers used within the thesis.

Compound (PEGylated alg)	Heterobifunctional PEG	Alg-PEG
3	PEG-sSH	ALG-sSH
4	PEG-ACR	ALG-ACR

5	**PEG-MAL**	**ALG-MAL**
6	**PEG-SH**	**ALG-SH**
	PEG-ACA	**ALG-ACA**

9	PEG-KET (ester)	ALG-KET (ester)
23	PEG-PFD	ALG-PFD
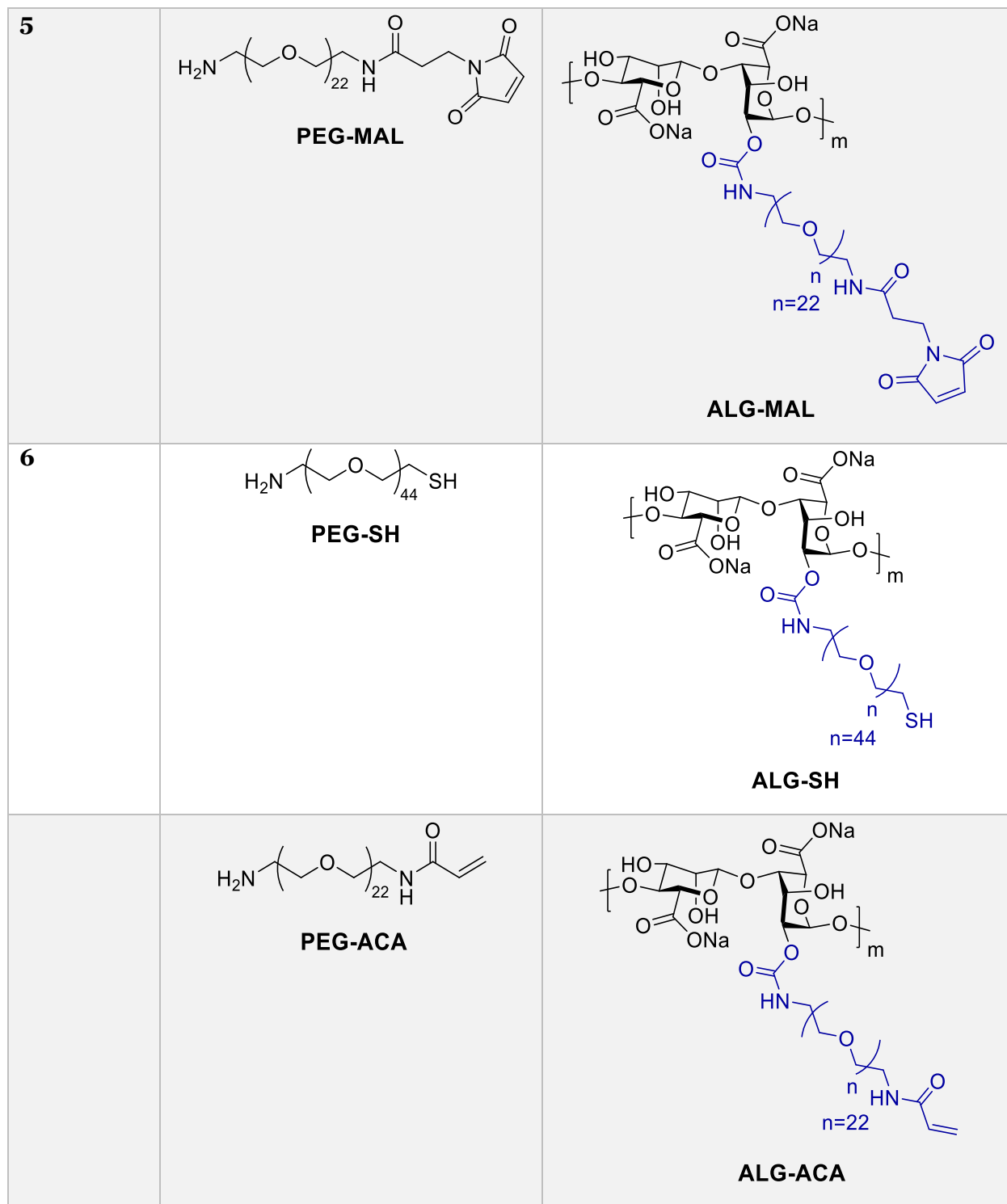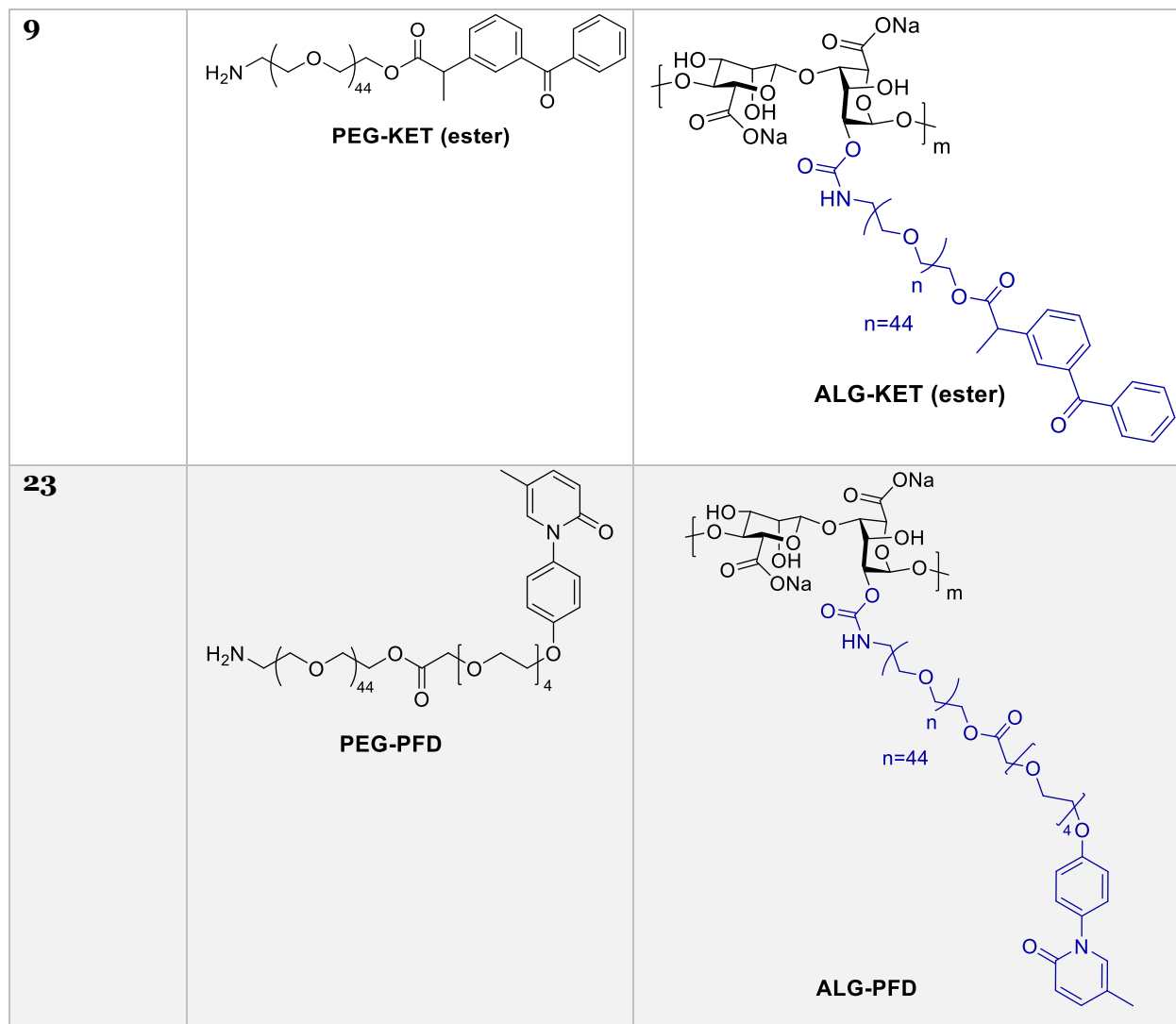
3.1.   Functionalization of Na-alg with cross-reactive PEG derivatives

This section is based on the manuscript entitled: "Synthesis Strategies to Extend the Variety of Alginate-Based Hybrid Hydrogels for Cell Microencapsulation", *Biomacromolecules*, **2017**, *18*, 2747−2755.

Clinical translation of encapsulated cell-based therapies is delayed partly due to the lack of biomaterials with perfect properties. Development of new alg-based materials was envisaged in a way that preserves the advantages and overcomes the drawbacks of pristine alg. Since the main

advantage of alg-based hydrogels is the fast physical cross-linking of the alg carboxyl groups with divalent cations, our target was functionalization of the hydroxyl group of alg. Combination of PEG with alg has been shown previously to improve biocompatibility,[260,261] and depending on the end-functionality of the PEG, it allows for introducing chemical cross-linking or active compounds. A main disadvantage of using unmodified alg is its poor mechanical properties. Addition of PEG on the polysaccharide backbone not only provides a hybrid hydrogel forming both ionic and covalent cross-linking, but also drastically improves the elastic behavior of the spherical hydrogel beads.

Previously in our group, covalent conjugation of heterobifunctional PEG on the alg hydroxyl group was developed by reaction with succinic anhydride, leading to an ester linkage between the alg backbone and PEG units. Functionalization of Na-alg in organic solvents requires good solubility of the polymer, therefore the first step of the synthesis was the conversion of Na-alg into its tetrabutylammonium (TBA) salt. Reaction with succinic anhydride led to an ester bond and generated a new carboxylic moiety, easily accessible for further modification with PEG (Scheme 3.1).
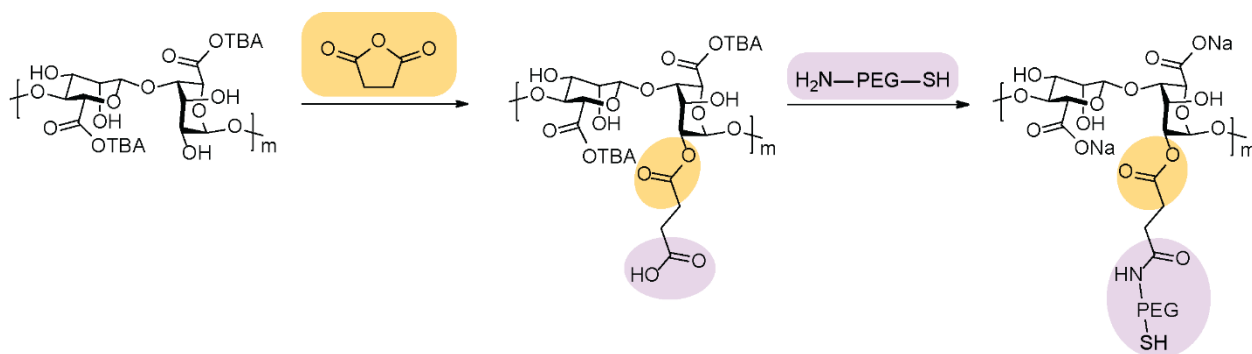
Scheme 3.1. Functionalization of Na-alg with PEG derivatives through ester linkage.

Using thiols as cross-reactive functionalities, dual ionic-covalent MS were obtained from the PEG-thiol functionalized alg and demonstrated favorable properties for the microencapsulation of human cells. However, due to the presence of ester grafting unit, long-term stability *in vivo* could not be achieved. Therefore, a new strategy was developed for the covalent conjugation of PEG on the alg hydroxyl groups through carbamate-bond formation, using imidazole chemistry. Reaction of TBA-alg with carbonyldiimidazole (CDI) activates the hydroxyl groups which can be further functionalized with the PEG cross-reactive derivatives (Scheme 3.2).
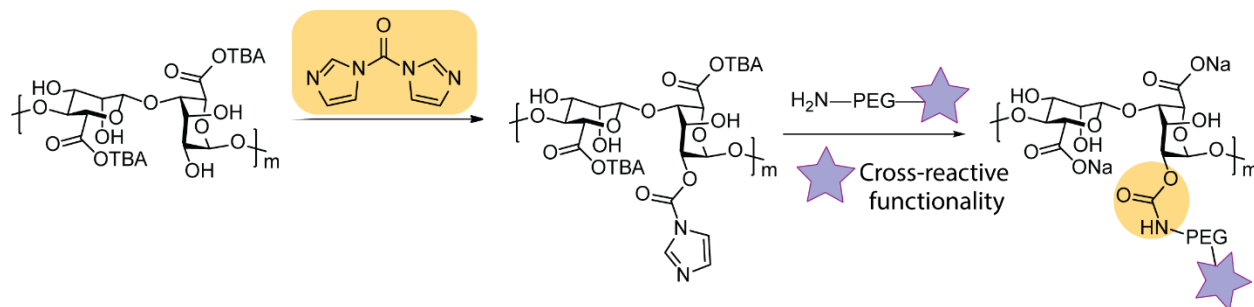
Scheme 3.2. Functionalization of Na-alg with PEG derivatives through carbamate linkage.

In the next section, the optimization of the different synthetic steps of the functionalization procedure will be presented.

3.1.1. Na-alg conversion into TBA-alg

In order to perform synthetic modification on alg, the polymer needs to be soluble in the organic solvent of use. Na-alg has a very poor solubility in organic solvents, but its TBA-alg salt has increased solubility in DMSO, which is the solvent used for the grafting of PEG on the alg hydroxyl groups. Conversion of Na-alg into TBA-alg happens in two consecutive steps: 1) formation of the carboxylic acid form by addition of acid 2) further transformation by TBAOH treatment of the precipitated acid (Scheme 3.3).
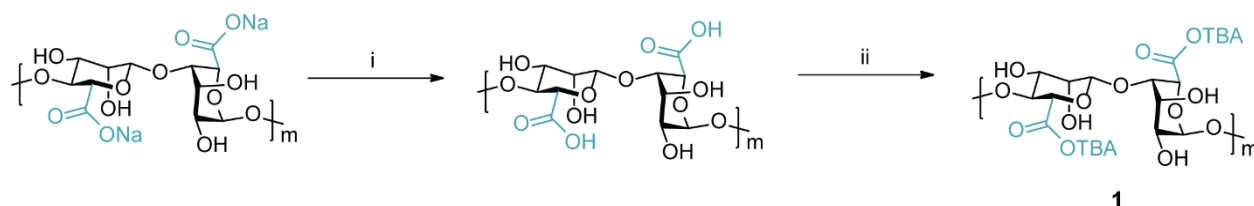
Scheme 3.3. Conversion of Na-alg to TBA-alg, with alginic acid as intermediate. Optimized reagents and conditions: i) HCOOH, EtOH, 0 °C ii) TBAOH, H₂O, rt.

One of the main goals of the present thesis was to optimize the polymer synthesis to minimize degradation, and obtain batches with good reproducibility. For this reason, the effect of many parameters of the TBA-alg synthesis were investigated: 1) type of acid 2) type of solvent 3) adjustment of pH during TBAOH addition 4) temperature.

Heterogeneous acidification of Na-alg is commonly performed using aqueous ethanolic hydrochloric acid (HCl) (0.6 or 6 N solutions), or aqueous formic acid.[262–265] Acidification with both HCl and formic acid were carried out for comparison, and the viscosities of the final aqueous TBA-alg solution were evaluated (Table 3.2). Formic acid, being a weaker acid, caused less degradation on the polymer backbone, and resulted in higher viscosity values of the TBA-alg

aqueous solutions. In addition, the variability in the viscosity values of the final TBA-alg polymer could be largely reduced by using formic acid (entries 3 and 4).

Table 3.2. Effect of the type of acid used for the synthesis of TBA-alg on the final viscosity of TBA-alg solution.

Entry	Type of acid	Solvent	Viscosity of TBA-alg[b]
1[a]	HCl	EtOH	133.1 mPa·s
2[a]	HCl	EtOH	86.51 mPa·s
3[a]	HCOOH, 20% aq. solution	H_2O	164.4 mPa·s
4[a]	HCOOH, 20% aq. solution	EtOH	157.7 mPa·s

[a] Reactions were performed on 1 g scale
[b] 2 wt% aqueous solution

The use of formic acid for the heterogeneous acidification of Na-alg was previously presented, however, only in aqueous media. Changing the solvent to ethanol significantly facilitated the implementation of the reaction. Two highly time-consuming steps were reduced: 1) since the reaction happens in a suspension, there is no need to wait for the solubilization of Na-alg in water 2) the filtration of the acid intermediate was simplified due to the change of the type of precipitate; instead of a gel-like precipitate formed in water, a powder-like precipitate was obtained in ethanol.

After precipitation of the alginic acid, this intermediate is resuspended in water and treated with TBAOH solution. The addition of TBAOH turned out to be a crucial step to obtain reproducible batches with minimal degradation. To ensure the complete exchange of protons to TBA-ions, the pH must be adjusted to 7. Further addition of TBAOH does not improve the TBA-ratio, nor the solubility in DMSO of the obtained TBA-alg. However, it does degrade the polymer chain and decreases the final viscosity of the polymer solution (Table 3.3). Therefore, stopping the addition of TBAOH at pH 7 is essential to deliver batches of TBA-alg polymer with reproducible viscosities in aqueous solution.

Table 3.3. Effect of pH adjustment on the final viscosity of TBA-alg.

Entry	TBAOH addition, pH	TBA-ratio	Viscosity of TBA-alg[b]
1[a]	9	2.1	89.4 mPa·s
2[a]	9	1.8	54.0 mPa·s
3[a]	7	2.0	146.6 mPa·s
4[a]	7	1.6	156.5 mPa·s

[a] Reactions were performed on 1 g scale
[b] 2 wt% aqueous solution

The temperature during the homogeneous acidification step was also found to have an influence on the degradation rate of the polymer, as expected. Previous studies reported the transformation of Na-alg into alginic acid at 4 °C during 12 h, or keeping the temperature at 4 °C for an hour and continue stirring for 12 h at room temperature. While performing the reaction at room temperature led to variations in the viscosity of the final polymer in aqueous solution, lowering the temperature ensured batch-to-batch reproducibility (Table 3.4).

Table 3.4. Effect of temperature on the final viscosity of TBA-alg.

Entry	Temperature	Viscosity of TBA-alg[c]
1[a]	Room temperature	76.5 mPa·s
1[b]	0 °C	155.5 mPa·s
2[a]	Room temperature	146.6 mPa·s
2[b]	0 °C	156.5 mPa·s

[a] and [b] were performed in parallel, only changing the temperature
[c] 2 wt% aqueous solution

The optimized parameters are summarized in Figure 3.1. To ensure good reproducibility, several batches were produced applying the parameters presented in Figure 3.1. The results are summarized in Table 3.5. All the viscosity values fall between the narrow range of 133.0−173.6 mPa·s.
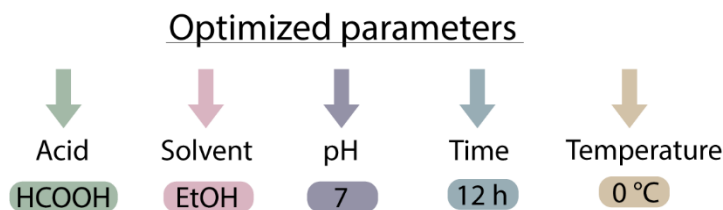
Figure 3.1. Optimized parameters for the synthesis of TBA-alg.

Finally, the optimized parameters were used to perform a scale-up of the reaction (Table 3.5, Entry 5). Very similar results were obtained when the reaction was performed on a 5 times larger scale, which is a very important asset in terms of future clinical applications.

Table 3.5. Results of the reproducibility experiments.

Entry	1[a]	2[a]	3[a]	4[a]	5[b]
TBA-ratio	1.7	2.0	1.5	2.0	2.2
Viscosity of TBA-alg (2% aq. solution)	133.0 mPa·s	155.5 mPa·s	146.3 mPa·s	157.7 mPa·s	173.6 mPa·s

[a] Reactions were performed on 1 g scale
[b] Reaction was performed on 5 g scale

3.1.2. Grafting of heterobifunctional PEG on TBA-alg

We first investigated the grafting of the thiol equipped PEG-sSH with the aim of forming disulfide bridges as complementary covalent network in the formation of hydrogel MS by ionotropic interactions. Conjugation of PEG derivatives on the hydroxyl group of TBA-alg required the activation of the hydroxyl groups. For this purpose, TBA-alg was treated with CDI for 0.5 h in DMSO, and the activated imidazolide alg **2** was subsequently precipitated. After thorough washing of the precipitate, it was dissolved in water and condensated with amino-terminated PEG derivatives for 2 h. The final product was obtained by exchange of TBA-ions to Na-ions, and subsequent purification by dialysis.
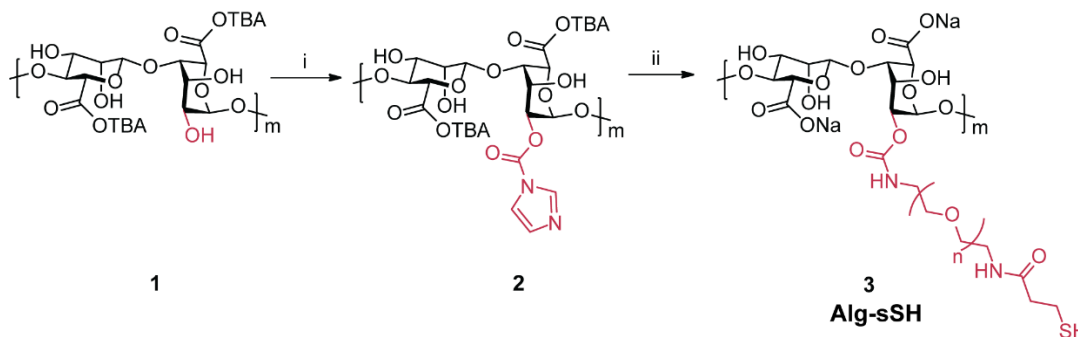
Scheme 3.4. Preparation of PEGylated alg. Reagents and conditions: i) CDI, DMSO, rt, 0.5 h ii) PEG-sSH, H₂O, rt, 2h.

At the end of the reaction, the desired form of the alg derivative is its Na-salt. Previous procedure developed in our lab involved the quenching of the reaction with 0.05 M NaOH solution (50 mL/1g of initial TBA-alg), to obtain the corresponding Na-alg derivative. This led to extensive and uncontrollable chain degradation of the polysaccharide, and consequently a high variety in the viscosity of the resulting polymer solutions. Taking into consideration that alg degrades in the presence of strong bases, we decided to reevaluate this step. All our attempts were targeted towards reducing the severity of the degradation by optimization of several parameters of the procedure.

a) First, we investigated the effect of controlled NaOH quenching, by adjusting the pH when adding the base. The aim of NaOH addition is to exchange TBA-ions to Na-ions, consequently, the amount of NaOH solution needed was to reach a pH in the range of 8–11. While the highest viscosities were observed by adjusting the pH to 8 or 11 (Table 3.6), no reproducible correlation between the pH value and extend of chain degradation could

be established. In addition, these results could not be precisely reproduced. Therefore, this strategy to exchange TBA-ions was discarded.

Table 3.6. Representative examples of the effect of precise pH adjustment when quenching the reaction.

Entry	Experiment	Viscosity of PEGylated-alg[b]
1	No pH adjustment	182.6 mPa·s
2	pH adjusted to 8	790.9 mPa·s
3[a]	pH adjusted to 9	387.4 mPa·s
4[a]	pH adjusted to 10	257.6 mPa·s
5[a]	pH adjusted to 11	709.1 mPa·s

[a] Reactions were performed in parallel, on a 100 mg scale.
[b] 3 wt% aqueous solution

b) Further attempt to decrease the degree of degradation included performing the quenching of the reaction at 0 °C, and continuing by dialysis at 4 °C. Unfortunately, this did not lead to improved results, but it made the implementation of the purification much more laborious.

c) Relatively fresh preparation of TBA-alg was evaluated to make a significant difference. Comparison assay of batches prepared from TBA-alg of 1 week-old or 2 or more weeks-old clearly suggested that preparation of TBA-alg 1 week prior to PEGylation results in higher viscosity ranges. The values are presented in Table 3.7.

Table 3.7. Influence of the age of TBA-alg on the final polymer solution viscosity.

TBA-alg	Viscosity of PEGylated-alg[b]
1 week-old[a]	628.0–870.5 mPa·s
2 or more weeks-old[a]	83.06–134.8 mPa·s

[a] Results are from min. 3 reactions
[b] 3 wt% aqueous solution

d) For the exchange of TBA-ions to Na-ions, ultrafiltration (UF) cell was also tested. The setup is presented on Figure 3.2. This method offers milder conditions, eliminating the use of a strong base, and the advantage of directly transferring the reaction solution into the cell. As an alternative to dialysis, the cell was also tested for further purification of the polymer. After transferring the reaction mixture to the UF cell, it was treated with NaCl solution. A low pressure of 3 bar was applied, and a cellulose membrane with MWCO of 3 kDa was chosen, in order to eliminate the potentially unreacted PEG-sSH, while retaining the Alg-sSH.
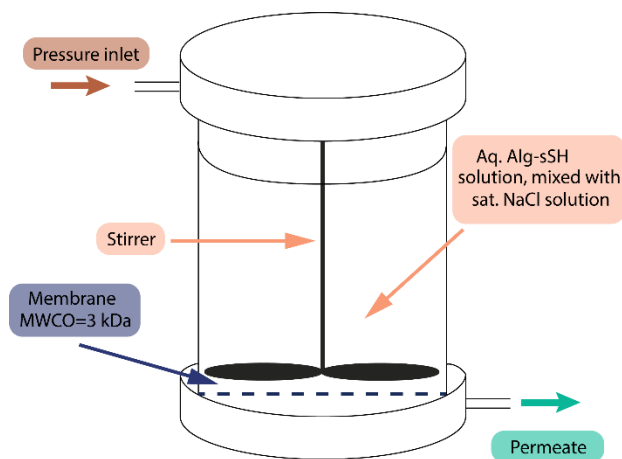
Figure 3.2. UF cell setup for the exchange of TBA to Na-ions.

Even though the technique offered a convenient and mild way of performing the ion exchange, and even potentially the purification, surprisingly, the amount of grafted PEG on the alg backbone was slowly reducing over time, as followed by ^{1}H-NMR (Figure 6.1, Annexes). Therefore, this technique was discarded.

e) Lastly, the best way of exchanging TBA-ions to Na-ions was found to be by addition of NaCl solution to the reaction mixture. After optimization of the concentration of NaCl solution and time needed for the exchange, the ideal conditions were concluded to be using 4M NaCl solution over 2 h.

3.1.3. Microsphere formation

Preparation of spherical hydrogel beads in our laboratory was performed using a coaxial air-flow droplet generator. The polymer solution is prepared in a concentration suitable for the encapsulator of intended use, and is extruded from a syringe through a needle into a gelation bath of CaCl$_2$. The air flow is applied to help the formation of spherical, and smaller MS compared to just dropping of the polymer solution in the ionic cross-linking bath by gravity (Figure 3.3).
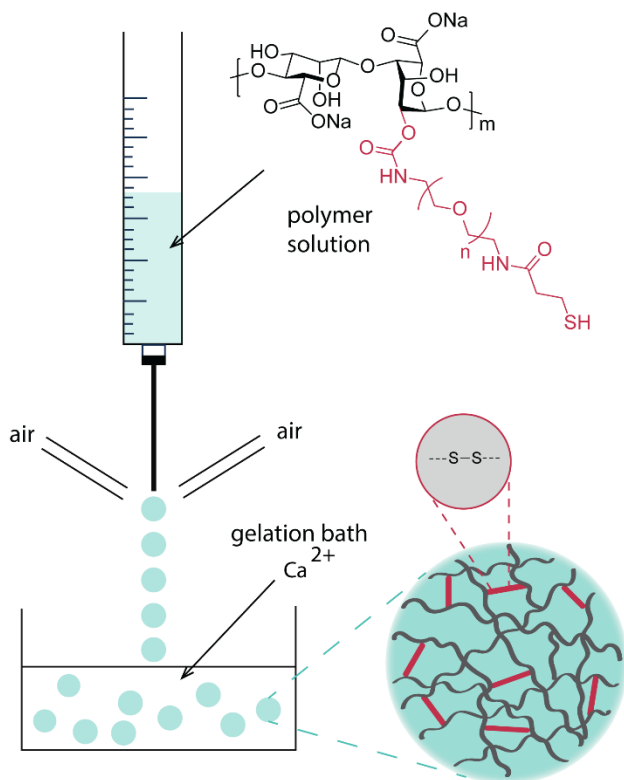
Figure 3.3. Formation of hybrid hydrogel MS with Alg-sSH.

Within a collaboration with the CEA (Commissariat à l'Ènergie atomique), in Grenoble, France, a microfluidic system was also developed for the preparation of PEGylated alg hydrogel MS. The motivation behind using microfluidics was the generation of MS with smaller diameter, better monodispersity, and homogeneity. Figure 3.4 presents an example of beads prepared from the polymer Alg-sSH using air-flow droplet generator and microfluidics. Droplet generation using microfluidics will be described more in details in Section 3.4.

1) Alg-sSH MS
Diameter: 741 ± 96 µm

2) Alg-sSH MS
Diameter: 385 ± 12 µm
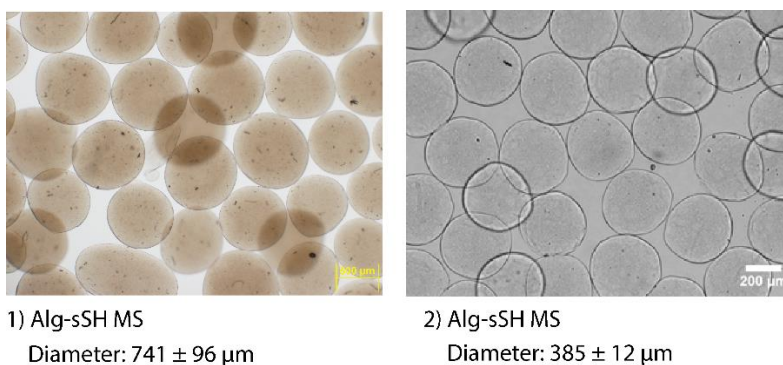
Figure 3.4. 1) Beads formed with coaxial air-flow droplet generator. The scale bar corresponds to 500 µm. 2) Beads formed with microfluidics. The scale bar corresponds to 200 µm. The mean diameter for both was measured 7 days after MS formation.

To reach the desired viscosity range compatible with the encapsulation setup, many parameters can be modified. The viscosity is dependent on the molecular mass of the polymer, the type of PEG grafted on the alg backbone, the grafting degree, the concentration of the solution, and also on the temperature. Optimized production of Alg-sSH MS was realized under the following conditions: Alg-sSH with a grafting degree of 7.1% (determined by ^{1}H-NMR) was dissolved at a concentration of 2 wt% in 3-(N-morpholino)propanesulfonic acid (MOPS) (10 mM, pH=7,4) (viscosity: 134.1 mPa·s), and extruded into a CaCl$_2$ (100 mM) containing bath. Measurement of the MS diameter at day 1 and day 7 after hydrogel formation revealed moderate shrinking of the MS. This observation is consistent with the slow completion of the covalent disulfide bridge network following fast initial gelation through ionic interactions with Ca^{2+} ions.
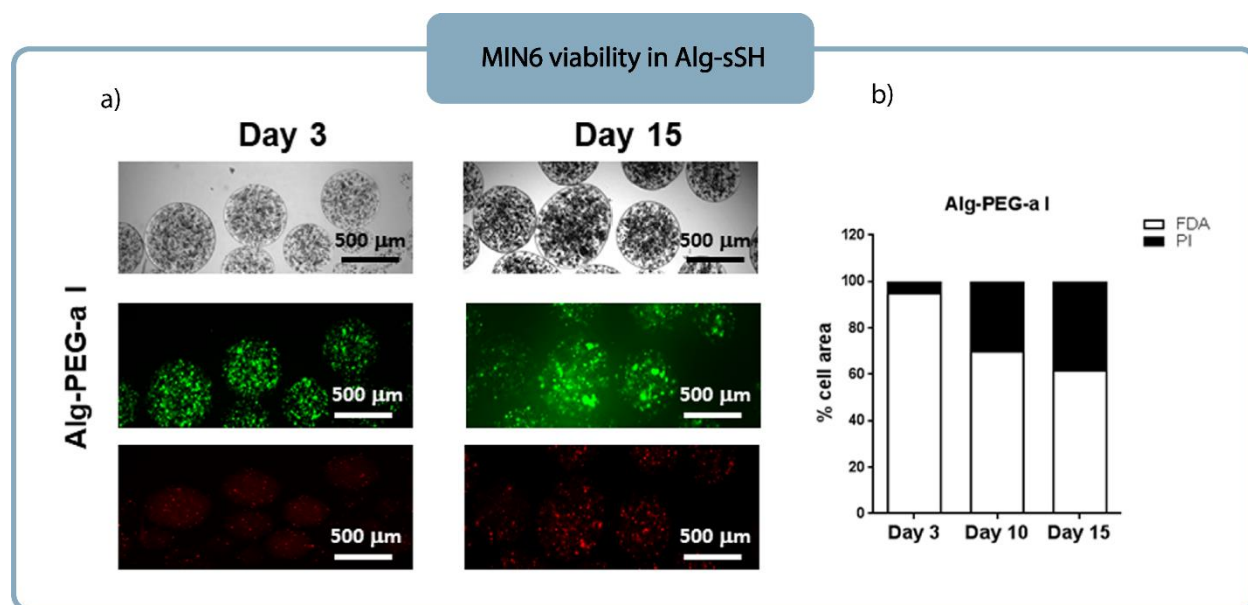
Figure 3.5. a) Microscopy images of MIN6 cells encapsulated in Alg-sSH at day 3 and day 15. Top: light microscopy images, middle: staining of live cells with FDA (green), bottom: staining of dead cells with PI (red). b) Quantification of viable and non-viable encapsulated MIN6 cells by FDA/PI staining at day 3, 10 and 10 expressed as % of the total cell area (n=6). "Reprinted (adapted) with permission from Synthesis Strategies to Extend the Variety of Alginate-based Hybrid Hydrogels for Cell Microencapsulation. Biomacromolecules. Copyright 2017 American Chemical Society."

Cell compatibility of Alg-sSH MS was assessed by encapsulation of MIN6 as a model for insulin producing cells (Figure 3.5). Encapsulation was performed using air-flow droplet generator, by homogeneously mixing MIN6 cells with the polymer solution and subsequently extruding it into a CaCl$_2$ containing gelation bath. MS with an average diameter of 500−600 µm were obtained, with homogeneous cell distribution within the MS core. Viability of the encapsulated cells was assessed at day 3, 10 and 15, by staining of live cells with fluorescein diacetate (FDA) and dead cells with propidium iodide (PI), as previously established.[266] Viability over time was slightly

decreasing, but it remained above 70% for all three time points. In fact, initial viability drop is a common phenomenon experienced in cell encapsulation, as these living entities need to adapt to their new environment. The relatively high cell viability suggests that functionalization of alg with thiolated PEG did not damage the cell compatibility of the alg hydrogel. Besides, the additional disulfide bridges efficiently stabilized the MS network, as presented by the intact integrity of beads *in vitro*. This was further confirmed by *in vivo* transplantation of empty MS in the peritoneal cavity of immune-competent mice. Macroscopic inspection 30 days after transplantation revealed the presence of free-floating MS in the peritoneal cavity with no sign of inflammation or PFO (Figure 3.6.a). Functionality of the cells was evaluated 3 days after encapsulation, by glucose stimulated insulin release assay. Basal insulin secretion at a glucose level of 2.8 mM was set at 1, and an almost 3-fold increase was experienced for the cells encapsulated in Alg-sSH MS, very similar to free cells (Figure 3.6.b). Therefore, encapsulation of MIN6 cells within the alg-based hydrogel did not affect their functionality.
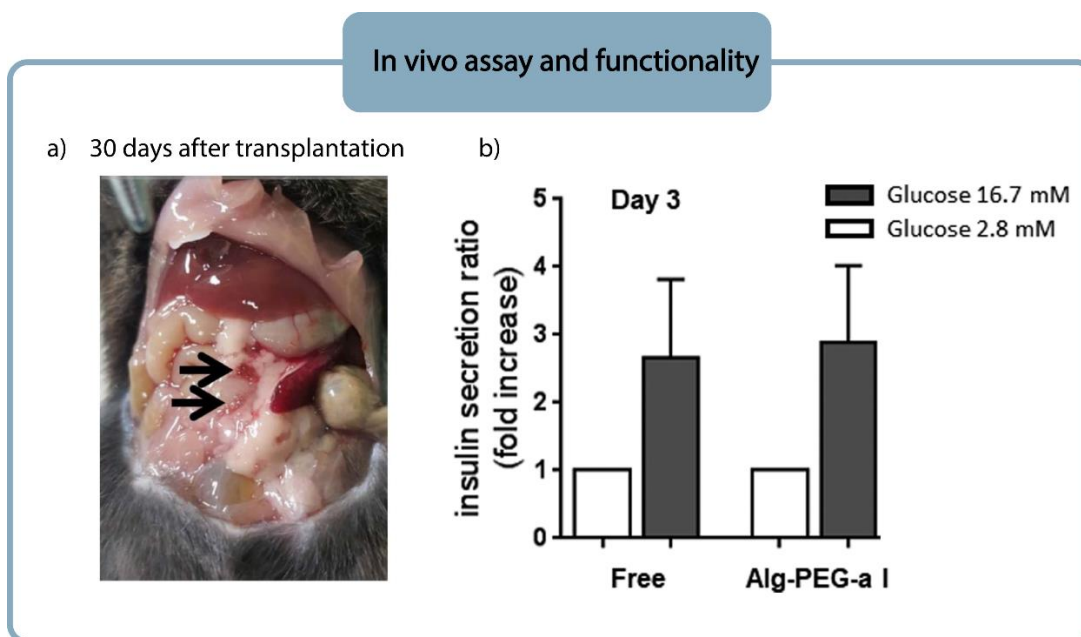
Figure 3.6. a) Macroscopic inspection after 30 days of intraperitoneal transplantation. The arrows indicate some of the MS. b) Glucose stimulated insulin secretion of free and Alg-sSH encapsulated MIN6 cells at day 3. "Reprinted (adapted) with permission from Synthesis Strategies to Extend the Variety of Alginate-based Hybrid Hydrogels for Cell Microencapsulation. Biomacromolecules. Copyright 2017 American Chemical Society."

Taken together, these data show the possibility to produce hybrid hydrogel MS using a one-component approach taking advantage of both carboxylic groups and thiol functionalities to form an interpenetrated network of ionic and covalent interactions. In the next section, variation of the nature of the covalent cross-linking reaction will be presented.

3.2.   Dual ionic and covalent cross-linking

This section is based on the manuscript entitled: "Cross-reactive Alginate Derivatives for the Production of Dual Ionic–Covalent Hydrogel Microspheres Presenting Tunable Properties for Cell Microencapsulation", *ACS Appl. Polym. Mater.* **2019**, *1*, 1326–1333.

Following the promising results obtained with Alg-sSH MS for the encapsulation of endocrine cells, other types of chemical cross-linkages were envisaged to modulate the physical properties and chemical stability of the resulting MS. Disulfide bond is often used in biochemical and biomedical fields, as it is easily achieved by oxidation of thiol groups. Unfortunately, oxidation can happen spontaneously when exposed to air, therefore, unwanted disulfide bridge formation might happen prior to formation of MS. Moreover, owing to the higher strength of thiol-carbon bond compared to thiol-thiol linkages, we envisaged to introduce covalent cross-linking based on sulfur and carbon electrophiles that can spontaneously undergo Michael addition reaction. The two complementary covalent cross-links investigated were the thiol-acrylate and thiol-maleimide systems (Figure 3.7).

3.2.1.   Preparation of Alg-PEG derivatives with cross-reactive functionalities

For the synthesis of the PEGylated alg polymers with cross-reactive functionalities, the same synthetic strategy was followed as previously described in section 3.1. Briefly, Na-alg was converted into TBA-alg for better solubility in DMSO. The hydroxyl groups of TBA-alg were activated with CDI, and functionalized with the corresponding heterobifunctional PEG derivatives PEG-ACR and PEG-MAL. The obtained structures are presented in Figure 3.7.
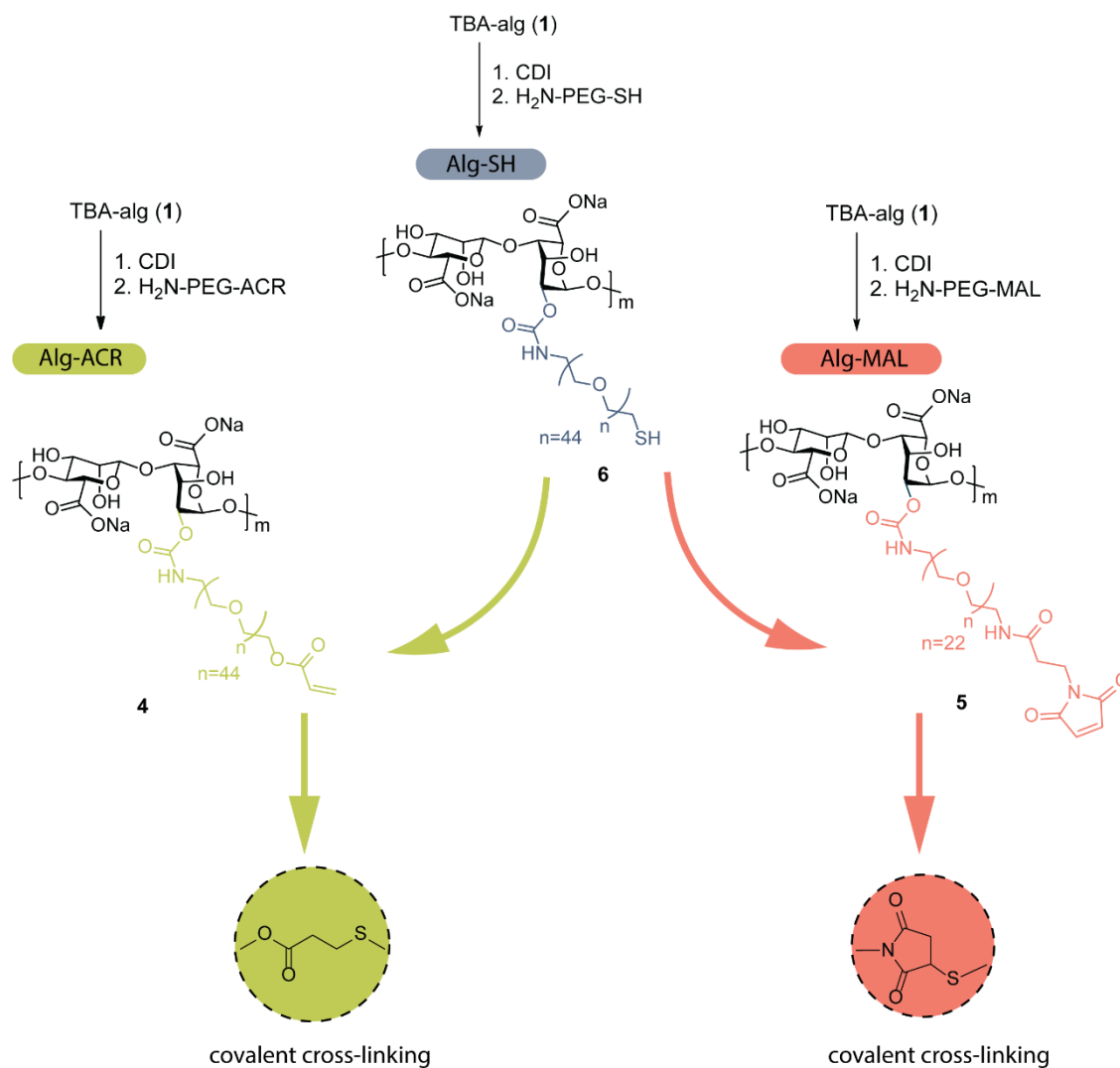
Figure 3.7. Formation of cross-functional hydrogels by mixing Alg-ACR or Alg-MAL with Alg-SH, resulting in the formation of two different types covalent cross-linking.

Since the viscosity range of the polymer solution is a crucial parameter in encapsulation techniques, we aimed at further optimizing the reaction conditions in order to obtain batches with adjustable values. To obtain higher viscosity, the degradation must be minimized. The activation of the hydroxyl groups with CDI generates a basic imidazole molecule, which could potentially lead to partial polysaccharide backbone degradation. We hypothesized that neutralization with the addition of 1 equiv. of acetic acid prior to CDI addition could decrease the chain degradation. Results of the experiments performed without or with the addition of acetic acid are presented in Table 3.8. Independently from the type of PEG grafted on the alg hydroxyl groups, neutralization of the imidazole by-product resulted in a fold-increase of the viscosity.

Table 3.8. Results of performing the grafting reaction with or without the addition of acetic acid, in terms of final viscosity value of the aqueous polymer solutions. Average grafting degree determined by ¹H-NMR.

Product	Viscosity without AcOH addition[a]	Viscosity with AcOH addition[a]	Grafting degree
Alg-ACR	57 mPa·s	654 mPa·s	29 %
Alg-MAL	201 mPa·s	749 mPa·s	26 %
Alg-SH	72 mPa·s	554 mPa·s	28 %

[a] The viscosity values correspond to 3 wt% aqueous solutions

The amount of grafted PEG on the alg backbone was optimized at a degree (25-30 %) that allowed the formation of spherical hydrogel beads, while also providing enough covalent cross-links to reinforce the hydrogel structure. The chemical structure and also the grafting degree of the PEGylated alg was confirmed by NMR spectroscopy. Figure 3.8 presents the section of the NMR spectra with the characteristic signals of the PEG end-functionalities: 6.47 (dd), 6.24 (dd), 6.02 (dd) ppm for the olefinic protons of acrylate functionality, 6.88 (s) ppm for the olefinic protons of maleimide functional group, 3.23 (t) ppm for the CH_2-SH.
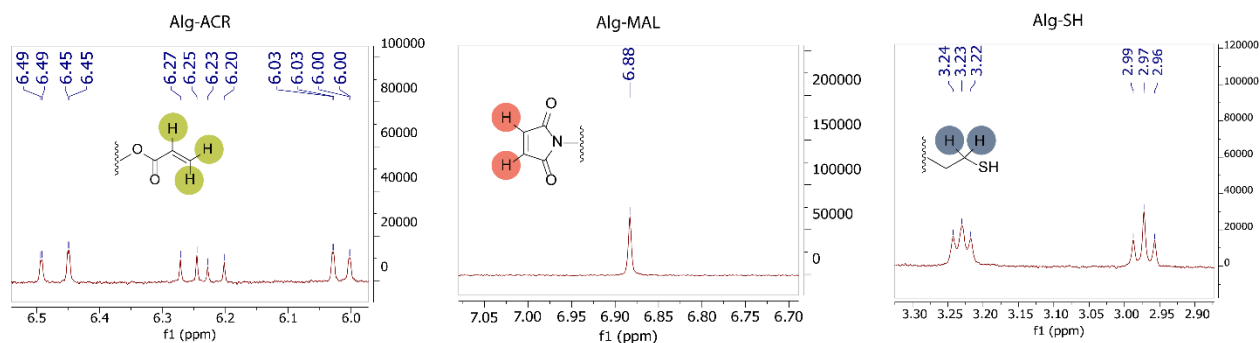
Figure 3.8. Characteristic NMR peaks of the Alg-ACR, Alg-MAL, and Alg-SH polymers.

The grafting degrees were deducted from ¹H-NMR spectra by a deconvolution method. The commonly used technique to determine the degree of grafting is by integration of characteristic peaks belonging to the alg and PEG polymers, and comparing their ratios. However, this method is not possible if there are signals overlapping in the spectra, which was the case for all Alg-PEG derivatives. Therefore, deconvolution by superimposition of the recorded spectra with a simulated spectra was used to assess the grafting degrees (Figure 3.9).
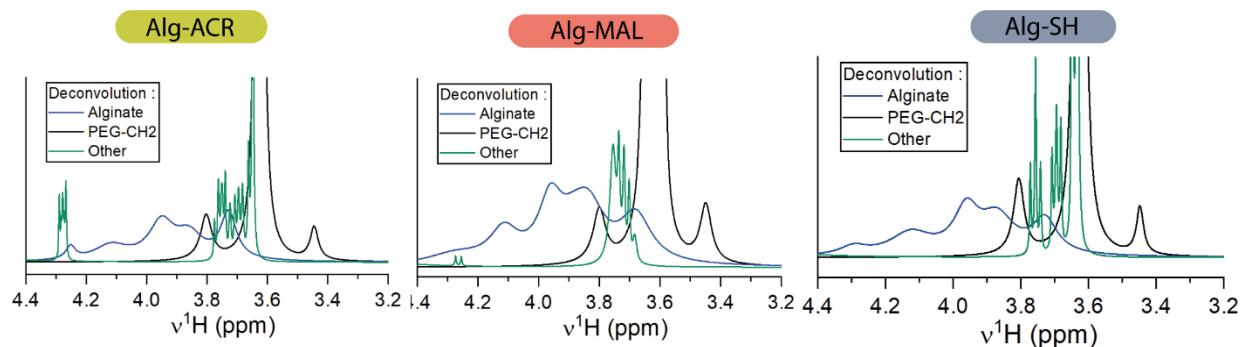
Figure 3.9. Deconvolution spectra of Alg-PEG derivatives. Deconvolution spectra decomposed in regions interpreted as part of alg signal contribution (blue), aliphatic PEG peak including ^{13}C satellites (black), and other functional groups belonging to the different components (green) that have been subtracted from the alg contribution.

To confirm the presence of covalent cross-linking between the PEG unit and the alg backbone, diffusion ordered spectroscopy (DOSY) was carried out. DOSY is the technique of choice for separation between NMR signals belonging to different species. A pair of gradient pulses are applied, and the relaxation time is analyzed to obtain diffusion coefficients. Since the diffusion coefficient is dependent on the radius of the molecule, different sizes of molecules will be separated. The presence of only one molecule in the DOSY spectra was a direct indication of the presence of covalent PEG conjugation. Figure 3.10 shows a superimposed DOSY spectra of Alg-ACR and PEG-ACR; the difference in the size of the two molecules is represented by the difference of the diffusion coefficients.
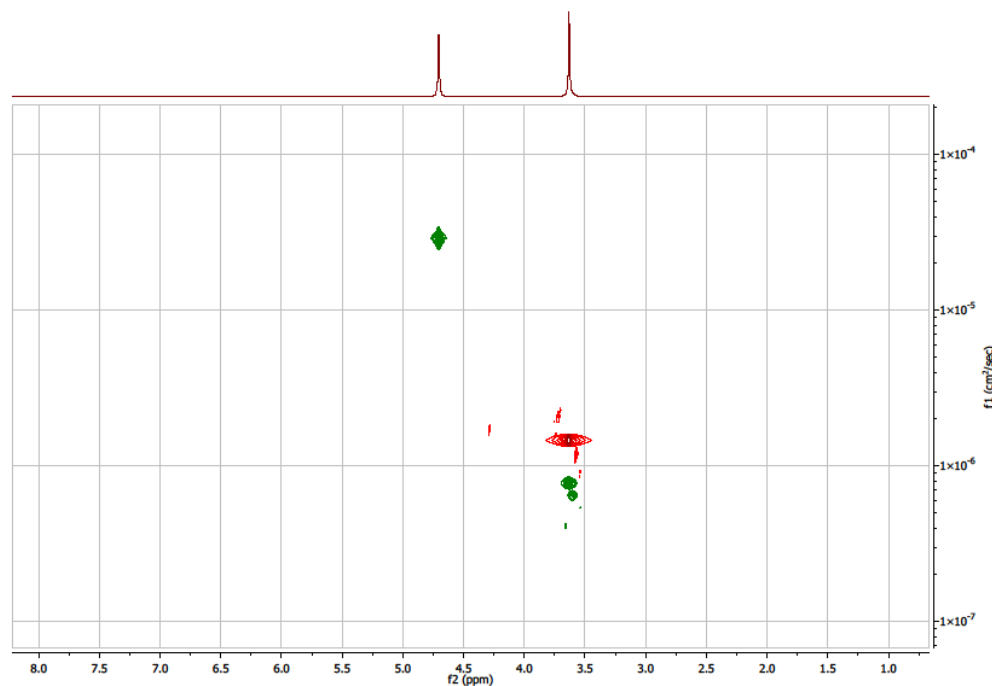
Figure 3.10. DOSY spectra of Alg-ACR (green) and un-grafted PEG ACR (red).

To sum up, our functionalization method allows for a straightforward, robust way of covalently grafting PEG on the alg hydroxyl group. The degree of grafted PEG, and the final viscosity of the polymer in aqueous solution are both adjustable, which allows for fine-tuning for the intended applications and encapsulation methods.

3.2.2. MS formation and subsequent characterization

While previous protocol was based on a one-component Alg-sSH polymer solution, dual ionic-covalent MS were prepared by mixing Alg-ACR or Alg-MAL with Alg- SH (Alg-ACR:Alg-SH 1:1, or Alg-MAL:Alg-SH 1:1). All polymers were dissolved at 3 wt% in aq. MOPS solution (10 mM, pH=7.4, with 0.4 % NaCl), and extruded into a $CaCl_2$ gelation bath (100 mM), keeping the coaxial air-flow at a constant rate. As a comparison, only ionic Ca-alg MS were prepared at the same time, under the same conditions. Figure 3.11 illustrates microscopic images of Ca-alg MS and beads prepared with the combination of Alg-SH:Alg-ACR or Alg-SH:Alg-MAL.
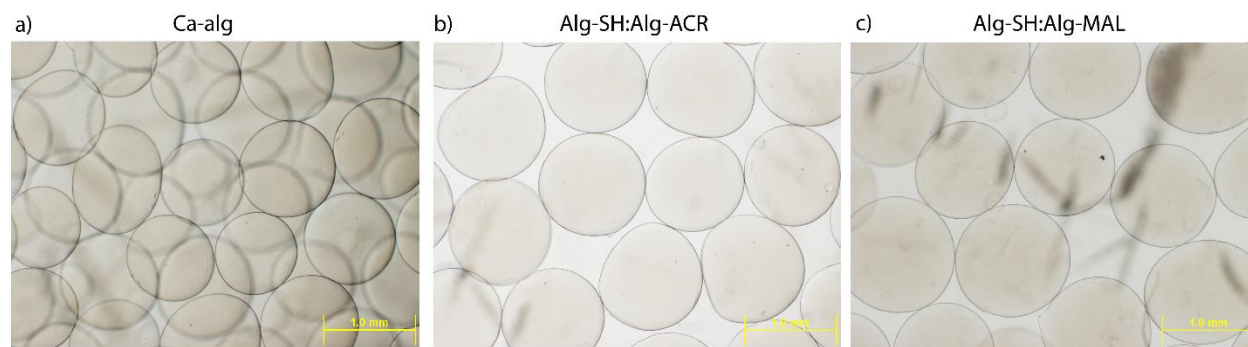
Figure 3.11. Microscopic images of MS prepared from a) Na-alg b) Alg-SH and Alg-ACR c) Alg-SH and Alg-MAL. The scale bar corresponds to 1.0 mm.

After preparation, MS were characterized at certain time points over one week for their diameter and mechanical properties, to assess the evolution of chemical cross-linking. Both the mechanical resistance of the MS and their capacity for shape recovery upon multiple successive compressions were evaluated with a texture analyzer. The resistance value corresponds to the force needed to compress the MS to 90% of their initial diameter. The application of ten repeated compressions to 90% of the initial MS diameter established the elasticity profile of the so-formed dual ionic-covalent MS. Results of the diameter and resistance changes over the course of one week are depicted in Table 3.9.

Table 3.9. Diameter and resistance to compression at 90% of initial MS diameter. For the diameter 30 MS were measured, for the resistance 10 MS were analyzed.

Day	Properties	Ca-alg	Alg-SH:Alg-ACR	Alg-SH:Alg-MAL
0	Diameter (μm)	1006 ± 114	1158 ± 125	1174 ± 149
	Resistance (N/mm³)	1.51 ± 0.36	1.29 ± 0.10	1.40 ± 0.23
3	Diameter (μm)	968 ± 59	1130 ± 71	1080 ± 115
	Resistance (N/mm³)	2.00 ± 0.56	1.60 ± 0.11	1.91 ± 0.25
7	Diameter (μm)	976 ± 69	1068 ± 89	1050 ± 125
	Resistance (N/mm³)	1.55 ± 0.40	1.74 ± 0.15	2.68 ± 0.12

The diameter of the two cross-linked systems showed a clear tendency to decrease over time, while the mechanical resistance was gradually increasing. Ca-alg MS exhibited an initial size decrease and resistance increase within the first days. However, the diameter was stabilized after 3 days, and the resistance value did not change over one week (1.51 N/mm³ at day 0, and 1.55 N/mm³ at day 7). The significant increase in the resistance of cross-linked systems from day 0 to day 7 (from 1.29 N/mm³ to 1.74 N/mm³ and from 1.40 N/mm³ to 2.68 N/mm³ for the acrylate-thiol and maleimide-thiol, respectively) is an indication for the slowly occurring covalent cross-linking over

time, and the result of the increasing network density. The rising amount of sulfur-carbon bonds and the evolution of the network density is reflected on the size decrease, as well. Assessment of the size and resistance was similarly performed 2 weeks after preparation, but no significant difference was experienced, indicating the completion of the covalent cross-links within the hydrogel network over 7 days.
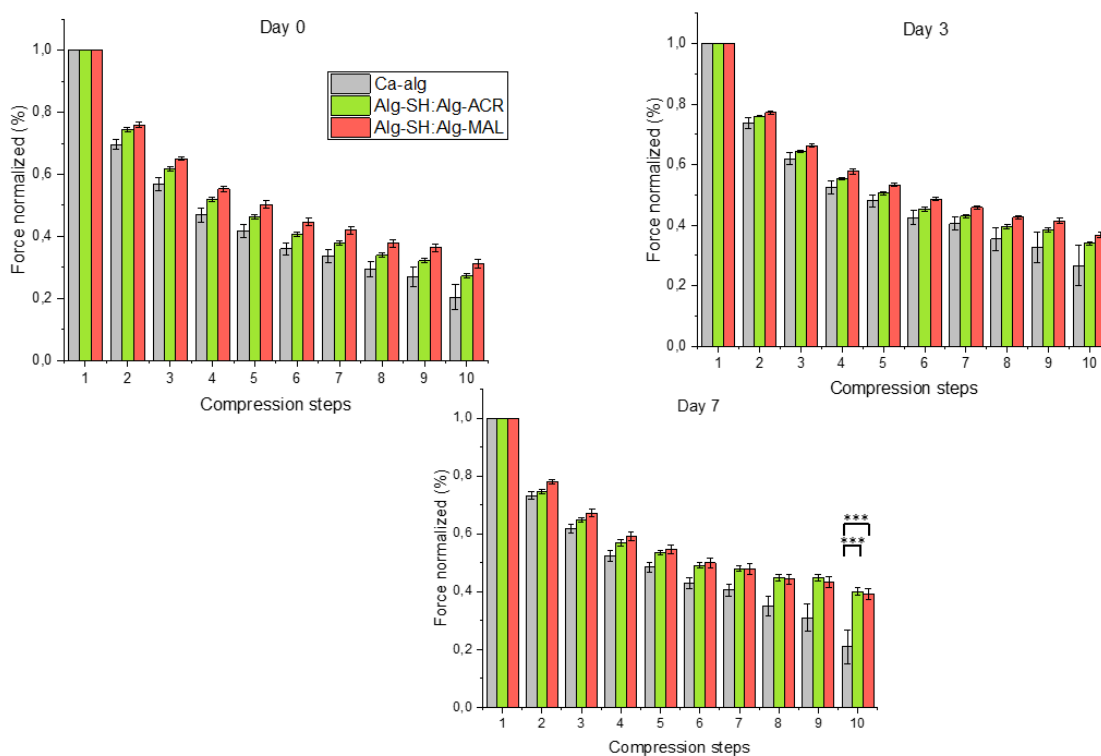
Figure 3.12. Shape recovery performance after 10 successive compressions to 90% of the initial diameter of Ca-alg, Alg-SH:Alg-ACR and Alg-SH:Alg-MAL MS, prepared from 3 wt% aqueous solutions. Measurements were done at day 0, 3 and 7, on 10 MS per condition. *** p < 0.001.

Hydrogels prepared purely by ionic gelation of Na-alg are known to display poor shape recovery performance.[156] Similarly, after 10 successive compressions, Ca-alg MS showed approximatively 20% shape recovery and this performance did not evolve over 7 days (Figure 3.12). Meanwhile, dual ionic-covalent MS exhibited an improved elasticity profile from the moment of preparation, and showed further enhancement over time, reaching 40% for both compositions 7 days after MS production. The measurement was repeated after 2 weeks of storage in MOPS media, but the results showed no more improvement, suggesting that formation of the covalent cross-links was completed within one week.

The type of covalent cross-link had a clear effect on the mechanical resistance of the beads, being significantly higher in the case of Michael addition of thiol to maleimide, compared to the addition

of thiol to acrylate. However, no substantial difference was observed for the shape recovery performance. The above mentioned observations were in correlation with our previous hypothesis, that ionic cross-linking happens very fast in the initial phase of MS formation, while covalent cross-links of the PEG end functionalities form more slowly, over the period of one week. However, these cross-links make the hydrogel network considerably more elastic and resistant to compression.

To further investigate the stability of MS, exposure to increasing concentration of Na-citrate was performed. MS were recovered by filtration 7 days after storage in the gelation bath and immersed in Na-citrate solutions of the indicated concentration. The microscopic images of MS after 24 h in the Na-citrate solutions are shown in Figure 3.13.
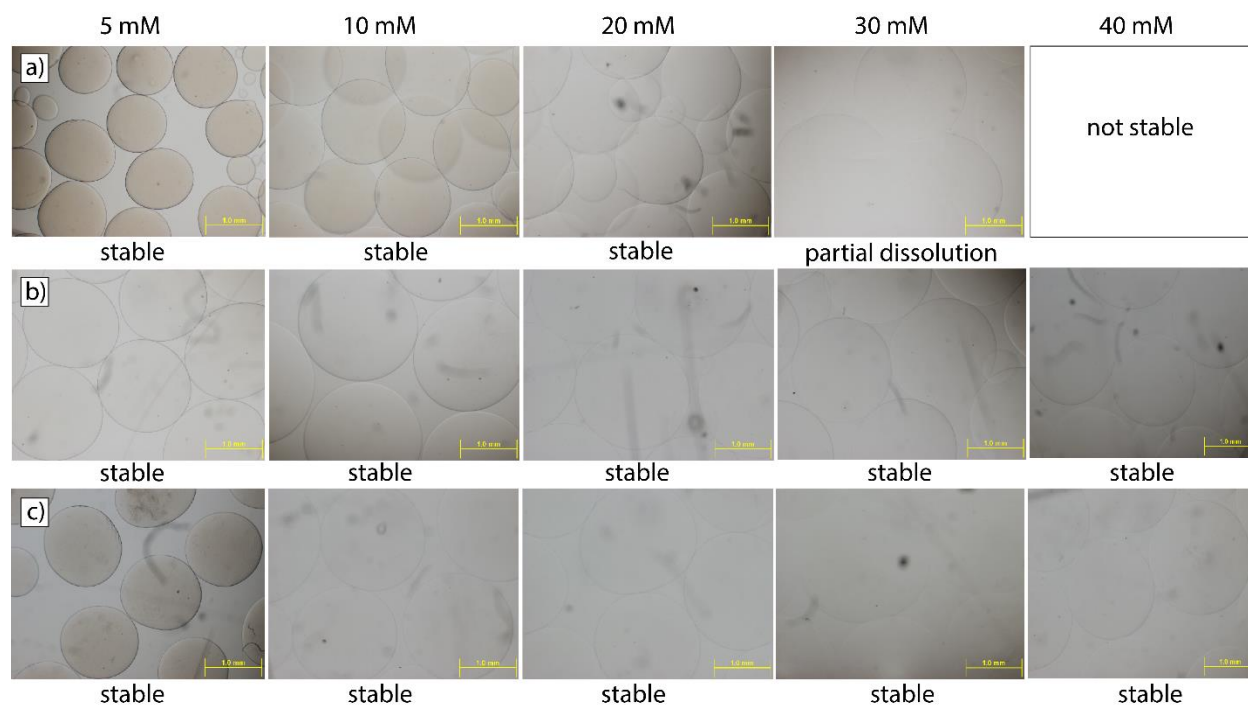
Figure 3.13. Stability of MS in increasing concentration of Na-citrate solution. a) Na-alg b) Alg-SH:Alg-ACR c) Alg-SH:Alg-MAL. The scale bar corresponds to 1.0 mm. After storage in the gelation bath for 7 days, MS were recovered by filtration (70 µm) and immersed in aqueous solution of sodium citrate at the indicated concentrations for 24 h. Stability was evaluated by observation of the MS under an Olympus AX70 microscope.

Merely ionic Ca-alg MS were expected to dissolve in Na-citrate solution above a certain concentration. Exchange of Ca^{2+} ions to non-gelling Na^+ ions damages the ionic hydrogel network and leads to the complete liquefaction of the MS. Dual cross-linked hydrogel systems, however, possess the advantage of additional covalent interactions that are not affected by the presence of non-gelling ions. The integrity of Ca-alg MS started to be visibly affected above 20 mM concentrations of Na-citrate, and there were no more beads present in 40 mM Na-citrate solution.

Cross-linked MS remained stable up to 40 mM Na-citrate solutions, the liquefaction of the Ca-alg ionic interactions did not affect the integrity of MS. Interestingly, as presented in Figure 3.14, MS prepared from Alg-SH:Alg-ACR did not show any swelling, and their diameter remained very similar. On the contrary, MS with Alg-SH:Alg-MAL interactions presented substantial increase in diameter. This, however, did not affect their stability. The different swelling behavior might be attributed to the different chemical composition of the MS, as well as the different molecular weight of the PEG grafted on the alg (PEG-ACR contains 2kDa PEG, while and PEG-MAL contains 1kDa PEG). MS prepared from both cross-linked systems remained spherical at concentrations of the current study, highlighting the stability enhancement by the introduction of covalent cross-linkings.
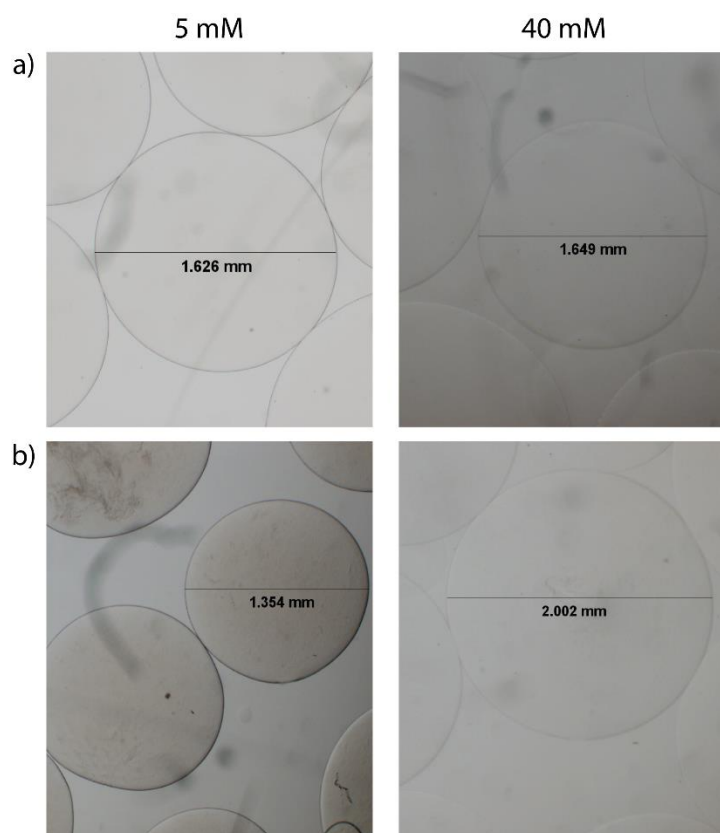
Figure 3.14. Diameter of MS in 5 and 40 mM Na-citrate solutions. a) Alg-SH:Alg-ACR c) Alg-SH:Alg-MAL MS.

For the viability of encapsulated cells, access to oxygen and nutrients is vital, which is only achievable if the permeability of the encapsulation membrane allows the diffusion of small molecules. Meanwhile, to avoid cell death by attack of immunoglobulins and T-cells, the biomaterial's permeability must exclude these larger size molecules. The permeability profile of Alg-SH:Alg-ACR and Alg-SH:Alg-MAL systems was compared to that of Ca-alg MS, by measuring the ratio of FITC-dextran solutions infiltrating within the MS core. MS were incubated with FITC-

dextran solutions (in MOPS) of 40, 150, 250 and 500 kDa size, and the ratio of passage was assessed by imaging with confocal microscopy and subsequent image analysis with ImageJ (examples of confocal images are given in Annexes, Figure 6.2). The presence of covalent cross-links did not have a negative impact on the permeability of MS, as shown by the very similar permeation values. Due to the difference in chemical composition, Alg-SH:Alg-MAL cross-linked MS exhibited slightly higher infiltration ratios than Alg-SH:Alg-ACR MS, which could be beneficial for oxygen and nutrients availability. However, the relatively high infiltration ratio of dextran molecules above 250 kDa could mean that antibodies can diffuse through the membrane and compromise the immune protection of cells. As the permeability of a molecule does not only depend on its size, but also on its configuration and the charges present, a better model could lead to more relevant result. Measuring the infiltration of fluorescently labeled antibodies could be a feasible alternative.
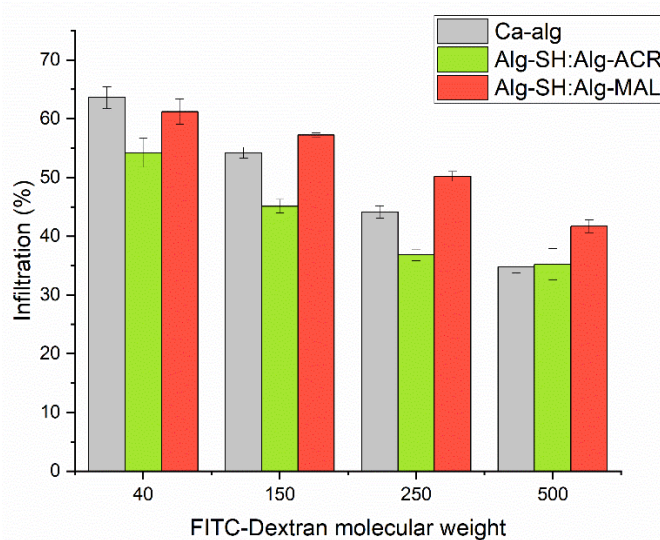
Figure 3.15. Relative permeability of FITC–dextrans within Ca-alg, Alg-SH:Alg-ACR and Alg-SH:Alg-MAL MS as a function of FITC–dextrans molecular weight after 36 h of incubation under gentle stirring. Error bars represent the standard deviation from n = 3 measurements. Quantification was performed using ImageJ.

3.2.3.   Dual ionic-covalent MS in cell microencapsulation

In view of the favorable physical properties and chemical stability demonstrated by Alg-SH:Alg-ACR and Alg-SH:Alg-MAL MS, these systems were assessed for the encapsulation of endocrine

cells. Huh7 were chosen as model cells, and were encapsulated using a coaxial air-flow droplet generator by extrusion in $CaCl_2$ containing gelation bath. The cells were homogeneously distributed within the hydrogel MS, and no cells were detected outside of the microcapsules (Figure 3.16.a). The viability of the cells was determined with FDA/PI staining at day 1, day 4 and day 7 after encapsulation. At each time point, the viability was higher than 90%, with very minimal cell death observed (Figure 3.16.b). Hence, we concluded that the covalent cross-linking of acrylate-thiol and maleimide-thiol did not interfere with cell viability.
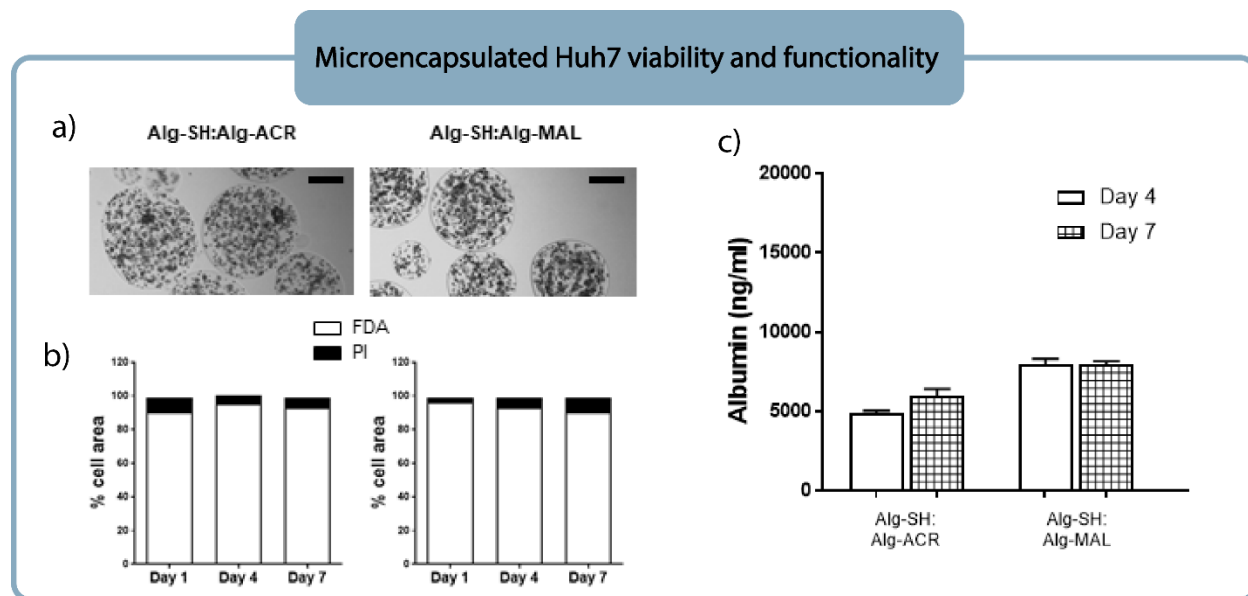
Figure 3.16. a) Huh7 cells encapsulated in Alg-SH:Alg-ACR and Alg-SH:Alg-MAL. b) Cell viability at day 1, day 4 and day 7 after encapsulation. c) Albumin secretion at day 4 and day 7. "Reprinted with permission from Cross-Reactive Alginate Derivatives or the Production of Dual Ionic-Covalent Hydrogel Microspheres Presenting Tunable Properties for Cell Microencapsulation. ACS Appl. Polym. Mater. Copyright 2019 American Chemical Society."

Since Huh7 cells are albumin secreting cells, the functionality of the encapsulated cells was determined by quantification of the amount of albumin secreted in the culture medium. High functionality was preserved for both polymer combinations at day 4 and day 7 after encapsulation (Figure 3.16.c). The secreted amount of albumin was moderately higher for cells encapsulated in Alg-SH:Alg-MAL which might be due to the higher diffusion efficiency of this composition, compared to the Alg-SH:Alg-ACR. These results indicated that dual ionic-covalent MS based on ionic interactions with Ca^{2+} ions and carbon-sulfur covalent bonds were suitable to maintain the viability and functionality of human endocrine cells. Further investigation addressed the biocompatibility of these encapsulation materials in a rodent model.
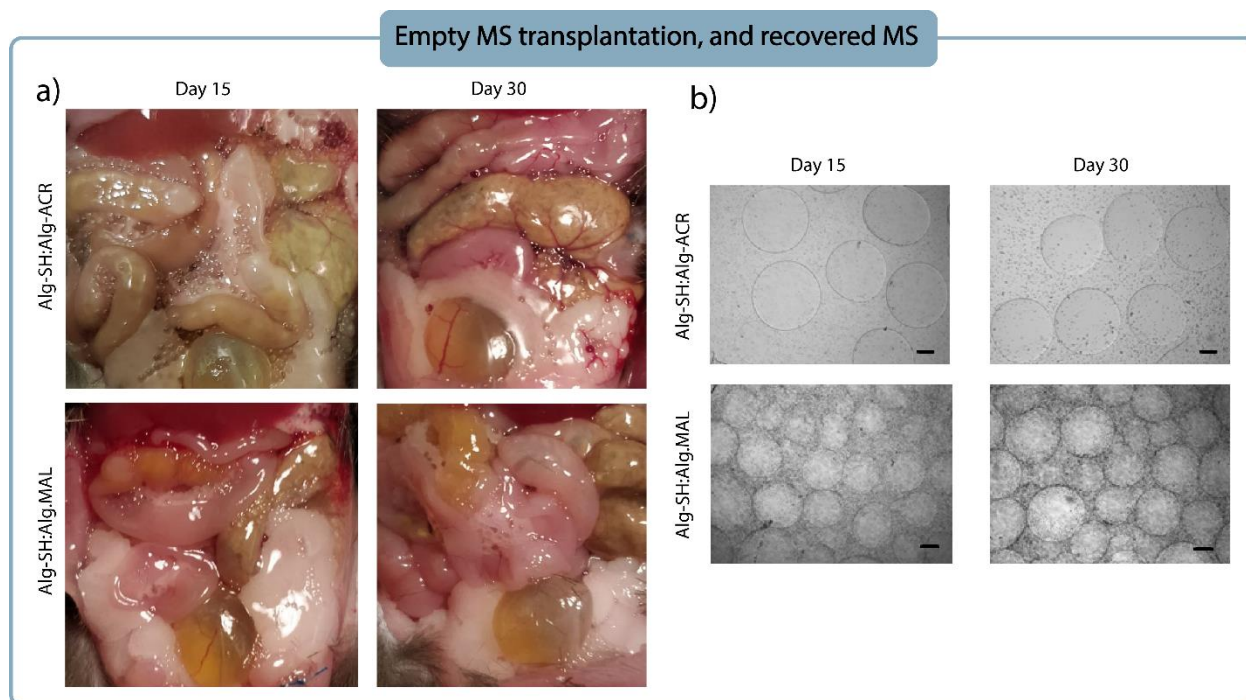
Figure 3.17. a) Macroscopic inspection of empty MS at 15 and 30 days after intraperitoneal transplantation. b) Microscopic images of recovered MS after 15 and 30 days of transplantation from the peritoneum. Scale bar: 200 µm. "Reprinted with permission from Cross-Reactive Alginate Derivatives or the Production of Dual Ionic-Covalent Hydrogel Microspheres Presenting Tunable Properties for Cell Microencapsulation. ACS Appl. Polym. Mater. Copyright 2019 American Chemical Society."

Transplantation of empty MS in the peritoneal cavity of immune-competent C57 BL/6 mice was performed. Mice were euthanized at two time points: day 15 and day 30 post transplantation. Both polymeric compositions (Alg-SH:Alg-ACR and Alg-SH:Alg-MAL) resulted in stable MS, as observed in the intraperitoneal cavity of mice after sacrifice (Figure 3.17.a). A representative amount of MS was investigated under light microscopy upon retrieval (Figure 3.17.b). MS kept their spherical shape and stability up to the 30 days of the experiment, with no sign of inflammation or fibrotic overgrowth around the transplanted microcapsules.

3.2.4.   Dual ionic-covalent MS formed by cross-reactive functionalities of thiol-acrylamide

Since acrylate contains a relatively labile ester bond, even though we did not experience any destabilization of the bond *in vivo*, we decided to also study the potential of using acrylamide instead of acrylate, and this way also broaden the variety of covalent cross-links used for dual cross-linked MS formation.

The feasibility of using acrylamide-thiol cross-coupling for the formation of MS was first studied. Alg-ACA and Alg-SH polymers were dissolved in MOPS solution in 3 wt% (10 mM, pH=7.4, containing 0.4% NaCl) and mixed in a weight ratio of 1:1. The resulted MS are displayed on Figure 3.18. MS displayed spherical geometry, and relatively high diameter, however, this can be reduced by optimization of the encapsulation parameters.
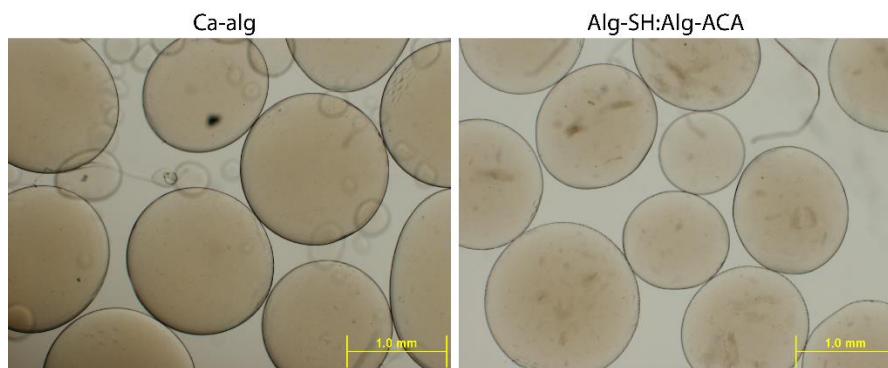
Figure 3.18. Microscopic images of Ca-alg and Alg-SH:Alg-ACA MS. The scale bar corresponds to 1.0 mm.

Next, the diameter changes and mechanical properties of MS were investigated in comparison to Ca-alg MS. (Table 3.10) The same tendency was observed as for the previously presented acrylate-thiol cross-linked MS: gradual decrease of the diameter and increase of mechanical resistance upon evolution of the slowly forming carbon-sulfur bonds. The resistance values for acrylamide-thiol were comparable to that of acrylate-thiol cross-linked MS, reaching 1.90 N/mm^3 and 1.74 N/mm^3 respectively, after 1 week of storage in MOPS buffer.

Table 3.10. Diameter and mechanical properties of Ca-alg and Alg:SH-Alg-ACA MS.

Day	Properties	Ca-alg[c]	Alg-SH:Alg-ACA[c]
1	Diameter (μm)[a]	1347 ± 297	1368 ± 191
	Resistance (N/mm^3)[b]	1.62 ± 0.54	1.31 ± 0.15
4	Diameter (μm) [a]	1363 ± 183	1330 ± 219
	Resistance (N/mm^3) [b]	1.83 ± 0.14	1.61 ± 0.12
7	Diameter (μm) [a]	1390 ± 297	1292 ± 182
	Resistance (N/mm^3) [b]	1.63 ± 0.44	1.90 ± 0.16

[a] Measured on an Olympus AX microscope, on 30 MS/conditions
[b] Measured with a Texture Analyzer, on 10 MS/conditions
[c] Prepared in a 3 wt% aqueous solution

This polymer system was further used in a multicomponent MS formation, which will be presented in Section 3.3.2.

In conclusion, the MS systems based on the dual cross-linking of Alg-SH:Alg-ACR, Alg-SH:Alg-MAL and Alg-SH:Alg-ACA and ionic interactions show superior mechanical properties compared to pure Ca-alg MS. These MS achieved improved mechanical resistance to compression and improved shape recovery performance. In addition, enhanced stability in Na-citrate solution compared to Ca-alg was obtained, without the addition of any chemical cross-linker.

3.3. Strategy to reduce fibrosis

Part of this section is based on the manuscript entitled: "Antifibrotic Effect of Ketoprofen-Grafted Alginate Microcapsules in the Transplantation of Insulin Producing Cells", *Bioconjugate Chem.* **2018**, *29*, 1932–1941.

A major issue that unquestionably needs to be solved in cell transplantation, is the inflammatory responses of the recipient to the transplanted MS. The fibrotic tissue formation around the capsules leads to fatal cell viability decrease and eventually graft failure. Many efforts are focused on reducing the foreign body response and minimize inflammation and fibrosis around the microcapsules. With this goal in mind, in our research group, a new strategy was developed by Dr. François Noverraz (EPFL Thesis N° 8949), for covalently conjugating anti-fibrotic molecules (drugs) on the alg hydrogel backbone. From a variety of drugs that were evaluated, ketoprofen showed excellent anti-inflammatory properties, therefore, was the main choice of further research. The main results obtained following this strategy will be briefly described in the upcoming section (Section 3.3.1).

3.3.1. Achievements with the strategy of covalent conjugation of ketoprofen for controlled release

A common way of including anti-inflammatory drugs within the hydrogel MS is co-encapsulation of the drug with Ca-alg, leading to a burst drug release. The work presented by Dr. F. Noverraz aimed at developing a system that provides a controlled, sustained drug release from the MS at the site of transplantation. In order to avoid burst release and achieve a controlled one, ketoprofen was covalently conjugated to a PEG derivative via an ester or amide functionality (Scheme 3.5). Following conjugation of PEG-KET on the hydroxyl groups of TBA-alg, combination of the resulted Alg-KET biopolymer with Na-alg led to spherical empty or cell-laden MS formation.
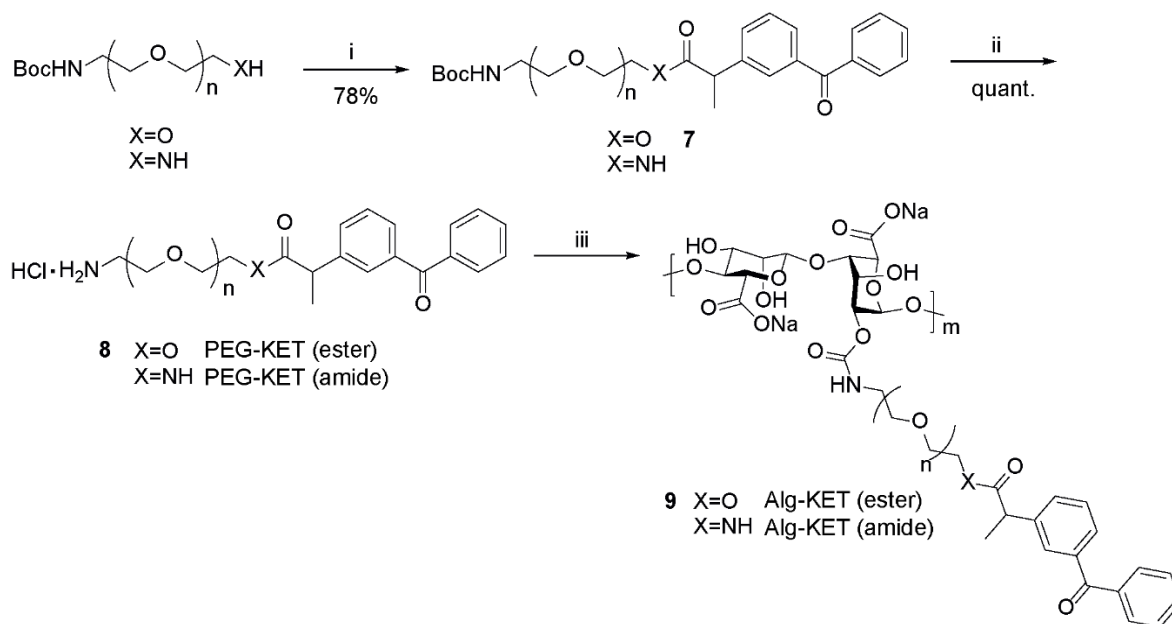
*Scheme 3.5. Ketoprofen conjugation to PEG, followed by grafting on the alg hydroxyl group. The numbering of the compounds refers to the ester derivative. Reagents and conditions for the synthesis of ester-conjugated ketoprofen, Alg-KET(ester) (**9**): i) DCC, DMAP, DCM, rt, 12 h ii) HCl (4N in dioxane), rt, 2 h iii) TBA-alg (**1**), CDI, DMSO, H₂O.*

The rate of the drug release was controlled by the type of covalent linkage, ester conjugated ketoprofen presenting a regular, sustained release up to two weeks via ester hydrolysis. This rate was accelerated in the presence of MIN6 cells, most likely as a result of cell esterase activity. On the contrary, amide conjugated ketoprofen allowed for only traces of ketoprofen being released (Figure 3.19).
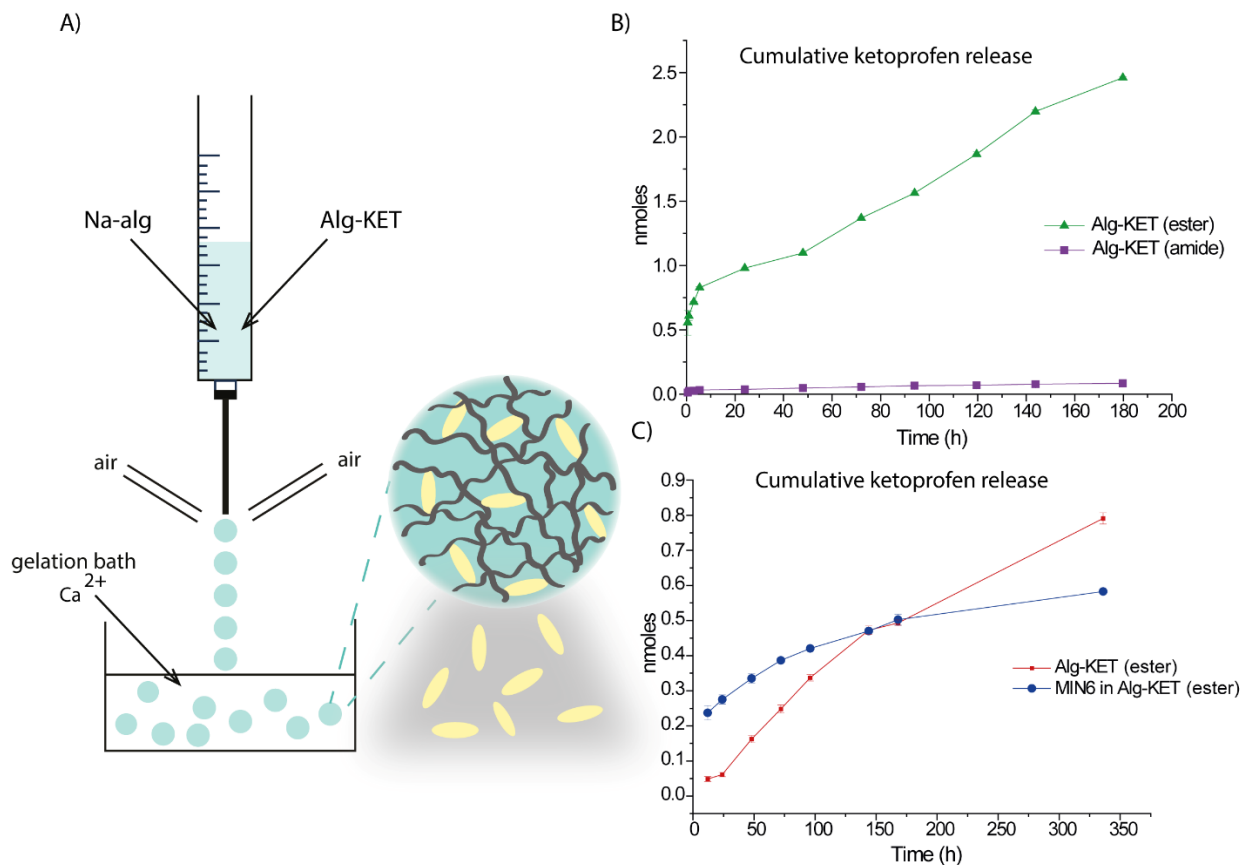
Figure 3.19. Formation of MS with the combination of Na-alg and Alg-KET using coaxial air-flow droplet generator. Cumulative ketoprofen release via ester (upper diagram, green) and amide (upper diagram, purple) bond hydrolysis. Cumulative ketoprofen release from empty (lower diagram, red) and MIN6 cell containing (lower diagram, blue) MS.

Transplantation of empty or MIN6 cell containing MS in immune-competent mice resulted in PFO, more noticeable in the case of cell-laden MS, highlighting the effect of cellular metabolic activity on the severity of fibrotic response. MS prepared from Na-alg, or Alg-KET containing ester or amide covalent bond were transplanted under the kidney capsule of C57BL/6 immune-competent mice to evaluate the anti-fibrotic potential of ketoprofen. As expected, transplantation of MS under the kidney capsule induced some fibrotic reaction, as shown by the amount of collagen deposition. Empty Ca-alg MS showed the lowest amount of collagen deposition, possibly due to the better sphericity and roundness of Ca-alg beads. However, retrieval of MS 4 weeks after transplantation followed by quantification of collagen deposition on the cell-loaded MS by histological analysis revealed the significant beneficial effect of using ester conjugated Alg-KET MS in reducing PFO (Figure 3.20).
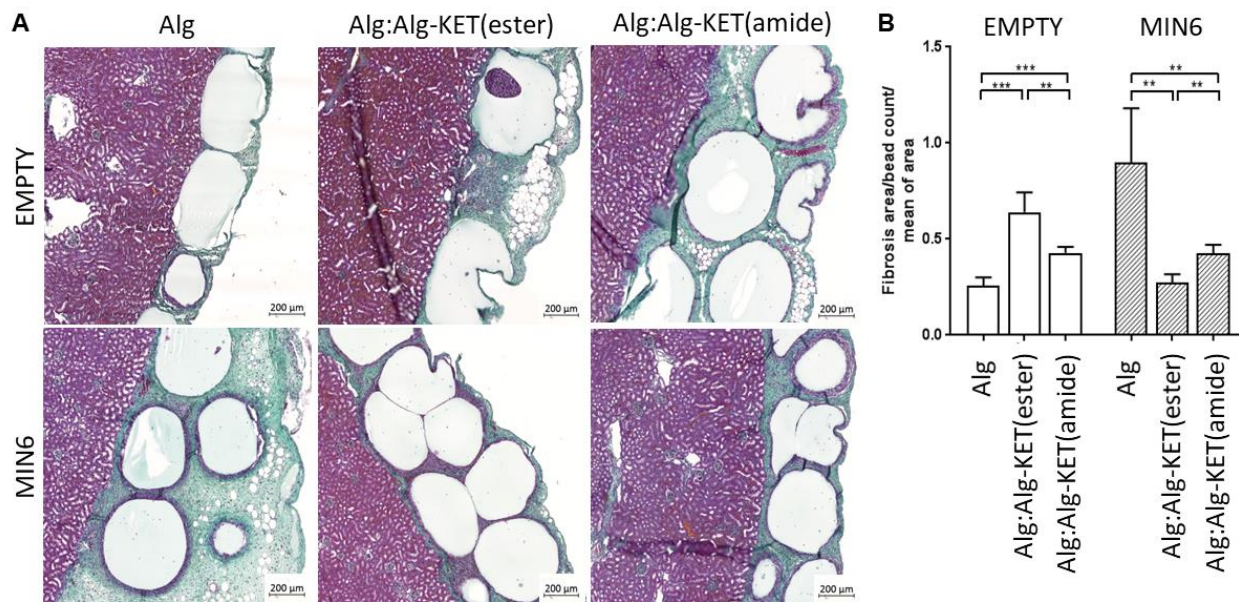
Figure 3.20. Quantification of collagen deposition around empty and MIN6 cell containing MS retrieved 4 weeks after transplantation under the kidney capsule. A) Sections of formalin-fixed and paraffin-embedded kidneys colored with Goldner's Thrichrome with Ca-alg MS (left row), Alg:Alg-KET (ester) (middle row), Alg-KET (amide) (right row); empty MS (upper panels) and MIN6 cell containing MS (lower panel). B) Empty (white bars) and MIN6 containing MS (grey bars). Quantification of collagen deposition was performed with Definiens software. All values are means ± standard deviations of 5 slides per condition. **p < 0.01, ***p < 0.001.

These results obtained with covalent conjugation of ketoprofen within the hydrogel network in reducing PFO confirmed our hypothesis that inclusion of anti-fibrotic compounds was important for *in vivo* applications. The higher drug release via ester bond hydrolysis led to more significant decrease of PFO, therefore, we continued the development of more complex systems involving covalently conjugated anti-fibrotic drugs with this composition.

3.3.2.   Multifunctional hybrid hydrogel MS

To combine the beneficial effects of the MS displaying enhanced mechanical properties and stability (Section 3.2.) with the covalent conjugation and subsequent sustained release of anti-fibrotic drug (Section 3.3.1.), we envisaged to design multifunctional MS, exhibiting both beneficial features. By mixing cross-reactive Alg-PEG derivatives with an Alg-PEG-drug component, we expected the formation of dual ionic-covalent MS, able to release the drug *in vivo* by hydrolysis of the ester linkage to the bioactive molecule under physiological conditions.

X=O   acrylate
X=NH   acrylamide

(drug) = HO

Multifunctional hydrogel
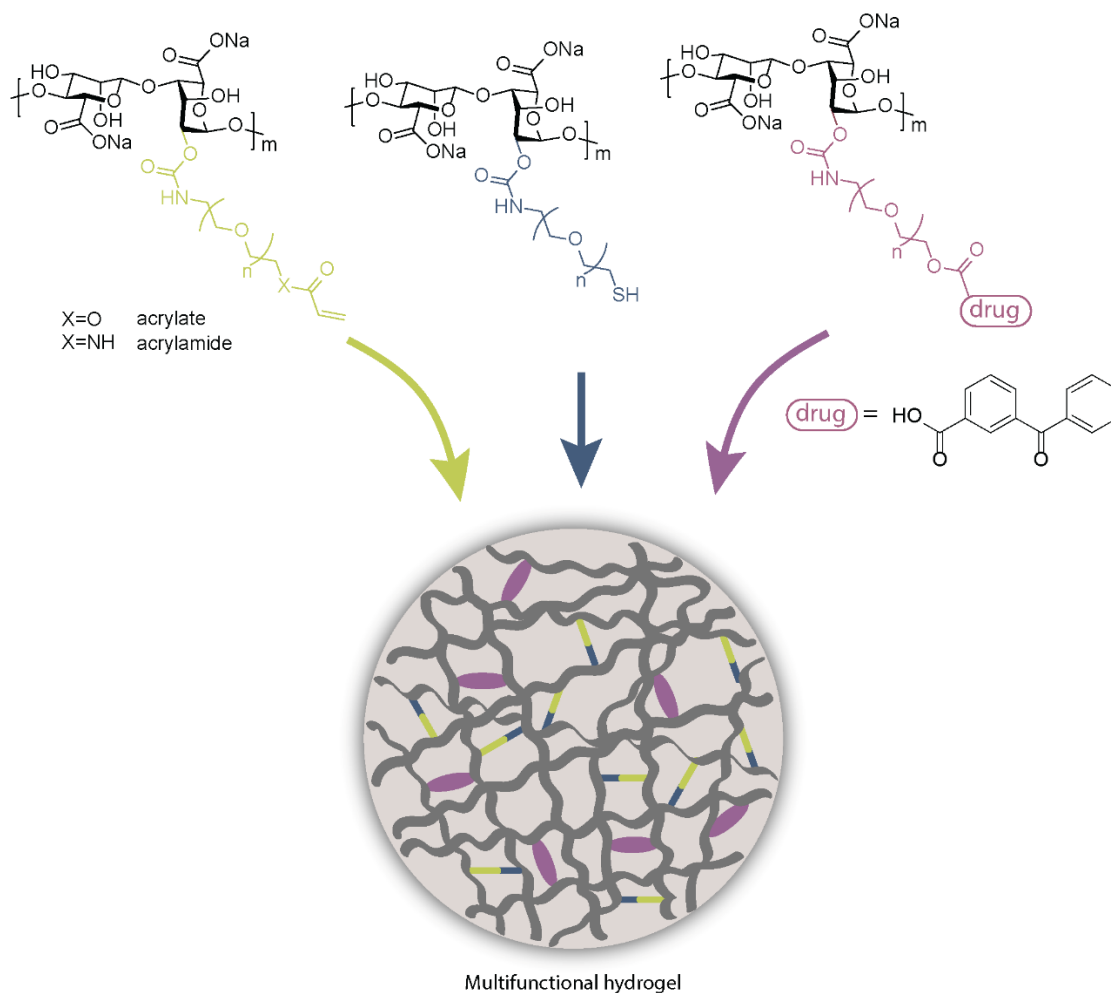
Figure 3.21. Components of multifunctional hydrogel beads.

3.3.2.1. Multicomponent MS formation

Based on the previous results obtained with the controlled release of ketoprofen from Alg:Alg-KET MS, we first investigated multicomponent MS based on the combination of Alg-KET with cross-reactive Alg-PEG derivatives. Most likely due to the high PEG content when mixing 3 PEGylated alg derivatives, formation of spherical MS with optimal diameter and good monodispersity was possible, but extremely challenging to achieve. Consequently, we decided to add unmodified Na-alg to the mixture prior to bead preparation to ease MS formation and achieve better sphericity. The composition of the two different polymer systems is described below. All polymers were mixed in a weight ratio of 1:1:1:1. The resulting MS are showed in Figure 3.22. Each of the PEGylated alg polymers was dissolved at a concentration, which allows for MS formation with the air-flow droplet generator. After mixing, the total concentration of the multicomponent

(ACR) and multicomponent (ACA) MS for the presented example were 2.75 and 3 wt%, respectively.

Multicomponent (ACR):

- Alg-ACR
- Alg- SH
- Alg-KET
- Na-alg

Multicomponent (ACA):

- Alg-ACA
- Alg-SH
- Alg-KET
- Na-alg
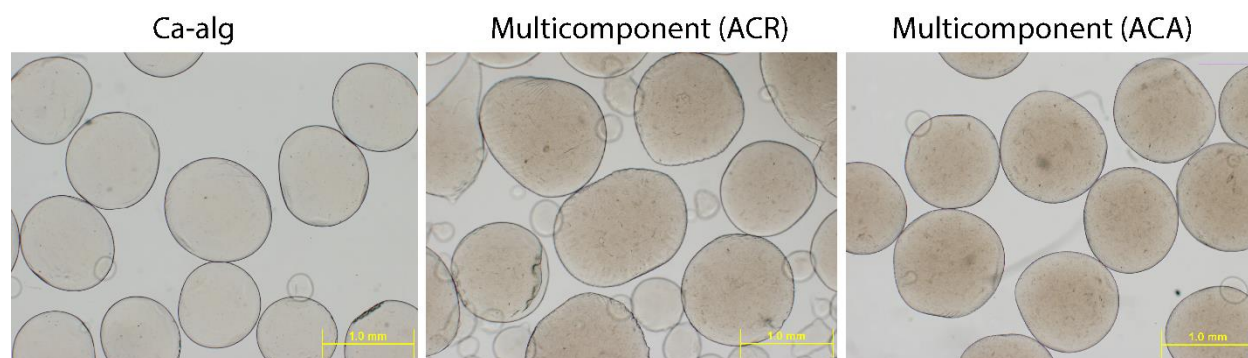
Figure 3.22. Brightfield microscopy images of Ca-alg, multicomponent (ACR) and (ACA) MS. Images were retrieved on the day of MS production (scale bar 1.0 mm).

Assessment of the mechanical properties was performed following the same techniques as previously described for the two-component cross-linked systems. There was a slight size decrease observed over time for all MS compositions (Table 3.11). However, due to the high standard deviation this cannot be concluded with complete certainty. On the other hand, resistance to a single compression up to 90% of the initial diameter clearly evolved over time in both multicomponent MS, reflecting the formation of covalent sulfur-carbon bonds over time. Multicomponent beads prepared with acrylate or acrylamide functionality increased from 0.72 N/mm^3 to almost 3 N/mm^3, and 1.14 N/mm^3 to 2.22 N/mm^3, respectively. Meanwhile, Ca-alg MS remained within the same range over one week.

Table 3.11. Diameter and mechanical properties of Ca-alg and multicomponent MS.

Day	Properties	Ca-alg	Multicomponent (ACR)	Multicomponent (ACA)
0	Diameter (μm)[a]	959 ± 80	1212 ± 133	1111 ± 199
	Resistance (N/mm³)[b]	1.68 ± 0.18	0.72 ± 0.33	1.14 ± 0.18
3	Diameter (μm)[a]	931 ± 115	1039 ± 133	1052 ± 189
	Resistance (N/mm³)[b]	1.45 ± 0.15	1.70 ± 0.29	1.76 ± 0.18
7	Diameter (μm)[a]	923 ± 103	943 ± 129	989 ± 92
	Resistance (N/mm³)[b]	1.70 ± 0.18	2.99 ± 0.27	2.22 ± 0.14

[a] Measured on a Leica DM 5500 microscope, 30 MS per condition
[b] Measured on a texture analyzer, using 10 MS per condition

Shape recovery performance profile was obtained by 10 successive compressions to 90% of the initial MS diameter. Ca-alg beads displayed a relatively stable elasticity profile, with no evolution over time. In contrast, multicomponent MS showed improved elasticity over time, exceeding more than 40% shape recovery by day 7 (Figure 3.23). A follow-up of multicomponent MS at day 11 and day 14 (data not shown) did not reveal any further evolution of the mechanical properties, suggesting that stabilization of the system was completed within one week.
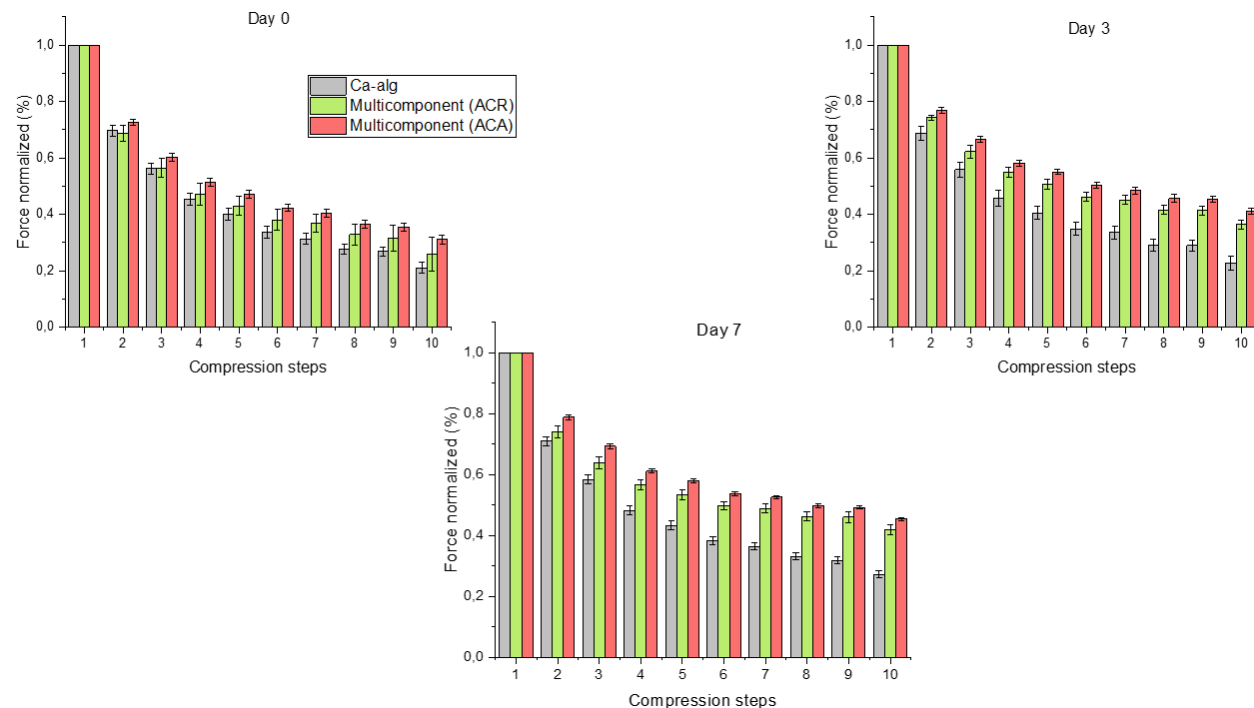
Figure 3.23. Shape recovery performance after 10 successive compressions to 90% of the initial diameter of Ca-alg and multicomponent MS prepared with either acrylate or acrylamide functionalized alg, n=10.

The stability of these multicomponent MS towards non-gelling ions was evaluated in Na-citrate solutions of 5, 10, 20 and 30 mM, and co·red with pure ionically cross-linked Ca-alg MS. Under the conditions of the experiment (MS formed with a total of 2.75 and 3 wt% solutions), Ca-alg MS (2 wt%) were degraded from 10 mM concentration (Figure 3.24). Multicomponent MS were stable up to 20 mM concentration, highlighting again the important contribution of the covalent carbon-sulfur bonds in the stability of the resulting MS against non-gelling ions. Moreover, due to a lower concentration of covalently cross-linked polymers in comparison with the previous dual systems, liquefaction of the MS was observed from 30 mM concentration. The lower stability is well explained by the lower concentration of covalently cross-linking polymers in the mixture. While the 2-component systems presented in Section 3.2 contained two polymers in a ratio of 1:1 to covalently cross-link, these multifunctional MS were composed of four polymers in equal ratios, and only two of them took part in the covalent cross-linking.
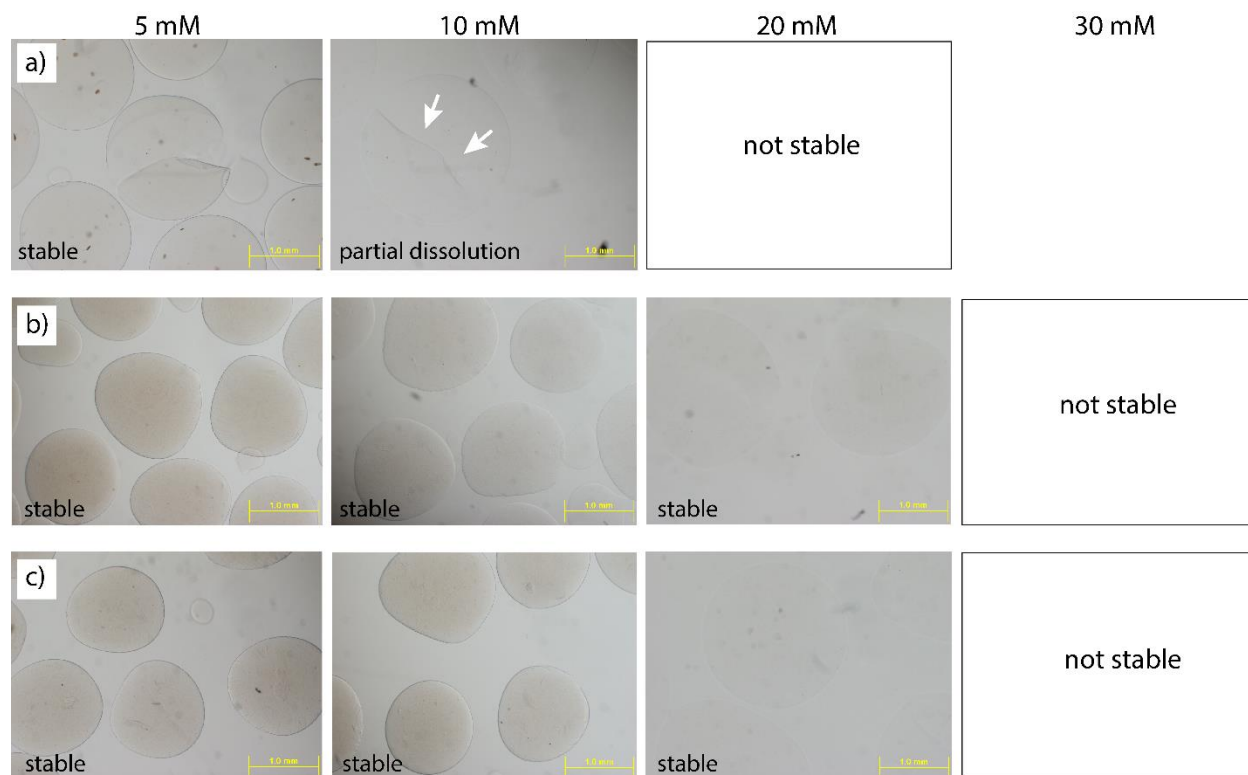
Figure 3.24. Stability of a) Ca-alg b) Multicomponent (ACR) and c) Multicomponent (ACA) MS in increasing concentrations of Na-citrate solutions. The white arrows indicate some of the partially damaged Ca-alg MS in 10 mM Na-citrate solutions. Scale bar: 1.0 mm.

3.3.2.2. Drug elution capacity of multicomponent MS

Further characterization of these drug-eluting MS focused on the quantification of ketoprofen released *in vitro* over 16 days. 1 ML polymer solution was extruded into the gelation bath, and beads were subsequently placed in 3 mL of MOPS medium (10 mM, containing $CaCl_2$) at pH=7.4. Aliquots of 1 mL were taken at the indicated time points over 17 days, and replaced with 1 mL of fresh medium. Quantification of the amount of ketoprofen released was performed by LC-MS analysis. Cumulative release of the drug showed a sustained delivery over more than 2 weeks, without any sign of burst release. Both acrylate and acrylamide containing multicomponent systems showed identical release profile, with very similar quantities of drug being released over time (Figure 3.25).
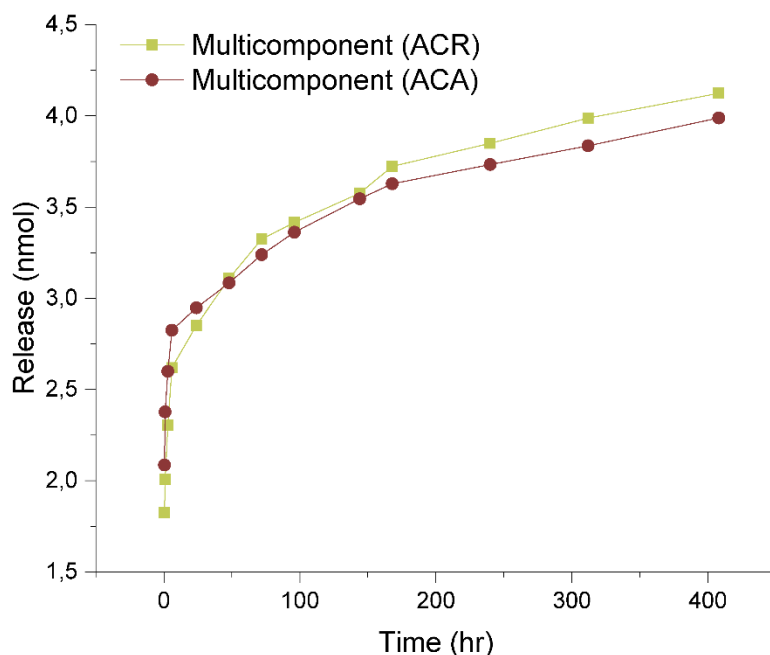
Time (hr)	0.5	1	3	6	24	48	72	96	144	168	240	312	408
Acr (nmol)	1,8255	2,0065	2,306	2,619	2,8515	3,109	3,3245	3,4155	3,5755	3,722	3,849	3,987	4,123
Aca (nmol)	2,08575	2,3766	2,59901	2,82394	2,9471	3,08441	3,23844	3,36131	3,54467	3,62762	3,73264	3,83497	3,98809

Figure 3.25. In vitro cumulative ketoprofen release from multicomponent MS in MOPS solution (pH=7.4). Aliquots of the supernatant were withdrawn at certain time points over two weeks after MS formation, and analyzed by LC-MS. At each time point, fresh supernatant was added to compensate for the withdrawn volume.

70

These results gave evidence that these multicomponent systems are able to perform better in terms of mechanical stability and durability than Ca-alg MS, while also providing a controlled anti-inflammatory drug release. These *in vitro* results are very promising, and will therefore shortly be tested for cell compatibility and potential in cell encapsulation and transplantation applications.

3.3.3. Pirfenidone and its derivatives as anti-fibrotic compounds

For *in vivo* applications, the improvement of biocompatibility and reduction of PFO is an extremely important requirement, since it will determine the usefulness of microcapsules for cell transplantation treatments. The promising results obtained with ketoprofen motivated us to investigate the potential of applying the developed strategy for other anti-fibrotic drugs for cell transplantation. Pirfenidone (PFD) was first approved in 2008 in Japan, as the first treatment for idiopathic pulmonary fibrosis (IPF).[267] Since then, it has been approved in many other places, such as China, Canada, the United States of America, Europe and Mexico. PFD exhibits both anti-fibrotic and anti-inflammatory effects.[268]

3.3.3.1. Synthesis of PFD derivatives

PFD derivatization was necessary for two reasons: 1) unmodified PFD does not contain any functional groups available for conjugation to PEG, 2) the efficiency of unmodified PFD is very low and high doses are needed to achieve the desired effect. This low efficiency is attributed to the very fast metabolism of PFD, which can be overcome by derivatization.[269] We planned modification of PFD starting from the previously reported analogue **11**.[270] Both aliphatic (propyl) (derivative **12**) and more polar tetra(ethylene glycol) (TEG) (derivative **13**) spacers were envisaged. A terminal carboxylic group was introduced to allow further conjugation to PEG derivatives through an ester linkage (Figure 3.26).
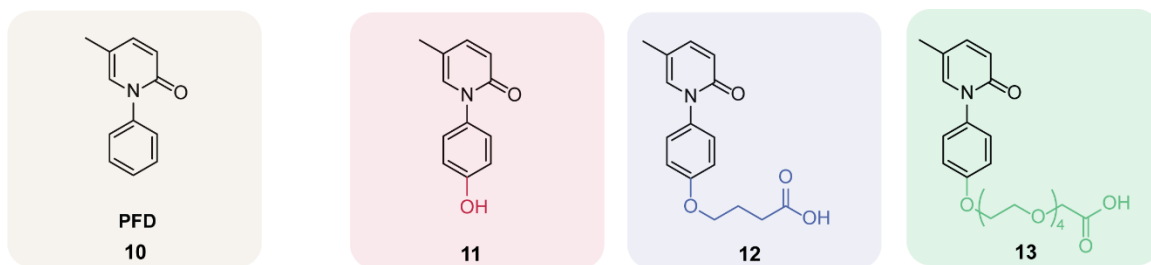
Figure 3.26. Pirfenidone and its synthesized derivatives.

Synthesis of derivative **11** has been already reported in the literature.[270] However, we introduced a slight modification at the benzyl deprotection step, which resulted in a higher yield. 2-Bromo-5-methylpyridine was converted into compound **14**, by first reaction with KO^{t}Bu, followed by acidic treatment. In parallel, 4-bromophenol was protected as a benzyl ether **15** in 85% yield. Ullmann-coupling with **14** afforded compound **16**. Deprotection of the benzyl group, under strong acidic conditions led to derivative **11** (Scheme 3.6).

For comparison, PFD **17** was produced by Ullmann-coupling of **14** with phenylbromide in 77% yield (Scheme 3.6).
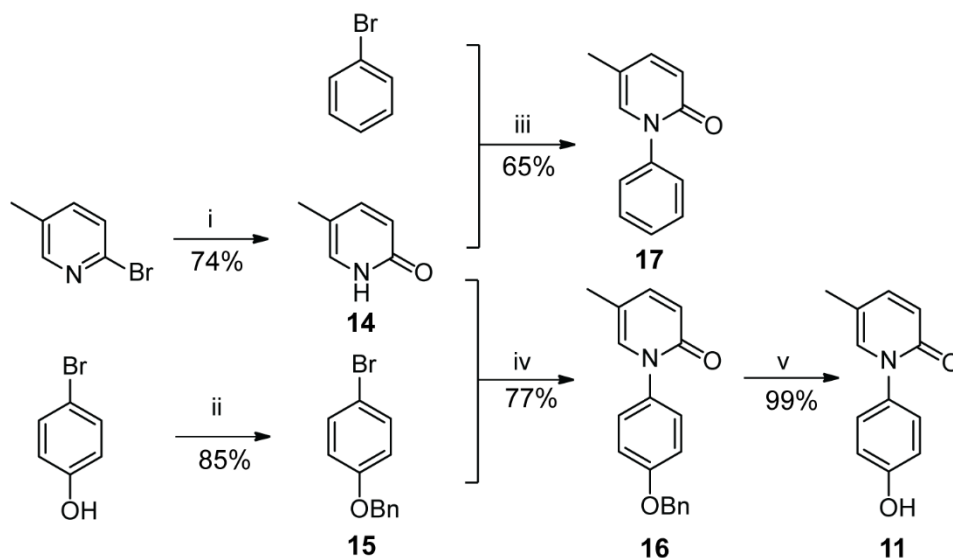
*Scheme 3.6. Synthesis of derivative **11**. Reagents and conditions: i) 1. KO^{t}Bu, 2-methylbutan-2-ol, 40 h, 100 °C 2. HCOOH, 24 h, ii) BrBn, NaH (60 %), anhydrous DMF, 2 h, rt, iii) CuI, K$_2$CO$_3$, anhydrous DMF, 12h, reflux iv) CuI, K$_2$CO$_3$, anhydrous DMF, 12h, reflux v) concd. HCl, MeOH/H$_2$O, concd. H$_2$SO$_4$, 4 h, reflux.*

Further derivatization of **11** involved a nucleophilic substitution on ethyl 4-bromobutyrate to obtain **18** in 89% yield, followed by ester saponification to obtain **12**. The generated carboxyl group would allow for coupling to a PEG with hydroxyl functionality (Scheme 3.7).
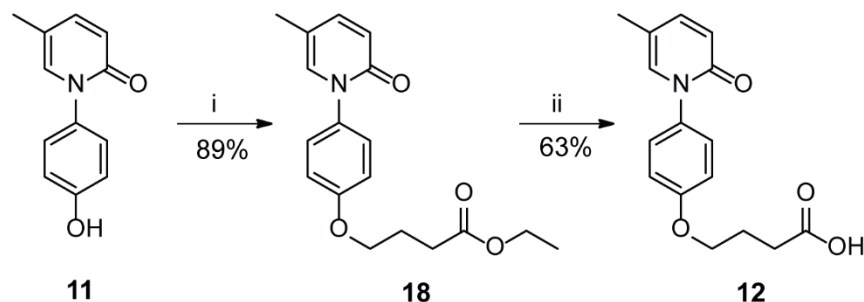
*Scheme 3.7. Synthesis of derivative **12**. Reagents and conditions: i) Ethyl 4-bromobutyrate, K_2CO_3, DMF, overnight, 80 °C ii) KOH (2M, aqueous), MeOH, 2h, reflux.*

In order to investigate the different effect of introducing a molar polar linker, previously prepared monotosylated TEG derivative **19** was reacted with **11** to afford **20** in 75% yield. Introduction of a carboxylic moiety was achieved by nucleophilic substitution on bromoacetic acid to afford **13** in 56% yield (Scheme 3.8).
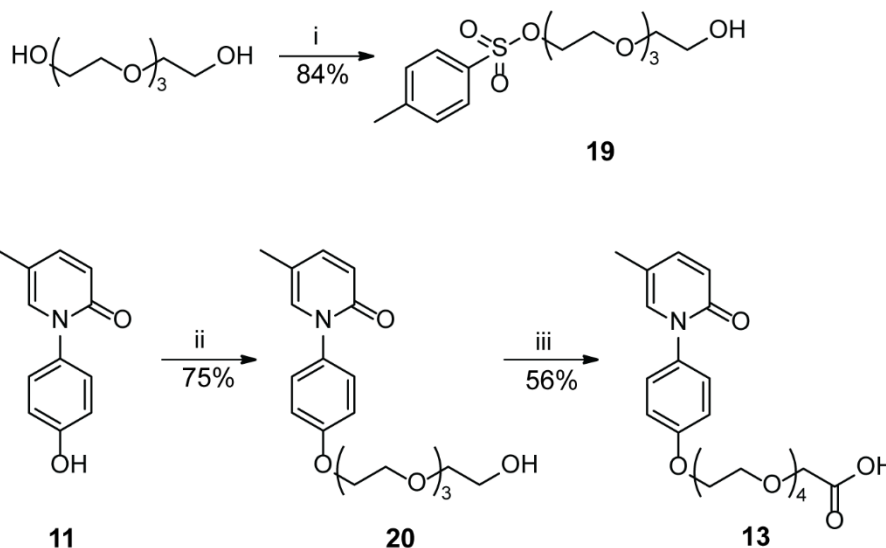
*Scheme 3.8. Synthesis of derivative **13**. Reagents and conditions: i) TsCl, Et$_3$N, DCM ii) **19**, K_2CO_3, anhydrous DMF, 16 h, 60 °C ii- Bromoacetic acid, NaH, anhydrous THF, rt, 5 h.*

3.3.3.2. The effect of PFD derivatives on insulin producing cells and fibroblasts

To assess the potential effects of PFD and its derivatives in the context of insulin producing cell microencapsulation, we first investigated their potential toxicity and impact on neonatal pig derived cell viability and metabolic activity. Then, we evaluated their anti-fibrotic effect *in vitro* on stimulated primary human fibroblasts. Lastly, we also assessed the effect of PFD and its most

promising derivative on the functionality of NPIs by performing a glucose-induced insulin secretion assay.

Effect of compounds on the metabolic activity of neonatal pig derived cells

The cytotoxicity and impact on cell metabolic activity of PFD and its derivatives were assessed by MTT assay on neonatal pig pancreatic-derived Mesenchymal Stromal Cells (pMSC). pMSCs were incubated with PFD and compounds **11-13** with concentrations ranging from 0.1 to 5 mM, using DMSO as control. Cell viability, measured by their metabolic activity, was assessed at day 1, 2 and 5 (Figure 3.27). Especially at higher concentrations, PFD and compound **11** and **12** showed a decrease of proliferation over time. However, cell proliferation in the presence of compound **13** remained relatively stable over 5 days. Interestingly, compound **13**, at 2 mM, did not induce significant detrimental effect on cell metabolic activity. In addition, it presented a higher MTT index than the other derivatives, at all concentrations tested.
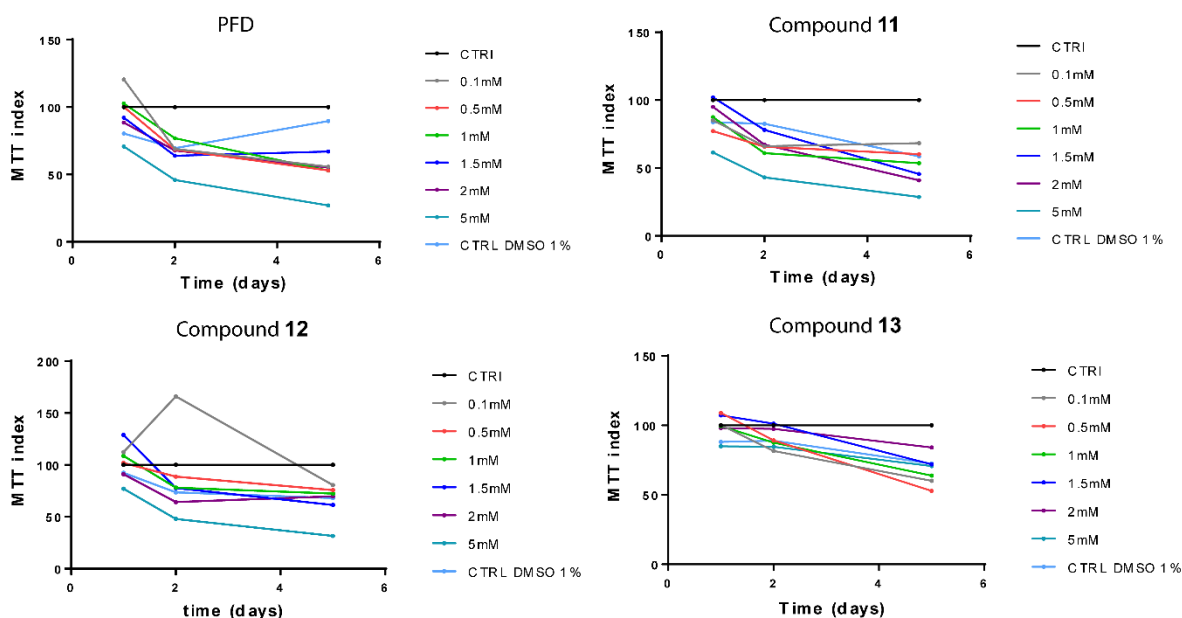
*Figure 3.27. MTT assay performed with PFD, compound **11**, **12** and **13** at concentrations between 0.1 and 5 mM. An untreated condition and 1% DMSO were used as controls. pMSCs were incubated with PFD and compounds **11-13**, and the number of viable cells was evaluated at day 1, 2 and 5.*

Evaluation of the potential anti-fibrotic effect of PFD and its derivatives

Next, evaluation of the anti-fibrotic effect of PFD and its derivatives prior to conjugation to PEG was performed on EDX1 human cell fibroblasts stimulated with the pro-inflammatory transforming growth factor beta 1 (TGFβ1). Under those conditions, fibroblasts are differentiated into myofibroblasts, which are the effector cells of fibrosis. Myofibroblasts typically express α-

smooth muscle actin (α-SMA), and quantification of α-SMA expression therefore allows to evaluate the anti-fibrotic potential of the different compounds. The values of α-SMA were obtained by quantification of western blot signals after normalization to total amounts of protein loaded. As depicted in Figure 3.28, stimulation of EDX1 cells with TGFβ1 enhanced α-SMA expression up to 2-4 times of control conditions. Cells were treated using increasing concentrations of PFD and compounds **11-13** for 5 days. We observed that the maximal fold decrease of α-SMA expression with the lowest concentration (1 mM) was observed for compound **13**. However, both compounds **11** and **12** resulted in a more notable decrease compared to the reference PFD drug but were most efficient at 1.5 mM.
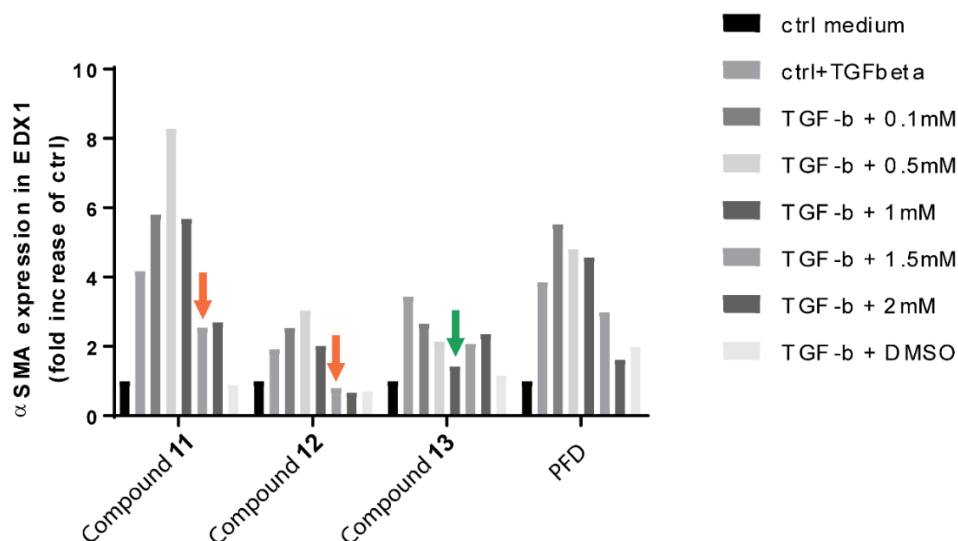
Figure 3.28. Quantification of α-SMA expression in EDX1 cells. The efficiency of reducing fibrosis (α-SMA expression) was evaluated for PFD, compound 11, 12 and 13 at different concentrations. Compound 13 was most efficient at 1 mM concentration (indicated by a green arrow), compound 11 and 12 at 1.5 mM concentrations (indicated by orange arrows).

Effect of PFD and compound 13 on the functionality of NPIs

Based on the previously presented results of MTT assay and anti-fibrotic effect, we concluded that compound **13** was the most promising anti-fibrotic drug candidate for our applications. PFD and its derivative were intended to be used for encapsulation of NPIs, therefore, an eventual deleterious effect on insulin secretion of the islets was evaluated. NPI functionality in the presence of PFD and compound **13** was assessed by incubation of free NPIs (1500 IEQ/condition) with the compounds at 0.5 mM and 1.5 mM concentrations for compound **13** and PDF, respectively, for 5 days, followed by glucose-induced insulin secretion assay. Untreated NPIs and NPIs incubated with DMSO (1%) were also evaluated. In the presence of both PFD and compound **13**, NPIs showed a tendency of increased secretion capacity upon stimulation with glucose (16.8 mM) and

theophylline (16.8 mM glucose supplemented with 5 mM theophylline), in comparison with untreated NPIs (Figure 3.29).
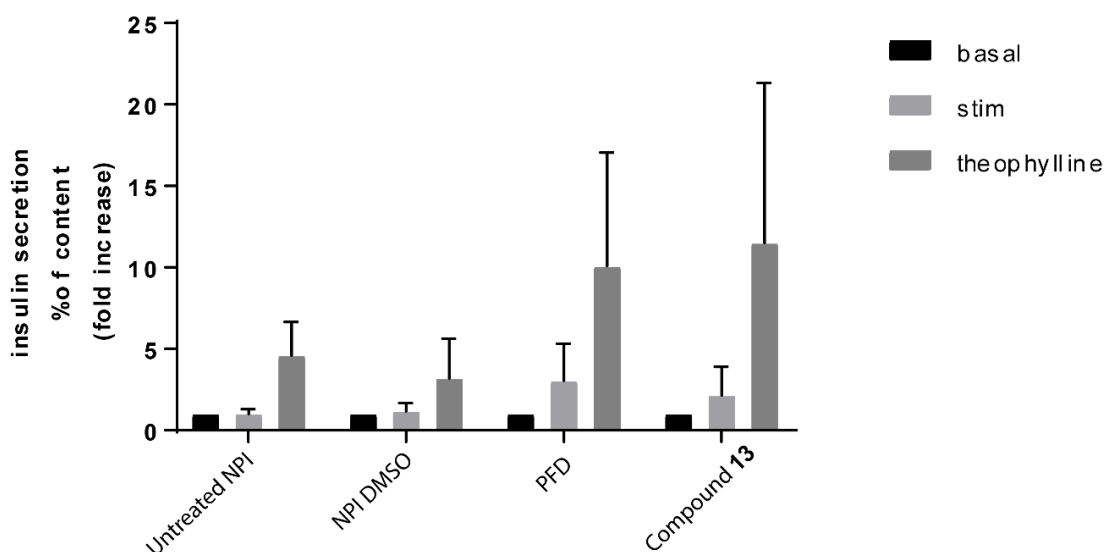
*Figure 3.29. Glucose-induced insulin secretion assay from NPIs after 5 days of culture with PFD and compound **13**. As a control untreated islets, and islets cultured in DMSO (1%) were used. The results represent the mean of two independent experiments with NPIs derived from two different isolations.*

All the above mentioned assays suggested that PFD and compound **13** could be a beneficial addition to MS in the microencapsulation of insulin producing cells. Therefore, we continued the development of hydrogel MS including PFD and compound **13**, followed by *in vivo* assays, which will be presented in the following sections.

3.3.3.3. Microencapsulation of insulin producing cells in PFD-modified hydrogels

Compound **13** was selected for further conjugation with PEG derivatives. Esterification in the presence of amino-PEG-NHBoc followed by acidic hydrolysis of the tert-butylcarbamate delivered PEG-PFD (**22**) in high yield. Using the grafting procedure presented in Section 3.1.2, PEG-PFD was conjugated to Na-alg for further encapsulation experiments.
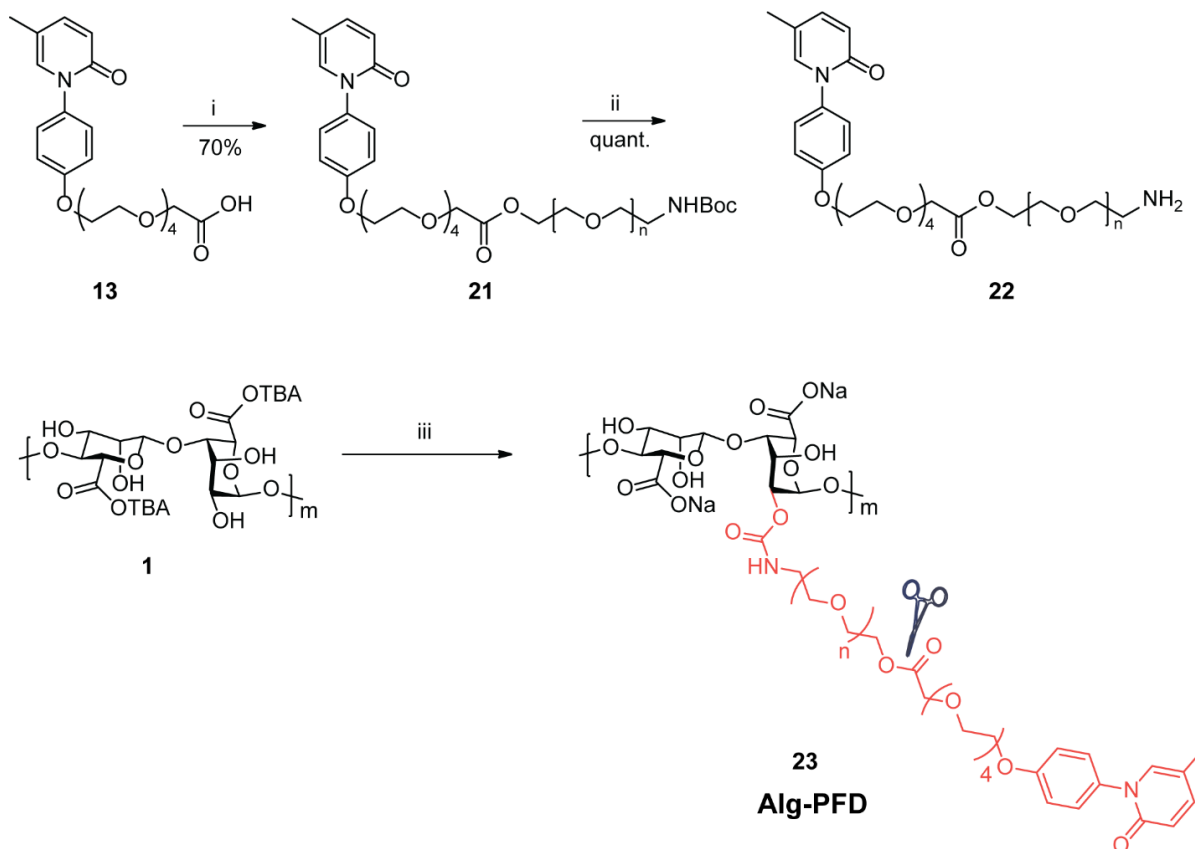
*Scheme 3.9. Synthesis of PEG-PFD **22** and further grafting on TBA-alg to obtain Alg-PFD (**23**). Reagents and conditions: i) BocNH-PEG(2K)-OH, EDCI, DMAP, DCM, 7 hr ii) HCl 4N in dioxane, 2h, rt iii) 1. CDI, DMSO 2. Compound **13**, H_2O.*

3.3.3.4. MS formation

To assess the potential of PFD and compound **13** in cell microencapsulation, drug eluting MS formation was performed, either by co-encapsulation or covalent conjugation of the anti-inflammatory drugs. Co-encapsulation of small drugs in alg-based hydrogel MS was reported to be successful in reducing fibrotic reactions.[207,209,210] However, co-encapsulation of small drugs is accompanied by a fast burst release from the MS. Thus, we aimed at forming MS by both co-encapsulation method, and following our strategy of covalent drug conjugation. In order to evaluate the difference between 1) covalently conjugated anti-fibrotic drug or co-encapsulated and 2) the difference between the effect of PFD and compound **13**, four different conditions of MS formation were tested:

1. Ca-alg as a reference (1.5 wt%)
2. Compound **13** covalently coupled to alg through the PEG-linker (compound Alg-PFD **23**), mixed with Na-alg (in a ratio of 1:2) for optimal MS formation (2.5 wt%) (Alg:Alg-PFD MS)
3. Compound **13** co-encapsulated with Na-alg (in a concentration of 3 mM, in 1.5 wt% alg)
4. PFD co-encapsulated with Na-alg (in a concentration of 3 mM, in 1.5 wt% alg).

MS formation was performed using a Büchi B-395 Pro encapsulator. Co-encapsulation was realized by first preparing a drug stock solution (3 mM), followed by dissolution of the alg biopolymer in the drug solution. The resulted empty beads are shown in Figure 3.30. Spherical beads of a size around 1000 μm were formed (the diameter of the MS is presented in Table 3.12).
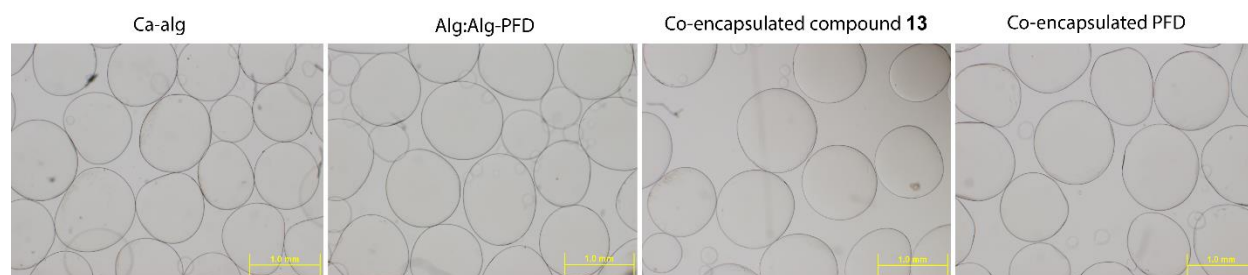
Figure 3.30. Images of empty beads produced with Büchi encapsulator. The scale bar corresponds to 1.0 mm.

We first evaluated the physical properties of the MS. Assessment of the mechanical properties was carried out only at one time point (at day 7), as evolution of these properties was not expected in the lack of covalent cross-linking. Mechanical resistance values at day 7 were similar for all conditions, ranging between 1.41 and 1.73 N/mm^3 (Table 3.12). Alg:Alg-PFD MS exhibited the highest value, it was slightly more resistant to 90% compression of the initial diameter compared to the other MS. Similarly, shape recovery performance at day 7 for Alg:Alg-PFD was higher compared to the other 3 conditions, indicating the beneficial effect of the presence of PEG. On the contrary, alg-based MS had a lover shape recovery performance, as expected for the pure Ca-alg MS compositions.

Table 3.12. Diameter and resistance to compression to 90% of the initial diameter, at day 7 post bead formation. For the diameter 30 MS were measured, for the resistance 10 MS were analyzed.

Properties (day 7)	Ca-alg	Alg:Alg-PFD	Co-encapsulated compound 13	Co-encapsulated PFD
Diameter (µm)	1010 µm ± 81	1019 µm ± 132	1030 µm ± 101	1022 µm ± 92
Resistance (N/mm³)	1.43 ± 0.15	1.73 ± 0.17	1.41 ± 0.12	1.65 ± 0.22
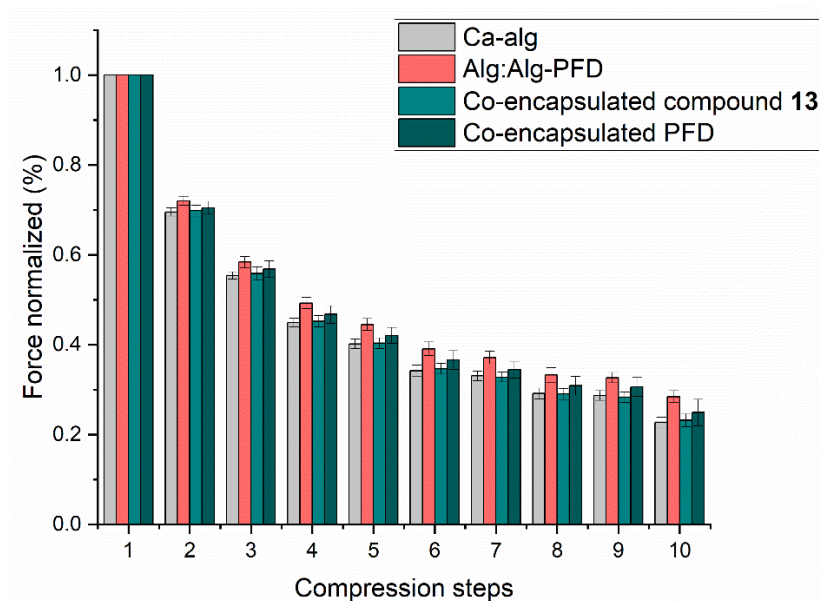
Figure 3.31. Shape recovery performance at day 7 of Ca-alg, Alg:Alg-PFD, compound 13 co-encapsulated and PFD co-encapsulated. The measurement was carried out using 10 MS/condition, using a Texture Analyzer.

3.3.3.5. Encapsulation of NPIs and NPIs with pMSCs

Upon successful MS formation with the above mentioned four conditions, the feasibility and potential beneficial effect on encapsulated cells was evaluated. Encapsulation of NPIs either alone or together with pMSCs was carried out. NPIs and NPIs with pMSCs entrapped within the above mentioned polymeric conditions are depicted in Figure 3.32. The encapsulation resulted in mostly spherical MS, a homogeneous cell distribution within the MS, with very minimal amount of empty beads. Live/dead staining of cells showed some cell death upon encapsulation, but the process

was not completely detrimental on cells, as indicated by the amount of live cells within the MS (Images of live/dead cell staining are presented in Annexes, Figure 6.3–6.6).
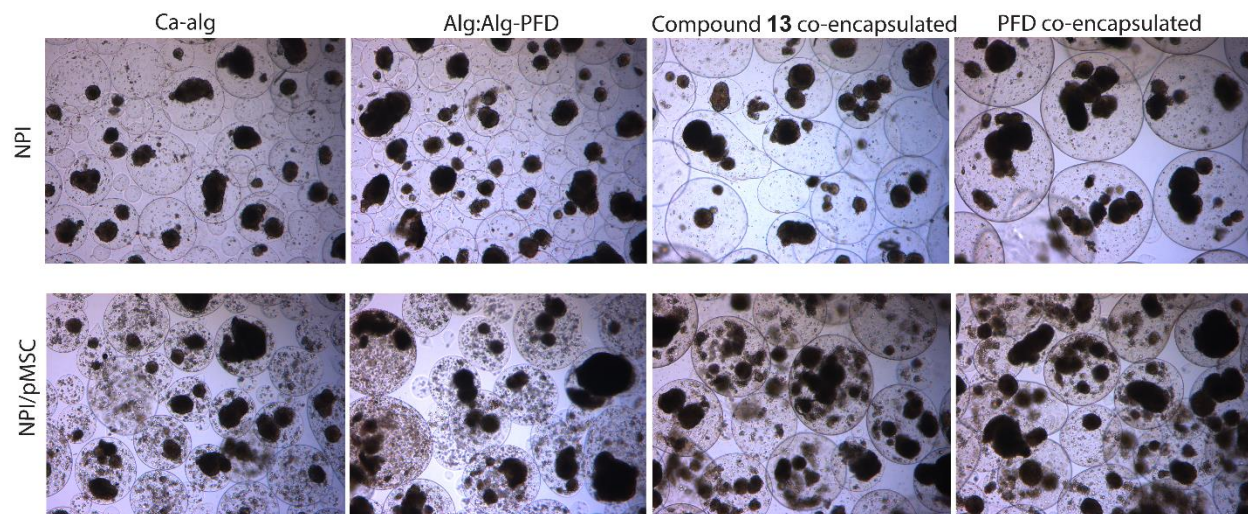
Figure 3.32. Microscopic images of NPIs or NPIs and pMSCs encapsulated as Ca-alg, Alg:Alg-PFD MS, or co-encapsulated with compound 13 or PFD.

Next, we evaluated the *in vivo* effect of the cell containing MS, and the ability of restoring normoglycemia in diabetic mice. After MS formation, NPI or NPI/pMSC containing microcapsules (~40 000 IEQ/1-1.5 mL of polymer) were transplanted in the peritoneal cavity of immune-competent streptozotocin-induced diabetic mice. The IEQ/mice was approximately 12-15 000, depending on the experiments and the availability of NPIs. The glycaemia of mice was measured every day to follow the possible changes *in vivo*. In the case of mice transplanted with only NPI containing microcapsules (Figure 3.33), there was a decrease observed in the case of Ca-alg or Alg:Alg-PFD MS. By day 6 the glycemic index was lowered to approximately 15 mmol/L for both conditions. PFD co-encapsulated in Ca-alg microcapsules transplanted to diabetic mice resulted in a decrease below 15 mmol/L by day 8. However, all conditions failed to maintain decreased glycaemia over several days, and by day 11, they were all hyperglycemic.
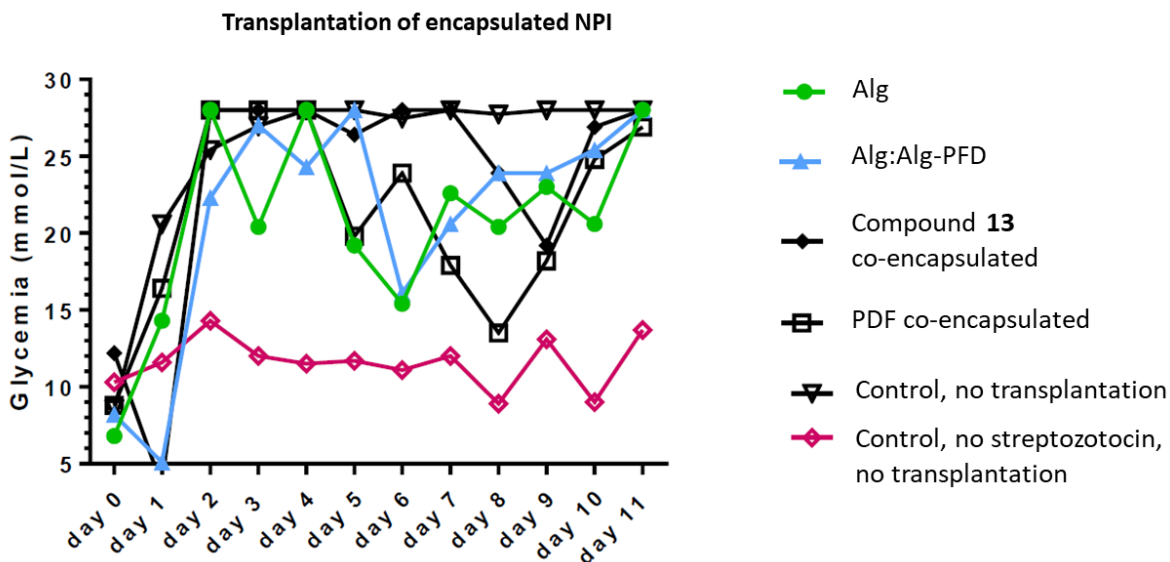
Figure 3.33. Blood glucose level changes in streptozotocin-induced diabetic mice transplanted with NPI containing microcapsules. Measurements were done daily, on one mouse/condition.

We aimed at investigating whether co-encapsulation of NPIs with pMSCs could have a beneficial effect on the insulin secreting capacity of NPI, and therefore have a favorable outcome of the transplantation. Thus, mice were transplanted with NPI and pMSC containing MS. This cell content showed potential in reaching a more significant decrease of glycemia at one time point, with Ca-alg and Alg:Alg-PFD MS. At day 6, these MS showed lowered glycemic index to ~10 and ~15 mmol/L, respectively. However, this could not be maintained for a longer period, and no long-term beneficial effect was observed with MS of any of the polymer compositions.

Transplantation of encapsulated NPI/pMSC

Legend:
- Alg
- Alg:Alg-PFD
- Compound **13** co-encapsulated
- PDF co-encapsulated
- Control, no transplantation
- Control, no streptozotocin, no transplantation
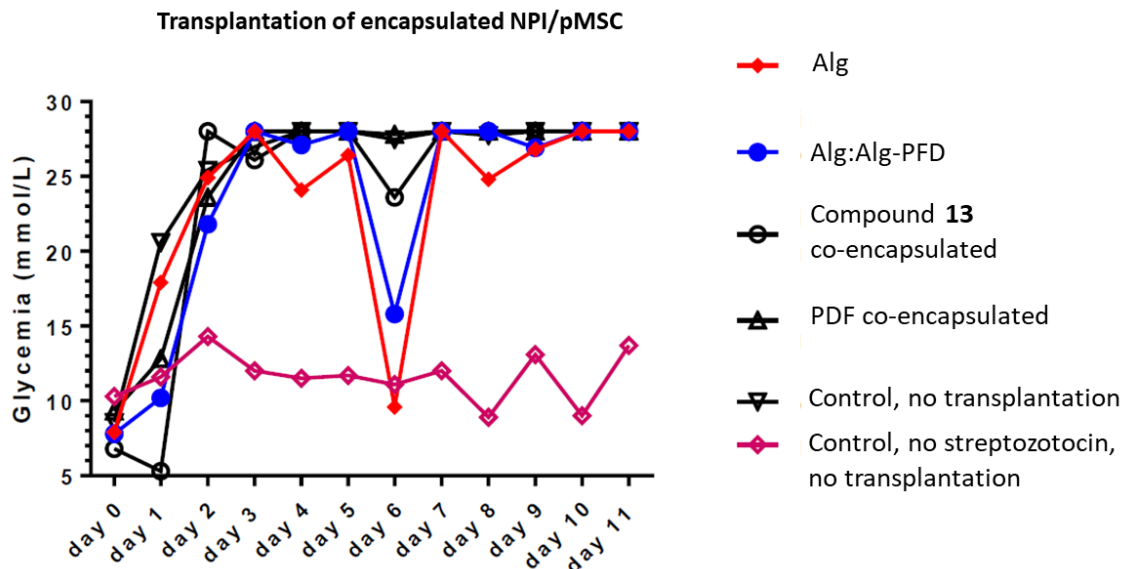
Figure 3.34. Blood glucose level changes in streptozotocin-induced diabetic mice transplanted with NPI and pMSC containing microcapsules. Measurements were done daily, on one mouse/condition.

To investigate the reason of the limited decrease of glycemic index achieved, at day 11, mice were euthanized and microcapsules were recovered from the peritoneum. The viability of encapsulated NPIs was assessed. Viable cells and islets were observed, however, NPI/pMSC containing Ca-alg microcapsules and PFD co-encapsulated NPI microcapsules had substantial PFO (Figure 6.7–6.8, Annexes). The exact reason for the graft failure remains unclear. We hypothesized that early graft failure in these first experiments was due to poor in vivo maturation of NPIs and the rapid cellular overgrowth around the microcapsules. This also suggests that the anti-fibrotic molecules were not sufficiently inhibiting the fibrotic reactions with the current settings. In addition, the experiments were performed on a single mouse per condition, due to the high number of conditions tested. As variations in animal models could be quite significant, the size of the experiment might have been a possible limitation, however, it was sufficient for an explorative observation.

Since co-encapsulation of pMSCs with NPIs did not result in significantly better outcomes compared to NPI encapsulation alone, the experiment was repeated using NPIs encapsulated alone. However, normoglycemia was again not achieved in diabetic mice (Figure 6.9, Annexes). We concluded that immunosuppression might still be necessary for studying the effectiveness of the compounds in pig to mouse xenotransplantation settings on fibrosis. The experiment will be repeated in immune-compromised mice to evaluate whether PFO can be reduced and allows to prolong graft function.

3.3.3.6. *In vitro* drug release

We next evaluated the i*n vitro* drug release from the three drug-containing MS. In order to ensure drug was released properly from the cell containing MS, and to investigate the difference between co-encapsulation and covalent drug conjugation, samples from the medium were taken at regular time points. NPI and NPI/pMSC containing MS were kept in the culture medium, and aliquots of 1 mL were taken for analysis, and replaced with 1 mL of fresh medium. The samples were analyzed by LC-MS, and the results are depicted in the form of cumulative release in Figure 3.35 (Alg:Alg-PFD) and 3.36 (compound **13** and PFD co-encapsulated).
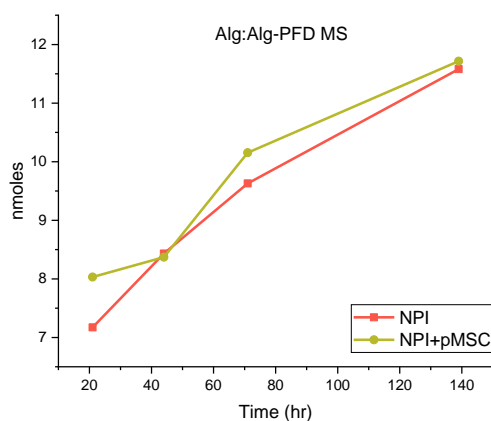
*Figure 3.35. In vitro cumulative release of compound **13** from NPI or NPI+pMSC containing Alg:Alg-PFD MS. MS were kept in NPI medium, aliquots of the supernatant were withdrawn at 21, 44, 71, 139 h after encapsulation, and analyzed by LC-MS. At each time point, fresh culture medium was added to compensate for the withdrawn volume.*

*Figure 3.36. In vitro cumulative release of compound **13** and PFD from NPI or NPI+pMSC containing Ca-alg MS, co-encapsulated with compound **13** or PFD, respectively. MS were kept in NPI medium, aliquots of the supernatant were*

withdrawn at 21, 44, 71, 139 h after encapsulation, and analyzed by LC-MS. At each time point, fresh culture medium was added to compensate for the withdrawn volume.
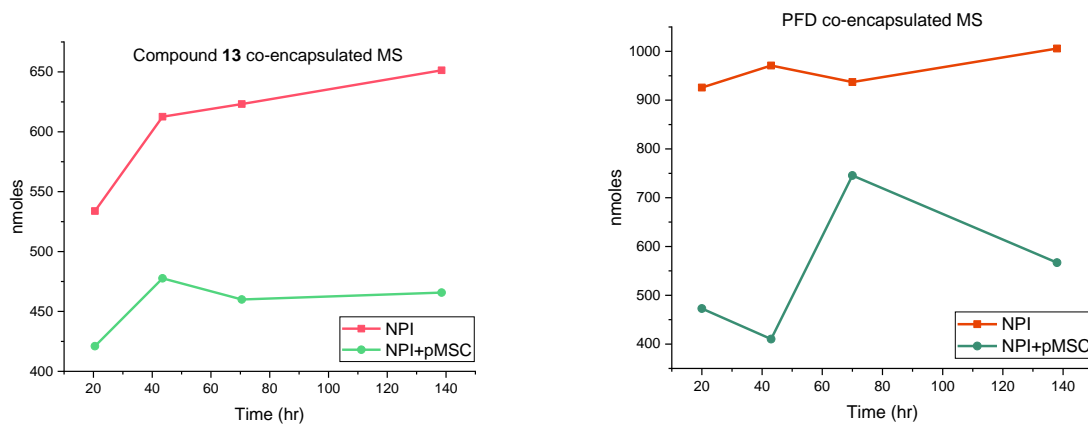
The release profile suggests that covalently grafted compound **13** via ester bond results in a controlled, sustained cumulative release. In the case of co-encapsulated drugs, the release profile does not follow a regular release pattern. PFD release from NPI containing MS remained approximately constant, suggesting that no more significant drug was released in the medium over the time of the experiment. Since the first sample was taken 20 h after encapsulation, it is likely that most of the drug had been released in the gelation bath prior to the culture of the microcapsules. Surprisingly, compound **13** co-encapsulated with NPI in Ca-alg MS showed a sustained release. However, NPI and pMSC containing MS co-encapsulated with either compound **13** or PFD exhibited a very irregular release profile. The results of the release samples might be slightly altered, as their analysis in the presence of cell medium is challenging due to the many salts present. Pre-treatment of the samples with a mixture of MeOH/HCOOH is required prior to injection.

3.3.3.7. *In vivo* anti-fibrotic effect

To evaluate the anti-fibrotic effect of PFD and compound **13**, we envisaged to transplant MS under the kidney capsule of immune-competent mice, and quantify the amount of PFO after retrieval of the kidney capsule. As we previously experienced with ketoprofen (presented in Section 3.3.1), the severity of cellular overgrowth in the presence of MIN6 cells was considerably increased, highlighting the importance of assessing the anti-fibrotic effect of the drugs with cell-containing MS. Thus, we prepared MS loaded with pMSC, with the above mentioned 4 polymeric conditions (Na-alg, Alg:Alg-PFD, compound **13** co-encapsulated and PFD co-encapsulated in Na-alg). Microscopic images of the resulted encapsulated pMSC are presented in the Annexes, Figure 6.10. Upon encapsulation, MS were transplanted under the kidney capsule of immune-competent mice. After 28 days the kidneys were recovered, fixed and embedded in paraffin. Analysis of the extent of the PFO on sections of the kidney is currently on going.

In conclusion, PFD and its derivatives **11**, **12** and **13** could be successfully synthesized, and the most promising compound **13** was covalently grafted on the alg hydroxyl group. This allowed us to investigate the effect of the drug release via ester hydrolysis compared to non-covalent drug encapsulation. *In vivo* results with NPI and NPI/pMSC encapsulated MS within the Alg:Alg-PFD polymer imply that covalent drug inclusion within the MS might be more beneficial. However, we

cannot draw conclusions with complete certainty yet, as analysis of results are still ongoing, and further experiments are needed to better understand this novel system.

3.4. Bead generation using microfluidics

Within the framework of a collaboration with CEA (Commissariat à l'Ènergie atomique), in Grenoble, France, a microfluidic method was developed for bead formation with the PEGylated alg polymers. Beads prepared with microfluidic technique could potentially lead to smaller diameter beads, less satellites and improve monodispersity. A brief description of the obtained results will be presented below.

3.4.1. Experimental setup

The microfluidic system was designed, set up and operated at CEA. The whole setup consists of a pressure control, an oil tank, the feed of the polymer solutions (mixed with cells for encapsulations), the microfluidic cartridge, and a recuperation falcon to collect the prepared MS. The bead formation takes place in the disposable microfluidic cartridges, which were designed and produced at CEA.

For our experiments, the geometries for each of the cartridges were kept the same for the droplet formation and pre-gelification, as shown in Figure 3.37. Figure 3.37/A shows a micro-flow-focusing droplet (MFFD) generation module, in which the polymer solution phase is sheared by two perpendicular soybean oil phases to form the droplets. The reason for the triangle chamber is to focus the droplet detachment exactly at the MFFD module.[271] Figure 3.37/B illustrates the pre-gelifying module;[272] the channel of soybean oil containing Ca-acetate is located in both sides of the channel containing the alg droplets and oil. As the Ca^{2+} containing oil meets the alg droplets, the gelification starts by diffusion of the gelifying ion.
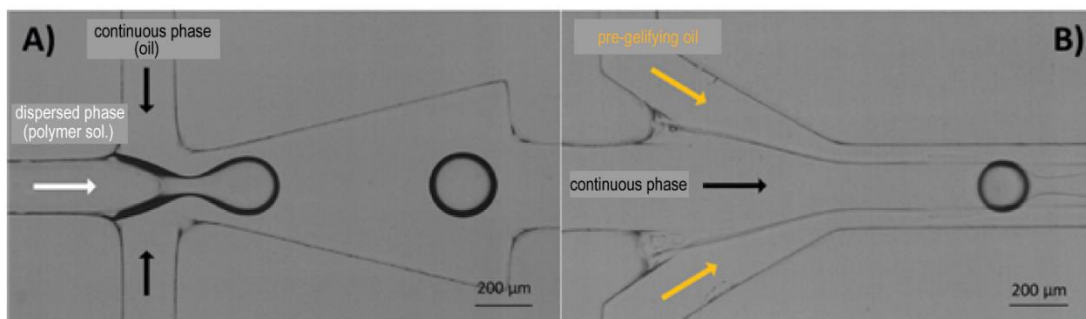

Figure 3.37. Images of the microfluidic cartridge modules. A) MFFD module for the generation of the beads. The continuous soybean oil phase shears the polymer solution to form droplets. B) Pre-gelification module. The pre-gelifying phase (soybean oil with Ca-acetate) gets in contact with the continuous phase containing the previously generated beads and oil.

The whole experimental setup (Figure 3.38) consisted of a cartridge containing the MFFD and pre-gelifying module, followed by a channel (with a diameter of 500 µm, big enough to encapsulate islet cells) that brings the microcapsules outside of the cartridge, where gelification is completed in a falcon tube. In the falcon tube the immiscible aqueous phase containing the MS and the oil phase are separated. The oil is withdrawn from the upper part, the MS are collected manually after 5 minutes of gelification, and then transferred manually in a physiological serum.
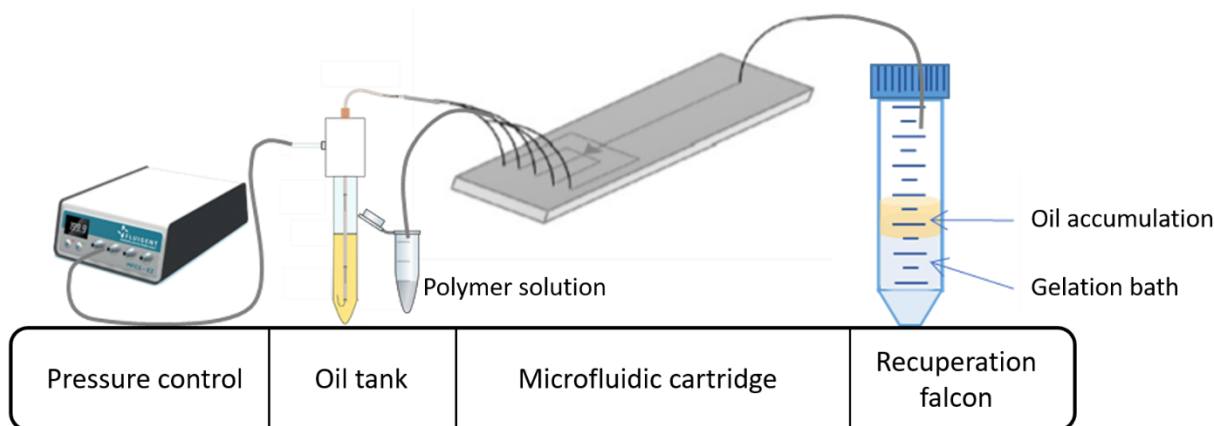
Figure 3.38. Experimental setup for microfluidic droplet generation.

3.4.2.   Empty MS formation using microfluidics

We used four different alg-based polymers to produce MS with microfluidics. As previously mentioned, different encapsulation techniques require different viscosities of the aqueous polymer solutions. Microfluidic generation of MS required highly viscous aqueous polymer solutions (above 4-500 mPa·s, in 4 wt% solution). Thus, the polymers were prepared following our strategy with the addition of acetic acid (presented in Section 3.2.1.) to minimize chain degradation and maximize the final polymer solution viscosity. The four polymer systems used with the microfluidic setup were:

- Na-alg (SLG100)
- Alg-sSH
- Alg-SH:Alg-ACA
- Alg:Alg-KET

The prepared empty MS were characterized for their average diameter, variation coefficient and aspect ratio (details of calculations are described in the Annexes). A representative example for each of the polymers is presented in Figure 3.39, with the characterization of MS.

Polymer	Average diameter (µm)	% of satellites	Variation coefficient (%)	Aspect ratio
Na-alg (2.5 wt%)	441	0	4.67	0.89
Alg-sSH (4 wt%)	385	1.29	2.89	0.94
Alg-SH:Alg-ACR (4 wt%)	418	0	2.89	0.98
Alg:Alg-KET (4 wt%)	346	9	10.67	0.92
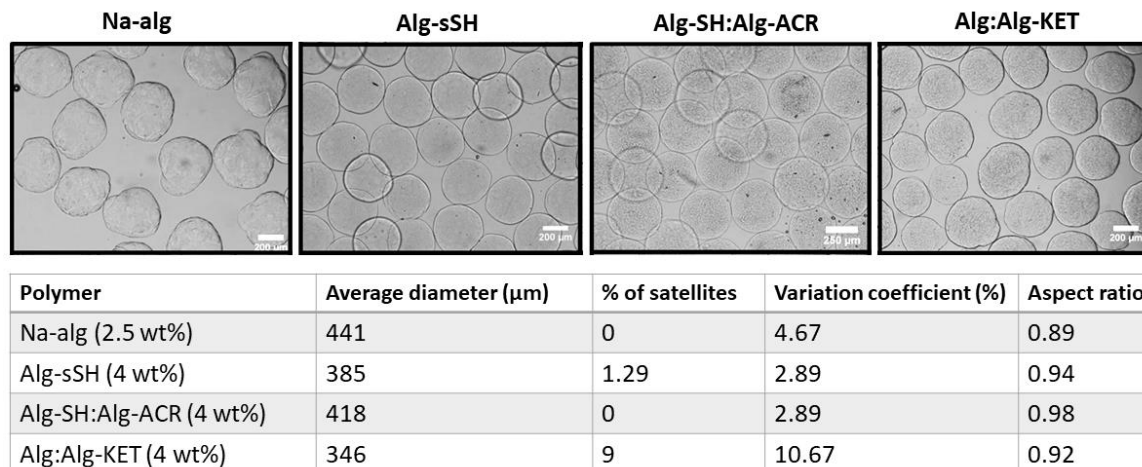
Figure 3.39. Empty MS prepared with microfluidics from polymers Na-alg, Alg-sSH, Alg-SH:Alg-ACR and Alg:Alg-KET. The scale corresponds to 200 µm. Characterization of the MS including average diameter, ratio of satellites formed, variation coefficient and the aspect ratio.

All polymer compositions resulted in spherical, monodisperse MS, with significantly smaller diameter than MS produced by air-flow droplet generator. The high aspect ratio values indicate the high sphericity of MS. Some satellites were formed mainly with the Alg:Alg-KET hydrogel MS but it was negligible.

Further characterization of MS produced by microfluidics focused on their permeability towards FITC-dextran of different molecular weights. The permeability was assessed the same way as previously described in Section 3.2.2. The permeability values of microcapsules prepared from the polymer composition Alg-SH:Alg-ACR resulted in very similar permeability values when prepared by air-flow droplet generator (Figure 3.14) or microfluidics (Figure 3.40). This suggests that the diameter of MS has no noticeable effect on the permeability of MS. Ca-alg beads prepared by microfluidics was found to be less permeable. However, Ca-alg prepared by air-flow droplet generator cannot be reliably compared to Ca-alg prepared by microfluidics, since the Na-alg used (Pronova SLG100 and Pronova UP LVG for microfluidics and for air-flow droplet generator, respectively) and its concentration were different.
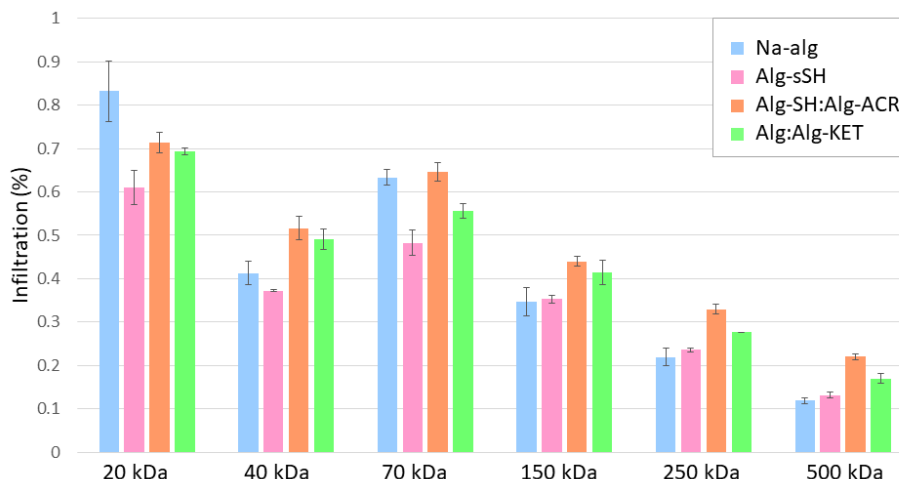
Figure 3.40. Permeability of microcapsules to different sizes of FITC-Dextran solutions. Na-alg was prepared in 2.5 %, while the other polymers were prepared at 4 wt% concentrations.

All in all, a microfluidic design was successfully applied to produce MS with PEGylated alg polymers. After optimizations, MS with small diameter and high sphericity could be obtained, providing a good basis for further developing the system in the presence of cells.

3.4.3. Encapsulation of NPIs using microfluidics

Next, the potential of using the microfluidic setup for the encapsulation of insulin producing cells was tested. The same polymer conditions were used to encapsulate NPIs as presented for the formation of empty MS. Examples of the resulted NPI containing microcapsules is illustrated in Figure 3.41.
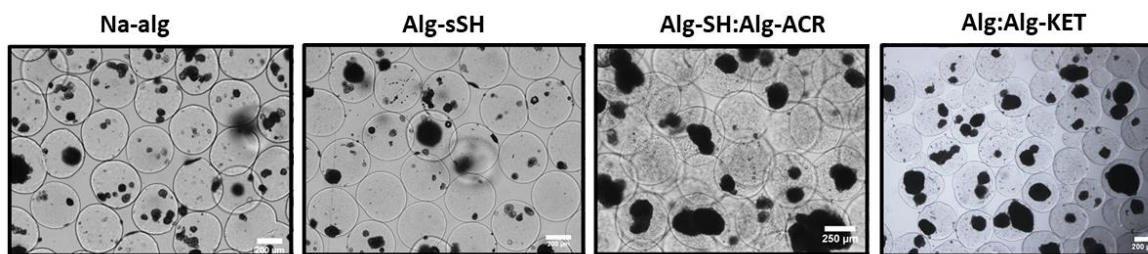
Figure 3.41. Encapsulated NPIs with microfluidics.

For encapsulation, NPIs were gently mixed with the aqueous polymer solutions, until homogeneously distributed within the viscous solution. The viability of islets was assessed right after the encapsulation, in order to see the effect of encapsulation on the cells. Encapsulated NPI viability was compared to the viability of non-encapsulated NPIs kept in NPI medium.

Figure 3.42 shows the viabilities obtained from 4 different encapsulation experiments performed with Na-alg and Alg-sSH polymers. The reason for the extremely low viabilities in the case of the first 2 encapsulations is due to the non-optimized transportation from one collaborator (from Geneva) to the other one (in Grenoble). Once the shipment protocol was optimized, cell viability was significantly improved (encapsulations 3 and 4). However, islets encapsulated in Alg-sSH still resulted in lower viabilities compared to Na-alg. Since we did not experience such a remarkable difference between Na-alg or Alg-sSH encapsulated cell viabilities when using other encapsulation techniques, we hypothesized, that the lower viability derived from the higher viscosity and concentration used. NPIs are extremely sensitive, a minimal change in their environment could possibly lead to such a drop of viability.

Figure 3.42. Viabilities of NPIs encapsulated with Na-alg or Alg-sSH polymers, assessed directly after encapsulation. The number of encapsulations correspond to different experiments, performed in a chronological order.

Figure 3.43 compares the viabilities derived from 3 different encapsulations with Na-alg, and Alg-SH:Alg-ACR polymers. The high viability results of the second and third encapsulations implied that encapsulation within these polymers did not damage NPIs and did not have a negative effect on NPI viability.

Figure 3.43. Viabilities of NPIs encapsulated with Na-alg or Alg-SH:Alg-ACR polymers, assessed directly after encapsulation. The number of encapsulations correspond to different experiments, performed in a chronological order.

Encapsulation of NPIs within the Alg:Alg-KET was expected to result in similar viabilities than encapsulation in pure Na-alg, due to the lack of reactive functionalities and the high amount of unmodified alg in this polymer composition. In 2 encapsulation experiments (2 and 3 in Figure 3.44), this expected tendency was achieved. No loss of viability was observed, indeed, even a slight increase was noticed in one case. However, encapsulation 1 and 4 resulted in decreased viabilities compared to free or Na-alg encapsulated NPIs.

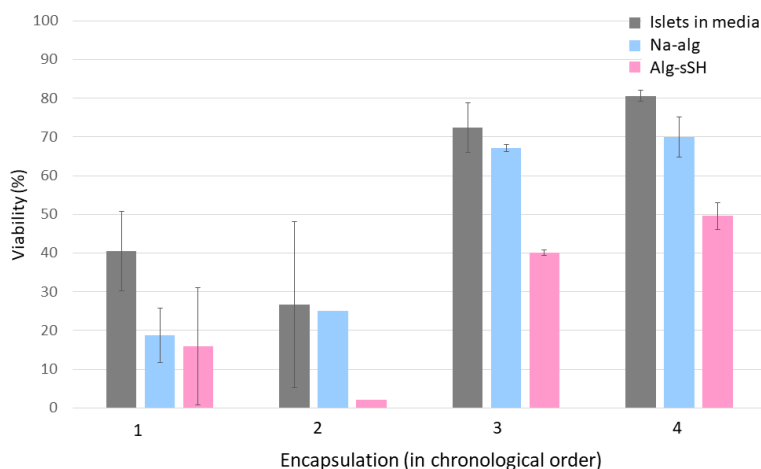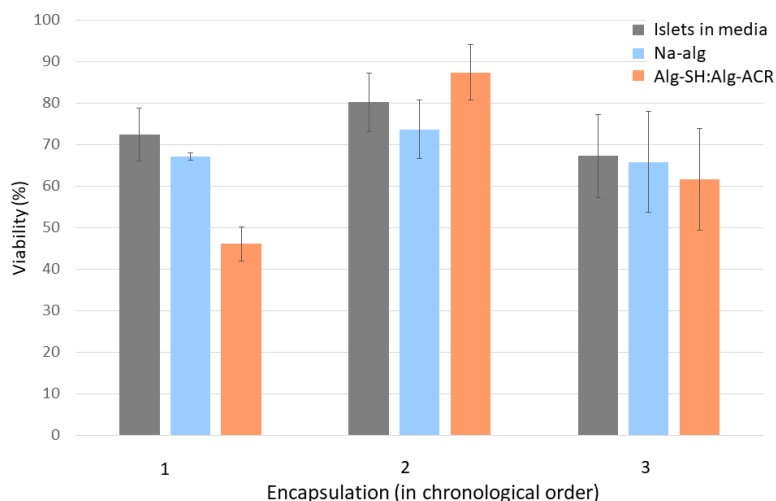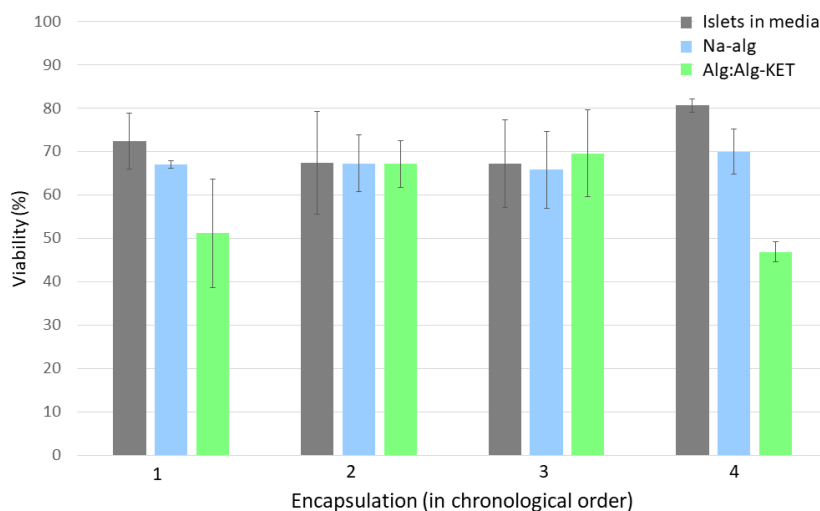*Figure 3.44. Viabilities of NPIs encapsulated with Na-alg or Alg:Alg-KET polymers, assessed directly after encapsulation. The number of encapsulations correspond to different experiments, performed in a chronological order.*

One considerable disadvantage of the microfluidics was the duration of the encapsulation process even with small amounts of polymer solution. A typical encapsulation procedure could take up to

3 hours, for which time some of the cells were suspended in the polymer solutions with minimal availability of oxygen. Implementation of a parallel setup for the droplet generation notably reduced the time needed to complete the encapsulation (1.5 h), and resulted in significantly improved viability results. The viability values of the experiment performed with the parallel setup are presented in Figure 6.12 in the Annexes. For each condition the viability was assessed to exceed the 80%.

In conclusion, we presented a successful microfluidic encapsulation of NPIs with the PEGylated alg polymers. This ensured us that PEG grafting on the alg hydroxyl group did not alter the characteristics of the alg-based hydrogels at a degree of preventing their use in a microfluidic setup. In addition, the resulting MS with smaller diameter could be beneficial. However, to properly evaluate the difference between larger and smaller diameter MS, *in vivo* experiments will be required.

4. Conclusion

Encapsulation of cells within a semipermeable membrane followed by their transplantation to replace damaged or non-functional cells and tissues could alleviate the life of many patients suffering from various types of diseases. The presence of the semipermeable membrane surrounding the cells allows the use of cells deriving from non-human species. Therefore, it could overcome the huge issue related to the limited availability of human donors. Additionally, cell microencapsulation could prevent the need for life-long immunosuppression. Alg-based cell encapsulation is a commonly used strategy to achieve cell immunoprotection. The biocompatibility and favorable gelling properties of alg make it a very promising candidate as a cell encapsulation material. However, some serious limitations, including defects in long-term durability *in vivo* as well as PFO leading to premature graft failure, prevented the transfer of alg encapsulated cells to routine clinical applications. Numerous research efforts are focused on overcoming these limitations, and eventually easing the translation of the technique from laboratory to clinics. Based on these limitations, the present thesis focused on the derivatization of alg into more stable hydrogels, and to improve as well as simplify the synthetic procedures to reach such derivatization. In addition, we aimed at reducing PFO in order to prevent restricted diffusion through the semipermeable membrane leading to early cell death. Finally, to benefit from the advantages of both strategies, we combined them into one multifunctional hydrogel MS.

First, novel alg-based hydrogels were developed, by functionalization with cross-reactive PEG derivatives, specifically on the hydroxyl group of alg. This way, complete preservation of the carboxylic groups for ionic cross-linking was achieved. The functionalization pathway was optimized using PEG-sSH as grafting polymer. Preparation of TBA-alg from Na-alg was necessary to achieve better solubility in organic solvents, and it involved treatment of Na-alg with formic acid followed by addition of TBAOH. Several parameters for the conversion of Na-alg into TBA-alg were optimized to ensure a robust and reproducible procedure. Then, activation of the hydroxyl groups with CDI allowed conjugation to the amine of PEG-sSH. Dissolution of this one-component Alg-sSH polymer and consequent extrusion into a Ca^{2+} containing gelation bath resulted in the formation of spherical, dual cross-linked hydrogel MS. Thiol-end functionalities of PEG-sSH provided disulfide bridges as covalent cross-linker. Fine-tuning of the grafting procedure by addition of acetic-acid prior to CDI addition led to decreased alg chain degradation, allowing fine tuning of the viscosity of the final polymer in aqueous solution, which is a key parameter to meet the requirements of several types of encapsulation procedures.

Next, we presented the possibility of extending the variety of covalent cross-links, applying the same synthesis procedure. We investigated the formation of carbon-sulfur covalent bonds via Michael addition between thiol-acrylate, thiol-acrylamide or thiol-maleimide. Hydrogel MS formation was realized by dissolution of the two-component system polymers (either Alg-SH:Alg-ACR, Alg-SH:Alg-MAL or Alg-SH:Alg-ACA) and extrusion of the solution into gelation bath. The beads presented increased mechanical resistance, shape recovery performance and stability towards Na-citrate solution compared to Ca-alg beads. The type of covalent cross-link had a clear effect on the permeability performance of the hydrogel MS. To further improve the immune-protective capabilities of these polymer systems, optimization of a more precise way to assess the permeability will be needed.

Furthermore, we showed that the strategy applied for alg functionalization with the aim of obtaining dual cross-linked hydrogels is also applicable to introduce anti-inflammatory drugs through a PEG spacer. Ketoprofen modification with PEG via ester or amide bond resulted in sustained, controlled drug release, significantly higher in the case of ester bond. Transplantation of MIN6 cell containing hydrogel beads prepared from a mixture of this polymer and Na-alg resulted in a notable decrease of fibrotic overgrowth around the microcapsules. Hence, we extended the variety of anti-fibrotic drugs, potentially decreasing PFO *in vivo*. PFD was modified to obtain three new derivatives, from which compound **13** showed the highest anti-fibrotic potential. It was thus further conjugated to PEG via an ester bond. After grafting on the alg backbone, formation of spherical beads was achieved by mixing with Na-alg. Preliminary *in vitro* and *in vivo* biological assessment involving this new PFD derivative was encouraging. However, several aspects are still under investigation and will be further addressed in the near future.

Finally, microcapsules involving both cross-reactive functionality and anti-fibrotic drugs were developed. To obtain such systems, Alg-KET/Alg-SH/Alg-ACR or Alg-ACA were combined, in the presence of Na-alg to ensure the formation of spherical hydrogels. Long-term sustained release of ketoprofen was observed, as well as enhanced microcapsule stability compared to Ca-alg.

In the framework of a collaboration with CEA (Grenoble, France), a microfluidic method was also developed for the formation of hydrogel MS, and encapsulation of islet cells was proved to be feasible. Noteworthy, adjustment of the viscosity of the PEG-grafted alg derivatives in aqueous solutions was crucial to adjust to the requirement of the MS formation, either by air-flow droplet generation of by microfluidic-assisted methodology.
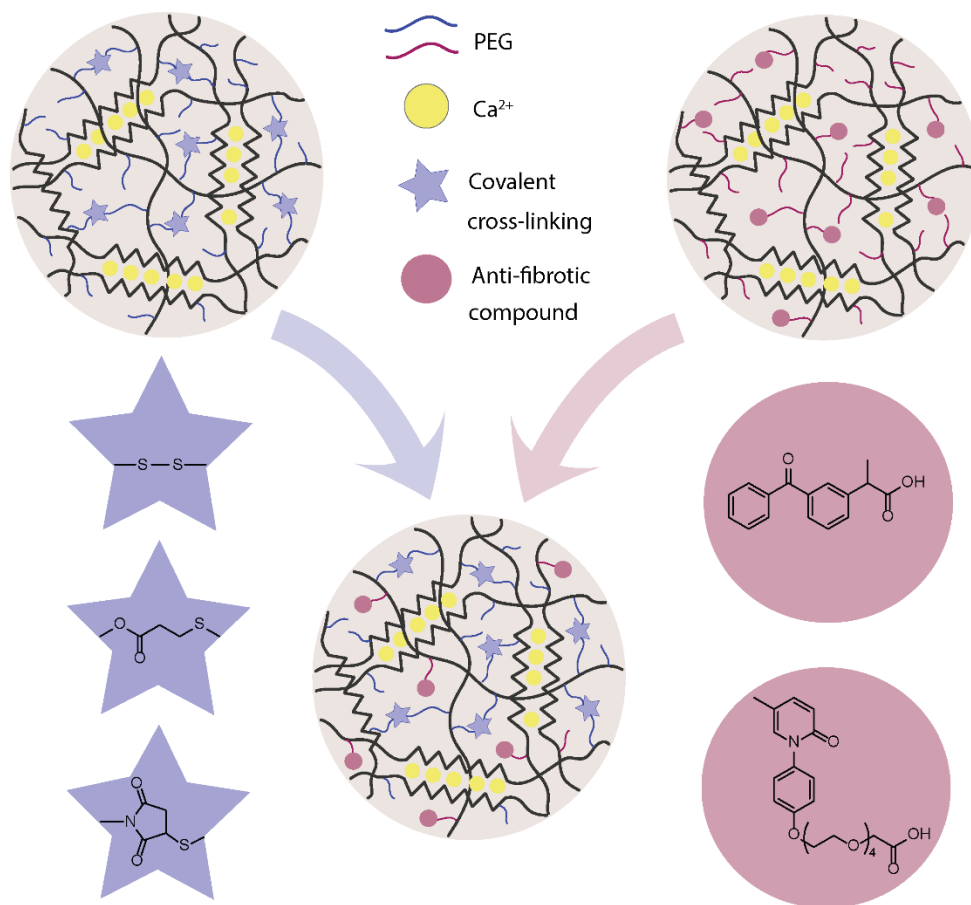
Figure 4.1. Schematic summary of the thesis achievements.

The above mentioned results provide the basis for further improvements and developments, which are the following:

- We showed a robust, straightforward and reproducible pathway for the derivatization of Na-alg into PEG-grafted derivatives, which will serve as a basis for the scaling-up of the procedure.

- Transplantation of microencapsulated NPIs into immune-competent diabetic mice could not yet ensure normoglycemia and maintain long-term glycemic control. However, decrease in the glycaemia was observed during the first days post-transplantation. Suspecting that the failure in glycemic control might result from the fragility and immaturity of NPIs, further experiments will be conducted with pig-derived pancreatic islets harvested from older specimens.

- In addition, the xenotransplantation model of pig to mice is not fully representative of the future use of pig to human transplantation. Therefore, the use of immune-compromised

mice next to an immune-competent model could be used as a control, to evaluate whether graft failure is due to fragility of the NPIs or a result of non-sufficient immune protection.

- The recently developed multicomponent hydrogel beads display favorable properties in terms of mechanical behavior, stability toward non-gelling ions and capability to ensure controlled release of bioactive molecular payloads. These compositions will be tested for the microencapsulation of endocrine cells and reduction of PFO *in vivo*, after transplantation. In particular, other clinical applications such as the treatment of acute liver failure might largely benefit from the newly developed hydrogels.

- In the search for alternative sources of insulin producing cells, a collaboration with the company Beta-Cell (Belgium) was initiated to investigate the potential of the multifunctional Alg-PEG hydrogels developed within the frame of this project for the microencapsulation and transplantation of fetal pig insulin producing cells.

5. Experimental section

5.1. Materials and methods

Na-alg Kelton HV (lot no. 61650A, [η] = 813 mL g⁻¹ in 0.1 M NaCl, T = 25 °C, G/M = 0.6) was obtained from Kelco (San Diego, USA, CA). Linear PEG derivatives were obtained from Biochempeg (Watertown, USA, MA) (Maleimide-PEG(1K)-NH$_2$, Acrylate-PEG(2K)-NH$_2$, Acrylamide-PEG(1K)-NH$_2$), Sigma (SH-PEG(2K)-NH$_2$) and Jenkem Technology (Beijin, China) (BocNH-PEG(2K)-OH). Other reagents and solvents were purchased from commercial sources (Fluka, Sigma, Switzerland; TCI Europe, Acros, Merck, VWR International) and were used without further purification. Dialysis membrane was purchased from Carl Roth (Karsruhe, Germany).

Unless special mention, all reactions were performed under argon (or nitrogen) atmosphere. Anhydrous solvents were either purchased as such, distilled prior to use or were obtained by filtration (Puresolv MD 5, Innovative Technology, Oldham, UK). When needed, glassware was dried for 12 h in an oven (T > 100 °C) or under vacuum with a heat gun (T > 200 °C).

Reactions were monitored by TLC using Merck Kieselgel 60F254 plates, or glass backed plates for preparative thin layer chromatography. Detection was performed by UV light (254 nm), followed by one of the following staining agents: KMnO$_4$, ninhydrin, molybdenate, pancaldi, vanillin, p-anisaldehyde or I$_2$. Flash column chromatography purifications were performed on Silicycle P60 Silica, 240-400 mesh.

NMR spectra were recorded on Bruker Avance III-400, Bruker Avance-400 or Bruker DRX-400 spectrometers at room temperature (rt) (400 MHz) (Bruker, Billerica, MA, USA). ¹H frequency is at 400.13 MHz, ¹³C frequency is at 100.62 MHz. Chemical shifts (δ) are expressed in parts per million (ppm) relative to residual solvent peaks rounded to the nearest 0.01 ppm for carbon (ref: CHCl$_3$ [¹H: 7.26 ppm, ¹³C: 77.2 ppm], MeOH [¹H: 3.31 ppm, ¹³C: 49.0 ppm], D$_2$O [¹H: 4.79 ppm]. Coupling constants (J) were reported in hertz (Hz) to the nearest 0.1 Hz. Peak multiplicity was indicated as follows s (singlet), d (doublet), t (triplet), q (quartet), m (multiplet), and br (broad). Attribution of peaks was done using the multiplicities and integrals of the peaks. When needed, COSY, HSQC and HMBC experiments were used to confirm the attribution.

Mass spectra were obtained by using a Waters ACQUITY H-class UPLC/MS ACQ-SQD by electron ionization (EI positive and negative) or a Finnigan TSQ7000 by electrospray ionization (ESI+). The accurate masses were measured by the mass spectrometry service of the EPFL by ESI-TOF using a QTOF Ultima from Waters. Quantitative MS analyses were performed on and Agilent Accurate Mass Q-TOF LCMS mass spectrometer coupled to an Agilent 1290 series UHPLC system (Agilent Technologies, USA). The separation was achieved using an ACQUITY UPLC® BEH C18 1.7μm column, 2.1 mm x 50 mm (Waters) heated at 30°C.

5.2. Synthesis of PEGylated alg derivatives for the production of covalently cross-linked microspheres
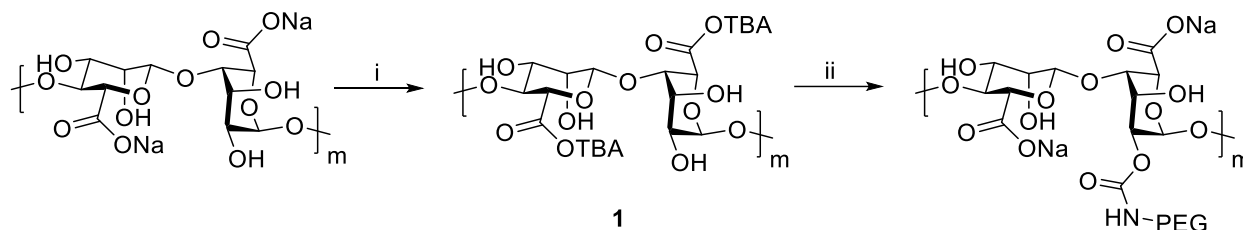
Scheme 5.1. PEGylation of Na-alg. Reagents and conditions: i) 1. HCOOH, EtOH, 12 h, 0 °C 2. TBAOH, H₂O, rt ii) 1. CDI, DMSO, CH₃COOH (0 or 1 equiv) 2. PEG-NH₂, H₂O.

TBA-alg (1)
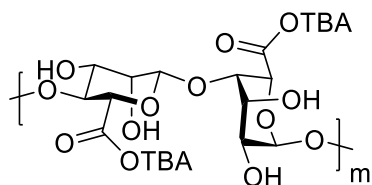
Na-alg (Kelton HV, 1.0 g) was suspended in EtOH (50 mL) and the solution was cooled down to 0 °C. Formic acid (20% aqueous solution, 50 mL) was added, and the mixture was stirred overnight at 0 °C. The resulting alginic acid powder was separated by vacuum filtration, washed with a mixture of EtOH/H₂0 1:1 (3 x 50 mL) and then acetone (3 x 50 mL). The resulting powder was further dried for 5 min under vacuum, and dispersed in water (50 mL). TBAOH (40% in water) was added dropwise until reaching pH 7. The solution was directly freeze-dried without dialysis to afford **TBA-alg** as a white solid.

¹H-NMR (400 MHz, Deuterium oxide): δ 4.18–3.76 (m, C*H*-Alg), 3.22–3.18 (m, 2H, C*H₂*-TBA), 1.70–1.62 (m, 2H, C*H₂*-TBA), 1.41–1.32 (m, 2H, C*H₂*-TBA), 0.95 (t, J = 7.4 Hz, 3H, C*H₃*-TBA) ppm.

¹H-NMR spectrum of **TBA-alg**
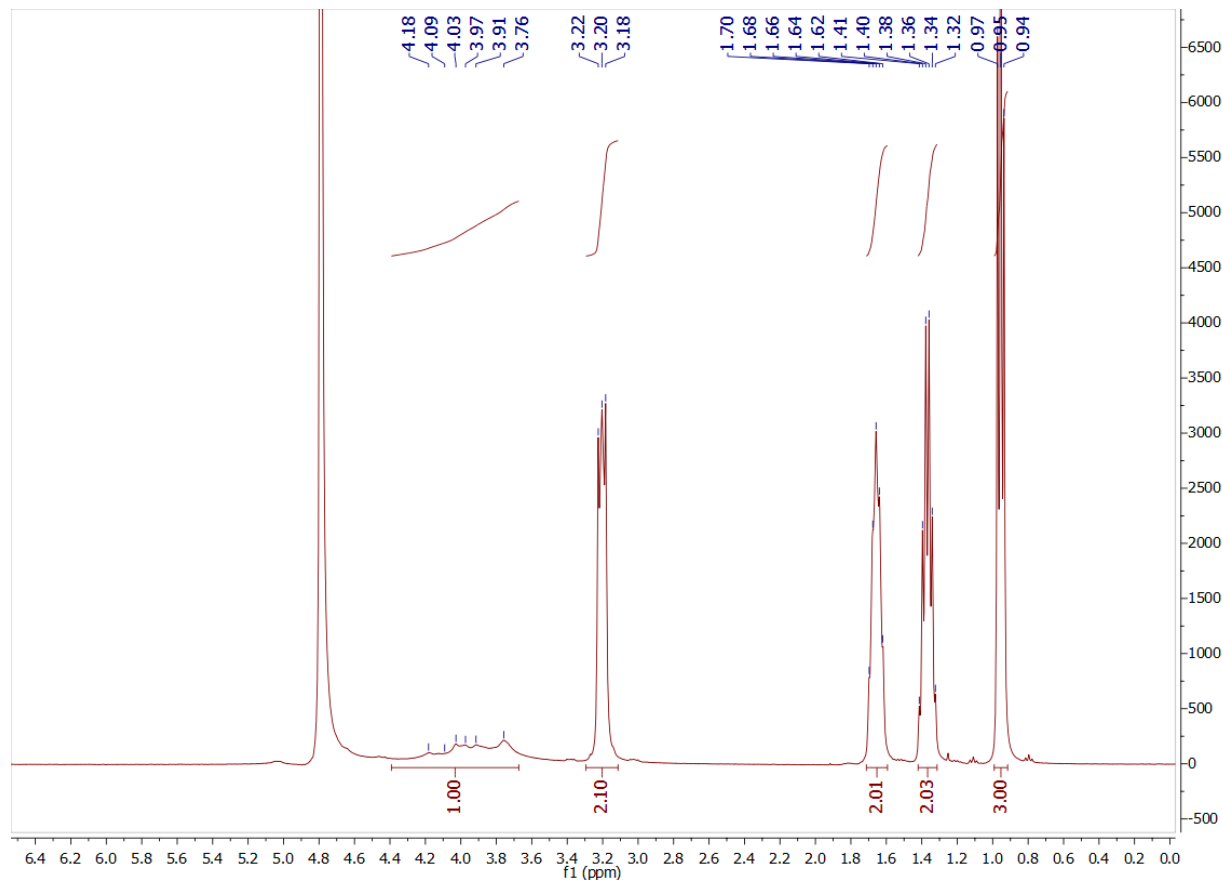
General procedure for the functionalization of TBA-alg with PEG derivatives.

For the preparation of lower viscosity Alg-PEG polymers, the procedure was the following. TBA-alg (100 mg) was dissolved in DMSO (20 mL) and the solution was stirred at 22 °C for 12 h to ensure homogeneous dissolution. 1,1'-Carbonyldiimidazole (CDI) (1 equiv, 0.239 mmol, 39 mg) previously dissolved in a minimum amount of DMSO was added and the reaction mixture was stirred for 30 min at rt. Acetone (40 mL) was added to enhance precipitation of the imidazolide-alg intermediate. The resulting precipitate was filtered (70 μm) and washed with acetone (3×10 mL). The solid was further dried for 15 min under vacuum at 40 °C and transferred to a round bottom flask. Distilled water was added (10 mL), and the mixture was stirred until complete dissolution. PEG derivative (1 or 2 equiv, 23.9 or 47.8 μmol) previously dissolved in a minimum volume of distilled water was added. In case of PEG derivatives standing as HCl salt, 1 equiv. of NaHCO₃ was added. The reaction mixture was stirred at 22 °C for 2 h. NaCl solution (4 mM, 40 mL) was added, and the reaction mixture was further stirred for 2 h. The solution was transferred

into a dialysis membrane (cut-off of 14 kDa) and dialyzed against distilled water for 3 days, changing water at least 3 times a day. The pH value was controlled at 7.0. The PEGylated alg polymers were obtained as white solids after freeze-drying.

For the preparation of polymers with higher viscosity in aqueous solution, acetic acid (1 equiv, 0.239 mmol, 0.014 mg, 0.015 mL) was added prior to the introduction of CDI.

Alg-sSH (3)
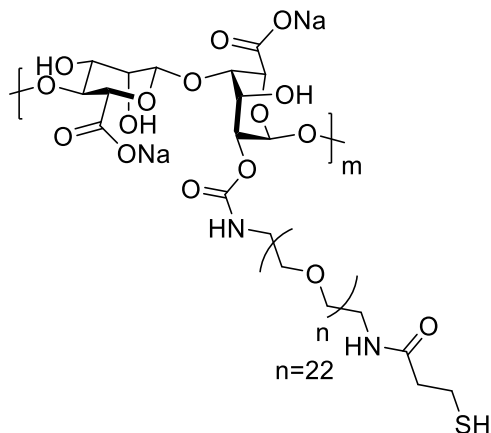
^{1}H-NMR (400 MHz, Deuterium oxide): δ 4.20–3.91 (m, CH-Alg), 3.79–3.63 (m, CH_2-O-CH_2), 3.42 (t, J=5.0 Hz, 2H, CH_2-NH-C(O)-O), 3.23 (t, J=5.0 Hz, 2H, CH_2-NH-C(O)-CH$_2$), 2.98 (t, J = 6.7 Hz, 2H, CH_2-C(O)-NH), 2.70 (t, J=6.7 Hz, 2H, CH_2-SH) ppm.

¹H-NMR spectrum of **Alg-sSH**
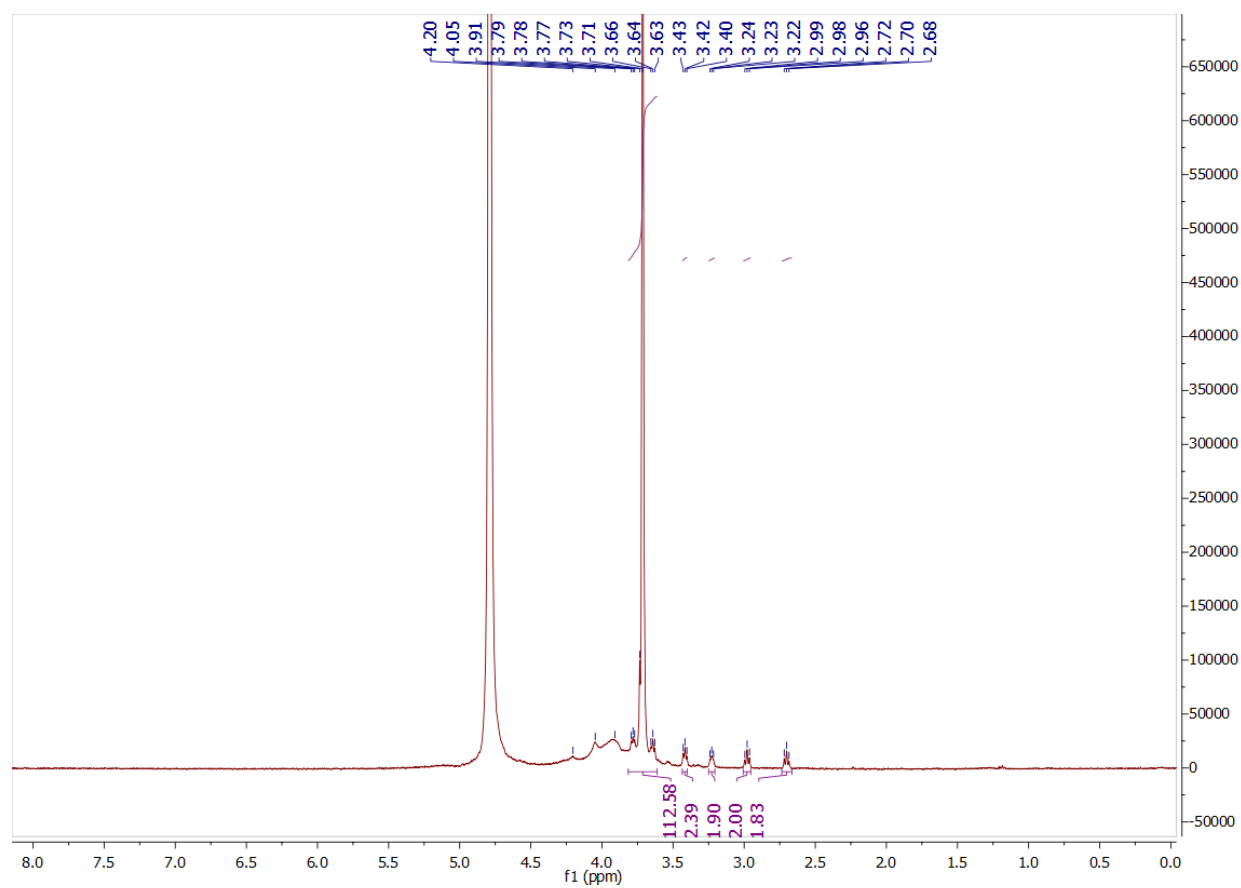
DOSY spectrum of **Alg-sSH**

Alg-ACR (4)

n=44
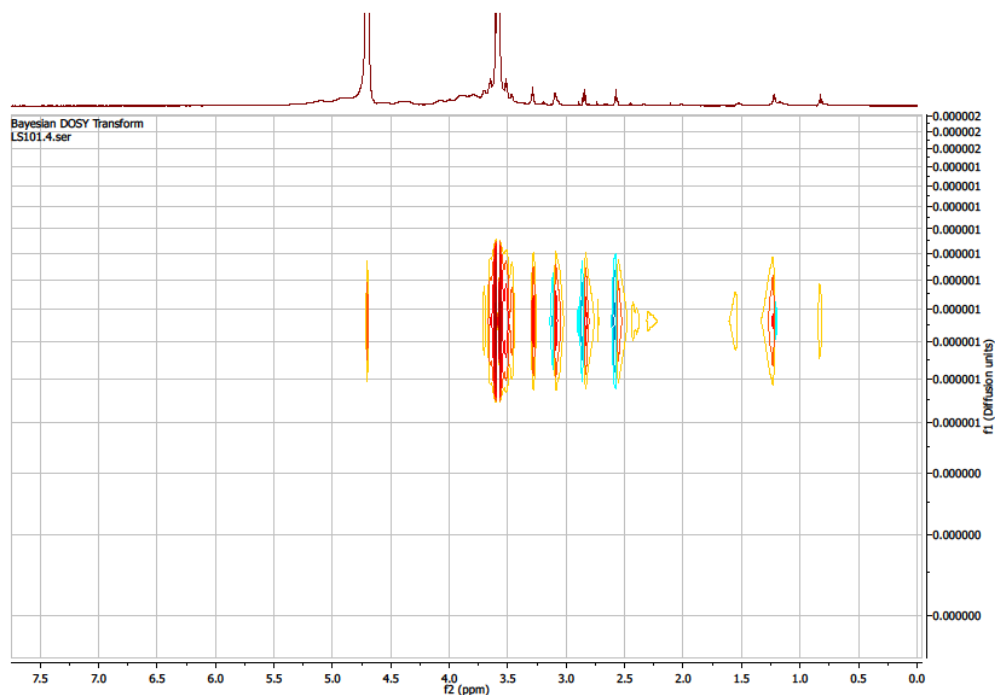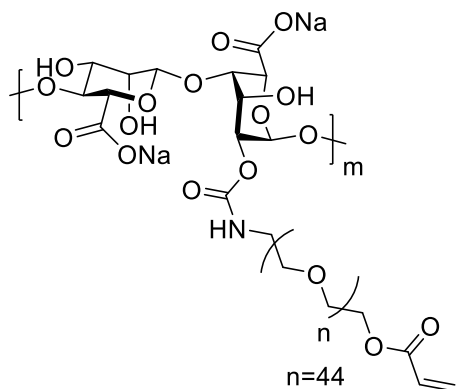
¹H-NMR (400 MHz, Deuterium oxide): δ 6.47 (dd, J = 17.3, 1.0 Hz, 1H, CH$_2$=CH-O), 6.24 (dd, J = 17.3, 10.5 Hz, 1H, CH$_2$=CH-O), 6.02 (dd, J = 10.7, 0.9 Hz, 1H, CH$_2$=CH-O), 4.35 − 4.34 (m, 2H, CH$_2$-O-C(O)), 3.88−3.52 (m, CH-Alg + CH$_2$-CH$_2$-O), 2.94 (t, J = 4.9 Hz, 2H, CH$_2$-NH) ppm.

¹H-NMR spectrum of **Alg-ACR**
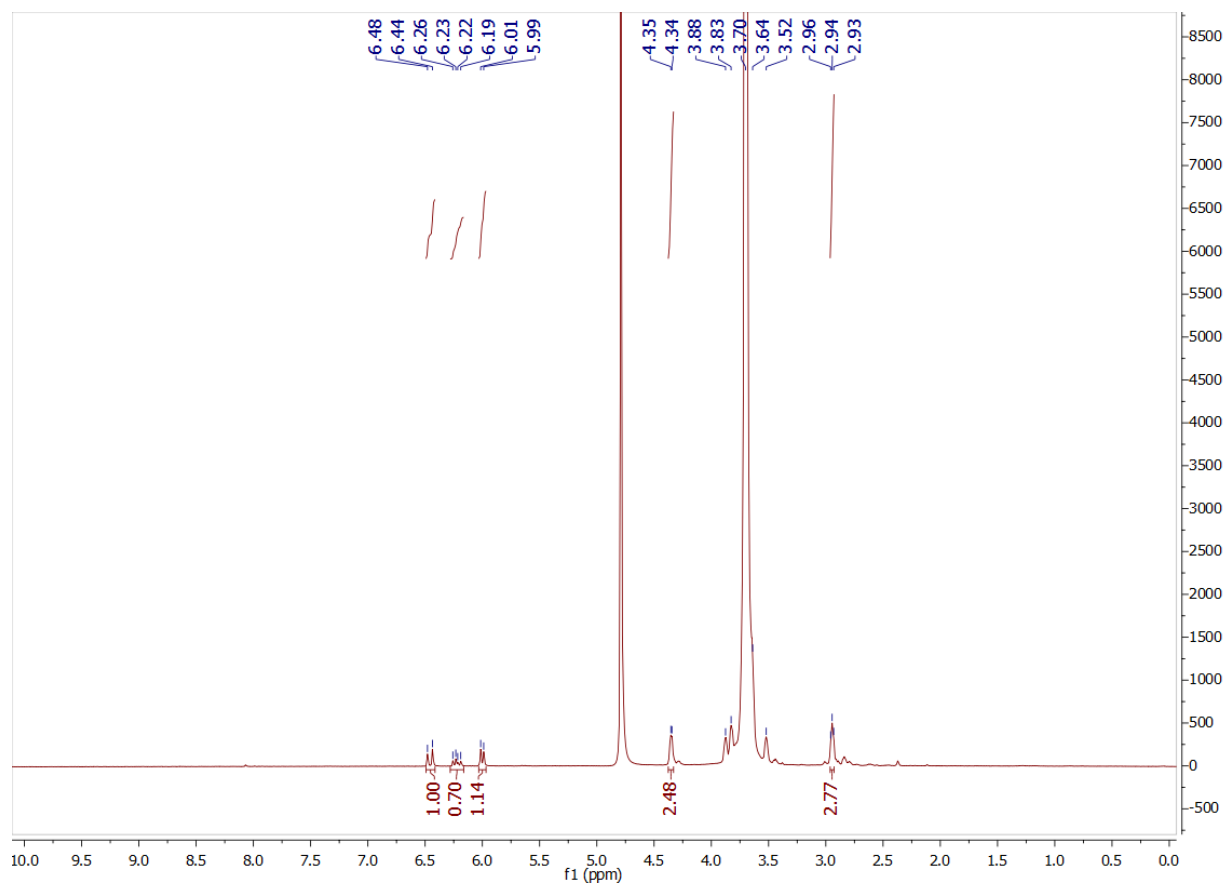
DOSY-NMR spectrum of **Alg-ACR** in comparison with ungrafted PEG-ACR
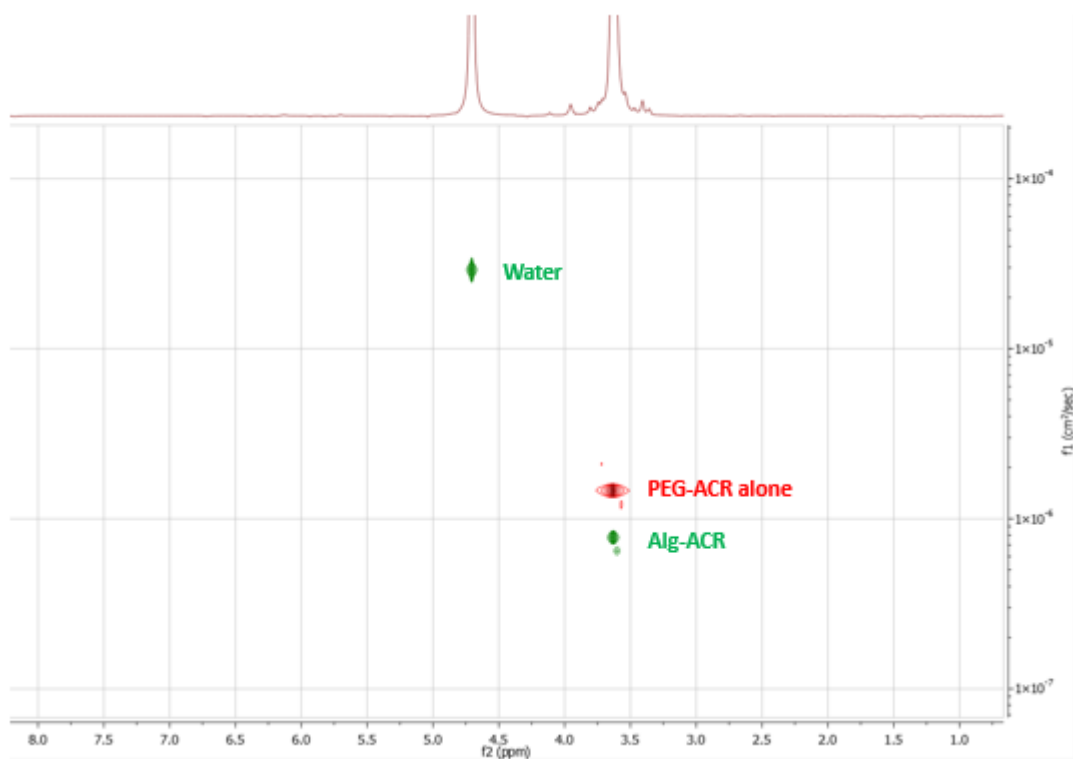
Alg-MAL (5)
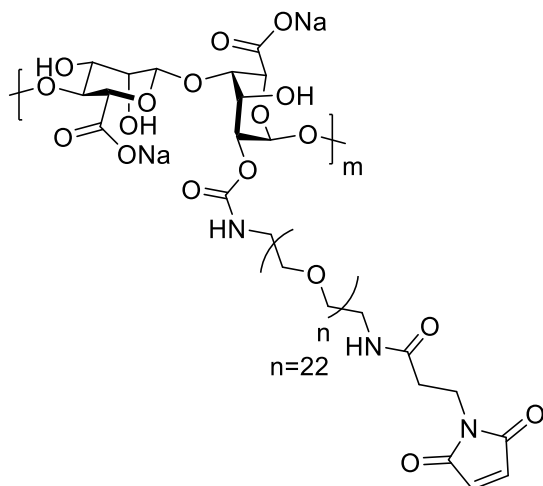
¹H-NMR (400 MHz, Deuterium oxide): δ 6.88 (s, 2H, 2 × =C*H*), 4.20 − 3.56 (m, C*H*-Alg + C*H₂*-C*H₂*-O), 3.38− 3.32 (m, 2H, C*H₂*-NH), 2.55-2.53 (m, 2H, C*H₂*-C(O)-NH) ppm.

¹H-NMR spectrum of **Alg-MAL**

Alg-SH (6)

n=44
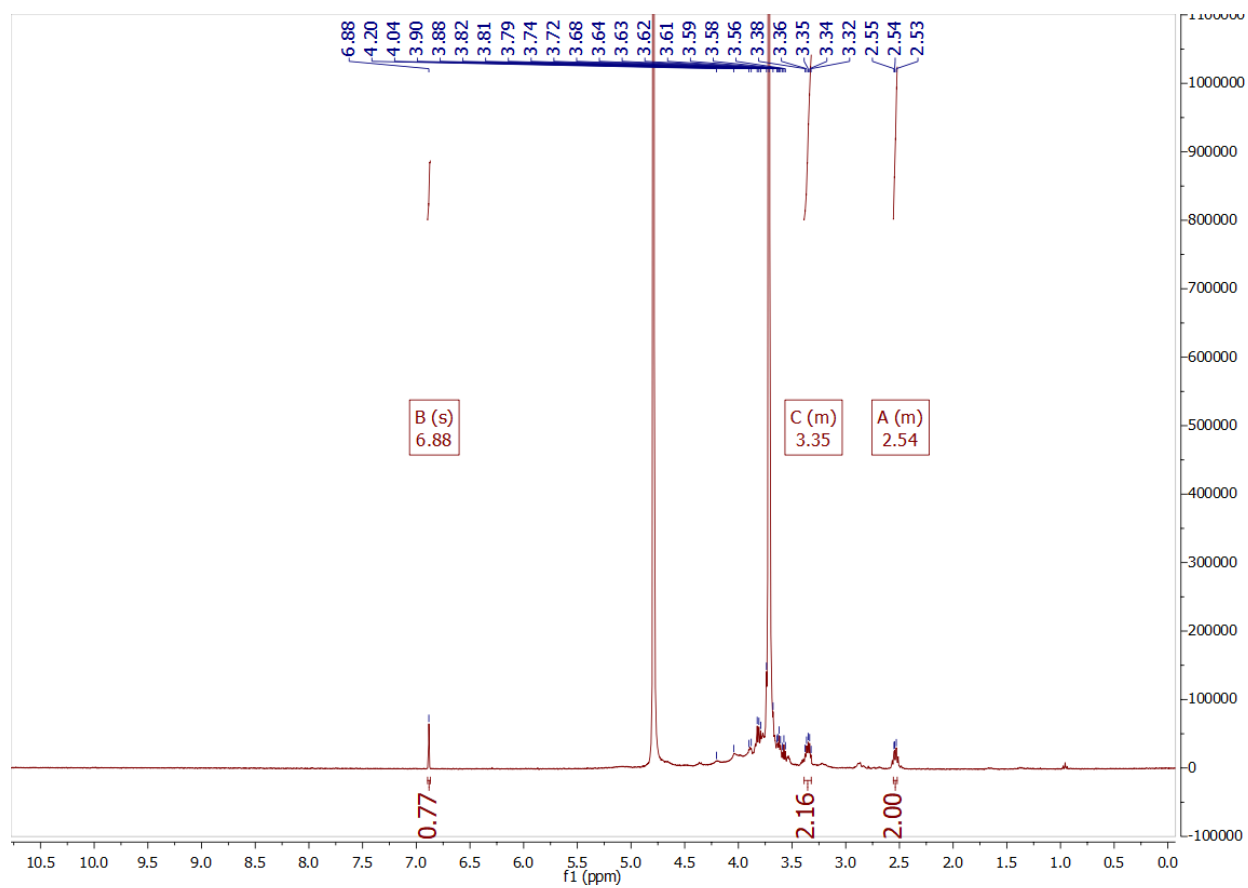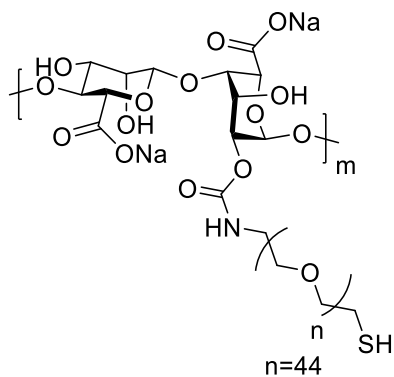
¹H-NMR (400 MHz, Deuterium oxide): δ 4.19 − 3.52 (m, C*H*-Alg + C*H*$_2$-C*H*$_2$-O), 3.23 (t, J = 5.0 Hz, 2H, C*H*$_2$-SH), 2.97 (t, J = 6.1 Hz 2H, C*H*$_2$-NH-C(O)-O) ppm.

¹H-NMR spectrum of **Alg-SH**

Alg-ACA

n=22
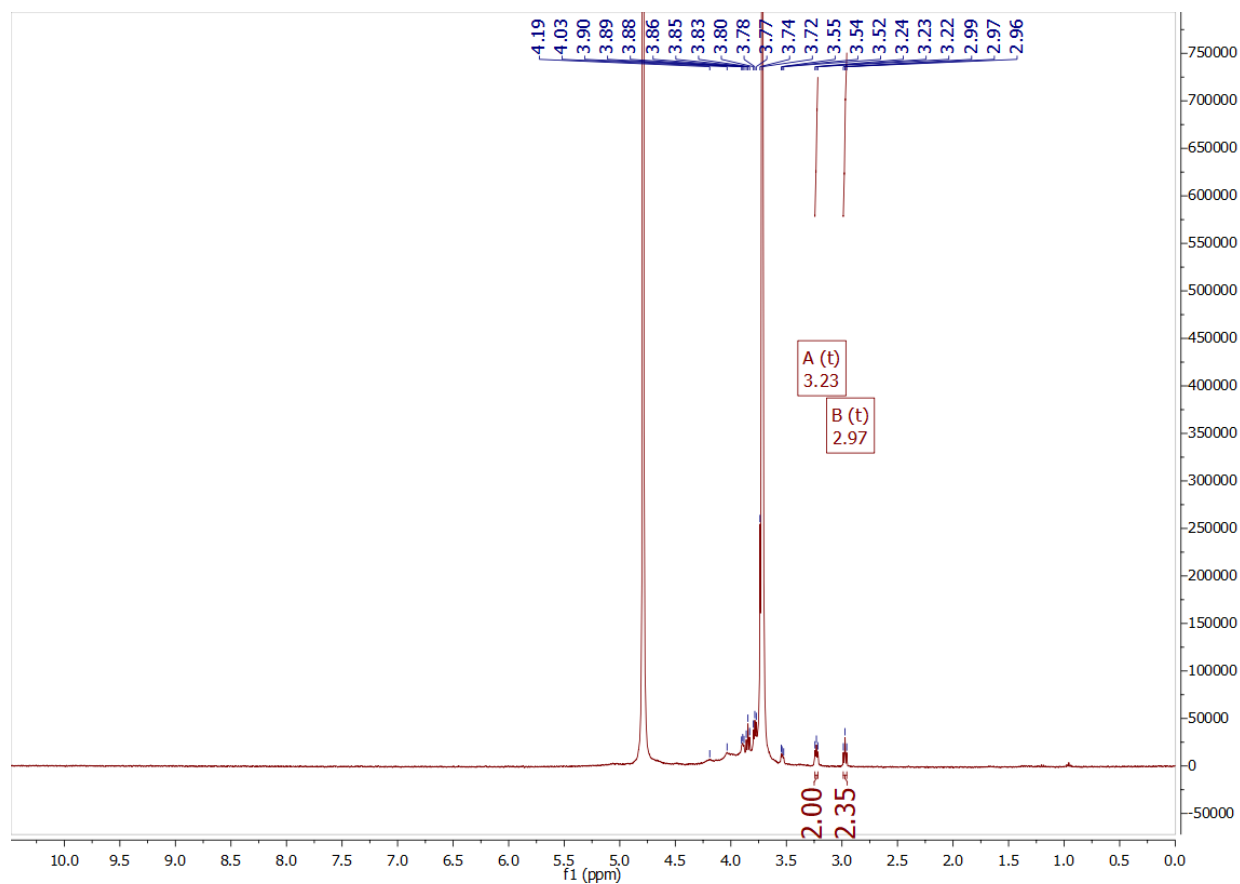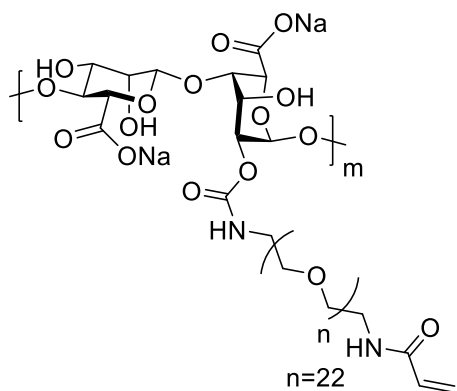
¹H-NMR (400 MHz, Deuterium oxide): δ 6.33 − 6.19 (m, 2H, CH_2-CH-C(O) + CH_2-CH-C(O)), 5.79 (dd, J = 9.9, 1.6 Hz, 1H, CH_2-CH-C(O)), 4.22 − 3.67 (m, CH-Alg + CH_2-CH_2-O), 3.49 (t, *J* = 5.2 Hz 2H, CH_2-NH-C(O)-O), 3.23 (m, CH_2-PEG) ppm.

¹H-NMR spectrum of **Alg-ACA**
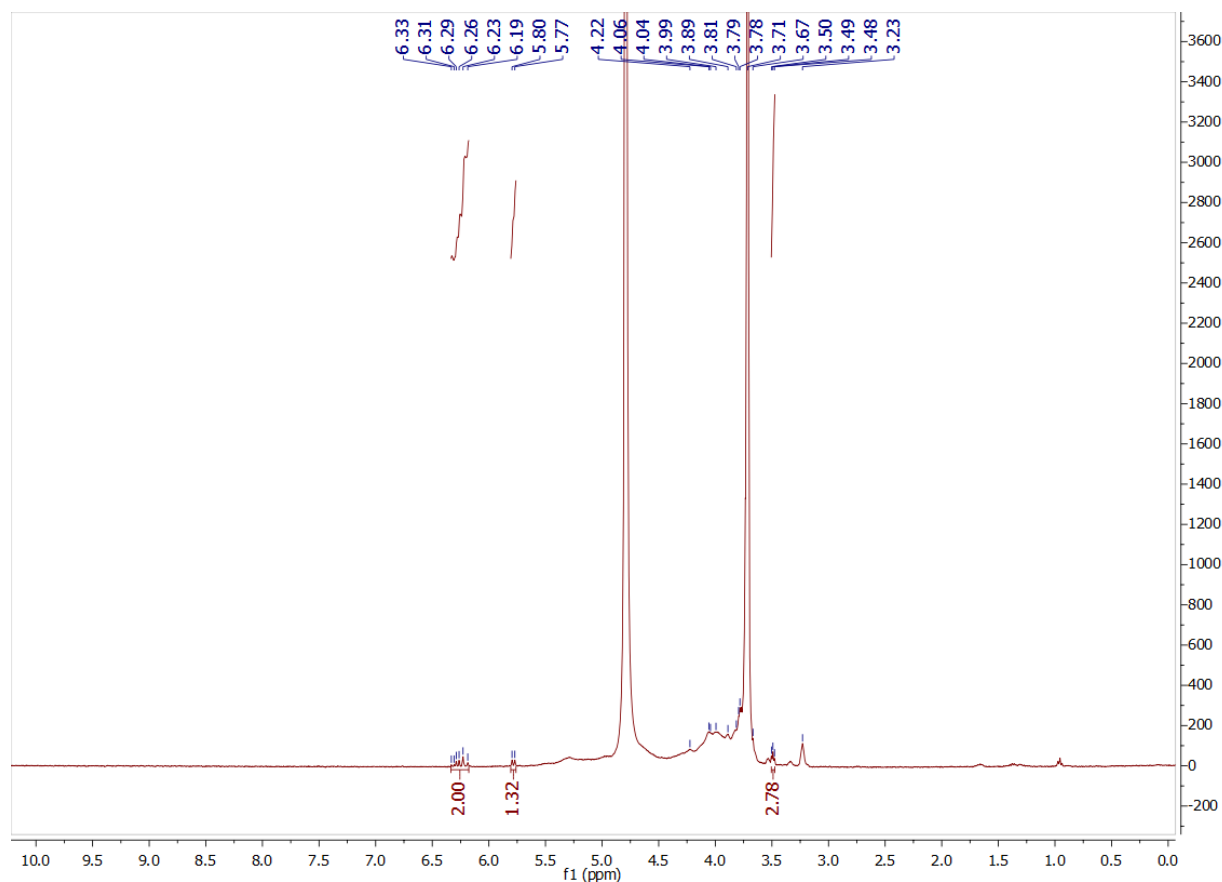
5.3.   Grafting degree determination

If the NMR spectra results in distinguishable signals derived from alg and the PEG derivative, integration under the specific peaks of the 1D ¹H-NMR spectra was used to determine the grafting degree.

To overcome difficulties resulting from signal overlaps, the following procedure was carried out: 1D ¹H-NMR of alg-PEG derivatives (Alg-ACR, Alg-MAL, Alg-SH) was run at 800 MHz with a repetition delay of 5 s as ¹H-longitudinal relaxation time constants (T_1) of PEG materials and alg were measured to be $T_1 < 1$ s. Line broadening was set to 0.3 Hz. The baseline was automatically corrected with the Bruker Topspin routine, using a degree 5 polynomial. The percentage of grafting was estimated by comparison of integration of ¹H resonances of PEG fragment (176 and 88 protons) and alg unit (five protons). Because of overlap, separation between PEG and alg resonances was performed by deconvolution with Lorentzian functions using Bruker Topspin curve fitting and the line-shape analysis tool.
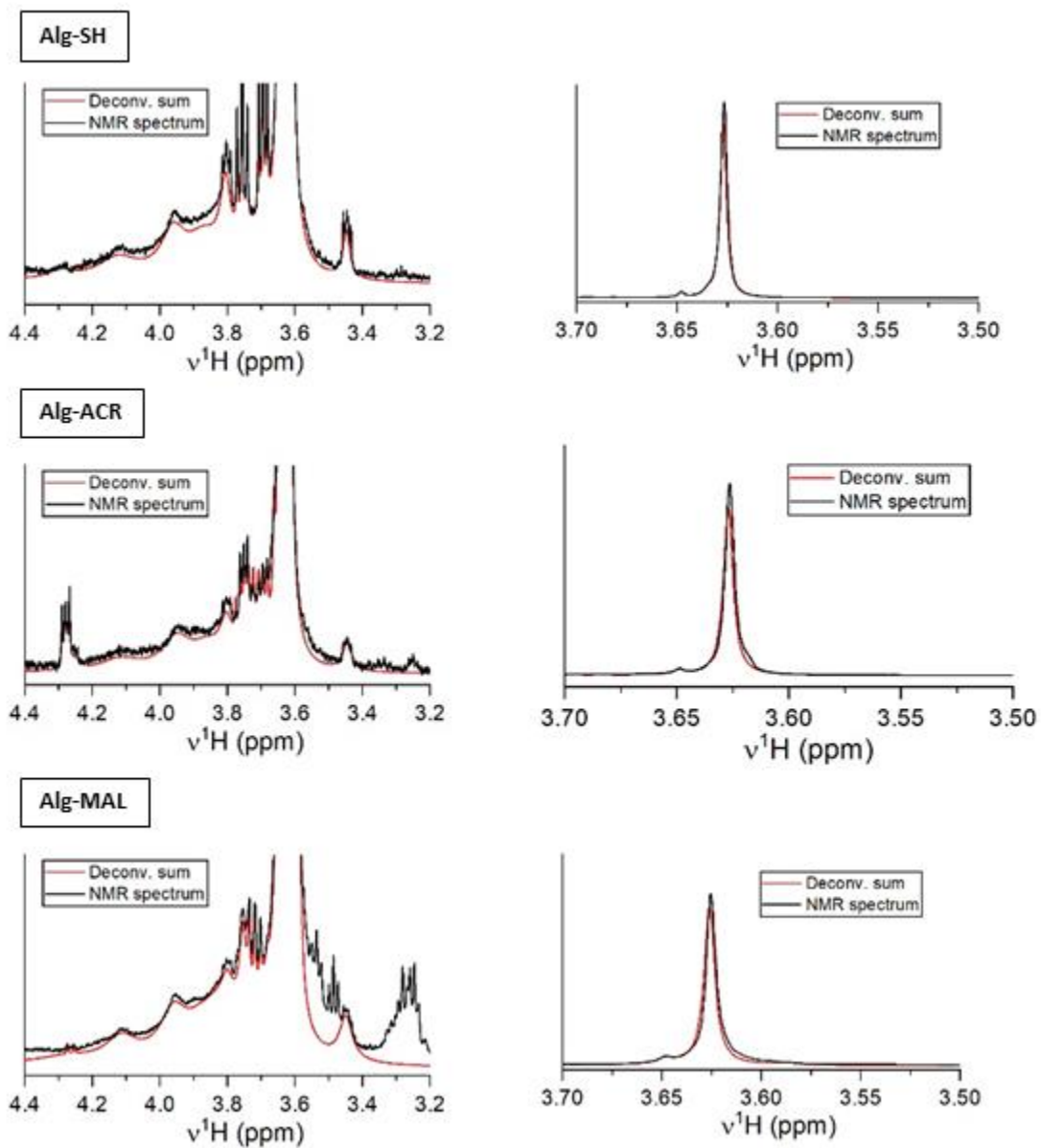
Superimposition of deconvoluted spectra and raw ¹H NMR data. Left row, zoom at alginate scale; right row, zoom at PEG scale.

5.4. Synthesis of PEGylated ketoprofen and grafting on alg
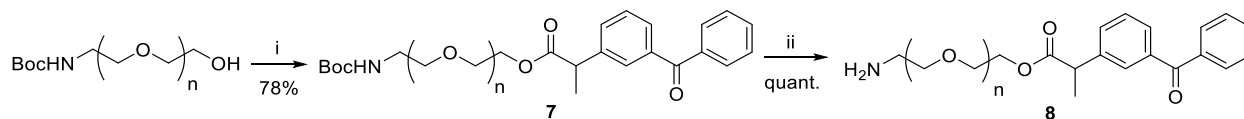
Scheme 5.2. Synthesis of PEGylated ketoprofen. Reagents and conditions: i) DCC, DMAP, DCM, rt, 12 h ii) HCl (4N in dioxane), rt, 2 h.

Boc-PEG-KET (7)
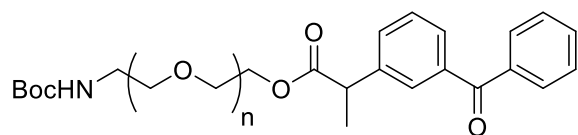
BocNH-PEG(2K)-OH (0.234 g, 0.111 mmol, 1.0 equiv) was dissolved in DCM (2 mL). Ketoprofen (29 mg, 0.112 mmol, 1.01 equiv), DCC (0.025 mg, 0.1224 mmol, 1.1 equiv) and DMAP (1 mg, 0.011 mmol, 0.1 equiv) were added to the reaction mixture. The reaction was stirred at 23 °C for 12 h. After concentration under reduced pressure, the crude residue was purified by FCC (DCM:MeOH = 30:1→10:1) to afford Boc-PEG-KET **7** as a white solid (0.202 g, 0.087 mmol, 78%).

^{1}H NMR (400 MHz, CDCl$_3$): δ 7.81 – 7.42 (m, 9H, 9 × Ar-*H*), 4.29 – 4.17 (m, 2H, C*H*$_2$- NHBoc), 3.84 – 3.80 (m, 2H, C*H*$_2$-OC(O)), 3.73 – 3.52 (s, 180H, C*H*$_2$, PEG), 3.48 – 3.45 (m, 1H, C*H*-Me), 3.32 – 3.29 (m 2H, C*H*$_2$-CH$_2$O), 1.75 (bs, 1H, N*H*), 1.54 (d, J = 7.2 Hz, 3H, CH$_3$), 1.44 (s, 9H, CH$_3$(Boc)) ppm.

¹H-NMR spectrum of **7**
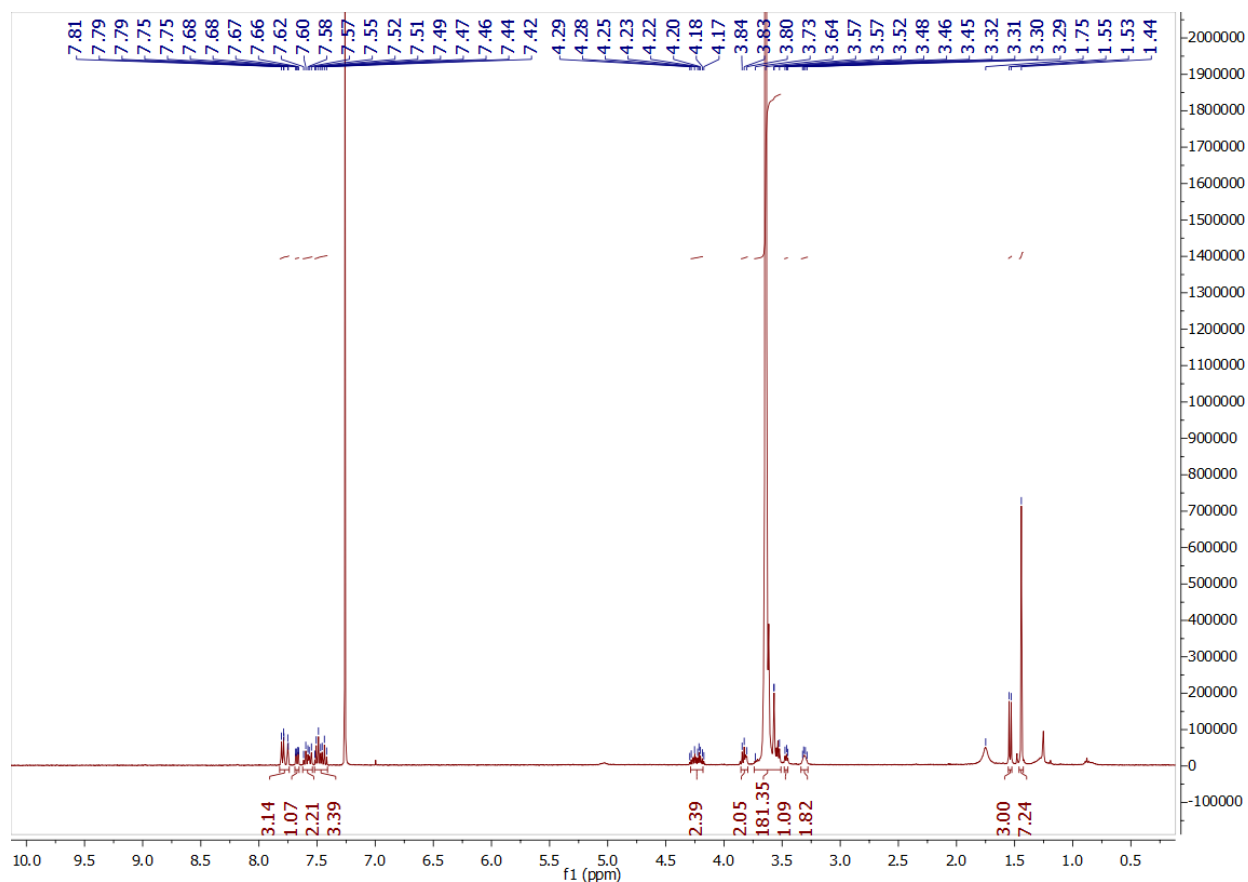
Amine-PEG-KET (8)
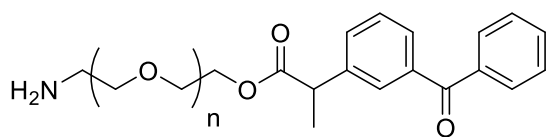
Boc-PEG-KET **7** (0.165 g, 0.071 mmol, 1.0 equiv) was dissolved in a solution of HCl 4N in dioxane (2 mL) and the reaction mixture was stirred at rt until complete disappearance of the starting material (2-3 h, monitored by TLC). The volatiles were removed under air flow and the product was dried in vacuo to afford amine-PEG-KET (**8**) as a beige, amorphous solid (162 g, quant.), which was used without further purification.

¹H NMR (400 MHz, CDCl₃): δ 7.81 − 7.42 (m, 9H, 9 × Ar-*H*), 4.29 − 4.17 (m, 2H, C*H₂*-NH₂), 3.94 (s, 2H, C*H₂*-OC(O)), 3.86 − 3.57 (s, 180H, PEG), 3.47 − 3.45 (m, 1H, C*H*-CH₃), 3.18 (s, 2H, C*H₂*-CH₂O), 1.54 (d, J = 7.2 Hz, 3H, CH₃) ppm.

111

¹H-NMR spectrum of **8**
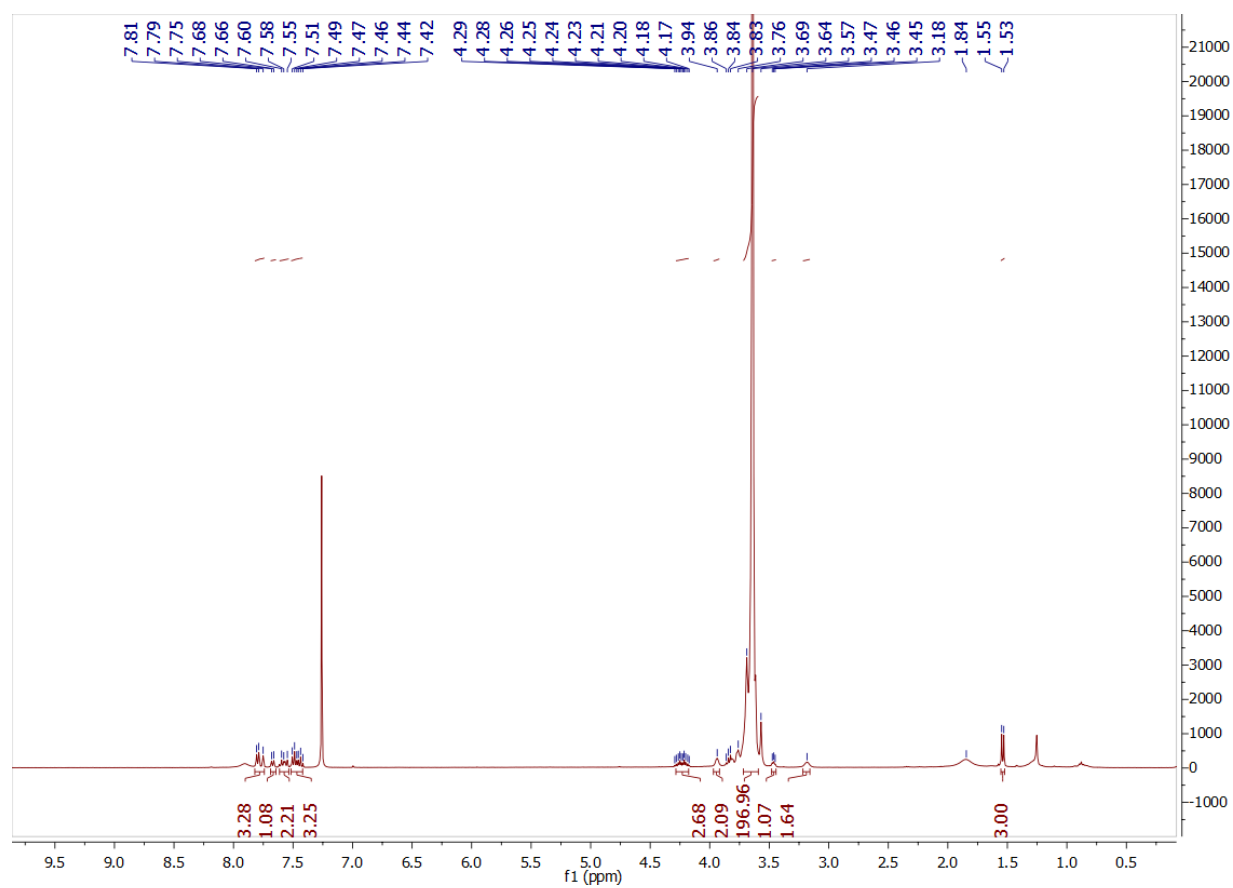
Alg-KET (9)
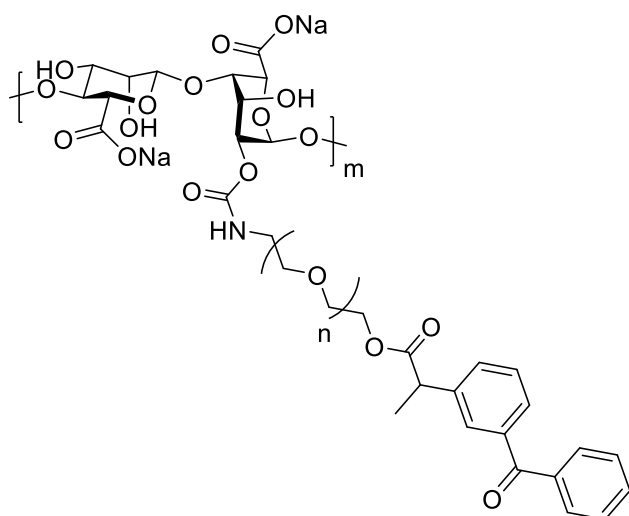
For grafting amine PEGylated ketoprofen **8** on the alginate, the same protocol was implemented as presented in Section 5.3 under "General procedure for the functionalization of TBA-alg with PEG derivatives".

¹H NMR (400 MHz, Deuterium oxide): δ 7.85 – 7.58 (m, Ar-*H*), 4.26 – 3.50 (m, C*H*-Alg + C*H₂*-PEG), 3.23 (m, C*H₂*-NHC(O)), 1.53 (d, J = 7.2 Hz, CH₃) ppm.

¹H-NMR spectrum of **9**

DOSY spectrum of **9**

Bayesian DOSY Transform
FN2.105DOSY2.5.ser
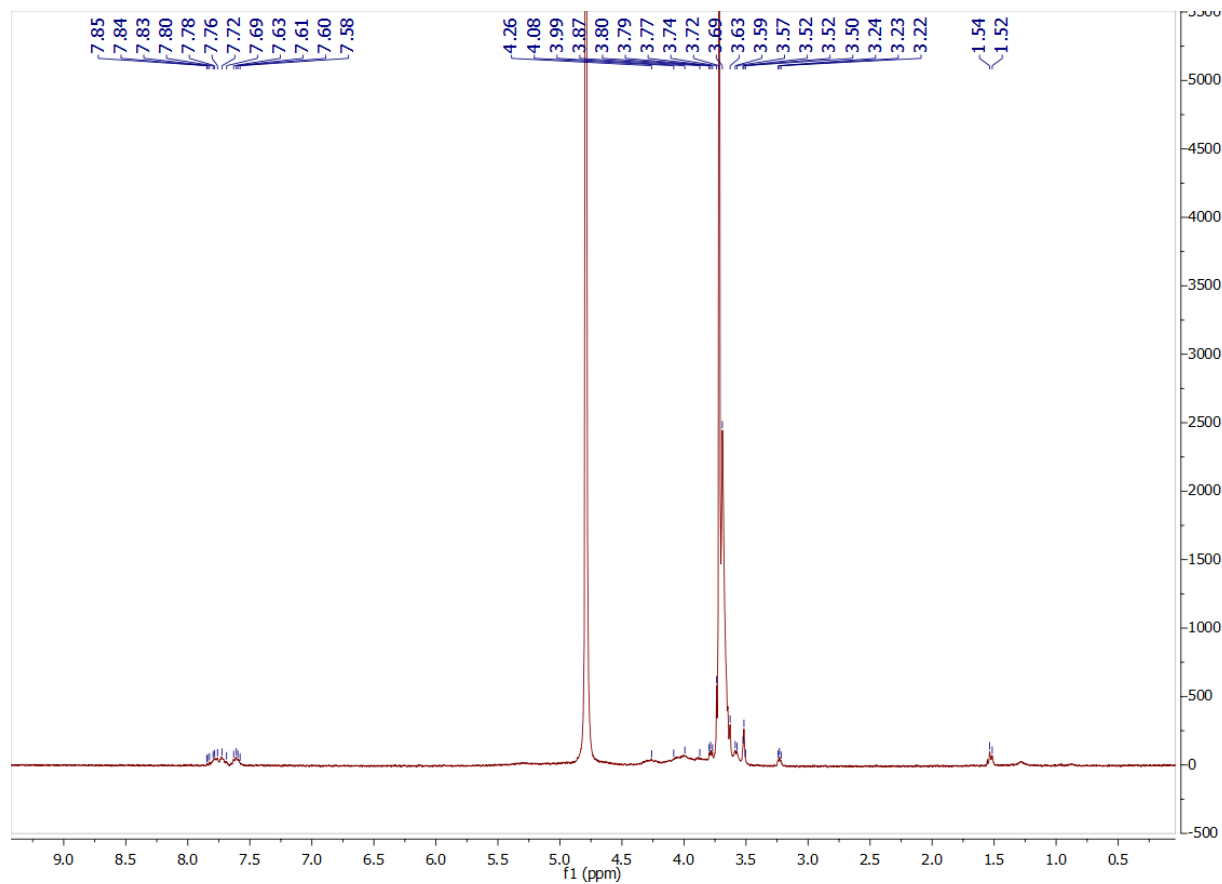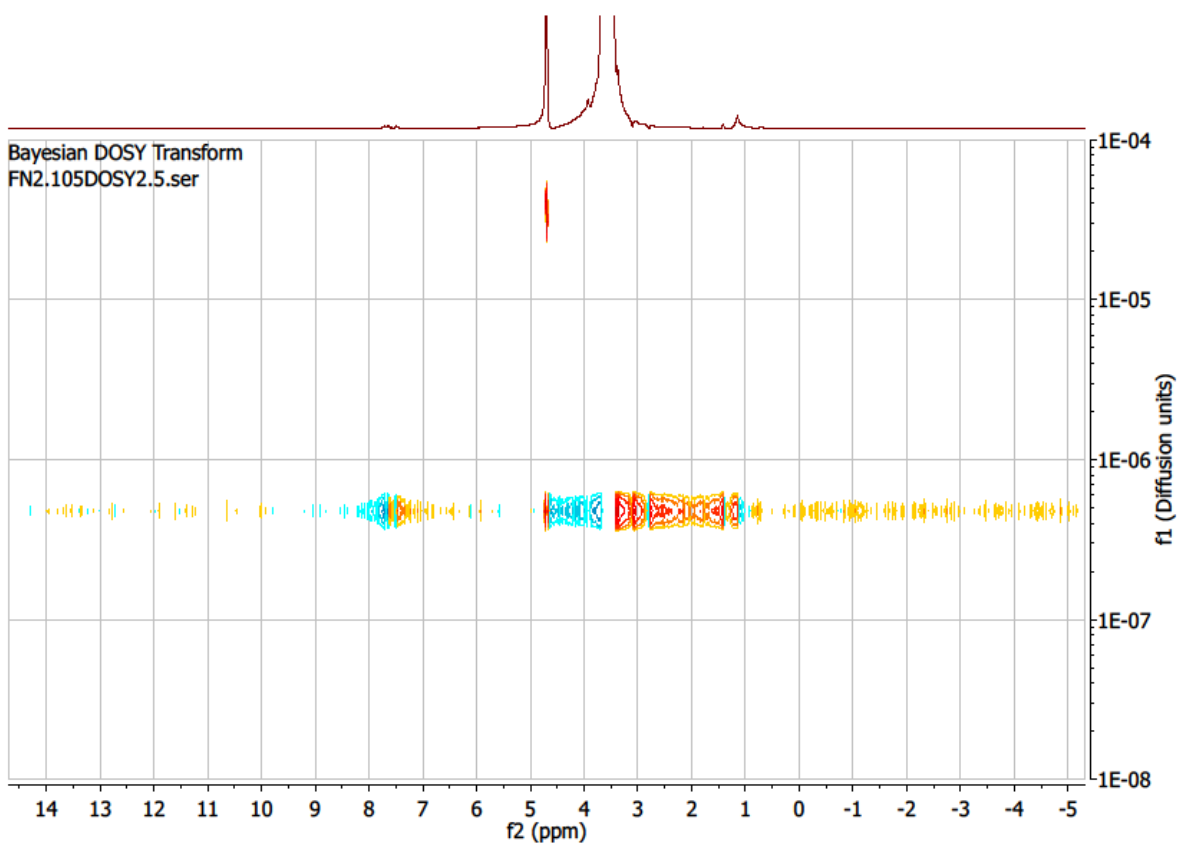
5.5. Synthesis of Pirfenidone derivatives and grafting on alg
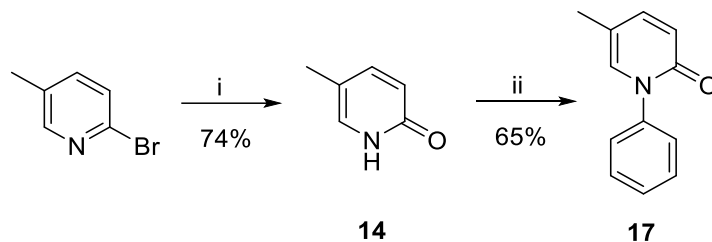
Scheme 5.3. Preparation of Pirfenidone. Reagents and conditions: i) 1. KO^{t}Bu, 2-methylbutan-2-ol, 40 h, 100 °C 2. HCOOH, 24 h ii) Bromobenzene, CuI, K$_2$CO$_3$, DMF, reflux, 12 h.

5-methylpyridin-2(1*H*)-one (14)
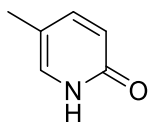
2-Bromo-5-methylpyridine (1.0 equiv, 17.4 mmol, 3.00 g) was dissolved in 2-methylbutan-2-ol (50 mL) under argon, and KO^{t}Bu (10 equiv, 174.4 mmol, 19.5 g) was added. The mixture was heated to 100 °C and stirred for 40 h. The solvent was removed under vacuo and the residue was dissolved in HCOOH (25 mL). After stirring for 24 h at rt, aq. KOH solution (2.4 M) was added until pH=6. The product was extracted with CHCl$_3$ (3×), and the combined organic phases were dried over MgSO$_4$, filtered and concentrated in vacuo. The crude product was purified by FCC (MeOH/DCM 1:25) to afford **14** as light brown powder (12.9 mmol, 1.414 g, 74%). The analytical data were in accordance with previously reported data.[273]

¹H NMR (400 MHz, CDCl$_3$): δ 7.34 (dd, J = 9.2, 2.6 Hz, 1H, C*H*-C(O)), 7.15 (m, 1H, C*H*-NH), 6.55 (d, J = 9.3 Hz, 1H, C*H*-CH-C(O)), 2.10 (s, 3H, C*H$_3$*) ppm.

¹H-NMR spectrum of **14**
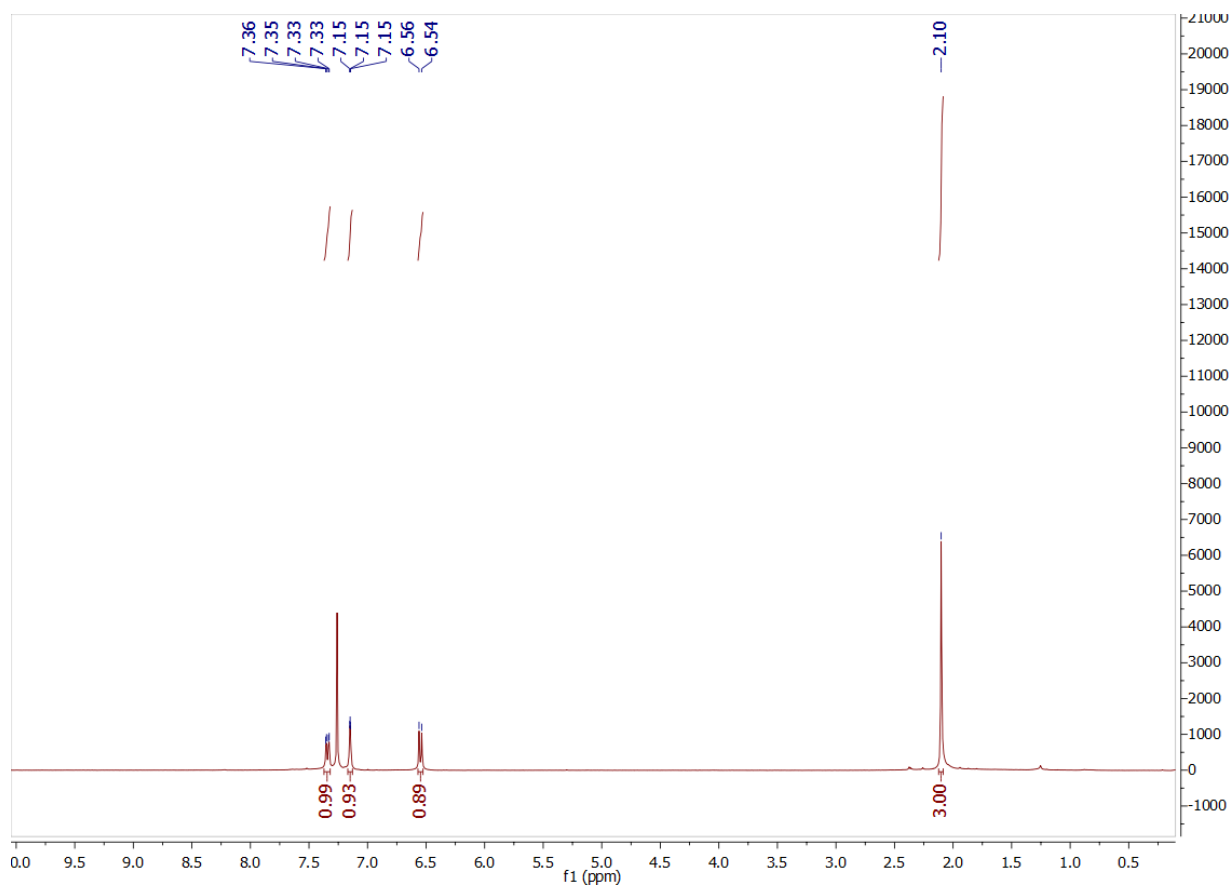
Pirfenidone (PFD) (17)
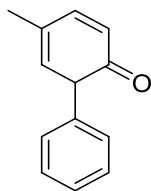
Bromobenzene (1.2 equiv, 1.737 mmol, 273 mg, 183 µL) and compound **14** (1 equiv, 1.448 mmol, 158 mg) were dissolved in anhydrous DMF (4 mL). CuI (0.2 equiv, 0.289 mmol, 55 mg) and K_2CO_3 (2 equiv, 2.896 mmol, 400 mg) were added. The reaction mixture was stirred at reflux for 12 h. The mixture was cooled down to rt, and quenched with the addition of sat. aq. $NaHCO_3$. The product was extracted with EtOAc (3×). The organic layers were combined, dried over $MgSO_4$, filtered and concentrated in vacuo. The crude product was purified by FCC (MeOH/DCM 1:50) to afford **PFD** as light yellow solid (0.945 mmol, 175 mg, 65%).

IR (neat): 3649, 2926, 2519, 2159, 2029, 1976, 1656, 1605, 1494, 1452, 1086, 825, 758 cm⁻¹.

¹H NMR (400 MHz, CDCl₃): δ 7.50 – 7.46 (m, 2H, 2 × Ar-*H*), 7.42 – 7.36 (m, 3H, 3 × Ar-*H*) 7.28 – 7.25 (m, 1H, Ar-*H*), 7.11 (s, 1H, Ar-*H*), 6.61 (d, J = 9.4 Hz, 1H, C*H*-C(O)), 2.10 (s, 3H, C*H₃*) ppm.

¹H-NMR spectrum of **PFD**
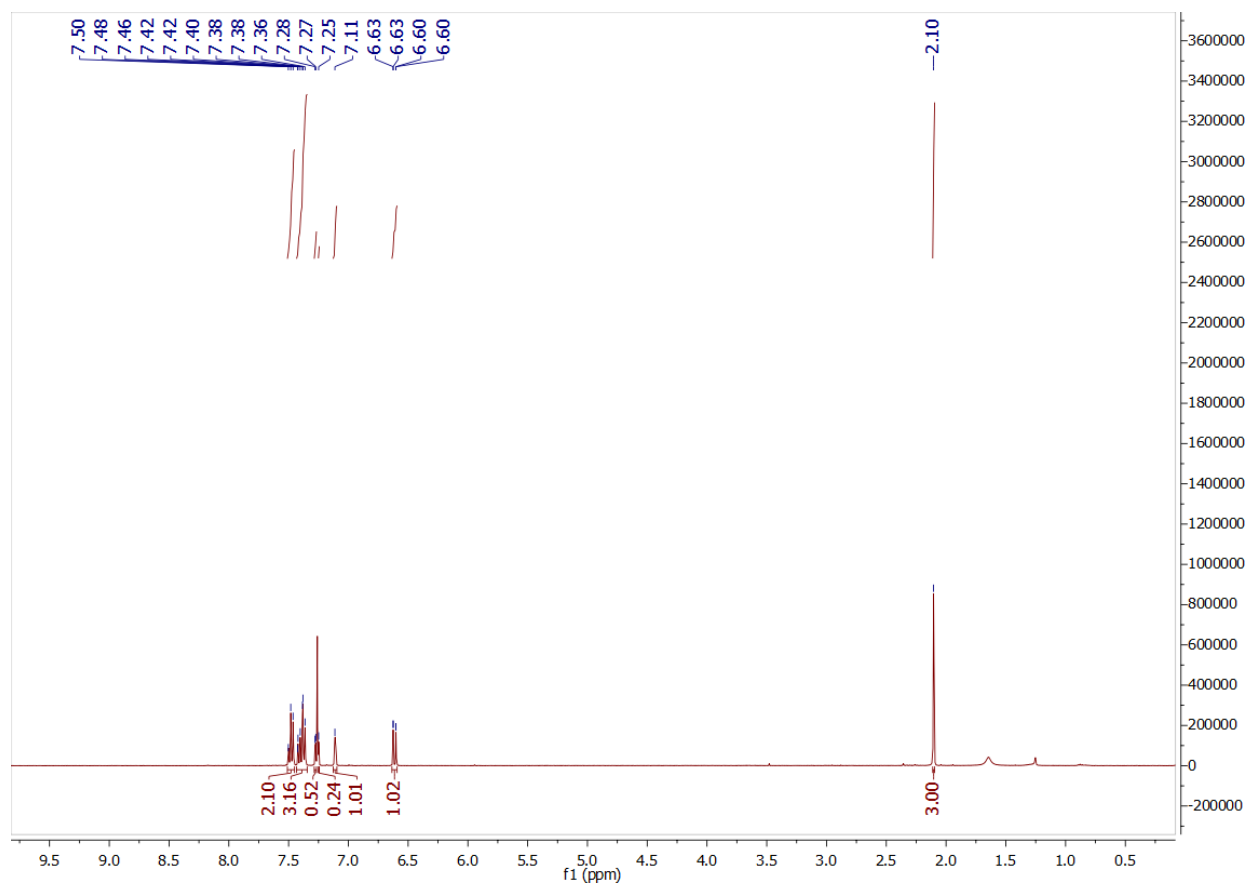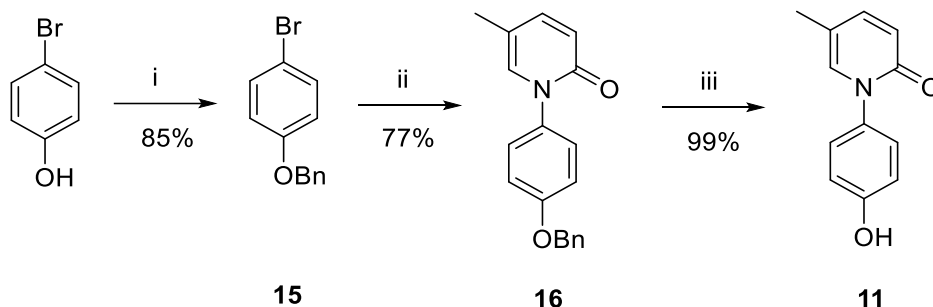
Scheme 5.4. Preparation of compound 11. Reagents and conditions: i) BrBn, NaH (60%), anhydrous DMF, 2 h, rt, ii) 14, CuI, K₂CO₃, anhydrous DMF, 12h, reflux iii) concd. HCl, MeOH/H₂O, concd. H₂SO₄, 4 h, reflux.

1-(benzyloxy)-4-bromobenzene (15)
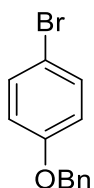
To a stirred solution of sodium hydride (1.2 equiv, 34.7 mmol, 1.387 g, 60%) in anhydrous DMF (40 mL), 4-bromophenol (1 equiv, 28.9 mmol, 5.00 g) was added at 0 °C under argon, and the mixture was stirred for 30 min at this temperature. Benzylbromide (1 equiv, 28.9 mmol, 4.943 g, 3.43 mL) was added, the cooling bath was removed, and the mixture was stirred for 3h at rt. The reaction mixture was treated with sat. aq. NH₄Cl (80 mL) and extracted with EtOAc (3×100 mL). The combined organic layers were dried over MgSO₄, filtered and concentrated in vacuo. The crude product was purified by FCC (PE/EtOAc 50:1) to afford **15** as white crystals (24.7 mmol, 6.5 g, 85%). The analytical data were in accordance with previously reported data.[274]

¹H NMR (400 MHz, CDCl₃): δ 7.42 – 7.33 (m, 7H, Ar-*H*), 6.86 – 6.84 (m, 2H, Ar-*H*), 5.04 (s, 2H, C*H*₂) ppm.

¹H-NMR spectrum of **15**
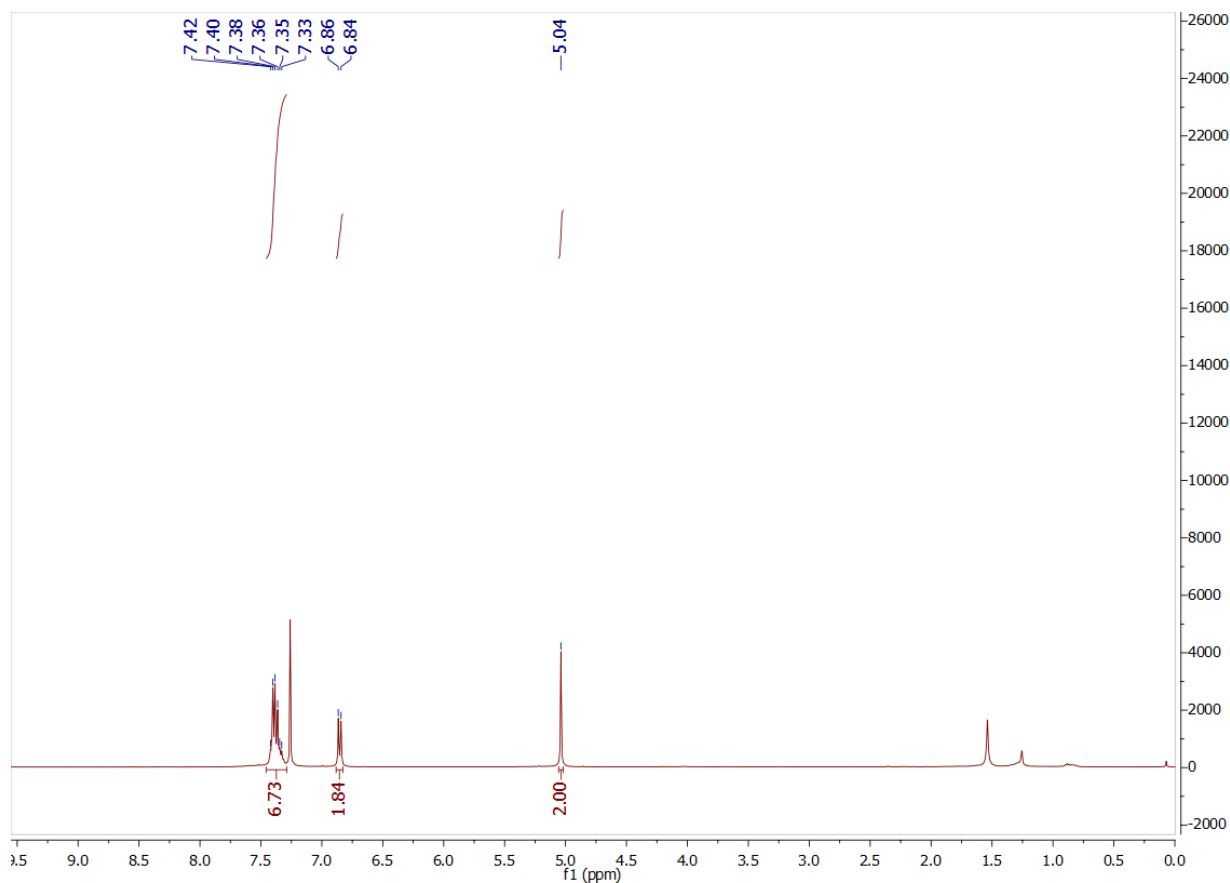
1-(4-(benzyloxy)phenyl)-5-methylpyridin-2(1*H*)-one (16)
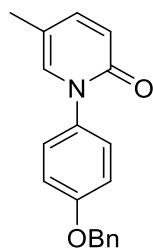
5-Methylpyridin-2(1*H*)-one (**14**) (1 equiv, 12.28 mmol, 1.34 g) and 1-(benzyloxy)-4-bromobenzene (**15**) (1.2 equiv, 14.73 mmol, 4.67 g) were dissolved in anhydrous DMF (30 mL). CuI (0.2 equiv, 2.46 mmol, 0.468 g) and K_2CO_3 (2 equiv, 24.6 mmol. 3.4 g) were added, and the mixture was heated to reflux. After 12 h of reflux, the mixture was cooled down to rt, and quenched with the addition of sat. aq. $NaHCO_3$ solution (25 ml). The product was extracted with EtOAc (3×), the organic layers were combined, dried over $MgSO_4$, filtered, and concentrated in vacuo. The crude product was purified by FCC (PE/EtOAc 1:1 to 1:2 and 1:3) to afford the product as a yellow

solid (9.445 mmol, 2.752 g, 77%). The analytical data were in accordance with previously reported data.[270]

¹H NMR (400 MHz, CDCl₃): δ 7.45 − 7.23 (m, 8H, Ar-*H*), 7.09 (m, 1H, Ar-*H*), 7.06−7.04 (m, 2H, Ar-*H*), 6.60 (d, J = 9.3 Hz, 1H), 5.10 (s, 2H, C*H₂*), 2.09 (s, 3H, C*H₃*) ppm.

¹H-NMR spectrum of **16**
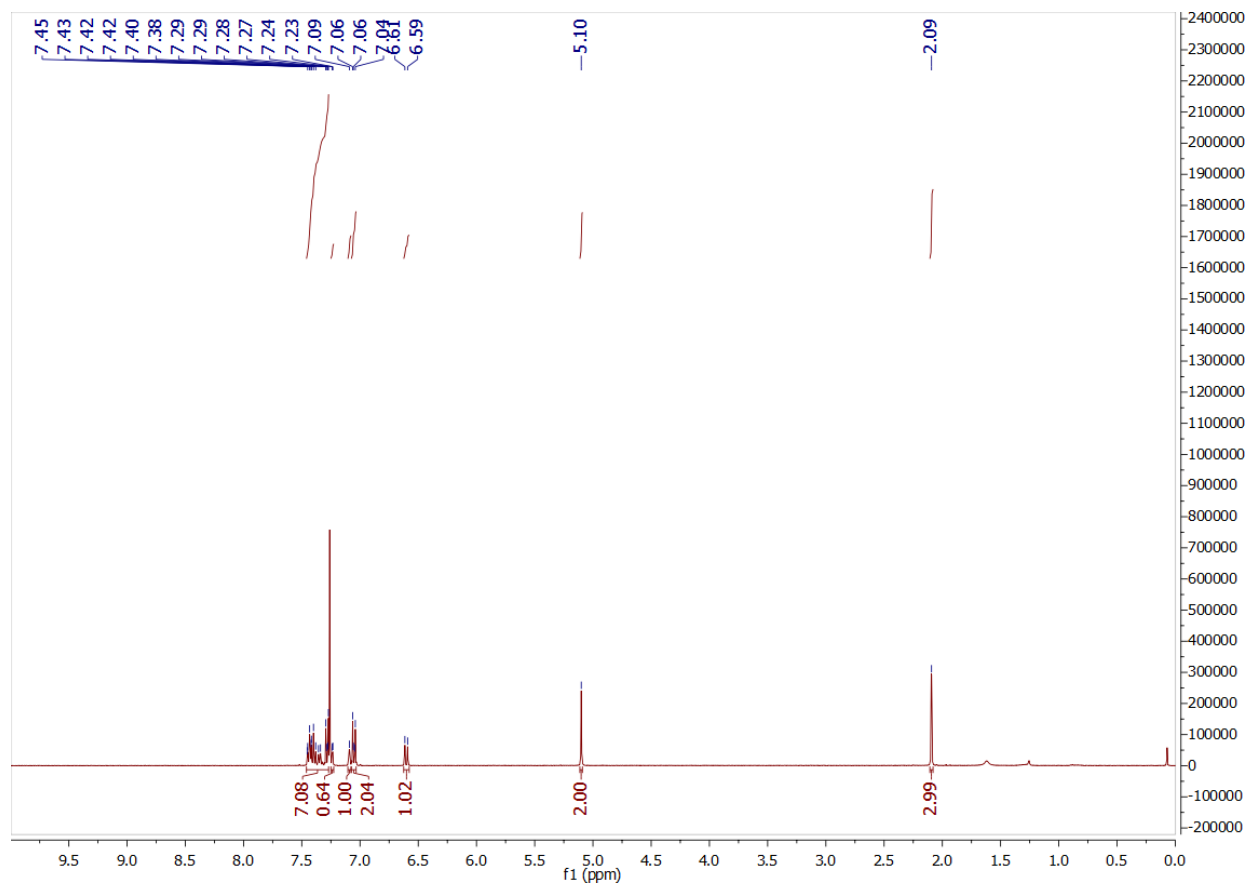
1-(4-hydroxyphenyl)-5-methylpyridin-2(1*H*)-one (11)

120
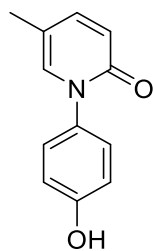
A mixture of 1-(4-(benzyloxy)phenyl)-5-methylpyridin-2(1*H*)-one (**16**) (6.43 mmol, 2.748 g), concentrated HCl (30 mL) in MeOH (30 mL) and H_2O (30 mL) was refluxed for 1 h. Concentrated H_2SO_4 (9 mL) was added, and the mixture was refluxed for an additional 3 h. The reaction mixture was diluted with H_2O (100 mL), and cooled down to rt. An airflow was applied to remove part of the volatiles and help precipitation of the product. The precipitate was collected, washed with cold water (3×), and dried to afford the product as a white solid (9.37 mmol, 1.887 g, 99%). The analytical data were in accordance with previously reported data.[270]

¹H NMR (400 MHz, CDCl₃): δ 7.36 (dd, J = 9.3, 2.6 Hz, 1H), 7.15 (s, 1H), 7.05 – 6.99 (m, 2H), 6.72 – 6.66 (m, 3H), 2.13 (s, 3H, C*H₃*) ppm.

¹H-NMR spectrum of **x**
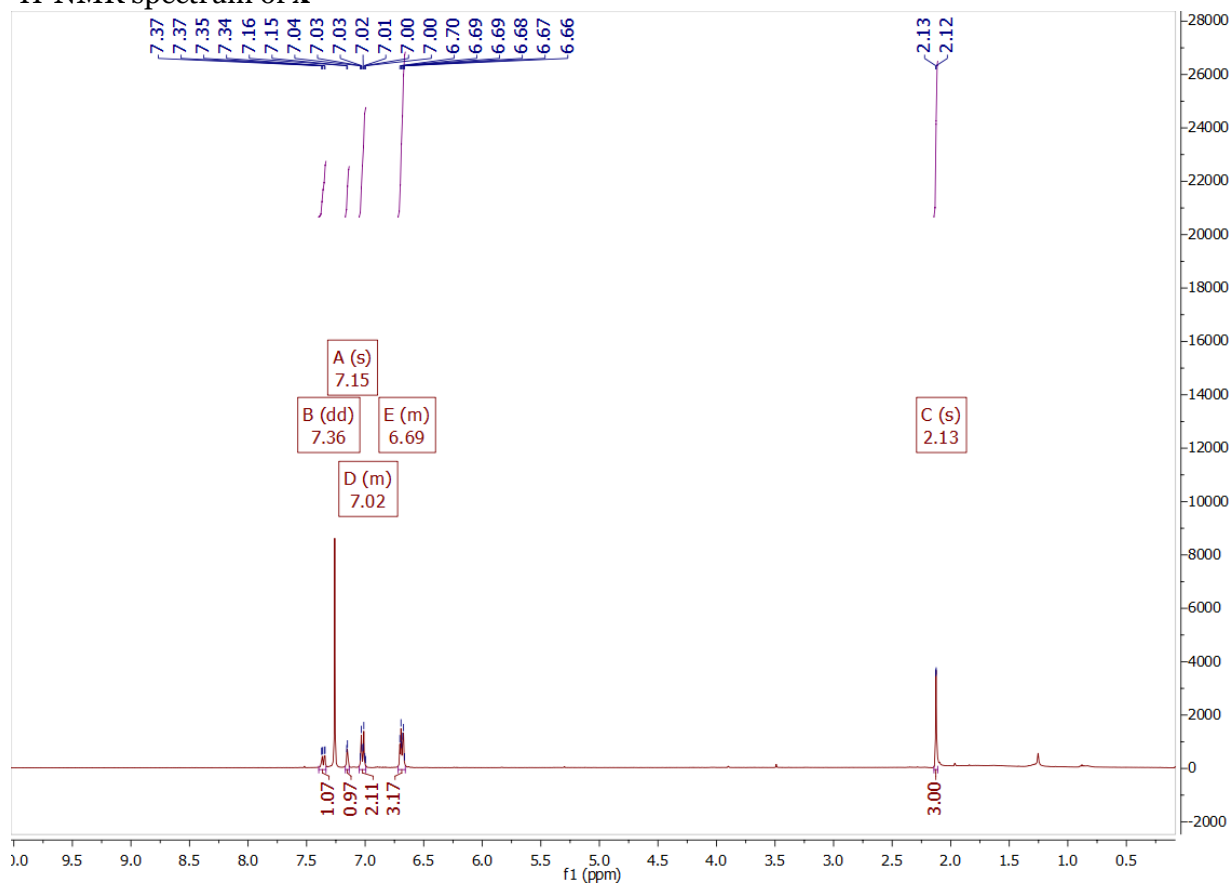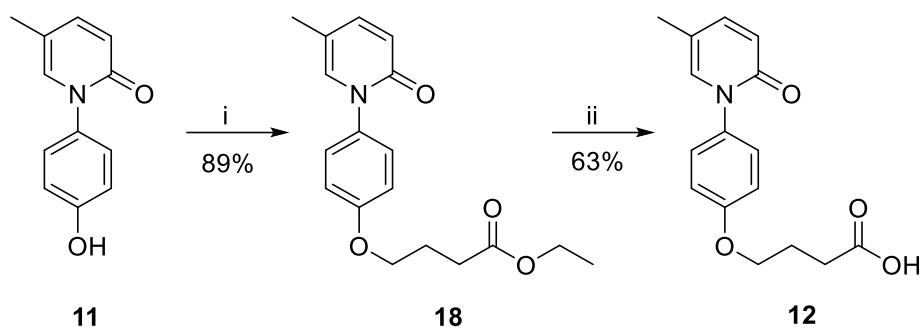
*Scheme 5.5. Preparation of compound **12**. Reagents and conditions: i) Ethyl 4-bromobutyrate, K₂CO₃, DMF, overnight, 80 °C ii) KOH (2M, aqueous), MeOH, 2h, reflux.*

Ethyl 4-(4-(5-methyl-2-oxopyridin-1(2*H*)-yl)phenoxy)butanoate (18)
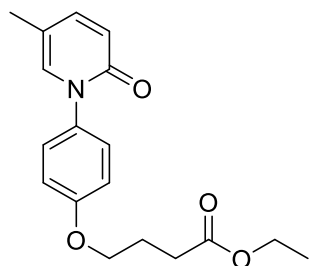
Ethyl 4-bromobutyrate (1.454 g, 7.455 mmol, 1.067 ml, 3 equiv) and K₂CO₃ (515 mg, 3.7275 mmol, 1.5 equiv) were added to a stirred solution of compound **11** (500 mg, 2.485 mmol, 1 equiv) in DMF (8 ml). The reaction mixture was stirred for 12 h at 80 °C. The reaction was quenched by the addition of 0.1M aq. HCl until pH~6 and extracted with EtOAc (3×). The combined organic phases were washed with brine, dried over MgSO₄, filtered and concentrated in vacuo. The crude product was purified by FCC (MeOH/DCM 1:40) to afford **18** as a white solid (2.2017 mmol, 696.3 mg, 89%).

HRMS-ESI: *m/z* 316.1549 (calcd. for C18H21NO4); 316.1546 (M+H) (found).

IR (neat): 2925, 1731, 1673, 1600, 1532, 1510, 1247, 1173, 1041, 828 cm⁻¹.

¹H NMR (400 MHz, CDCl₃) δ 7.28 − 7.24 (m, 3H, 3 × Ar-*H*), 7.11 − 7.08 (m, 1H, Ar-*H*), 6.98 − 6.94 (m, 2H, 2 × Ar-*H*), 6.62 (d, J = 9.3 Hz, 1H, Ar-*H*), 4.15 (q, J = 7.1 Hz, 2H, C*H*₂-CH₃), 4.04 (t, J = 6.1 Hz, 2H, O-C*H*₂-CH₂), 2.52 (t, J = 7.3 Hz, 2H, C*H*₂-C(O)-O), 2.16 − 2.08 (m, 5H, CH₂-C*H*₂-CH₂, C*H*₃), 1.27 (t, J = 7.1 Hz, 3H, CH₂-C*H*₃) ppm.

¹H-NMR spectrum of **18**
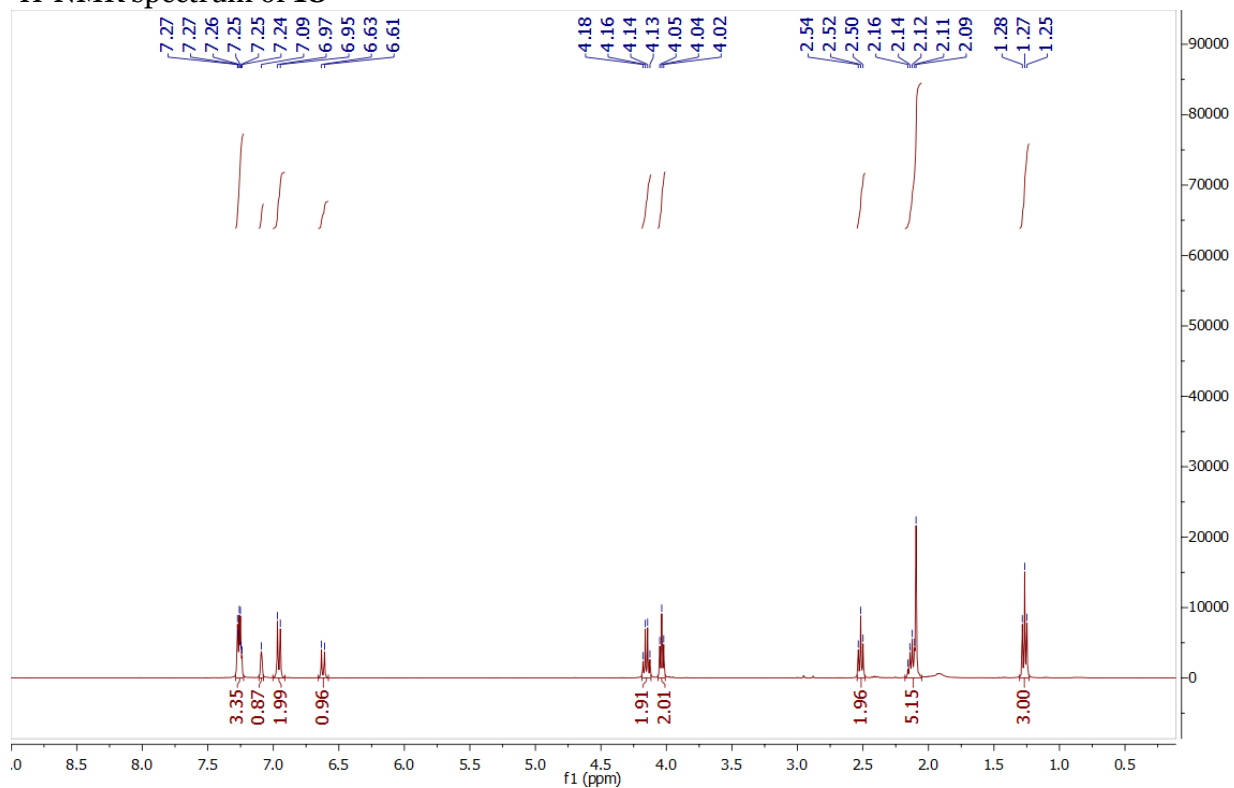
¹³C NMR (101 MHz, CDCl₃): δ 173.3 (C(O)-O), 162.1 (C(O)), 158.7 (C-O-CH₂), 142.7 (C_{ar}), 135.8 (C_{ar}), 134.1 (C_{ar}), 127.8 (2 × C_{ar}), 121.4 (C_{ar}), 115.2 (2 × C_{ar}), 115.0 (C_{ar}), 67.2 (CH₂), 60.6 (CH₂), 30.9 (CH₂), 24.7 (CH₂), 17.1 (CH₃), 14.4 (CH₃).

¹³C-NMR spectrum of **18**
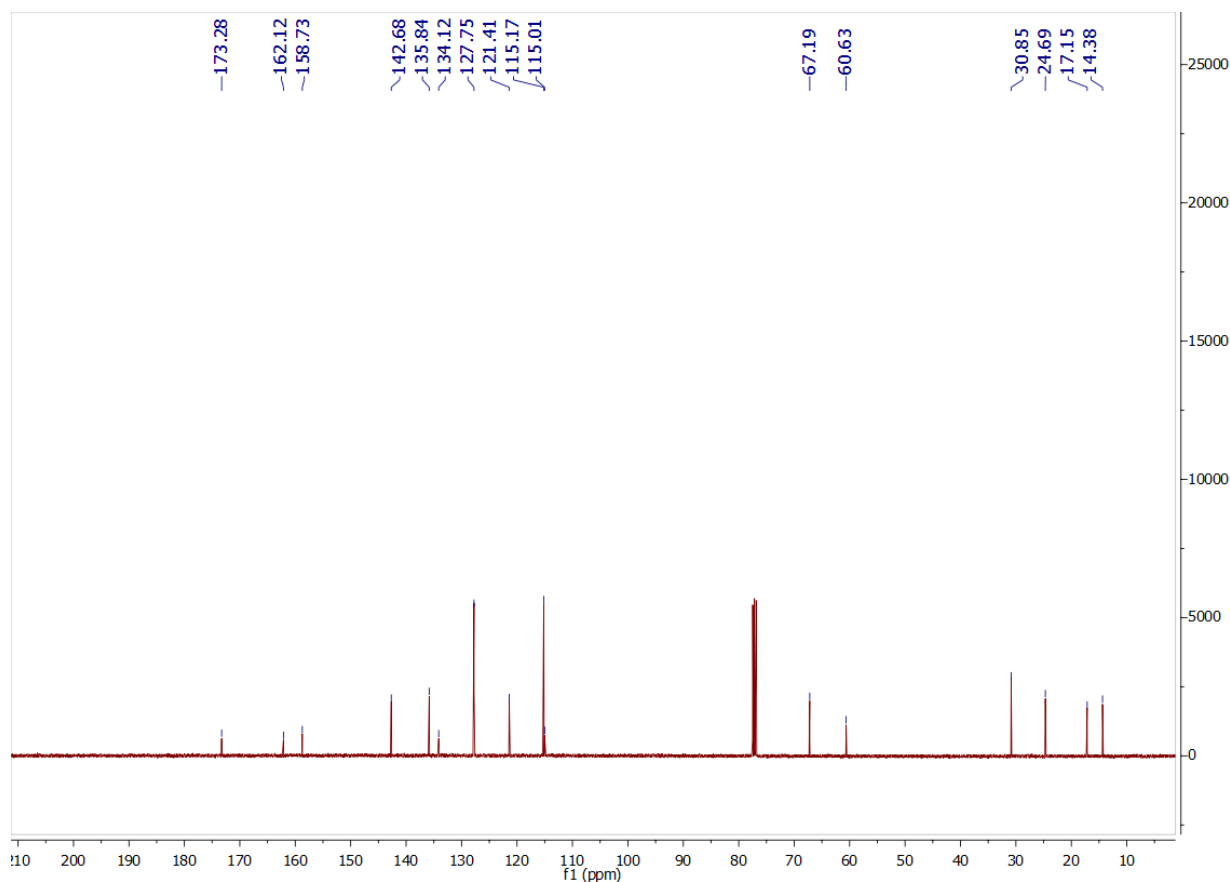
4-(4-(5-methyl-2-oxopyridin-1(2*H*)-yl)phenoxy)butanoic acid (12)
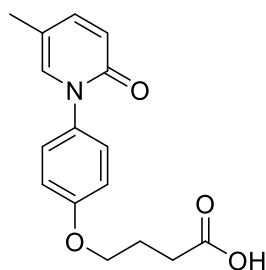
Compound **12** (529 mg, 1.677 mmol, 1 equiv) was dissolved in MeOH (20 mL). 2.4 M aq. KOH solution (235.2 mg, 4.1925 mmol, 1.75 mL, 2.5 equiv) was added dropwise. The reaction mixture was refluxed for 2 h. The volatile organic solvent was removed in vacuo, and the remaining aq. phase was acidified to pH=1 by the addition of 1M aq. HCl solution. The precipitate was collected by filtration, washed with cold water (3×) and dried completely under vacuo to afford the product as a white powder (1.058 mmol, 304.1 mg, 63%).

HRMS-ESI: *m/z* 288.1236 (calcd. for C18H21NO4); 288.1237 (M+H) (found).

IR (neat): 2872, 1715, 1509, 1454, 1294, 1245, 1158, 1042, 941, 829 cm⁻¹.

¹H NMR (400 MHz, CDCl₃): δ 7.31 − 7.25 (m, 3H, 3 × Ar-*H*), 7.13 − 7.10 (m, 1H, Ar-*H*), 6.98 − 6.94 (m, 2H, 2 × Ar-*H*), 6.68 (d, J = 9.3 Hz, 1H, Ar-*H*), 4.04 (t, J = 6.1 Hz, 2H, O-C*H*₂-CH₂), 2.55 (t, J = 7.2 Hz, 2H, C*H*₂-COOH), 2.15 − 2.09 (m, 5H, CH₂-C*H*₂-CH₂, C*H*₃) ppm.

¹H-NMR spectrum of **12**
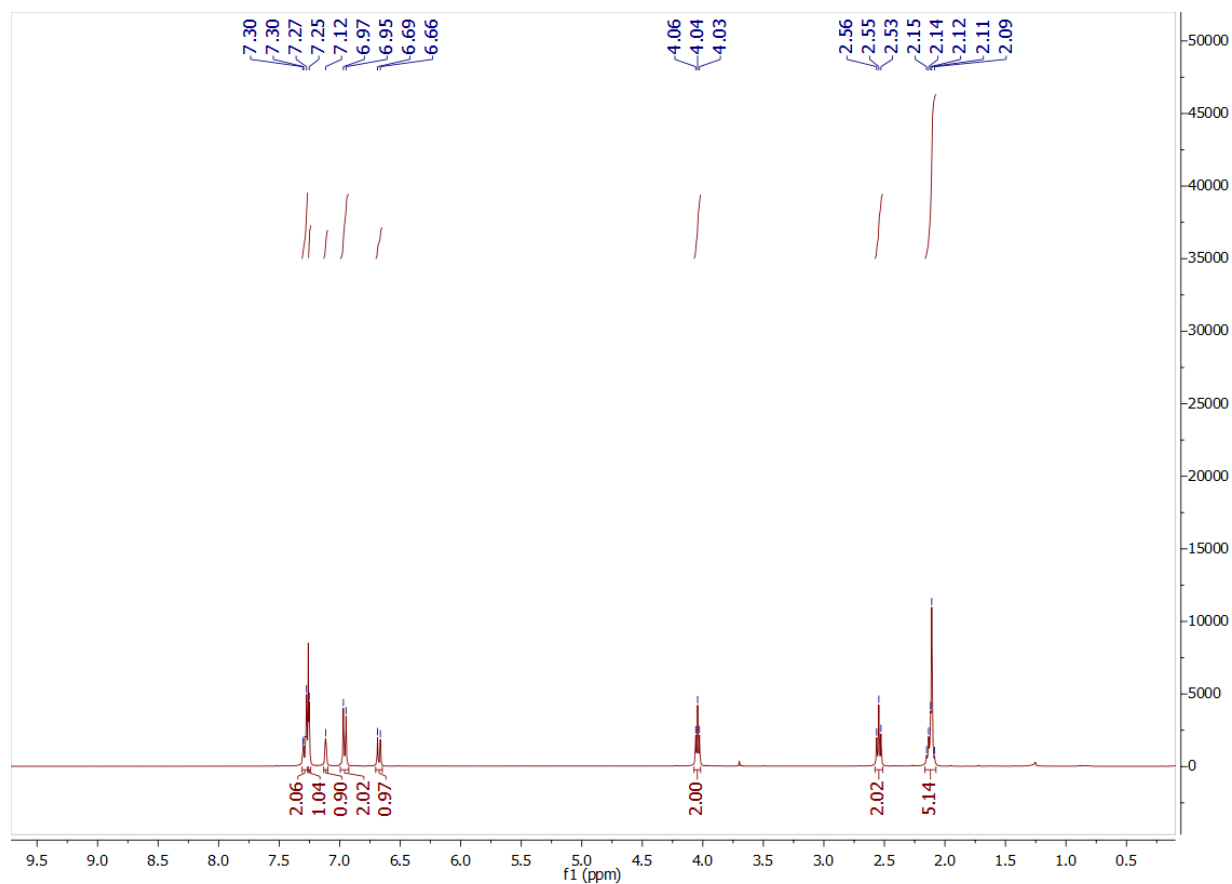
¹³C NMR (101 MHz, CDCl₃): δ 176.6 (*C*OOH), 162.3 (*C*(O)), 158.8 (*C*-O-CH₂), 143.0 (*C*ₐᵣ), 135.9 (*C*ₐᵣ), 134.0 (*C*ₐᵣ), 127.8 (2 × *C*ₐᵣ), 121.3 (*C*ₐᵣ), 115.6 (*C*ₐᵣ), 115.2 (2 × *C*ₐᵣ), 67.1 (*C*H₂), 30.4 (*C*H₂), 24.5 (*C*H₂), 17.2 (*C*H₃).

125

¹³C-NMR spectrum of **12**
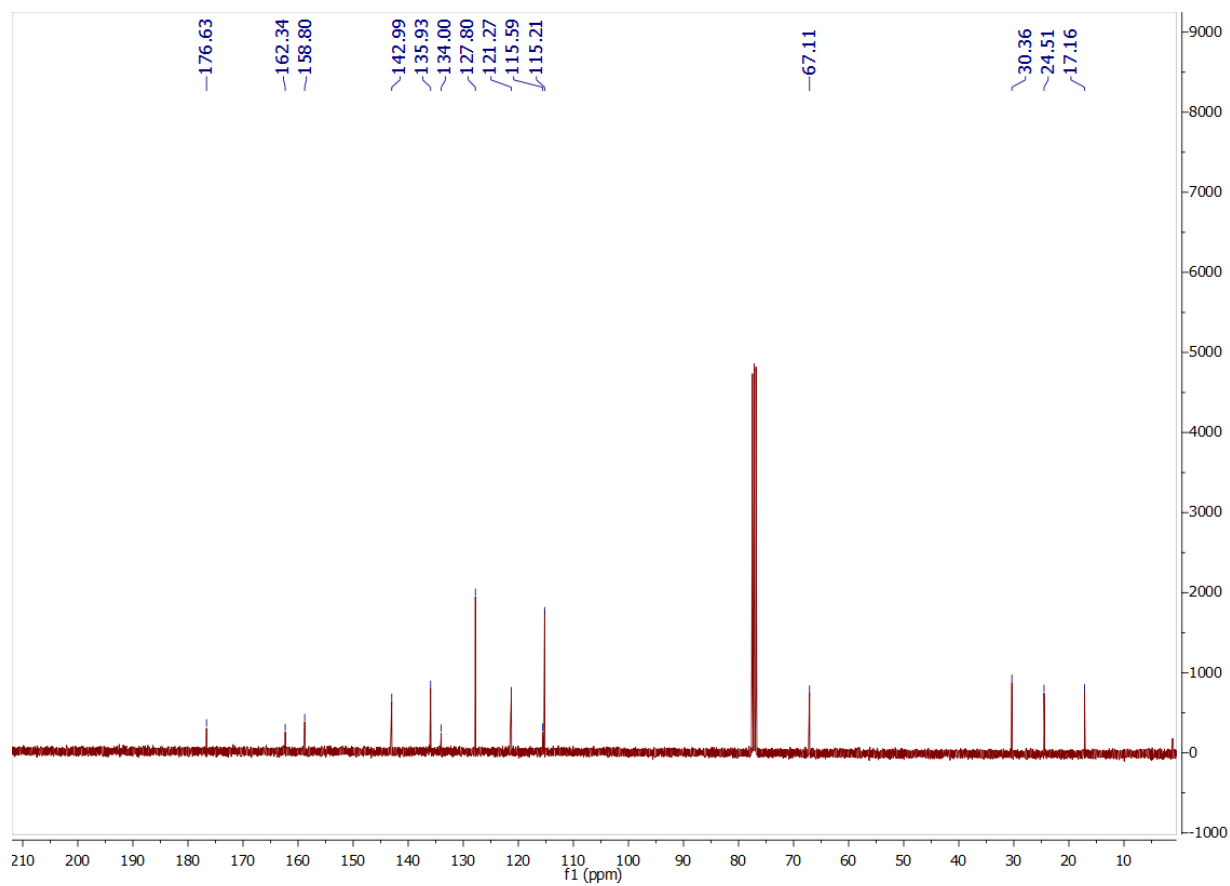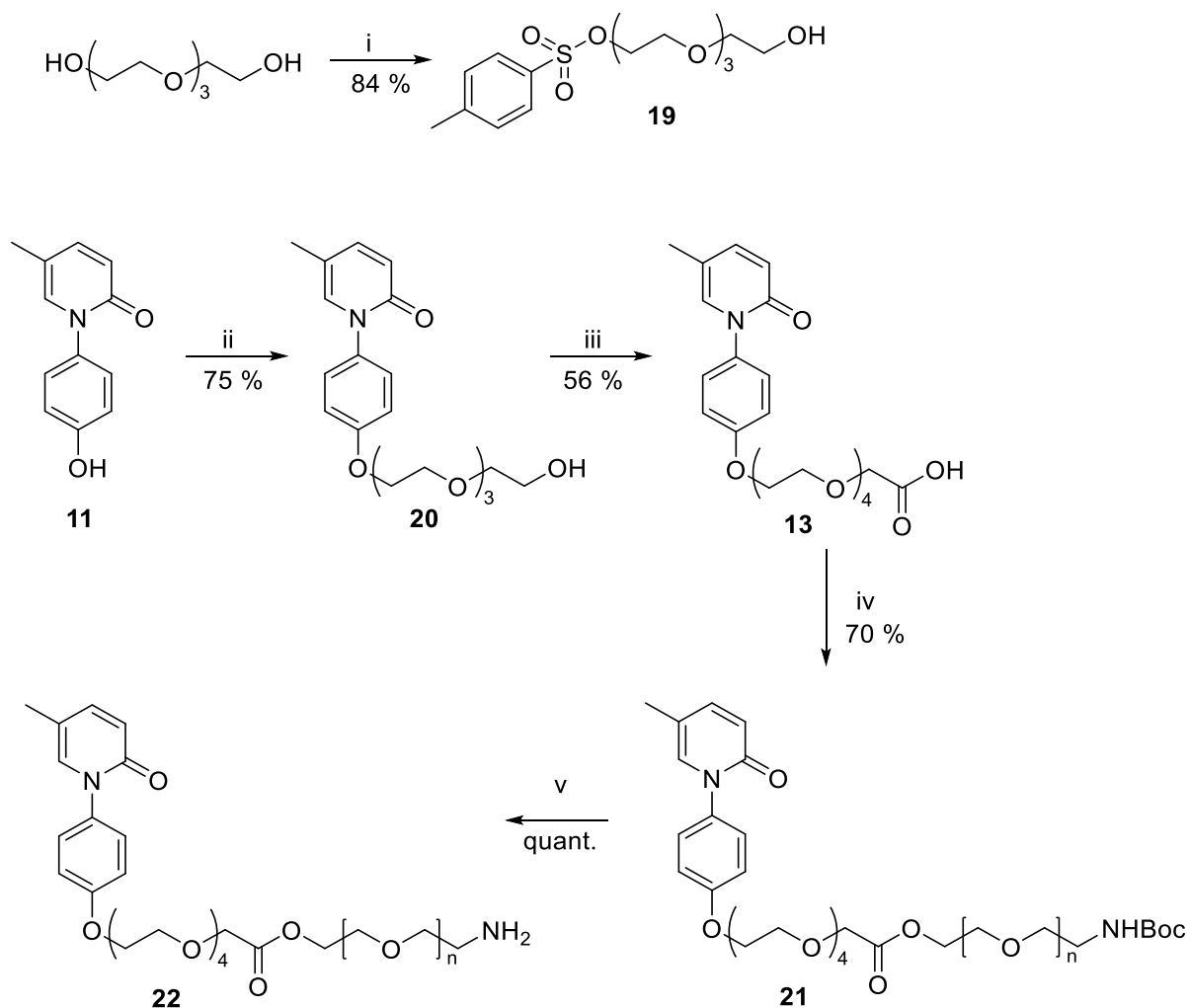
Scheme 5.6. Preparation of compound **13**, and its PEGylation. Reagents and conditions: i) TsCl, Et₃N, DCM ii) **19**, K₂CO₃, anhydrous DMF, 16 h, 60 °C iii) Bromoacetic acid, NaH, anhydrous THF, rt, 5 h iv) BocNH-PEG(2K)-OH, EDCI, DMAP, rt v) HCl 4N in dioxane, 2h, rt.

2,2'-((oxybis(ethane-2,1-diyl))bis(oxy))bis(ethan-1-ol) (19)
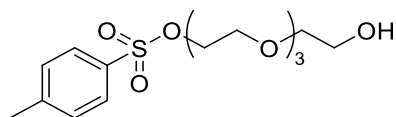
Tetraethylene glycol (10 g, 51.48 mmol, 10 equiv) was dissolved in DCM.(10 mL). The mixture was cooled to 0 °C, tosyl chloride (0.981 g, 5.148 mmol, 1 equiv) and Et₃N (1.472 g, 7.722 mmol, 2.027 mL, 1.5 equiv) were added. The mixture was stirred at rt overnight. The reaction mixture was washed with water (3×). The organic phase was dried over MgSO₄, filtered, and concentrated in vacuo. The crude product was purified by FCC (MeOH/DCM 1:30 to 1:20) to afford the product

as a colorless oil (4.328 mmol, 1.508 g, 84%). The analytical data were in accordance with previously reported data.[275]

¹H NMR (400 MHz, CDCl₃): δ 7.80 (d, J = 8.3 Hz, 2H), 7.34 (d, J = 8.0 Hz, 2H), 4.20 − 4.14 (m, 2H), 3.74 − 3.57 (m, 14H), 2.45 (s, 3H).

¹H-NMR spectrum of **19**
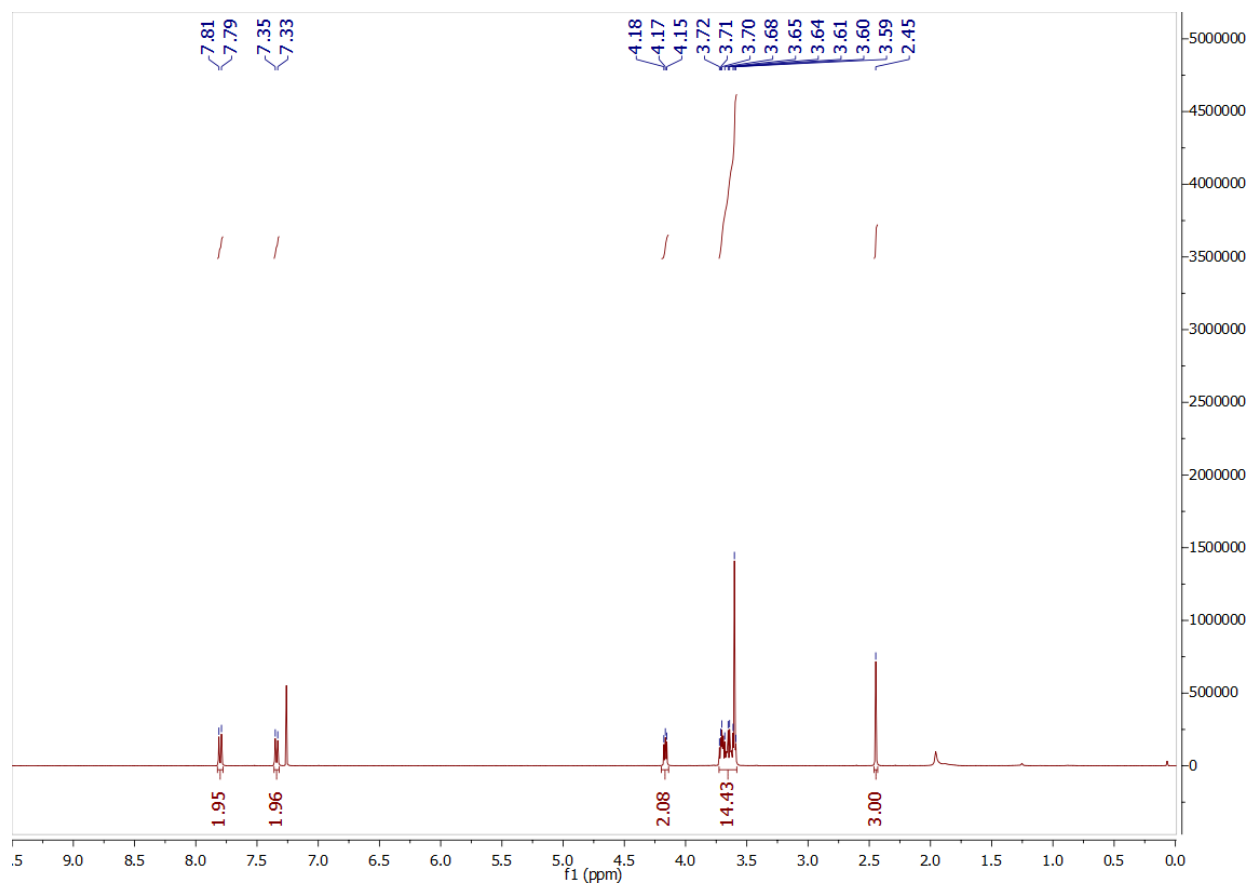
1-(4-(2-(2-(2-(2-hydroxyethoxy)ethoxy)ethoxy)ethoxy)phenyl)-5-methylpyridin-2(1*H*)-one (20)
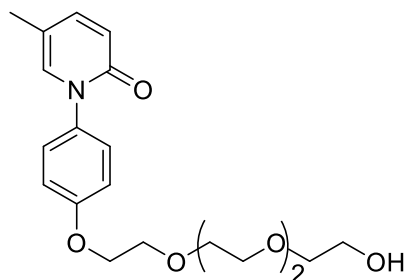
To a stirred solution of compound **11** (300 mg, 1.49 mmol, 1 equiv) and compound **19** (670 mg, 1.924 mmol, 1.3 equiv) in anhydrous DMF (27 ml), K_2CO_3 (515 mg, 3.725 mmol, 2.5 equiv) was added under argon atmosphere. The reaction mixture was heated to 60 °C and stirred overnight at this temperature. Water was added, and the product was extracted with EtOAc (5×), adjusting the pH of the aq. phase to 7 with 1M HCl solution (aq). The organic layers were combined, dried over $MgSO_4$, filtered and concentrated in vacuo. The crude product was purified by FCC (MeOH/DCM 1:20) to afford the product as a yellow oil (1.121 mmol, 423 mg, 75%).

HRMS-ESI: *m/z* 378.1917 (calcd. for C20H27NO6); 378.1916 (M+H) (found).

IR (neat): 3383, 2869, 1714, 1667, 1585, 1532, 1508, 1453, 1350, 1288, 1247, 1172, 1110, 943, 873, 830, 735, 688, 624 cm^{-1}.

¹H NMR (400 MHz, CDCl$_3$): δ 7.31 − 7.22 (m, 3H, 3 × Ar-*H*), 7.09 (s, 1H, Ar-*H*), 6.99 (d, J = 8.5 Hz, 2H, 2 × Ar-*H*), 6.61 (d, J = 9.3 Hz, 1H, Ar-*H*), 4.16 (t, J = 4.8 Hz, 2H, C*H*$_2$), 3.87 (t, J = 4.8 Hz, 2H, C*H*$_2$), 3.78 − 3.64 (m, 10H, 5×C*H*$_2$), 3.60 (t, J = 4.7 Hz, 2H, 1×C*H*$_2$), 2.09 (s, 3H, C*H*$_3$) ppm.

¹H-NMR spectrum of **20**
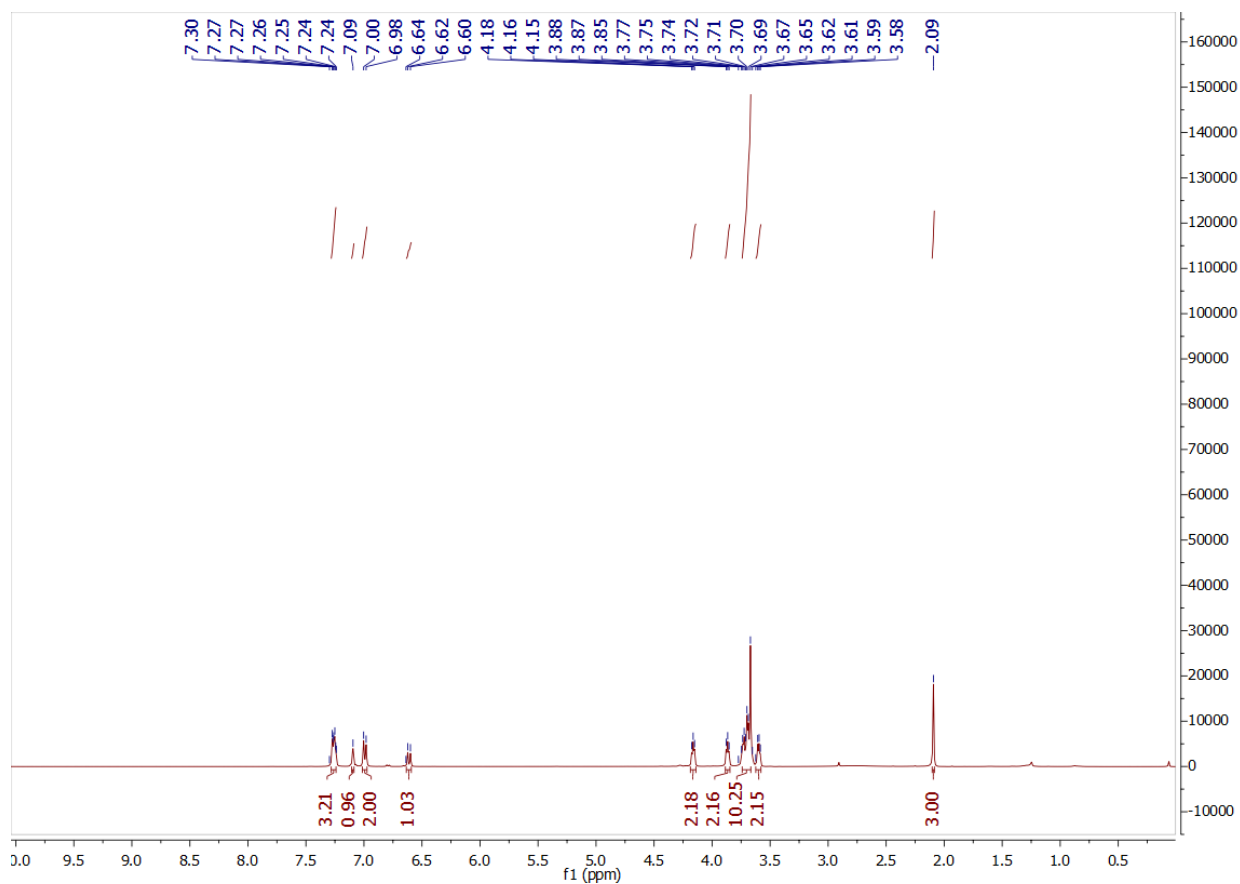
¹³C NMR (101 MHz, CDCl₃): δ 162.1 (C(O)), 158.7 (*C*-O), 142.7 (*C*$_{ar}$), 135.8 (*C*$_{ar}$), 134.2 (*C*$_{ar}$), 127.7 (2 × *C*$_{ar}$), 121.4 (*C*$_{ar}$), 115.4 (2 × *C*$_{ar}$), 115.1 (*C*$_{ar}$), 72.6 (*CH₂*), 71.0 (*CH₂*), 70.8 (*CH₂*), 70.7 (*CH₂*), 70.5 (*CH₂*), 69.8 (*CH₂*), 67.9 (*CH₂*), 61.9 (*CH₂*), 17.1 (*CH₃*).

¹³C-NMR spectrum of **20**
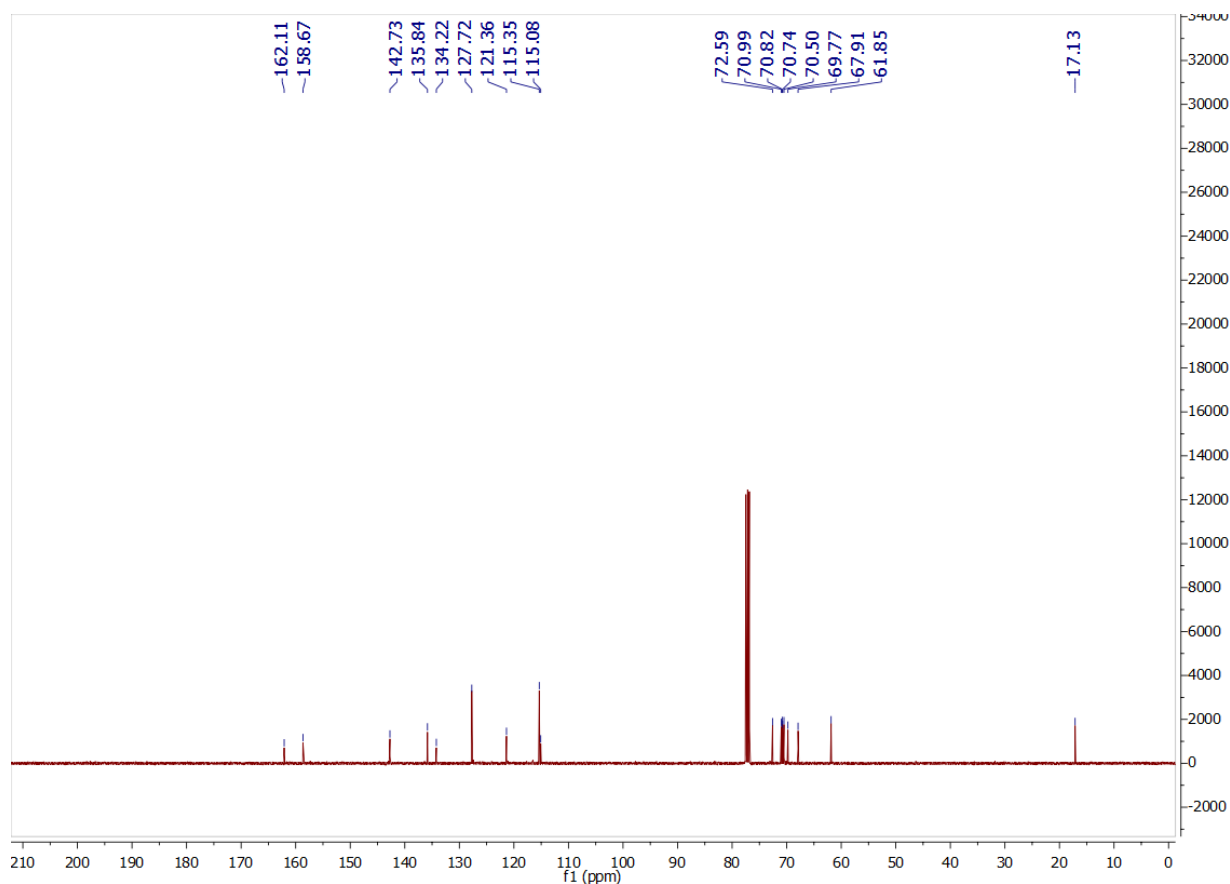
14-(4-(5-methyl-2-oxopyridin-1(2*H*)-yl)phenoxy)-3,6,9,12-tetraoxatetradecanoic acid (13)
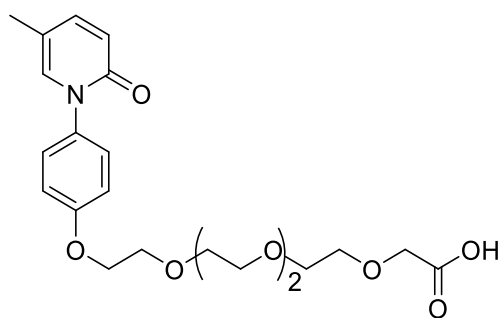
To a stirred solution of sodium hydride (60% in mineral oil, 70 mg, 1.746 mmol, 6 equiv) in anhydrous THF (3.5 mL), compound **20** (110 mg, 0.291 mmol, 1 equiv) dissolved in a minimum of anhydrous THF was slowly added under argon, at 0 °C. The reaction mixture was stirred for 1 h at rt. Bromoacetic acid (81 mg, 0.582 mmol, 2 equiv) dissolved in a minimum of anhydrous THF was added dropwise to the mixture at 0 °C. The reaction mixture was allowed to warm to rt and

was stirred for an additional 6 h. The reaction was quenched by addition of water (3 mL) and THF was evaporated. The remaining aq. phase was acidified with 1 M HCl solution to pH=1, and the precipitate was extracted with EtOAc (5 × mL). The combined organic layers were dried over MgSO₄, filtered and concentrated in vacuo. The crude product was purified by preparative TLC (MeOH/DCM 1:10) to afford the product as a light yellow oil (0.163 mmol, 71.2 mg, 56%).

HRMS-ESI: *m/z* 436.1699 (calcd. for C22H29NO8); 436.1692 (M+H) (found).

IR (neat): 3413, 2870, 1715, 1669, 1597, 1532, 1509, 1453, 1291, 1247, 1110, 945, 830, 688 cm⁻¹.

¹H NMR (400 MHz, CDCl₃): δ 7.26 – 7.22 (m, 3H, 3 × Ar-*H*), 7.10 (s, 1H, Ar-*H*), 6.99 (d, J = 8.5 Hz, 2H, 2 × Ar-*H*), 6.57 (d, J = 9.3 Hz, 1H, Ar-*H*), 4.17 (m, 2H, C*H₂*), 3.86 – 3.57 (m, 16H, 8×C*H₂*), 2.09 (s, 3H, C*H₃*).

¹H-NMR spectrum of **13**
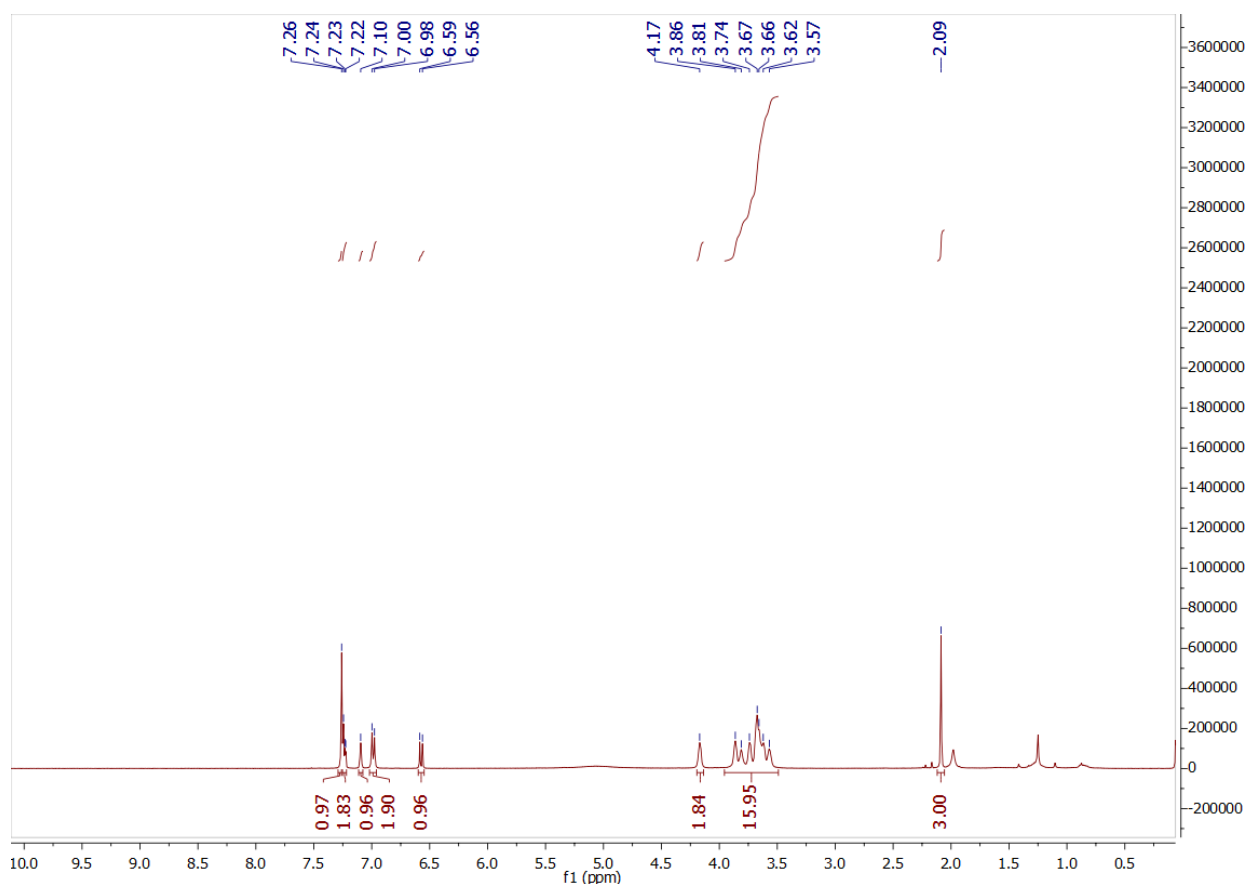
¹³C NMR (101 MHz, CDCl₃) δ 162.2 (C(O)), 158.6 (*C*-O), 142.8 (*C*ₐᵣ), 135.9 (*C*ₐᵣ), 134.3 (*C*ₐᵣ), 127.8 (2 × *C*ₐᵣ), 121.3 (*C*ₐᵣ), 115.4 (2 × *C*ₐᵣ), 115.2 (*C*ₐᵣ), 70.5 (*CH₂*), 70.1 (*CH₂*), 70.1 (*CH₂*), 70.1 (*CH₂*), 70.0 (*CH₂*), 70.0 (*CH₂*), 70.0 (*CH₂*), 69.6 (*CH₂*), 67.9 (*CH₂*), 17.1 (*CH₃*).

¹³C-NMR spectrum of **13**
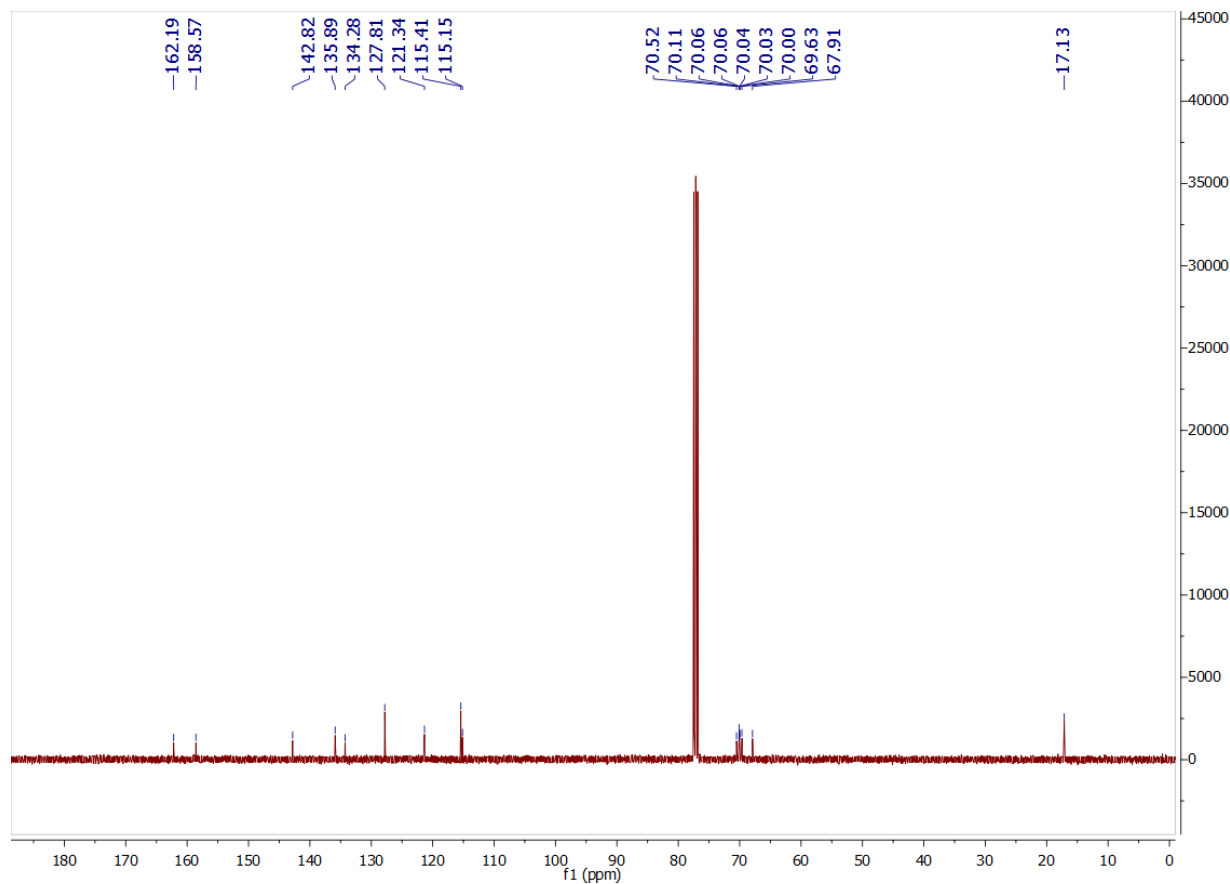
Boc-PEG-PFD (21)
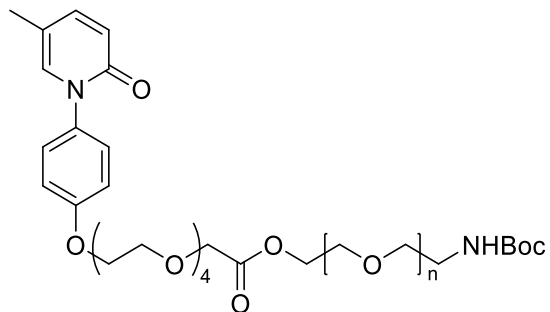
To a stirred solution of compound **21** (52 mg, 0.119 mmol, 1.01 equiv) in anhydrous DCM (2.5 mL) EDCI (40.7 mg, 0.212 mmol, 1.8 eq) and DMAP (2.8 mg, 0.0236 mmol, 0.2 equiv) were added under argon atmosphere, and were stirred for 5 min. Boc-PEG(2K)-hydroxyl (248 mg, 0.118 mmol, 1 equiv) dissolved in a minimum of DCM was added. The reaction mixture was stirred at rt until complete disappearance of the starting materials, as followed by TLC. Upon completion

of the reaction, the solvent was evaporated, and the crude was purified by FCC (MeOH/DCM 1:18 to 1:5) to afford the product **21** as a white amorphous solid (0.082 mmol, 207 mg, 70%).

¹H NMR (400 MHz, CDCl$_3$): δ 7.28 – 7.23 (m, 3H, Ar-*H*), 7.09 (m, 1H, Ar-*H*), 6.99 (d, J = 8.7 Hz, 2H, 2 × Ar-*H*), 6.60 (d, J = 9.7 Hz, 1H, Ar-*H*), 4.29 (t, J= 4.9 Hz, 2H, C*H*$_2$-C(O)-O), 4.18 – 4.14 (m, 4H, C*H*$_2$-O), 3.87 (t, J= 4.9 Hz, 2H, C*H*$_2$-O), 3.82 (t, J= 4.9 Hz, 2H, C*H*$_2$-O) 3.74 – 3.60 (m, C*H*$_2$-O), 3.54 (t, J=4.9 Hz, 2H, C*H*$_2$-O), 3.46 (m, 2H, C*H*$_2$-O), 3.31 (m, 2H, C*H*$_2$-O), 2.09 (s, 3H, C*H*$_3$), 1.44 (s, 9H, Boc) ppm.

¹H-NMR spectrum of **21**
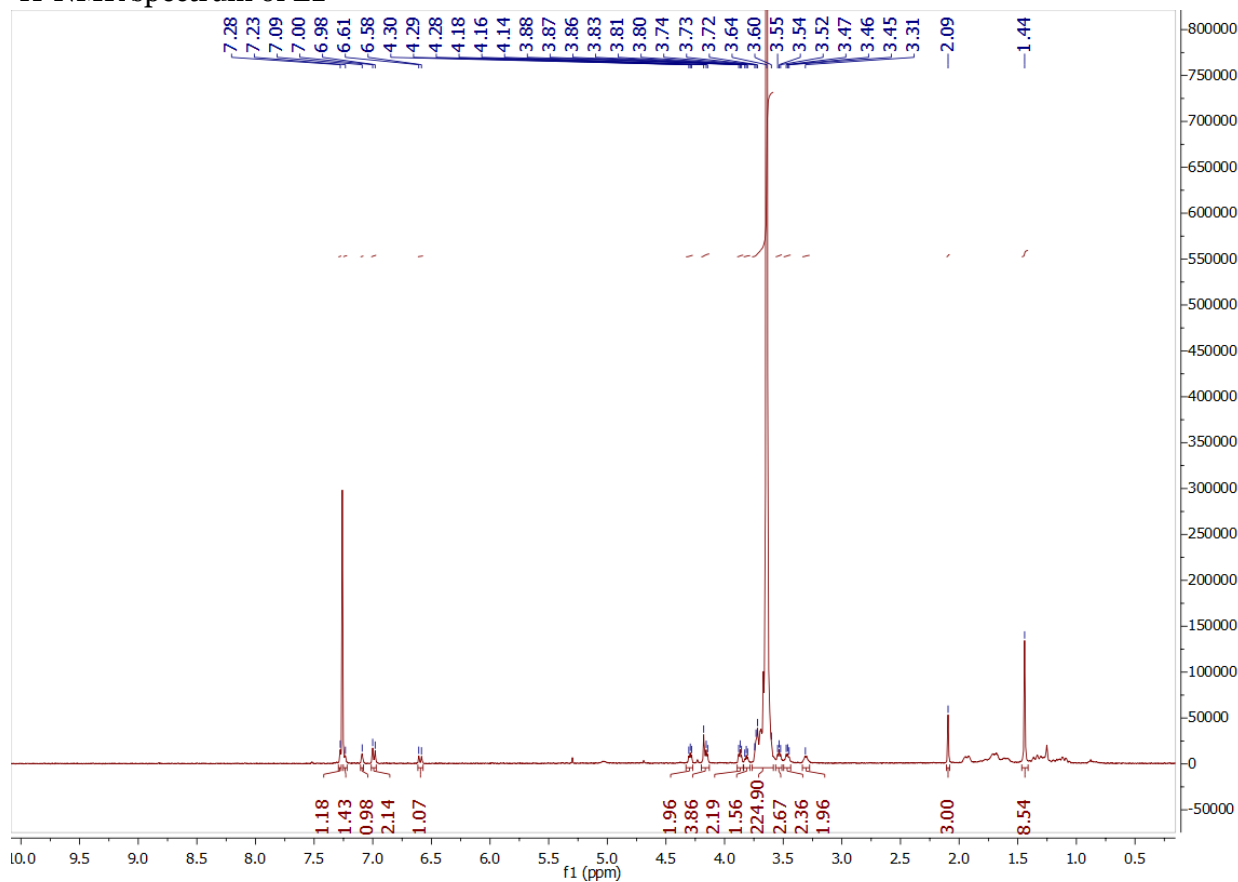
Amine-PEG-PFD (22)
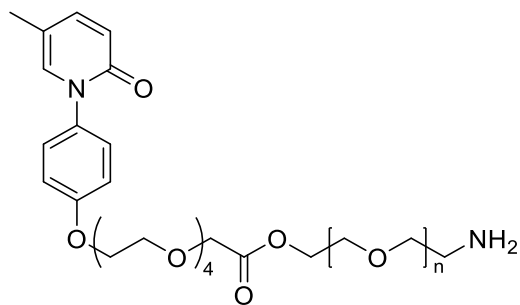
Compound **21** (192 mg, 0.076 mmol, 1 equiv) was dissolved in a solution of HCl 4N in dioxane (2.5 mL) and the reaction mixture was stirred at rt until completion of the reaction (monitored by TLC). The volatiles were removed under air flow and the product was dried under vacuo to afford the product **22** as a white amorphous solid (195 mg, quant.), which was used without further purification.

HRMS-ESI: *m/z* 2416.3922 (calcd. for C112H211N2O52); 2416.1995 (M+H) (found).

¹H NMR (400 MHz, CDCl₃): δ 7.64 (s, 2H, N*H*₂), 7.31 – 7.24 (m, 3H, 3 × Ar-*H*), 7.13 (m, 1H, Ar-*H*), 6.99 (d, J = 8.7 Hz, 2H, 2 × Ar-*H*), 6.71 (d, J = 9.4 Hz, 1H, Ar-*H*), 4.29 (t, J= 4.9 Hz, 2H, C*H*₂-C(O)-O), 4.18 – 4.15 (m, 4H, C*H*₂-O), 3.94 (m, 2H, C*H*₂-O), 3.87 (t, J= 4.9 Hz, 2H, C*H*₂-O), 3.82 – 3.64 (m, C*H*₂-O), 3.46 (t, J=5.5 Hz, C*H*₂-O), 2.11 (s, 3H, C*H*₃) ppm.

¹H-NMR spectrum of **22**
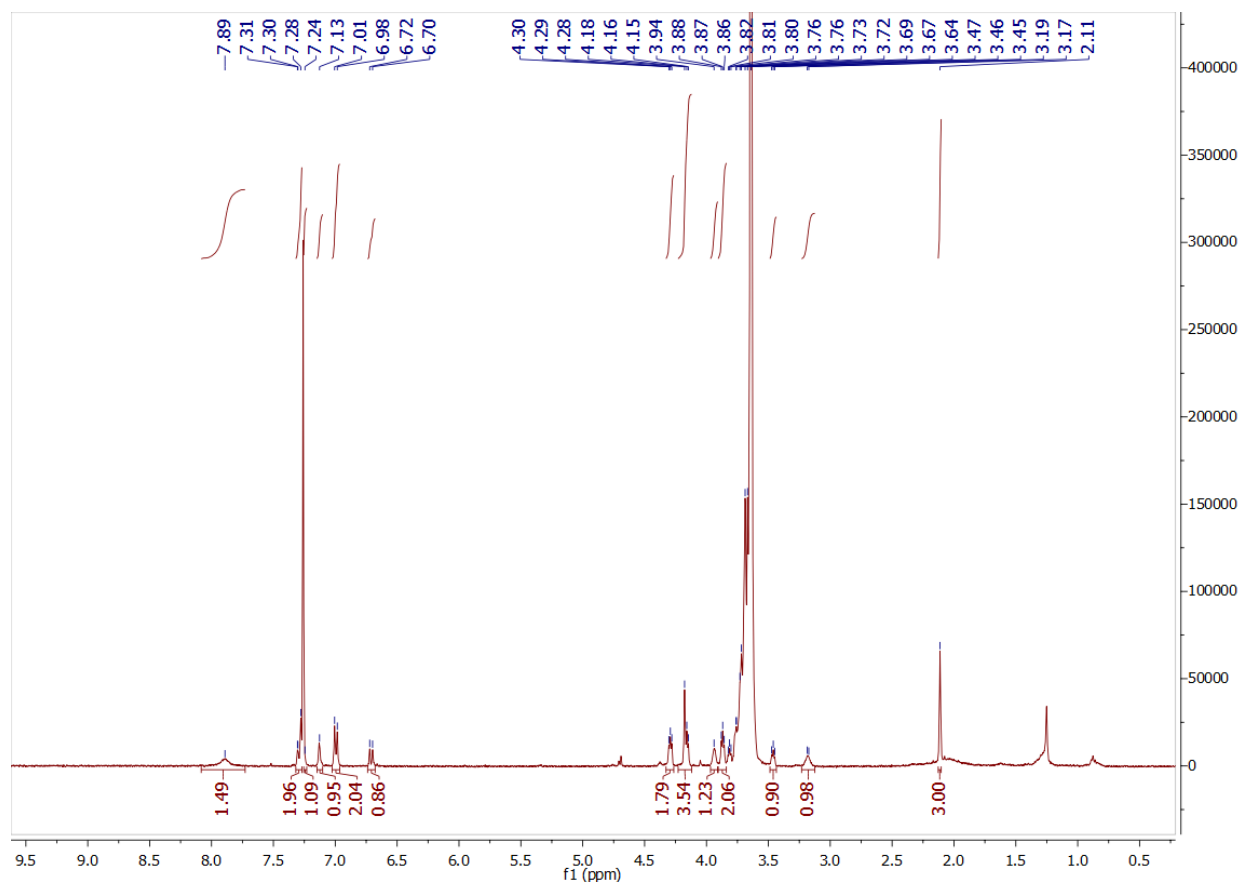
¹³C NMR (100 MHz, CDCl₃): δ 170.6 (*CO*), 162.1 (*CO*), 158.7 (*CO*), 142.9 (*C_ar*), 135.9 (*C_ar*), 134.1 (*C_ar*), 127.9 (*C_ar*), 127.7 (2 × *C_ar*), 121.2 (*C_ar*) 115.5 (*C_ar*), 115.3 (2 × *C_ar*), 72.7 (*CH₂*), 72.4 (*CH₂*), 71.0 (*CH₂*), 71.0 (*CH₂*), 70.7 (n × *CH₂*), 70.4 (*CH₂*), 70.3 (*CH₂*), 70.2 (*CH₂*), 70.2 (*CH₂*), 70.2 (*CH₂*), 70.1 (*CH₂*), 70.0 (*CH₂*), 69.8 (*CH₂*), 69.7 (*CH₂*), 69.1 (*CH₂*), 68.6 (*CH₂*), 67.9 (*CH₂*), 66.9 (*CH₂*), 63.9 (*CH₂*), 61.8 (*CH₂*), 43.0 (*CH₂*), 42.8 (*CH₂*), 40.7 (*CH₂*), 29.8 (*CH₂*), 17.1 (*CH₃*) ppm.

¹³C-NMR spectrum of **22**

170.57
162.05
158.73
142.88
135.93
134.07
127.88
127.67
121.18
115.51
115.33
72.65
72.39
71.02
70.97
70.68
70.43
70.27
70.22
70.18
70.16
70.08
69.99
69.81
69.73
69.08
68.63
67.90
66.93
63.89
61.83
43.01
42.79
40.74
29.81
17.13
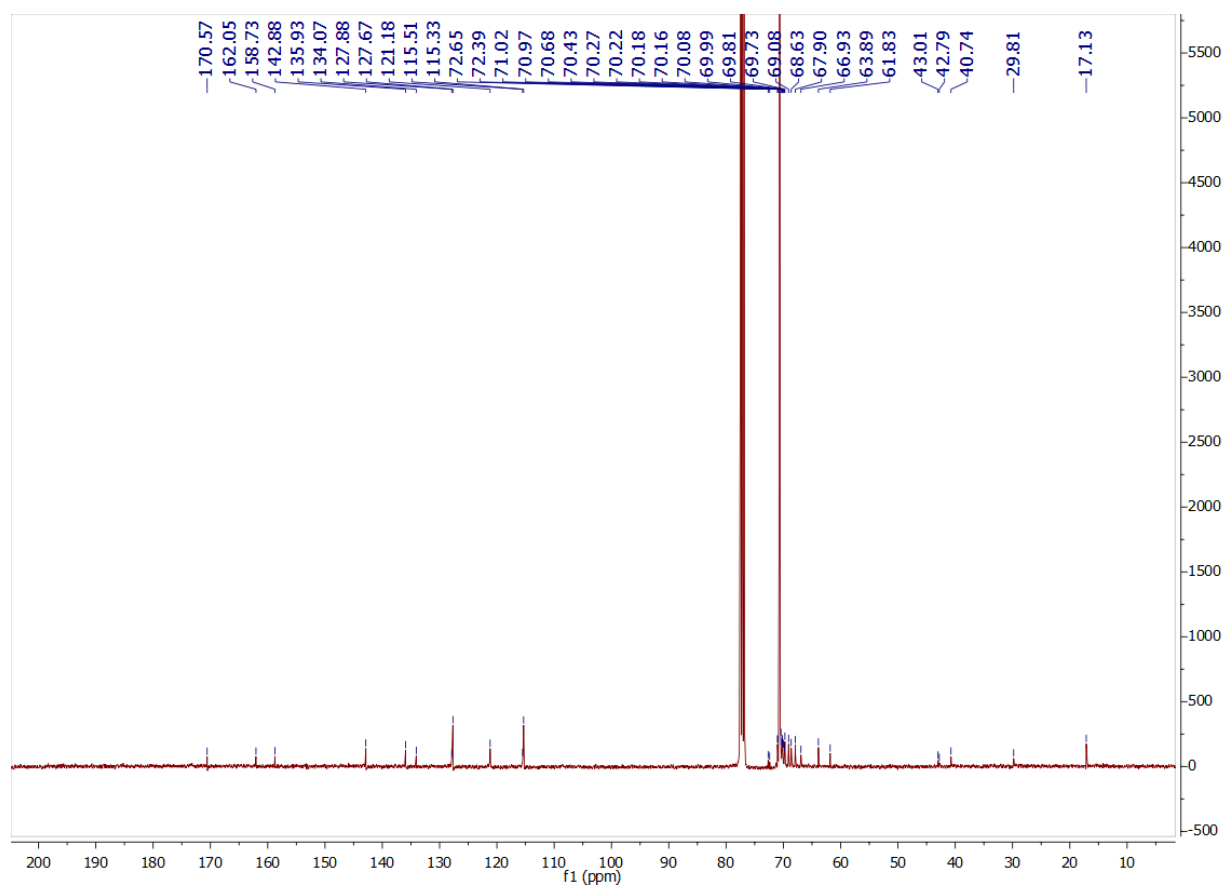
Alg-PFD (23)
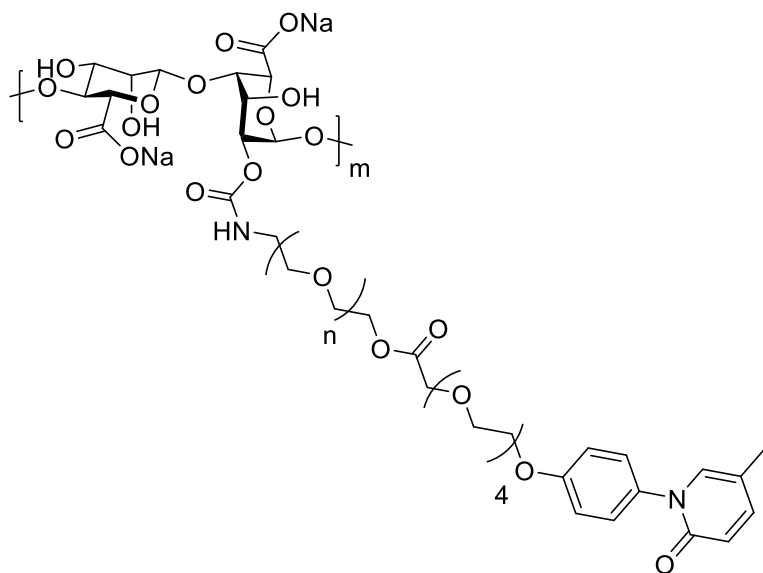
For grafting amine-PEG-PFD (**22**) on the alg, the same protocol was implemented as presented in Section 5.2 under "**General procedure for the functionalization of TBA-alg with PEG derivatives**".

¹H NMR (400 MHz, Deuterium oxide): δ 7.67 (d, J = 8.9 Hz, Ar-*H*), 7.47 (s, Ar-*H*), 7.35 (d, J = 8.8 Hz, Ar-*H*), 7.17 (d, J = 8.2, Ar-*H*), 6.68 (d, J = 9.1 Hz, Ar-*H*), 4.35 − 4.26 (m, C*H*₂-TEG), 4.16 − 3.52 (m, C*H*-Alg + C*H*₂-PEG), 3.23 (m, C*H*₂-NHC(O)), 2.17 (s, C*H*₃) ppm.

¹H-NMR spectrum of **23**
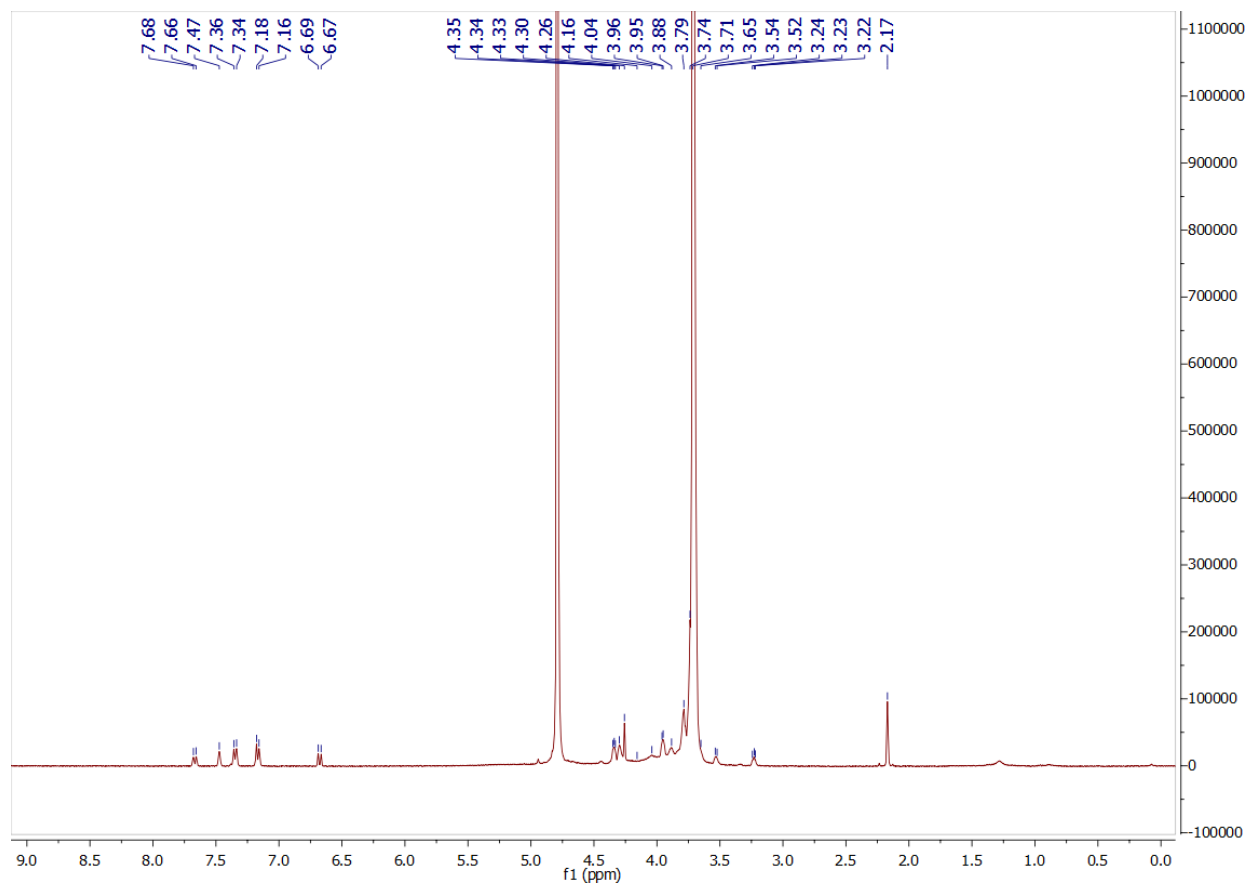
5.6. Microspheres formation

Formation of empty MS using a one-component protocol (Na-alg, Alg-sSH)

Na-alg or Alg-sSH were dissolved in MOPS buffer (10 mM, pH=7.4) containing 0.4% NaCl at the indicated concentrations (2-3 wt%). The polymer solution was extruded into a gelation bath (100

mM CaCl$_2$ in 10 mM MOPS buffer, pH=7.4) containing tween (diluted 1/10 000) using a coaxial air-flow droplet generator. MS were collected by filtration, rinsed with MOPS buffer containing CaCl$_2$ (100 mM), and stored in this solution until further use.

Formation of empty MS using a two-component protocol (Alg-SH:Alg-ACR, Alg-SH:Alg-MAL or Alg-SH:Alg-ACA)

Alg-ACR, Alg-MAL, Alg-ACA or Alg-SH were dissolved in MOPS buffer (10 mM, pH=7.4), containing 0.4% NaCl at the indicated concentrations (2-3 wt%). Alg-SH polymer solution was mixed with either Alg-ACR or Alg-MAL or Alg-ACA solutions in a molar ratio of 1:1. The resulting solutions were gently mixed for 5 to 15 minutes, to ensure homogeneous distribution. Extrusion into a gelation bath (100 mM CaCl$_2$ in 10 mM MOPS buffer, pH=7.4) containing tween (diluted 1/10 000) using a coaxial air-flow droplet generator resulted in the production of spherical MS which were collected by filtration, rinsed with MOPS buffer containing CaCl$_2$ (100 mM), and stored in this solution until further use.

Formation of empty MS functionalized with anti-inflammatory and anti-fibrotic compounds (MS of Alg:Alg-KET or Alg:Alg-PFD)

Na-alg and either Alg-KET, or Alg-PFD were dissolved in MOPS buffer (10 mM, pH=7.4), containing 0.4% NaCl. The two polymer solutions were mixed in a weight ratio of 2 (Na-alg) to 1 (PEGylated alg) and stirred until reaching a homogeneous solution. Extrusion of the polymer solution into a gelation bath (100 mM CaCl$_2$ in 10 mM MOPS buffer, pH=7.4) containing tween (diluted 1/10 000) with a coaxial air-flow droplet generator resulted in MS formation.

Formation of empty MS by co-encapsulation of anti-fibrotic compounds

Anti-fibrotic compounds were prepared in a concentration of 3 mM, by dissolution in MOPS buffer (10 mM, pH=7.4) containing 0.4% NaCl. 1.5 wt% alg solution was prepared by dissolving the corresponding amount of alg powder in the previously prepared 3 mM drug solution. Bead formation was achieved as previously described, using a coaxial air-flow droplet generator.

Formation of empty MS from a mixture of polymers (Multicomponent hydrogel microspheres)

The PEGylated polymers were dissolved in a concentration that allowed for a homogeneous distribution of all the components. In the example presented in Section 3.3.2.1, Alg-KET and Alg-ACA were prepared as a 3 wt%, Alg-SH 4wt %, Alg-ACR and Na-alg as 2wt % solutions, by dissolving them in MOPS buffer (10 mM, pH=7.4) containing 0.4 % NaCl. The polymer solutions

were mixed in a weight ratio of 1:1:1:1, either as Na-alg, Alg-KET, Alg-SH, Alg-ACR or as Na-alg, Alg-KET, Alg-SH, Alg-ACA. The resulting solutions were gently mixed for 5 to 15 minutes, to ensure homogeneous distribution. Extrusion into a gelation bath (100 mM $CaCl_2$ in 10 mM MOPS buffer, pH=7.4) containing tween (diluted 1/10 000) using a coaxial air-flow droplet generator resulted in the production of spherical MS which were collected by filtration, rinsed with MOPS buffer containing $CaCl_2$ (100 mM), and stored in this solution until further use. For the release of ketoprofen, 1 mL of polymer solution was extruded into the gelation bath, MS were collected by filtration, rinsed with MOPS buffer containing $CaCl_2$ (100 mM), and 3 mL of the same media was freshly added. Aliquots of the media at certain time points were obtained by withdrawing 1 mL of media, and replacing it with 1 mL of fresh media. The release of ketoprofen was quantified by LC-MS measurements.

5.6.1. Encapsulation of cells, transplantation and follow-up procedures

Cell encapsulation was performed under sterile conditions, using a Büchi coaxial air-flow droplet generator (Encapsulator B-395 Pro, Büchi Labortechnik AG, Flawil, Switzerland).

Encapsulation of MIN6 cells

1 mL of polymer solution containing MIN6 cells (10×10^6) previously cultured in Dulbecco Modified Eagle's Medium (DMEM) complete medium were suspended in 1 mL of polymer solution (previously prepared in MOPS buffer (10 mM, pH=7.4) containing 0.4% NaCl). The DMEM medium was supplemented with 1 mM Na-pyruvate, 71 µM β-mercaptoethanol, 15% decomplemented Fetal Calf Serum, 25 mM glucose, penicillin, and streptomycin. The resulting cell suspension was extruded using the same protocol as described above for the empty MS formation.

Encapsulation of Huh7 cells

1 ML of polymer solution containing Huh7 cells (5×10^6) previously cultured in DMEM complete medium and centrifuged at 250g for 5 min was placed in a 10 mL syringe. The resulting cell suspension was extruded using the same protocol as described above for the empty MS formation.

Encapsulation of NPIs

NPIs were cultured in neonatal porcine islet culture medium from Corning. The NPIs were placed in a falcon tubes for 5 min and after sedimentation the supernatant was removed. The remaining

cell pellet was dispersed in 1 mL of the polymer solutions using a 10 mL syringe to obtain 10000 or 20000 IEQ / ml of polymer. MS were produced using the same procedure described above. Encapsulated NPIs were then cultured in NPI culture medium from Corning at 37°C with 5% CO_2 and the medium was changed two times per week.

Albumin secretion assay

Microencapsulated Huh7 cells (0.2×10^6) were seeded in 1 mL complete culture medium in a 24-well Corning Primaria Cell Culture Multiwell Plate. Albumin secretion was measured in 24 hour-supernatants at day 4 and 7. Supernatants were frozen until albumin was measured using a 100% specific human albumin ELISA kit (Abcam, Cambridge, UK) applying manufacturer's instructions.

Insulin secretion assay

Insulin secretion assay consists of inducing insulin secretion from NPI through incubation of encapsulated NPI (150 islet equivalents (IEQ)) in different conditions: basal (5.6 mM glucose), high (16.7 mM glucose) and maximal stimulation (16.7 mM glucose + 5 mM theophylline). The encapsulated islets (placed in semipermeable transwells) are successively placed into basal, stimulating and maximal stimulating conditions during 1 hours at 37 °C to release insulin. Insulin released was then measured using a porcine insulin ELISA assay (Mercodia, Uppsala, Sweden). Insulin secretion is expressed as fold increase, where basal release was set as 1.

MTT assay

Cells (12.10^4) were seeded per 96-well and treated with compounds (PFD, **11**, **12** and **13**) at different concentration. To check for metabolic activity after treatment, culture media was removed and 150 µl of MTT at 0.2 mg/ml in complete culture media were added for 2 h into each well at day 1, 2 and 5. Thereafter, media were aspirated and 150 µl of 0.1 M HCl isopropanol was added. Plates were gently rotated on an orbital shaker for 5 min to completely dissolve the precipitation. The absorbance was detected at 540 nm with a Microplate Reader (SpectraMax Paradigm Multi-Mode Microplate Reader, Molecular Devices, San Jose, CA). Values were expressed as percentages of untreated control condition, which was set as 100 percent.

Quantification of α-SMA expression

50.10^4 cells/well were plated into 24 well plates and cultured for 5 days in media containing increasing amounts of compounds. α-SMA expression was evaluated by performing a SDS-PAGE analysis, followed by a Western blot analysis using a specific antibodies directed against α-SMA and GAPDH a protein used for loading control. The α-SMA level was quantified using a Fusion solo S software. α-SMA values were then normalized by values obtained for GAPDH. α-SMA expression in the different conditions was expressed as fold increase where the control condition was set as 1.

Transplantation of empty MS in the peritoneal cavity

All animal experiments were approved by the Geneva veterinary authorities. Prior to transplantation, MS were rinsed three times for 15 min in Hank's Balanced Salt Solution (HBSS), containing Ca^{2+}. Once MS have settled on the bottom of the tube, the supernatant was removed and remaining MS were dispersed in a minimal amount of HBBS for transplantation. MS were introduced through a small incision into the peritoneal cavity of C57BL/6 mice, anesthetized by isoflurane. For cross-reactive MS, transplantation was performed three days after MS formation to ensure formation of covalent cross-links.

Transplantation of microbeads under the kidney capsules

For transplantation under the kidney capsule, kidneys were exposed through a small dorsal incision and ~100 µL of MS were injected under the kidney capsule using a 18G catheter. For quantification of PFO mice were sacrificed and kidneys were retrieved for histological analysis.

5.7.   Physical characterization of microspheres

Diameter measurement

The measurement of the diameter of MS was performed on a 30 MS/batch, at the given time points, using an Olympus AX70 microscope equipped with an Olympus DP70 color digital camera.

Mechanical resistance and elasticity

The mechanical resistance to the compression to 90% of the initial diameter was analyzed using a texture analyzer (TA-XT2i, software Texture Exponent 32, Stable Micro Systems, Godalming, UK) equipped with a force transducer (1 mN resolution). A single MS was placed below the probe, for which a constant speed was set as 0.5 mm s^{-1}. Ten MS of each batch were included in the analysis. To obtain the elasticity, the same measurement was repeated ten times on one MS, and ten MS per batch were included in the analysis.

Permeability measurement of MS

Alg-based MS and control glass beads were incubated for 36 h with fluorescein isothiocyanate (FITC)-labeled dextran solution (0.033 mg/mL prepared in MOPS buffer, pH=7.4) of 40, 150, 250 and 500 kDa molecular weight. Images of alg-based MS (3/condition) and glass beads (2/condition) were taken with a confocal microscope (LSM 510 meta ConfoCor3, Zeiss). The permeability of FITC-dextrans was quantified by using ImageJ software, as a ratio between the fluorescence intensity inside and outside of the MS. The infiltration value is given as a percentage, considering the glass beads as reference value of 0%.

Stability in Na-citrate

Beads stored in MOPS solution (10 mM MOPS buffer, pH=7.4, containing 100 mM CaCl$_2$) were collected by filtration, dried and placed in 1 mL of Na-citrate solutions (prepared in MOPS buffer, pH=7.4) of 5, 10, 20, 30 and 40 mM, for 24 h. The MS were than imaged using an Olympus AX70 microscope equipped with an Olympus DP70 color digital camera.

Quantitative analysis of ketoprofen, PFD and compound 13 release by UHPLC-ESI-HRMS

MS quantitative analysis were performed on a Agilent 6530 Accurate Mass Q-TOF LCMS mass spectrometer coupled to an Agilent 1290 series UHPLC system (Agilent Technologies, USA). The separation was achieved using an ACQUITY UPLC® BEH C18 1.7μm column, 2.1 mm x 50 mm (Waters) heated at 30°C. Mobile phase consisted of 0.1% formic acid in water as eluent A and 0.1% formic acid in acetonitrile as eluent B. The separation was carried out at 0.4 mL/min over a 6 min total run time using the following program: 0-0.5 min, 1-5% B; 0.5-3 min, 5-95% B; 3-3.5 min, 95-1% B; 3.5-6 min, 1% B to re-equilibrate the system in initial conditions. The sample

manager was system temperature was fixed at 10 °C and the injection volume was 5µL. Mass spectrometer detection was operated in positive ionization using the Dual AJS Jet stream ESI Assembly. The QTOF instrument was operated in the 4 GHz High Resolution mode in profile mode. The Instrument was calibrated in positive full scan mode using ESI-L+ solution (Agilent Technologies, USA). The TOF mass spectra were acquired over the range of m/z 100-1000 at an acquisition rate of 3 spectra/s. ESI AJS settings were as follows RF drying gas flow, 8 L/min; drying gas temperature, 300°C; nebulizer pressure, 35psi; capillary voltage, 3500V; nozzle voltage, 1000V; fragmentor voltage, 175V; skimmer voltage, 65V; octopole 1 RF voltage, 750V; Sheath gas temperature, 350°C; Sheath gas low; 11L/min. Data was processed using the MassHunter Workstation (Agilent Technologies, USA). Extracted ions chromatograms (XIC) were based on a retention time (RT) window of ±0.2 min with a mass-extraction-window (MEW) of ±50 ppm centered on m/z_{theor}. Calibration curves were fitted with a polynomial order 2 equation, with R2 > 0.995.
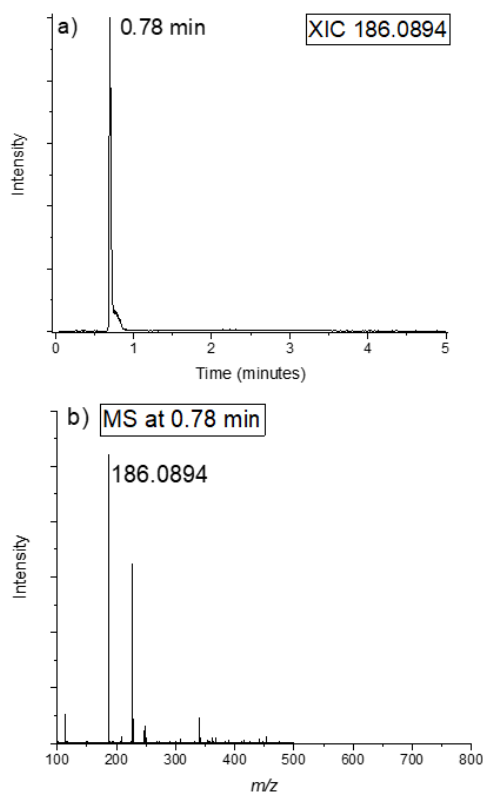
Figure 5.1. a) Typical XIC (186.0894 MEW) of PFD standard b) Typical MS of PFD standard at 0.78 min.
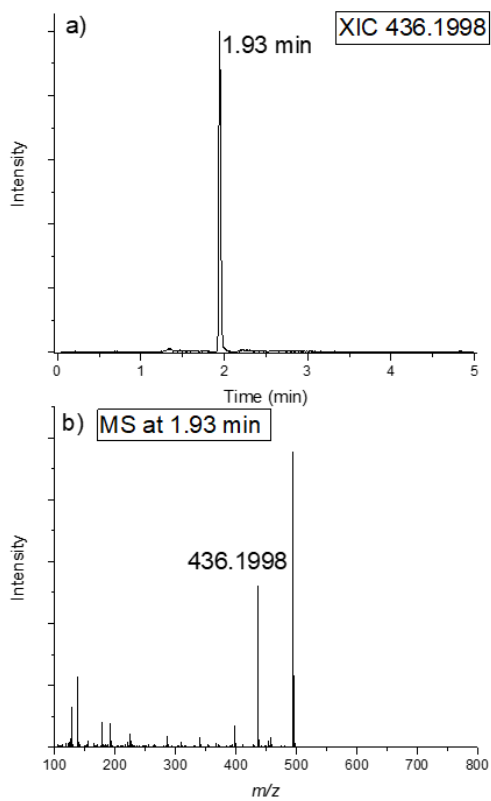
*Figure 5.2. a) Typical XIC (436.1998 MEW) of compound **13** standard b) Typical MS of compound **13** standard at 1.93 min.*

6. Annexes
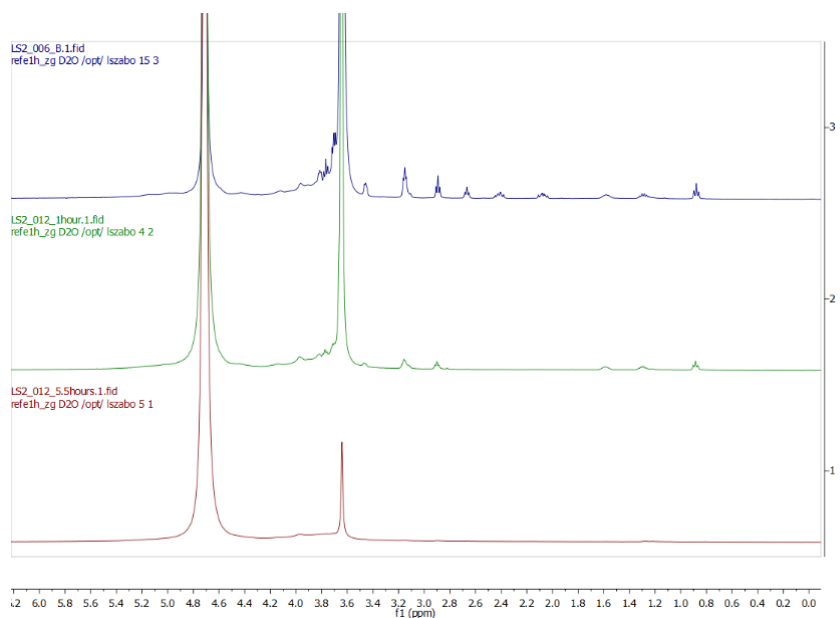
Figure 6.1. ¹H-NMR spectra of Alg-sSH polymer treated in ultrafiltration cell for TBA to Na-ion exchange. The upper spectra was recorded prior to treatment, the middle spectra 1 h and the lower one 5 h after stirring the polymer solution in the UF cell.
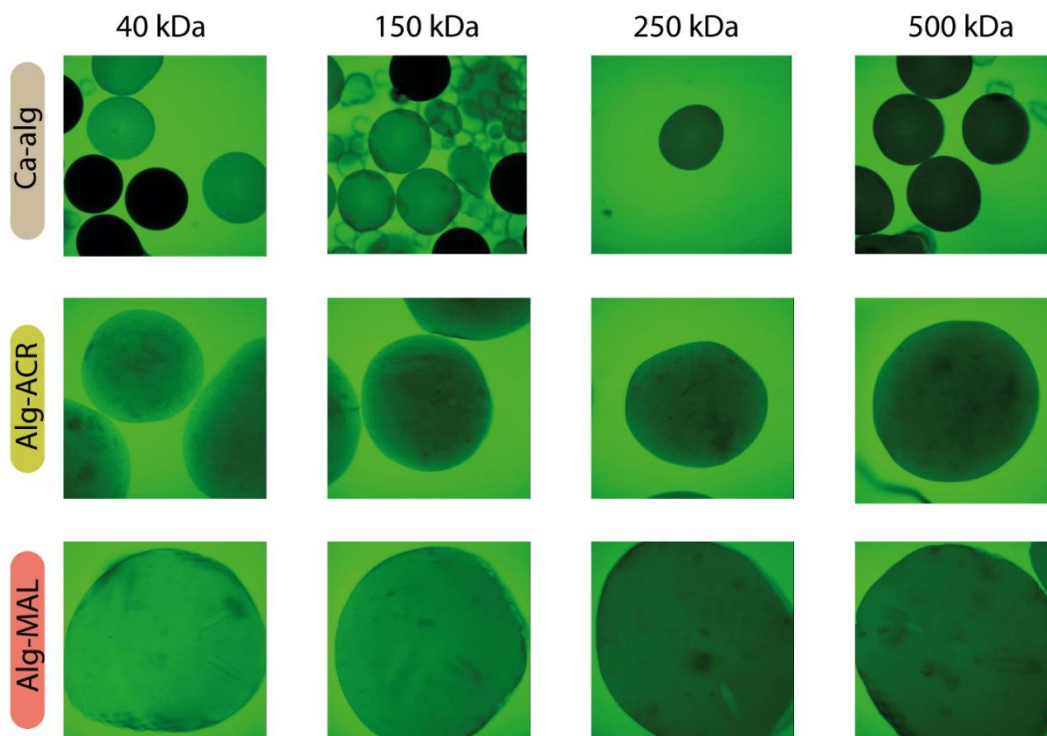
Figure 6.2. Confocal microscope images of MS in 40, 150, 250 and 500 kDa FITC-Dextran solutions.

Day 1 after encapsulation
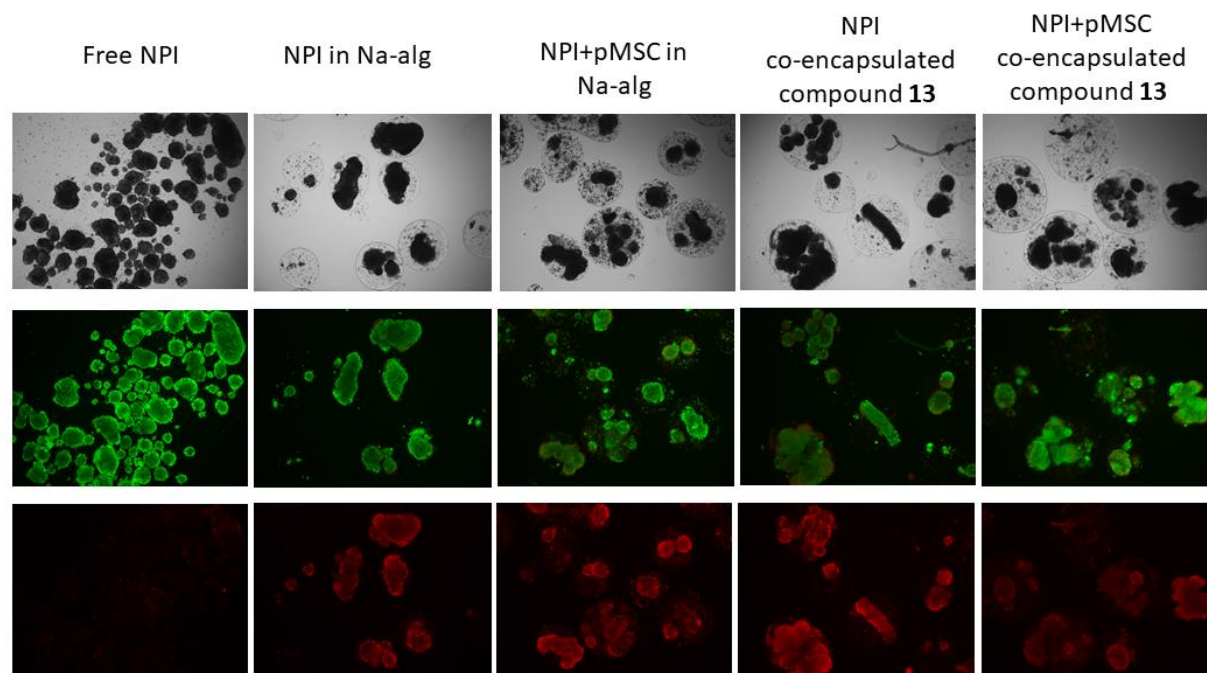
Figure 6.3. Microscopy images of free NPI and NPI or NPI+pMSC encapsulated in Na-alg, and co-encapsulated with compound 13, at day 1. Top panel: light microscopy, middle panel: staining of live cells with FDA (green), bottom panel: staining of dead cells with PI (red).

Day 1 after encapsulation
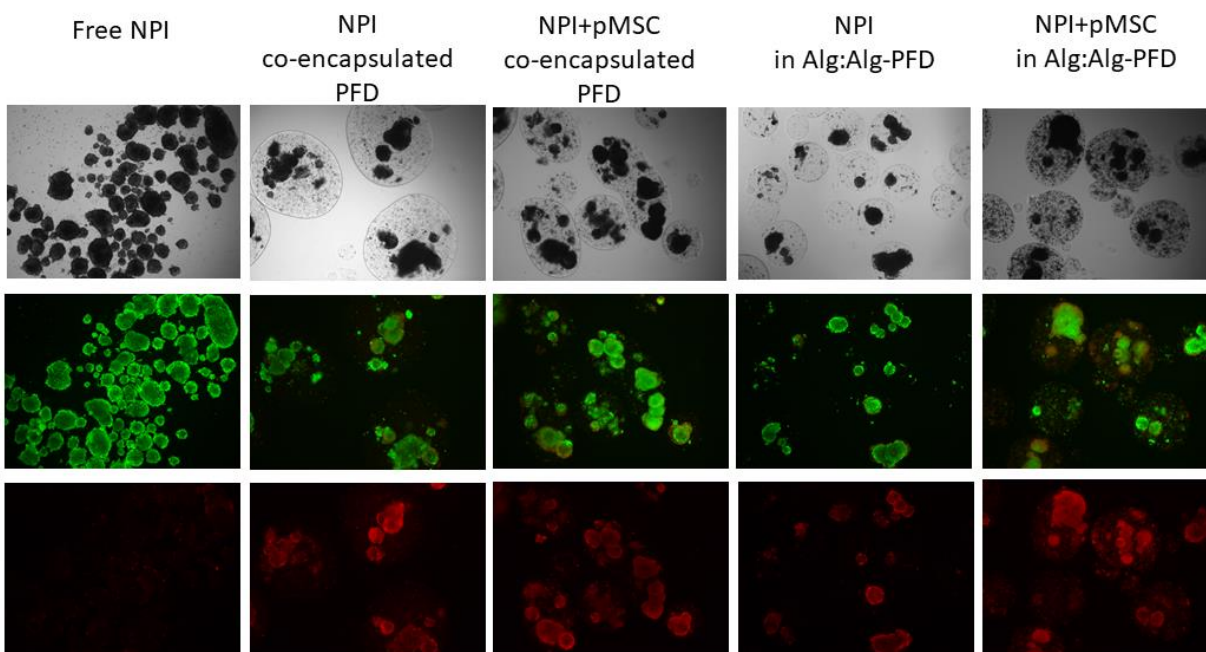
Figure 6.4. Microscopy images of free NPI and NPI or NPI + pMSC co-encapsulated with PFD, and encapsulated in Alg:Alg-PFD at day 1. Top panel: light microscopy, middle panel: staining of live cells with FDA (green), bottom panel: staining of dead cells with PI (red).

Day 7 after encapsulation
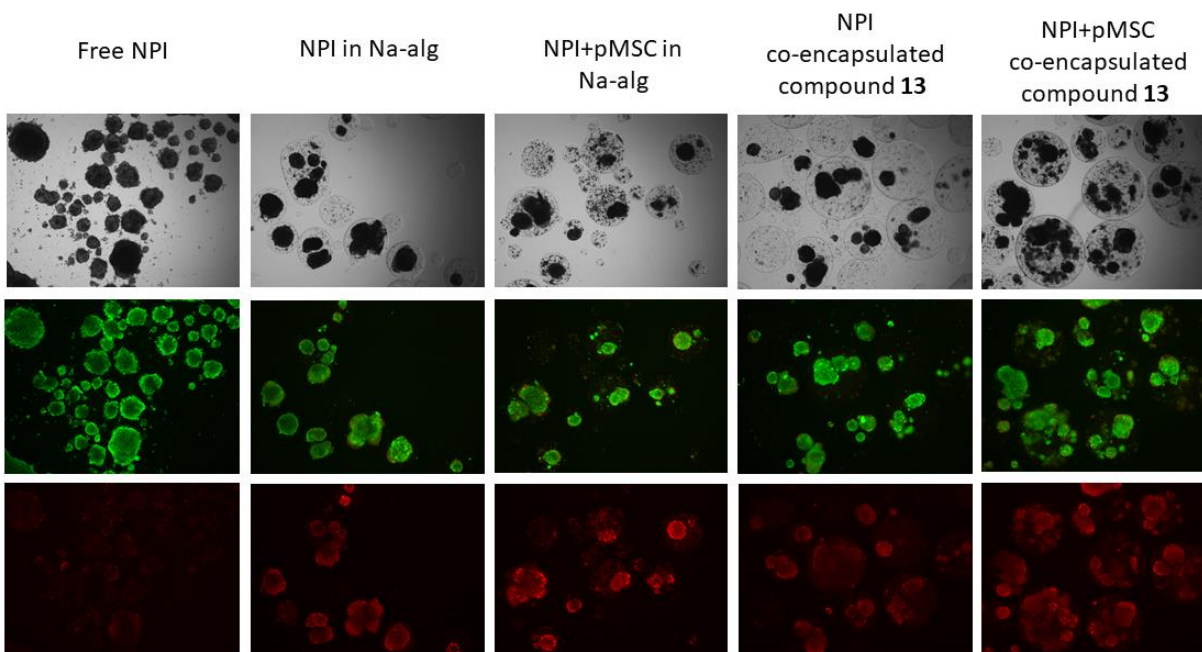
*Figure 6.5. Microscopy images of free NPI and NPI or NPI+pMSC encapsulated in Na-alg, and co-encapsulated with compound **13**, at day 7. Top panel: light microscopy, middle panel: staining of live cells with FDA (green), bottom panel: staining of dead cells with PI (red).*

Day 7 after encapsulation
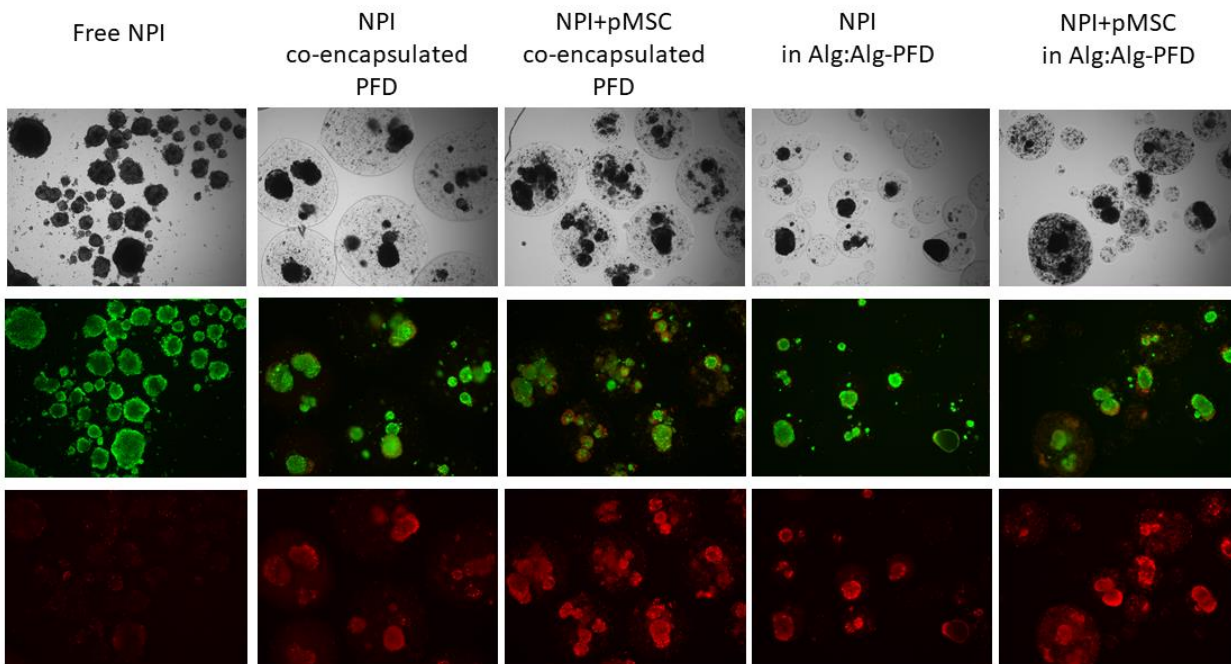
Figure 6.6. Microscopy images of free NPI and NPI or NPI + pMSC co-encapsulated with PFD, and encapsulated in Alg:Alg-PFD at day 7. Top panel: light microscopy, middle panel: staining of live cells with FDA (green), bottom panel: staining of dead cells with PI (red).
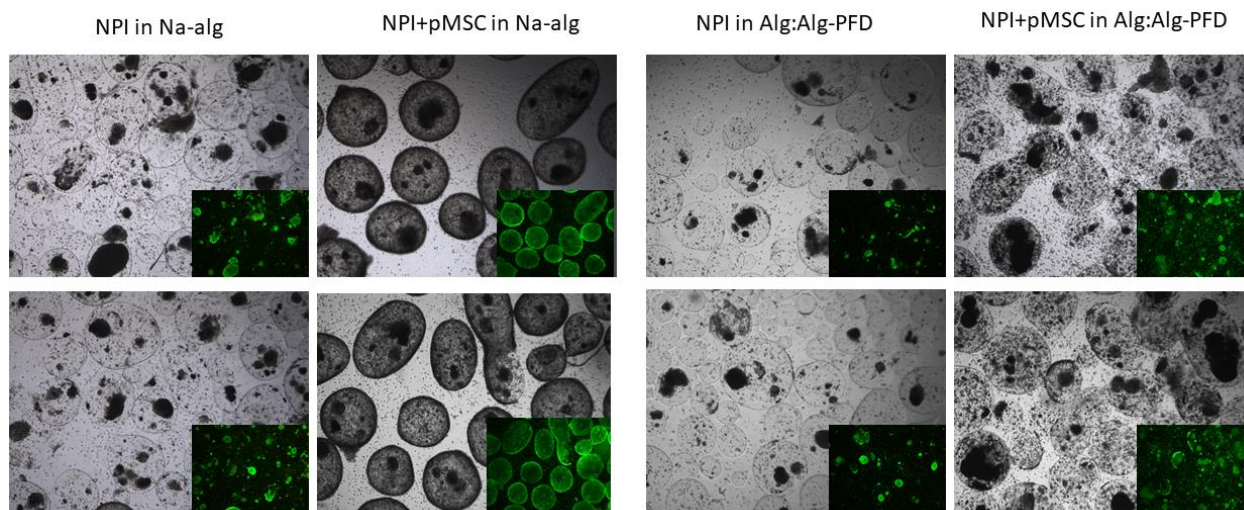
Figure 6.7. NPI and NPI+pMSC containing microcapsules of Na-alg and Alg:Alg-PFD recovered from the peritoneum of mice, 13 days after transplantation. Light microscopy images, and live cell staining with FDA (green).
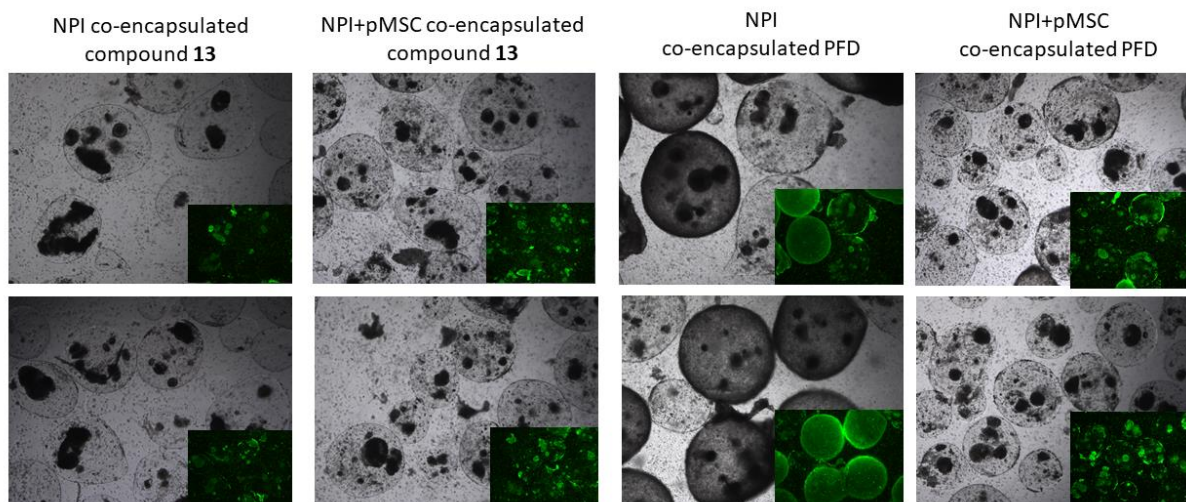
*Figure 6.8. NPI and NPI+pMSC containing microcapsules co-encapsulated with compound **13** and PFD recovered from the peritoneum of mice, 13 days after transplantation. Light microscopy images, and live cell staining with FDA (green).*
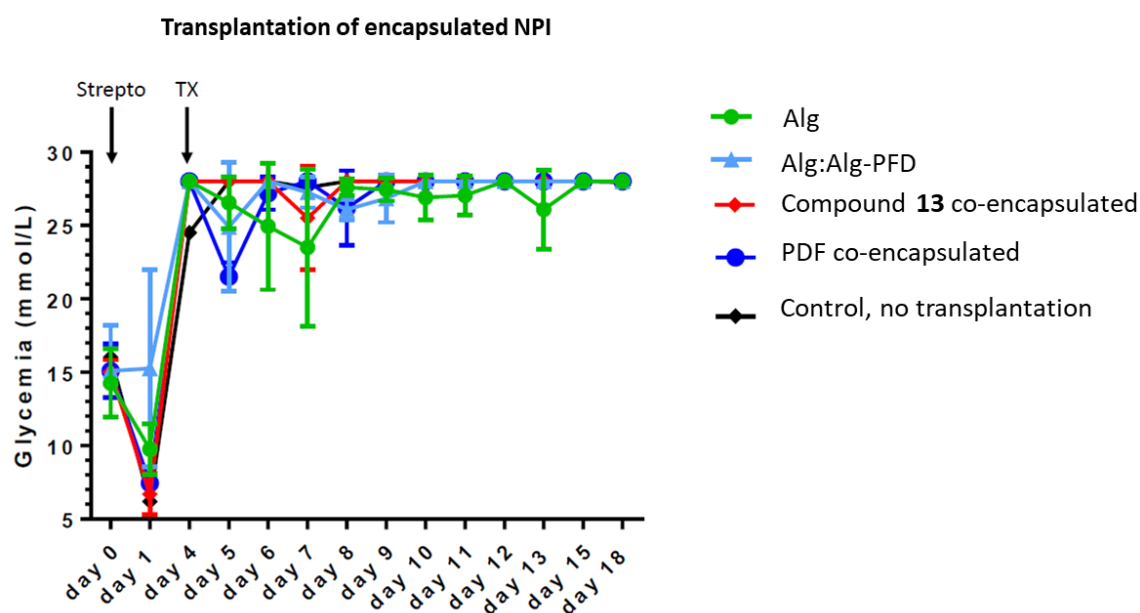
Figure 6.9. Blood glucose level changes in streptozotocin-induced diabetic mice transplanted with NPI containing microcapsules. Measurements were done daily, on two mouse/condition.
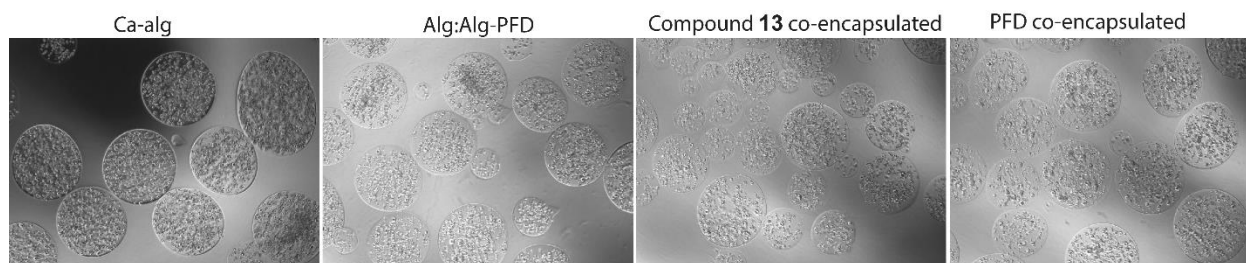
*Figure 6.10. pMSC encapsulated for in vivo evaluation of anti-fibrotic effect of Compound **13** and PFD. The microcapsules were further transplanted under the kidney capsule of immune-competent mice.*
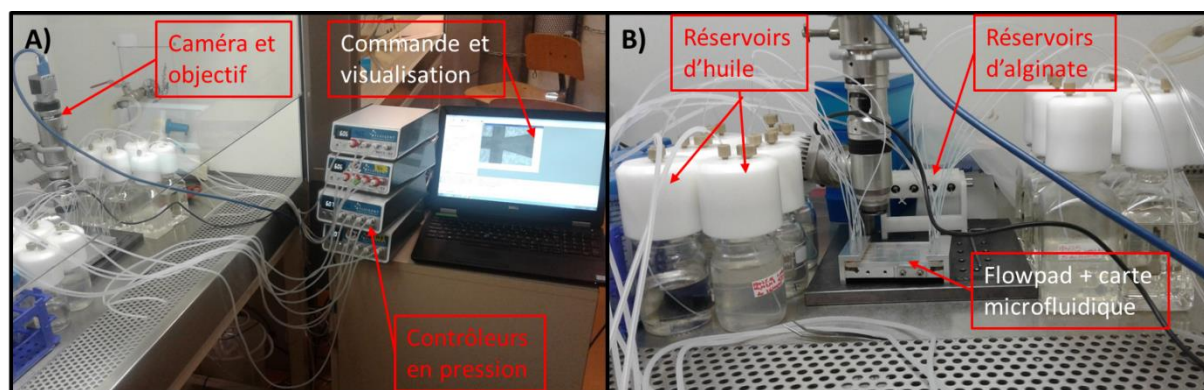
Figure 6.11. The microfluidic setup at CEA, Grenoble, for MS production.
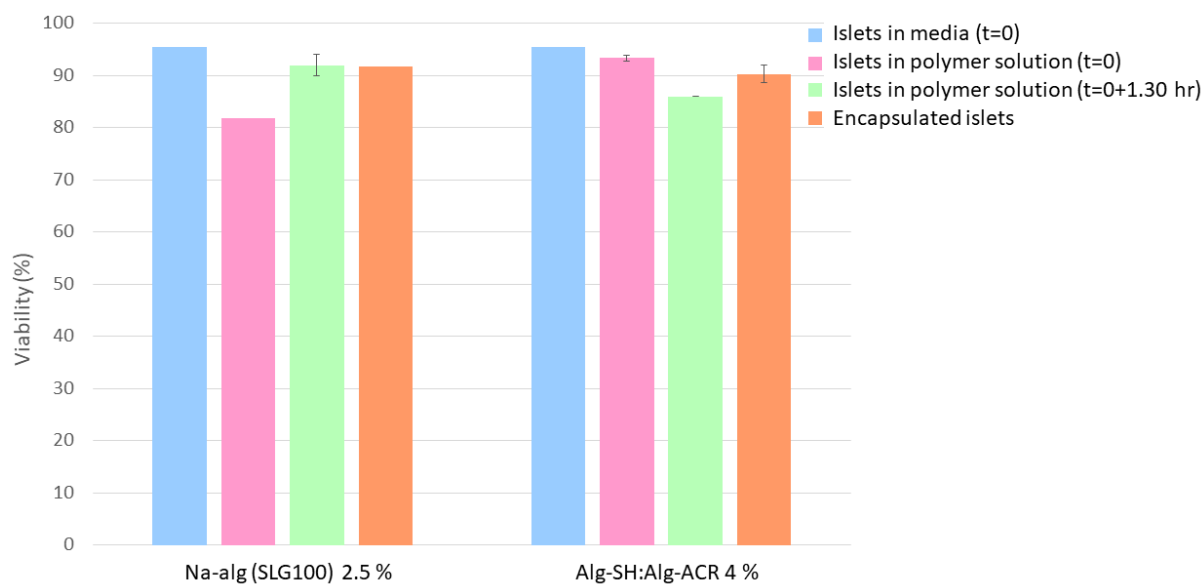
Figure 6.12. Viabilities of NPI right after encapsulation in a parallel microfluidic setup with Na-alg and Alg-SH:Alg-ACR polymers.

Characterization of MS prepared with microfluidics:
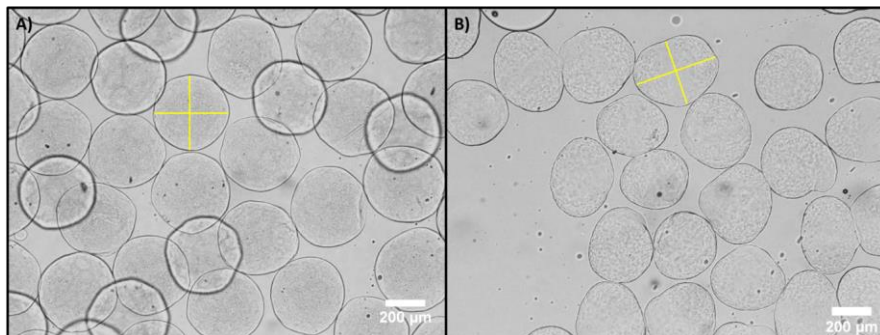
Characterization with ImageJ, on around 100 capsules :

- Take maximal (d_{max}) and minimal (d_{min}) diameter of a bead
- Aspect Ratio AR : $AR = \frac{d_{max}}{d_{min}}$

  (A perfectly spherical capsule has an AR of 1). In the example capsule in image A has an AR of 0,99, the capsule in image B has an AR of 0,79.
- For the monodispersity: Average of the 2 diameters for each capsule is measured, then the average of those mean diameters is calculated, and their standard deviation
- Coefficient of variation CV : $CV = \frac{standard\ deviation}{mean\ average}$

  It gives an idea about the monodispersity of capsules (we were aiming for a CV under 5%).

7. References

(1)   Application of Current Statutory Authorities to Human Somatic Cell Therapy Products and Gene Therapy Products, Notice. *Fed. Regist.* **1993**, *58*, 53247–53251.

(2)   Mason, C.; Brindley, D. A.; Culme-Seymour, E. J.; Davie, N. L. Cell Therapy Industry: Billion Dollar Global Business with Unlimited Potential. *Regen. Med.* **2011**, *6*, 265–272.

(3)   Tavassoli, M.; Crosby, W. Transplantation of Marrow to Extramedullary Sites. *Science* **1968**, *161*, 54–46.

(4)   Fischbach, M. A.; Bluestone, J. A.; Lim, W. A. Cell-Based Therapeutics: The next Pillar of Medicine. *Sci. Transl. Med.* **2013**, *5*, 1–7.

(5)   Heathman, T. R.; Nienow, A. W.; McCall, M. J.; Coopman, K.; Kara, B.; Hewitt, C. J. The Translation of Cell-Based Therapies: Clinical Landscape and Manufacturing Challenges. *Regen. Med.* **2015**, *10*, 49–64.

(6)   Anassi, E.; Ndefo, U. A. Sipuleucel-T (Provenge) Injection the First Immunotherapy Agent (Vaccine) for Hormone-Refractory Prostate Cancer. *Pharm. Ther.* **2011**, *36*, 197–202.

(7)   Aiuti, A.; Roncarolo, M. G.; Naldini, L. Gene Therapy for ADA-SCID, the First Marketing Approval of an Ex Vivo Gene Therapy in Europe: Paving the Road for the next Generation of Advanced Therapy Medicinal Products. *EMBO Mol. Med.* **2017**, *9*, 737–740.

(8)   Zheng, P. P.; Kros, J. M.; Li, J. Approved CAR T Cell Therapies: Ice Bucket Challenges on Glaring Safety Risks and Long-Term Impacts. *Drug Discov. Today* **2018**, *23*, 1175–1182.

(9)   Labanieh, L.; Majzner, R. G.; Mackall, C. L. Programming CAR-T Cells to Kill Cancer. *Nat. Biomed. Eng.* **2018**, *2*, 377–391.

(10)   Graham, C.; Hewitson, R.; Pagliuca, A.; Benjamin, R. Cancer Immunotherapy with CAR-T Cells - Behold the Future. *Clin. Med.* **2018**, *18*, 324–328.

(11)   Mardiana, S.; Solomon, B. J.; Darcy, P. K.; Beavis, P. A. Supercharging Adoptive T Cell Therapy to Overcome Solid Tumor-Induced Immunosuppression. *Sci. Transl. Med.* **2019**, *11*, 1–9.

(12)   Kimbrel, E. A.; Lanza, R. Current Status of Pluripotent Stem Cells: Moving the First Therapies to the Clinic. *Nat. Rev. Drug Discov.* **2015**, *14*, 681–692.

(13)   Thomson, J. A. Embryonic Stem Cell Lines Derived from Human Blastocysts. *Science* **1998**, *282*, 1145–1147.

(14)   Bobba, S.; Di Girolamo, N.; Munsie, M.; Chen, F.; Pébay, A.; Harkin, D.; Hewitt, A.; O'Connor, M.; McLenachan, S.; Shadforth, A. M. A.; et al. The Current State of Stem Cell Therapy for Ocular Disease. *Exp. Eye Res.* **2018**, *177*, 65–75.

(15)   Chen, H.; Zhang, A.; Wu, J. C. Harnessing Cell Pluripotency for Cardiovascular Regenerative Medicine. *Nat. Biomed. Eng.* **2018**, *2*, 392–398.

(16)   Rahim, F.; Arjmand, B.; Shirbandi, K.; Payab, M.; Larijani, B. Stem Cell Therapy for Patients with Diabetes: A Systematic Review and Meta-Analysis of Metabolomics-Based Risks and Benefits. *Stem Cell Investig.* **2018**, *5*, 40.

(17)   Sneddon, J. B.; Tang, Q.; Stock, P.; Bluestone, J. A.; Roy, S.; Desai, T.; Hebrok, M. Stem Cell Therapies for Treating Diabetes: Progress and Remaining Challenges. *Cell Stem Cell* **2018**, *22*, 810–823.

(18)   Garcia, O.; Carraro, G.; Navarro, S.; Bertoncello, I.; McQualter, J.; Driscoll, B.; Jesudason, E.; Warburton, D. Cell-Based Therapies for Lung Disease. *Br. Med. Bull.* **2012**, *101*, 147–161.

(19)   Serrano-Mollar, A. Cell Therapy in Idiopathic Pulmonary Fibrosis. *Med. Sci.* **2018**, *6*, 64.

(20)   Wattanapanitch, M. Recent Updates on Induced Pluripotent Stem Cells in Hematological Disorders. *Stem Cells Int.* **2019**, *2019*, 1–15.

(21)   Claudio, B. Stem-Cell Therapies for Blood Diseases. *Nature* **2006**, *441*, 1100–1102.

(22)   Ruiz, M. A.; Junior, R. L. K.; Piron-Ruiz, L.; Peña-Arciniegas, T.; Saran, P. S.; De Quadros, L. G. Hematopoietic Stem Cell Transplantation for Crohn's Disease: Gaps, Doubts and Perspectives. *World J. Stem Cells* **2018**, *10*, 134–137.

(23)   Schulte, L.; Hohwieler, M.; Müller, M.; Klaus, J. Intestinal Organoids as a Novel Complementary Model to Dissect Inflammatory Bowel Disease. *Stem Cells Int.* **2019**, *2019*.

(24)   Mohamed, M. S.; Chen, Y.; Yao, C. L. Intestinal Stem Cells and Stem Cell-Based Therapy for Intestinal Diseases. *Cytotechnology* **2015**, *67*, 177–189.

(25)   Song, C. G.; Zhang, Y. Z.; Wu, H. N.; Cao, X. L.; Guo, C. J.; Li, Y. Q.; Zheng, M. H.; Han, H. Stem Cells: A Promising Candidate to Treat Neurological Disorders. *Neural Regen. Res.* **2018**, *13*, 1294–1304.

(26)   Ogliari, K. S.; Marinowic, D.; Brum, D. E.; Loth, F. Stem Cells in Dermatology. *An. Bras. Dermatol.* **2014**, *89*, 286–291.

(27)   Volarevic, V.; Markovic, B. S.; Gazdic, M.; Volarevic, A.; Jovicic, N.; Arsenijevic, N.; Armstrong, L.; Djonov, V.; Lako, M.; Stojkovic, M. Ethical and Safety Issues of Stem Cell-Based Therapy. *Int. J. Med. Sci.* **2018**, *15*, 36–45.

(28)   Poulos, J. The Limited Application of Stem Cells in Medicine: A Review. *Stem Cell Res. Ther.* **2018**, *9*, 1–11.

(29)   Martin, U. Therapeutic Application of Pluripotent Stem Cells: Challenges and Risks. *Front. Med.* **2017**, *4*, 229.

(30)   Kahanovitz, L.; Sluss, P. M.; Russell, S. J. Type 1 Diabetes-a Clinical Perspective. *Point Care* **2017**, *16*, 37–40.

(31)   Lind, M.; Svensson, A.-M.; Kosiborod, M.; Gidbjörnsdottir, S.; Pivodic, A.; Wedel, H.; Dahlqvist, S.; Clements, M.; Rosengren, A. Glycemic Control and Excess Mortality in Type 1 Diabetes. *N. Engl. J. Med.* **2014**, *371*, 1972–1982.

(32)   Livingstone, S. J.; Levin, D.; Looker, H. C.; Lindsay, R. S.; Wild, S. H.; Joss, N.; Leese, G.; Leslie, P.; McCrimmon, R. J.; Metcalfe, W.; et al. Estimated Life Expectancy in a Scottish Cohort with Type 1 Diabetes, 2008-2010. *JAMA* **2015**, *313*, 37–44.

(33)   Vantyghem, M.-C.; de Koning, E. J. P.; Pattou, F.; Rickels, M. R. Advances in β-Cell Replacement Therapy for the Treatment of Type 1 Diabetes. *The Lancet.* **2019**, 1274–1285.

(34)   Bottino, R.; Knoll, M. F.; Knoll, C. A.; Bertera, S.; Trucco, M. M. The Future of Islet

Transplantation Is Now. *Front. Med.* **2018**, *5*, 1–13.

(35) Kelly, W.; Lillehei, R.; Merkel, F.; Idezuki, Y.; Goetz, F. Allotransplantation of the Pancreas and Duodenum along with the Kidney in Diabetic Nephropathy. *Surgery* **1967**, *61*, 827–837.

(36) Ballinger, W.; Lacy, P. Transplantation of Intact Pancreatic Islets in Rats. *Surgery* **1972**, *72*, 175–186.

(37) Scharp, D. W.; Lacy, P. E.; Santiago, J. V.; Mccullough, C. S.; Weide, L. G.; Falqui, L.; Marchetti, P.; Gingerich, R. L.; Jaffe, A. S.; Cryer, P. E.; et al. Insulin Independence after Islet Transplantation into Type I Diabetic Patient. *Diabetes* **1990**, *39*, 515–518.

(38) Shapiro, J. A. M.; Lakey, J. R. T.; Edmond, R. A.; Korbutt, G. S.; Toth, E.; Warnock, G. L.; Kneteman, N. M.; Rajotte, R. V. Islet Transplantation in Seven Patients with Type 1 Diabetes Mellitus Using a Glucocorticoid-Free Immunosuppressive Regimen. *N. Engl. J. Med.* **2000**, *343*, 230–238.

(39) Hering, B. J.; Raja, K.; Jeffrey D., A.; Eckman, P. M.; Masahiko, N.; Sawada, T.; Matsumoto, I.; Ihm, S.-H.; Zhang, H.-J.; Parkey, J.; et al. Single-Donor, Marginal-Dose Islet Transplantation in Patients With Type 1 Diabetes. *JAMA* **2005**, *293*, 830–836.

(40) Anazawa, T.; Okajima, H.; Masui, T.; Uemoto, S. Current State and Future Evolution of Pancreatic Islet Transplantation. *Ann. Gastroenterol. Surg.* **2019**, *3*, 34–42.

(41) Abou-El-Enein, M.; Hey, S. P. Cell and Gene Therapy Trials: Are We Facing an 'Evidence Crisis'? *EClinicalMedicine* **2019**, *7*, 13–14.

(42) Aijaz, A.; Li, M.; Smith, D.; Khong, D.; Leblon, C.; Fenton, O. S.; Olabisi, R. M.; Libutti, S.; Tischfield, J.; Maus, M. V.; et al. Biomanufacturing for Clinically Advanced Cell Therapies. *Nat. Biomed. Eng.* **2018**, *2*, 362–376.

(43) Ponte, G. M.; Pileggi, A.; Messinger, S.; Alejandro, A.; Ichii, H.; Baidal, D. A.; Khan, A.; Ricordi, C.; Goss, J. A.; Alejandro, R. Toward Maximizing the Success Rates of Human Islet Isolation: Influence of Donor and Isolation Factors. *Cell Transplant.* **2007**, *16*, 595–607.

(44) Horner, R.; Gassner, J. G. M. V.; Kluge, M.; Tang, P.; Lippert, S.; Hillebrandt, K. H.; Moosburner, S.; Reutzel-Selke, A.; Pratschke, J.; Sauer, I. M.; et al. Impact of Percoll Purification on Isolation of Primary Human Hepatocytes. *Sci. Rep.* **2019**, *9*, 2–11.

(45) Nanji, A. S.; Shapiro, J. A. M. Islet Transplantation in Patients with Diabetes Mellitus. *Biodrugs* **2004**, *18*, 315–328.

(46) Duncan, M. D.; Wilkes, D. S. Transplant-Related Immunosuppression: A Review of Immunosuppression and Pulmonary Infections. *Proc. Am. Thorac. Soc.* **2005**, *2*, 449–455.

(47) Pazetti, R.; Pêgo-Fernandes, P. M.; Jatene, F. B. Adverse Effects of Immunosuppressant Drugs upon Airway Epithelial Cell and Mucociliary Clearance: Implications for Lung Transplant Recipients. *Drugs* **2013**, *73*, 1157–1169.

(48) Diehl, R.; Ferrara, F.; Müller, C.; Dreyer, A. Y.; McLeod, D. D.; Fricke, S.; Boltze, J. Immunosuppression for in Vivo Research: State-of-The-Art Protocols and Experimental Approaches. *Cell. Mol. Immunol.* **2017**, *14*, 146–179.

(49) Yang, Y. G.; Sykes, M. Xenotransplantation: Current Status and a Perspective on the Future. *Nat. Rev. Immunol.* **2007**, *7*, 519–531.

(50) Meier, R. P. H.; Muller, Y. D.; Balaphas, A.; Morel, P.; Pascual, M.; Seebach, J. D.; Buhler, L. H. Xenotransplantation: Back to the Future? *Transpl. Int.* **2018**, *31*, 465–477.

(51) Dong, N.; Hong-Jiang, W.; Lin, L.; Haydy, George; Tao, W.; I-Hsiu, L.; Hong-Ye, Z.; Yong, W.; Yinan, K.; Ellen, S.; et al. Inactivation of Porcine Endogenous Retrovirus in Pigs Using CRISPR-Cas9. *Science* **2017**, *357*, 1303–1307.

(52) Richter, B.; Neises, G. Human versus Animal Insulin in People with Diabetes Mellitus: A Systematic Review. *Cochrane Database Syst. Rev.* **2005**.

(53) Van Der Windt, D. J.; Bottino, R.; Kumar, G.; Wijkstrom, M.; Hara, H.; Ezzelarab, M.; Ekser, B.; Phelps, C.; Murase, N.; Casu, A.; et al. Clinical Islet Xenotransplantation: How Close Are We? *Diabetes* **2012**, *61*, 3046–3055.

(54) Nagaraju, S.; Bottino, R.; Wijkstrom, M.; Trucco, M.; Cooper, D. K. C. Islet Xenotransplantation: What Is the Optimal Age of the Islet-Source Pig? *Xenotransplantation* **2015**, *22*, 7–19.

(55) Zhu, H.-T.; Yu, L.; Lyu, Y.; Wang, B. Optimal Pig Donor Selection in Islet Xenotransplantation: Current Status and Future Perspectives. *J Zhejiang Univ-Sci B (Biomed Biotechnol)* **2014**, *15*, 681–691.

(56) Hecht, G.; Eventov-Friedman, S.; Rosen, C.; Shezen, E.; Tchorsh, D.; Aronovich, A.; Freud, E.; Golan, H.; El-Hasid, R.; Katchman, H.; et al. Embryonic Pig Pancreatic Tissue for the Treatment of Diabetes in a Nonhuman Primate Model. *Proc. Natl. Acad. Sci. U. S. A.* **2009**, *106*, 8659–8664.

(57) Eventov-Friedman, S.; Tchorsh, D.; Katchman, H.; Shezen, E.; Aronovich, A.; Hecht, G.; Dekel, B.; Rechavi, G.; Blazar, B. R.; Feine, I.; et al. Embryonic Pig Pancreatic Tissue Transplantation for the Treatment of Diabetes. *PLoS Med.* **2006**, *3*, 1165–1177.

(58) Korbutt, G. S.; Elliott, J. F.; Ao, Z.; Smith, D. K.; Warnock, G. L.; Rajotte, R. V. Large Scale Isolation, Growth, and Function of Porcine Neonatal Islet Cells. *J. Clin. Invest.* **1996**, *97*, 2119–2129.

(59) Weir, G. C.; Quickel, R. R.; Yoon, K.; Ulrich, T. R.; Bonner-weir, J. H. S. Porcine Neonatal Pancreatic Cell Clusters (NPCCs): A Potential Source of Tissue for Islet Transplantation. *Ann. Transplant.* **1997**, *2*, 63–68.

(60) Emamaullee, J. A.; Shapiro, A. M. J.; Rajotte, R. V.; Korbutt, G.; Elliott, J. F. Neonatal Porcine Islets Exhibit Natural Resistance to Hypoxia-Induced Apoptosis. *Transplantation* **2006**, *82*, 945–952.

(61) Orive, G.; Hernández, R. M.; Gascón, A. R.; Calafiore, R.; Chang, T. M. S.; De Vos, P.; Hortelano, G.; Hunkeler, D.; Lacík, I.; Shapiro, A. M. J.; et al. Cell Encapsulation: Promise and Progress. *Nat. Med.* **2003**, *9*, 104–107.

(62) Olabisi, R. M. Cell Microencapsulation with Synthetic Polymers. *J. Biomed. Mater. Res. Part A* **2015**, *103*, 846–859.

(63) Rossow, T.; Lienemann, P. S.; Mooney, D. J. Cell Microencapsulation by Droplet Microfluidic Templating. *Macromol. Chem. Phys.* **2017**, *218*, 1–14.

(64) Omami, M.; McGarrigle, J. J.; Reedy, M.; Isa, D.; Ghani, S.; Marchese, E.; Bochenek, M. A.; Longi, M.; Xing, Y.; Joshi, I.; et al. Islet Microencapsulation: Strategies and Clinical Status in Diabetes. *Curr. Diab. Rep.* **2017**, *17*, 1–7.

(65) Bisceglie, V. Uber Die Antineoplastische Immnnitat; Heterologe Einpflanzung von Tumoren in Huhner-Embryonen. *V. Zeitschrift für Krebsforsch.* **1933**, *40*, 122–140.

(66) Glenn H. A.; James M. W.; Richmond T. P. Growth of Cells In Vivo in Diffusion Chambers. I. Survival of Homografts in Immunized Mice. *J. Natl. Cancer Inst.* **1954**, *15*, 493–507.

(67) Chang, T. M. Semipermeable Microcapsules. *Sci. New Ser.* **1964**, *146*, 524–525.

(68) Chang, T. M. S. 50th Anniversary of Artificial Cells: Their Role in Biotechnology, Nanomedicine, Regenerative Medicine, Blood Substitutes, Bioencapsulation, Cell/Stem Cell Therapy and Nanorobotics. *Artif. Cells, Blood Substitutes, Biotechnol.* **2007**, *35*, 545–554.

(69) Franklin, L.; Anthony M. S. Microencapsulated Islets as Bioartificial Endocrine Pancreas. *Science* **1980**, *210*, 908–910.

(70) Soon-Shiong, P.; Heintz, R. E.; Merideth, N.; Yao, Q. X.; Yao, Z.; Zheng, T.; Murphy, M.; Moloney, M. K.; Schmehl, M.; Harris, M.; et al. Insulin Independence in a Type 1 Diabetic Patient after Encapsulated Islet Transplantation. *Lancet* **1994**, *343*, 950–951.

(71) Ernst, A. U.; Wang, L. H.; Ma, M. Interconnected Toroidal Hydrogels for Islet Encapsulation. *Adv. Healthc. Mater.* **2019**, *1900423*, 1–8.

(72) Weaver, J. D.; Headen, D. M.; Hunckler, M. D.; Coronel, M. M.; Stabler, C. L.; García, A. J. Design of a Vascularized Synthetic Poly(Ethylene Glycol) Macroencapsulation Device for Islet Transplantation. *Biomaterials* **2018**, *172*, 54–65.

(73) Evron, Y.; Colton, C. K.; Ludwig, B.; Weir, G. C.; Zimermann, B.; Maimon, S.; Neufeld, T.; Shalev, N.; Goldman, T.; Leon, A.; et al. Long-Term Viability and Function of Transplanted Islets Macroencapsulated at High Density Are Achieved by Enhanced Oxygen Supply. *Sci. Rep.* **2018**, *8*, 1–13.

(74) Willem M., K.; Robert P., L.; William L., C. *Cell Encapsulation Technology and Therapeutics*; **1999**.

(75) Bitar, C. M. E.; Markwick, K. E.; Treľová, D.; Kroneková, Z.; Pelach, M.; Selerier, C. M. O.; Dietrich, J.; Lacík, I.; Hoesli, C. A. Development of a Microchannel Emulsification Process for Pancreatic Beta Cell Encapsulation. *Biotechnol. Prog.* **2019**, *35*, e2851.

(76) Hoesli, C. A.; Raghuram, K.; Kiang, R. L. J.; Mocinecová, D.; Hu, X.; Johnson, J. D.; Lacík, I.; Kieffer, T. J.; Piret, J. M. Pancreatic Cell Immobilization in Alginate Beads Produced by Emulsion and Internal Gelation. *Biotechnol. Bioeng.* **2011**, *108*, 424–434.

(77) Yaakov, N.; Ananth Mani, K.; Felfbaum, R.; Lahat, M.; Da Costa, N.; Belausov, E.; Ment, D.; Mechrez, G. Single Cell Encapsulation via Pickering Emulsion for Biopesticide Applications. *ACS Omega* **2018**, *3*, 14294–14301.

(78) Prüsse, U.; Bilancetti, L.; Bučko, M.; Bugarski, B.; Bukowski, J.; Gemeiner, P.; Lewińska, D.; Manojlovic, V.; Massart, B.; Nastruzzi, C.; et al. Comparison of Different Technologies for Alginate Beads Production. *Chem. Pap.* **2008**, *62*, 364–374.

(79) Utech, S.; Prodanovic, R.; Mao, A. S.; Ostafe, R.; Mooney, D. J.; Weitz, D. A. Microfluidic Generation of Monodisperse, Structurally Homogeneous Alginate Microgels for Cell Encapsulation and 3D Cell Culture. *Adv. Healthc. Mater.* **2015**, *4*, 1628–1633.

(80) Headen, D. M.; García, J. R.; García, A. J. Parallel Droplet Microfluidics for High Throughput Cell Encapsulation and Synthetic Microgel Generation. *Microsystems*

Nanoeng. **2018**, *4*, 1–9.

(81)   Brouzes, E.; Medkova, M.; Savenelli, N.; Marran, D.; Twardowski, M.; Hutchison, J. B.; Rothberg, J. M.; Link, D. R.; Perrimon, N.; Samuels, M. L. Droplet Microfluidic Technology for Single-Cell High-Throughput Screening. *Proc. Natl. Acad. Sci. U. S. A.* **2009**, *106*, 14195–14200.

(82)   Bučko, M.; Vikartovská, A.; Lacík, I.; Kolláriková, G.; Gemeiner, P.; Pätoprstý, V.; Brygin, M. Immobilization of a Whole-Cell Epoxide-Hydrolyzing Biocatalyst in Sodium Alginate-Cellulose Sulfate-Poly(Methylene-Co-Guanidine) Capsules Using a Controlled Encapsulation Process. *Enzyme Microb. Technol.* **2005**, *36*, 118–126.

(83)   Passemard, S.; Szabó, L.; Noverraz, F.; Montanari, E.; Gonelle-Gispert, C.; Bühler, L. H.; Wandrey, C.; Gerber-Lemaire, S. Synthesis Strategies to Extend the Variety of Alginate-Based Hybrid Hydrogels for Cell Microencapsulation. *Biomacromolecules* **2017**, *18*, 2747–2755.

(84)   Bugarski, B.; Li, Q.; Goosen, M. F. A.; Poncelet, D.; Neufeld, R. J.; Vunjak, G. Electrostatic Droplet Generation: Mechanism of Polymer Droplet Formation. *AIChE J.* **1994**, *40*, 1026–1031.

(85)   Manojlovic, V.; Djonlagic, J.; Obradovic, B.; Nedovic, V.; Bugarski, B. Investigations of Cell Immobilization in Alginate: Rheological and Electrostatic Extrusion Studies. *J. Chem. Technol. Biotechnol.* **2006**, *81*, 505–510.

(86)   Micheal, W.; Ian W., M. Microencapsulation Using Vibrating Technology. *J. Microencapsul.* **2011**, *28*, 669–688.

(87)   Prüße, U.; Jahnz, U.; Wittlich, P.; Breford, J.; Vorlop, K.-D. Bead Production with JetCutting and Rotating Disk/Nozzle Technologies. *Landbauforsch. Völkenrode SH.* **2002**, *241*, 1–10.

(88)   Teunou, E.; Poncelet, D. Rotary Disc Atomisation for Microencapsulation Applications-Prediction of the Particle Trajectories. *J. Food Eng.* **2005**, *71*, 345–353.

(89)   Prüße, U.; Dalluhn, J.; Breford, J.; Vorlop, K. D. Production of Spherical Beads by JetCutting. *Chem. Eng. Technol.* **2000**, *23*, 1105–1110.

(90)   Wu, Z.; Su, X.; Xu, Y.; Kong, B.; Sun, W.; Mi, S. Bioprinting Three-Dimensional Cell-Laden Tissue Constructs with Controllable Degradation. *Sci. Rep.* **2016**, *6*, 1–10.

(91)   Sittadjody, S.; Saul, J. M.; McQuilling, J. P.; Joo, S.; Register, T. C.; Yoo, J. J.; Atala, A.; Opara, E. C. In Vivo Transplantation of 3D Encapsulated Ovarian Constructs in Rats Corrects Abnormalities of Ovarian Failure. *Nat. Commun.* **2017**, *8*, 1858.

(92)   Wang, J.; Huang, R.; Chen, H.; Qiao, X.; Shi, X.; Wang, X.; Cheng, Y.; Tan, W.; Tan, Z. Personalized Single-Cell Encapsulation Using E-Jet 3D Printing with AC-Pulsed Modulation. *Macromol. Mater. Eng.* **2019**, *304*, 1–8.

(93)   Mazzitelli, S.; Capretto, L.; Quinci, F.; Piva, R.; Nastruzzi, C. Preparation of Cell-Encapsulation Devices in Confined Microenvironment. *Adv. Drug Deliv. Rev.* **2013**, *65*, 1533–1555.

(94)   Kang, A. R.; Park, J. S.; Ju, J.; Jeong, G. S.; Lee, S. H. Cell Encapsulation via Microtechnologies. *Biomaterials* **2014**, *35*, 2651–2663.

(95)   Zhu, K.; Yu, Y.; Cheng, Y.; Tian, C.; Zhao, G.; Zhao, Y. All-Aqueous-Phase Microfluidics for

Cell Encapsulation. *ACS Appl. Mater. Interfaces* **2019**, *11*, 4826–4832.

(96) Mahou, R.; Passemard, S.; Carvello, M.; Petrelli, A.; Noverraz, F.; Gerber-Lemaire, S.; Wandrey, C. Contribution of Polymeric Materials to Progress in Xenotransplantation of Microencapsulated Cells: A Review. *Xenotransplantation* **2016**, *23*, 179–201.

(97) Mitrousis, N.; Fokina, A.; Shoichet, M. S. Biomaterials for Cell Transplantation. *Nat. Rev. Mater.* **2018**, *3*, 441–456.

(98) Augst, A. D.; Kong, H. J.; Mooney, D. J. Alginate Hydrogels as Biomaterials. *Macromol. Biosci.* **2006**, *6*, 623–633.

(99) Wichterle, O.; Lim, D. Hydrophilic Gels for Biological Use. *Nature* **1960**, 117–118.

(100) Gauvin, R.; Parenteau-Bareil, R.; Dokmeci, M. R.; Merryman, W. D.; Khademhosseini, A. Hydrogels and Microtechnologies for Engineering the Cellular Microenvironment. *Wiley Interdiscip. Rev. Nanomedicine Nanobiotechnology* **2012**, *4*, 235–246.

(101) Vermonden, T.; Klumperman, B. The Past, Present and Future of Hydrogels. *Eur. Polym. J.* **2015**, *72*, 341–343.

(102) Foyt, D. A.; Norman, M. D. A.; Yu, T. T. L.; Gentleman, E. Exploiting Advanced Hydrogel Technologies to Address Key Challenges in Regenerative Medicine. *Adv. Healthc. Mater.* **2018**, *7*, 1700939.

(103) Zheng, S. Y.; Ding, H.; Qian, J.; Yin, J.; Wu, Z. L.; Song, Y.; Zheng, Q. Metal-Coordination Complexes Mediated Physical Hydrogels with High Toughness, Stick-Slip Tearing Behavior, and Good Processability. *Macromolecules* **2016**, *49*, 9637–9646.

(104) Okay, O. Semicrystalline Physical Hydrogels with Shape-Memory and Self-Healing Properties. *J. Mater. Chem. B* **2019**, *7*, 1581–1596.

(105) Guo, H.; Nakajima, T.; Hourdet, D.; Marcellan, A.; Creton, C.; Hong, W.; Kurokawa, T.; Gong, J. P. Hydrophobic Hydrogels with Fruit-Like Structure and Functions. *Adv. Mater.* **2019**, *31*, 1–8.

(106) Ye, X.; Li, X.; Shen, Y.; Chang, G.; Yang, J.; Gu, Z. Self-Healing PH-Sensitive Cytosine- and Guanosine-Modified Hyaluronic Acid Hydrogels via Hydrogen Bonding. *Polymer* **2017**, *108*, 348–360.

(107) Zhang, G.; Chen, Y.; Deng, Y.; Ngai, T.; Wang, C. Dynamic Supramolecular Hydrogels: Regulating Hydrogel Properties through Self-Complementary Quadruple Hydrogen Bonds and Thermo-Switch. *ACS Macro Lett.* **2017**, *6*, 641–646.

(108) Tuncaboylu, D. C.; Sari, M.; Oppermann, W.; Okay, O. Tough and Self-Healing Hydrogels Formed via Hydrophobic Interactions. *Macromolecules* **2011**, *44*, 4997–5005.

(109) Mihajlovic, M.; Staropoli, M.; Appavou, M. S.; Wyss, H. M.; Pyckhout-Hintzen, W.; Sijbesma, R. P. Tough Supramolecular Hydrogel Based on Strong Hydrophobic Interactions in a Multiblock Segmented Copolymer. *Macromolecules* **2017**, *50*, 3333–3346.

(110) Kuo, C. K.; Ma, P. X. Ionically Crosslinked Alginate Hydrogels as Scaffolds for Tissue Engineering: Part 1. Structure, Gelation Rate and Mechanical Properties. *Biomaterials* **2001**, *22*, 511–521.

(111) Sánchez, P.; Hernández, R. M.; Pedraz, J. L.; Orive, G. Encapsulation of Cells in Alginate

Gels. In *Immobilization of Enzymes and Cells. Methods in Molecular Biology (Methods and Protocoles), Humana Press* **2013**, 313–323.

(112) Urtuvia, V.; Maturana, N.; Acevedo, F.; Peña, C.; Díaz-Barrera, A. Bacterial Alginate Production: An Overview of Its Biosynthesis and Potential Industrial Production. *World J. Microbiol. Biotechnol.* **2017**, *33*, 1–10.

(113) Clark, D. E.; Green, H. C. Alginic Acid and Process of Making Same. US Patent 2036922, **1936**.

(114) Gacesa, P. Alginates. *Carbohydr. Polym.* **1988**, *8*, 161–182.

(115) Haug, A.; Myklestad, S.; Larsen, B.; Smidsrød, O.; Eriksson, G.; Blinc, R.; Paušak, S.; Ehrenberg, L.; Dumanović, J. Correlation between Chemical Structure and Physical Properties of Alginates. *Acta Chem. Scand.* **1967**, *21*, 768–778.

(116) Draget, K. I.; Simensen, M. K.; Onsøyen, E.; Smidsrød, O. Gel Strength of Ca-Limited Alginate Gels Made in Situ. *Hydrobiologia* **1993**, *260–261*, 563–565.

(117) Fu, S.; Thacker, A.; Sperger, D. M.; Boni, R. L.; Buckner, I. S.; Velankar, S.; Munson, E. J.; Block, L. H. Relevance of Rheological Properties of Sodium Alginate in Solution to Calcium Alginate Gel Properties. *AAPS PharmSciTech* **2011**, *12*, 453–460.

(118) Lee, K. Y.; Mooney, D. J. Alginate: Properties and Biomedical Applications. *Prog. Polym. Sci.* **2012**, *37*, 106–126.

(119) Grant, G. T.; Morris, E. R.; Rees, D. A.; Smith, P. J. C.; Thom, D. Biological Interactions between Polysaccharides and Divalent Cations: The Egg-Box Model. *FEBS Lett.* **1973**, *32*, 195–198.

(120) Sikorski, P.; Mo, F.; Skjåk-Bræk, G.; Stokke, B. T. Evidence for Egg-Box-Compatible Interactions in Calcium - Alginate Gels from Fiber x-Ray Diffraction. *Biomacromolecules* **2007**, *8*, 2098–2103.

(121) Duvivier-Kali, V. F.; Omer, A.; Lopez-Avalos, M. D.; O'Neil, J. J.; Weir, G. C. Survival of Microencapsulated Adult Pig Islets in Mice in Spite of an Antibody Response. *Am. J. Transplant.* **2004**, *4*, 1991–2000.

(122) Qi, M.; Mørch, Y.; Lacík, I.; Formo, K.; Marchese, E.; Wang, Y.; Danielson, K. K.; Kinzer, K.; Wang, S.; Barbaro, B.; et al. Survival of Human Islets in Microbeads Containing High Guluronic Acid Alginate Crosslinked with Ca^{2+} and Ba^{2+}. *Xenotransplantation* **2012**, *19*, 355–364.

(123) Strand, B. L.; Coron, A. E.; Skjak-Braek, G. Current and Future Perspectives on Alginate Encapsulated Pancreatic Islet. *Stem Cells Transl. Med.* **2017**, *6*, 1053–1058.

(124) Nicodemus, G. D.; Bryant, S. J. Cell Encapsulation in Biodegradable Hydrogels for Tissue Engineering Applications. *Tissue Eng. - Part B Rev.* **2008**, *14*, 149–165.

(125) Mironi-Harpaz, I.; Wang, D. Y.; Venkatraman, S.; Seliktar, D. Photopolymerization of Cell-Encapsulating Hydrogels: Crosslinking Efficiency versus Cytotoxicity. *Acta Biomater.* **2012**, *8*, 1838–1848.

(126) Almany, L.; Seliktar, D. Biosynthetic Hydrogel Scaffolds Made from Fibrinogen and Polyethylene Glycol for 3D Cell Cultures. *Biomaterials* **2005**, *26* (15), 2467–2477.

(127) Hong, Y.; Song, H.; Gong, Y.; Mao, Z.; Gao, C.; Shen, J. Covalently Crosslinked Chitosan

Hydrogel: Properties of in Vitro Degradation and Chondrocyte Encapsulation. *Acta Biomater.* **2007**, *3*, 23–31.

(128) Brunsen, A.; Ritz, U.; Mateescu, A.; Höfer, I.; Frank, P.; Menges, B.; Hofmann, A.; Rommens, P. M.; Knoll, W.; Jonas, U. Photocrosslinkable Dextran Hydrogel Films as Substrates for Osteoblast and Endothelial Cell Growth. *J. Mater. Chem.* **2012**, *22*, 19590–19604.

(129) Moreira Teixeira, L. S.; Feijen, J.; van Blitterswijk, C. A.; Dijkstra, P. J.; Karperien, M. Enzyme-Catalyzed Crosslinkable Hydrogels: Emerging Strategies for Tissue Engineering. *Biomaterials* **2012**, *33*, 1281–1290.

(130) Sakai, S.; Hashimoto, I.; Ogushi, Y.; Kawakami, K. Peroxidase-Catalyzed Cell Encapsulation in Subsieve-Size Capsules of Alginate with Phenol Moieties in Water-Immiscible Fluid Dissolving H_2O_2. *Biomacromolecules* **2007**, *8*, 2622–2626.

(131) Sakai, S.; Ito, S.; Ogushi, Y.; Hashimoto, I.; Hosoda, N.; Sawae, Y.; Kawakami, K. Enzymatically Fabricated and Degradable Microcapsules for Production of Multicellular Spheroids with Well-Defined Diameters of Less than 150 Mm. *Biomaterials* **2009**, *30*, 5937–5942.

(132) Yigit, S.; Sanyal, R.; Sanyal, A. Fabrication and Functionalization of Hydrogels through "Click" Chemistry. *Chem. Asian J.* **2011**, *6*, 2648–2659.

(133) Madl, C. M.; Heilshorn, S. C. Bioorthogonal Strategies for Engineering Extracellular Matrices. *Adv. Funct. Mater.* **2018**, *28*, 1–21.

(134) Gopinathan, J.; Noh, I. Click Chemistry-Based Injectable Hydrogels and Bioprinting Inks for Tissue Engineering Applications. *Tissue Eng. Regen. Med.* **2018**, *15*, 531–546.

(135) Jiang, Y.; Chen, J.; Deng, C.; Suuronen, E. J.; Zhong, Z. Click Hydrogels, Microgels and Nanogels: Emerging Platforms for Drug Delivery and Tissue Engineering. *Biomaterials* **2014**, *35*, 4969–4985.

(136) Kolb, H. C.; Finn, M. G.; Sharpless, K. B. Click Chemistry: Diverse Chemical Function from a Few Good Reactions. *Angew. Chem. Int. Ed. Engl.* **2001**, *40*, 2004–2021.

(137) Ossipov, D. A.; Hilborn, J. Poly(Vinyl Alcohol)-Based Hydrogels Formed by "Click Chemistry." *Macromolecules* **2006**, *39*, 1709–1718.

(138) Crescenzi, V.; Cornelio, L.; Di Meo, C.; Nardecchia, S.; Lamanna, R. Novel Hydrogels via Click Chemistry: Synthesis and Potential Biomedical Applications. *Biomacromolecules* **2007**, *8*, 1844–1850.

(139) Breger, J. C.; Fisher, B.; Samy, R.; Pollack, S.; Wang, N. S.; Isayeva, I. Synthesis of "Click" Alginate Hydrogel Capsules and Comparison of Their Stability, Water Swelling, and Diffusion Properties with That of Ca^{+2} Crosslinked Alginate Capsules. *J. Biomed. Mater. Res. Part B Appl. Biomater.* **2015**, *103*, 1120–1132.

(140) Henan, Z.; Heleen, de J.; Dennis W. P. M., L. Comparison of Bioorthogonally Cross-Linked Hydrogels for in Situ Cell Encapsulation. *ACS Appl. Bio Mater.* **2019**, *2*, 2862–2871.

(141) Vinh X. T.; Kelly M. T.; George P. S.; Richard L. B.; Richard A. E.; Helmut, T.; John S. F. Photodegradable Gelatin-Based Hydrogels Prepared by Bioorthogonal Click Chemistry for Cell Encapsulation and Release. *Biomacromolecules* **2015**, *16*, 2246–2253.

(142) Han, S. S.; Yoon, H. Y.; Yhee, J. Y.; Cho, M. O.; Shim, H. E.; Jeong, J. E.; Lee, D. E.; Kim,

K.; Guim, H.; Lee, J. H.; et al. In Situ Cross-Linkable Hyaluronic Acid Hydrogels Using Copper Free Click Chemistry for Cartilage Tissue Engineering. *Polym. Chem.* **2018**, *9*, 20–27.

(143) Yu, F.; Cao, X.; Li, Y.; Zeng, L.; Zhu, J.; Wang, G.; Chen, X. Diels-Alder Crosslinked HA/PEG Hydrogels with High Elasticity and Fatigue Resistance for Cell Encapsulation and Articular Cartilage Tissue Repair. *Polym. Chem.* **2014**, *5*, 5116–5123.

(144) Madl, C. M.; Heilshorn, S. C. Rapid Diels–Alder Cross-Linking of Cell Encapsulating Hydrogels. *Chem. Mater.* **2019**, 31, 8035–8043.

(145) Fu, Y.; Kao, W. J. In Situ Forming Poly(Ethylene Glycol)-Based Hydrogels via Thiol-Maleimide Michael-Type Addition. *J. Biomed. Mater. Res. A* **2011**, *98,* 201–211.

(146) Silviya P. Z.; Jennie B. L. Hydrolytically Degradable Poly(Ethylene Glycol) Hydrogel Scaffolds with Tunable Degradation and Mechanical Properties. *Biomacromolecules* **2011**, *11*, 1348–1357.

(147) Stewart, S. A.; Coulson, M. B.; Zhou, C.; Burke, N. A. D.; Stöver, H. D. H. Synthetic Hydrogels Formed by Thiol-Ene Crosslinking of Vinyl Sulfone-Functional Poly(Methyl Vinyl Ether-: Alt -Maleic Acid) with α,ω-Dithio-Polyethyleneglycol. *Soft Matter* **2018**, *14*, 8317–8324.

(148) Chatani, S.; Nair, D. P.; Bowman, C. N. Relative Reactivity and Selectivity of Vinyl Sulfones and Acrylates towards the Thiol-Michael Addition Reaction and Polymerization. *Polym. Chem.* **2013**, *4*, 1048–1055.

(149) Junpeng, X.; Yi, L.; Shan-hui, H. Hydrogels Based on Schiff Base Linkages for Biomedical Applications. *Molecules* **2019**, *24*, 1–21.

(150) Jalalvandi, E.; Hanton, L. R.; Moratti, S. C. Schiff-Base Based Hydrogels as Degradable Platforms for Hydrophobic Drug Delivery. *Eur. Polym. J.* **2017**, *90*, 13–24.

(151) Somo, S. I.; Langert, K.; Yang, C. Y.; Vaicik, M. K.; Ibarra, V.; Appel, A. A.; Akar, B.; Cheng, M. H.; Brey, E. M. Synthesis and Evaluation of Dual Crosslinked Alginate Microbeads. *Acta Biomater.* **2018**, *65*, 53–65.

(152) Jeon, O.; Shin, J. Y.; Marks, R.; Hopkins, M.; Kim, T. H.; Park, H. H.; Alsberg, E. Highly Elastic and Tough Interpenetrating Polymer Network-Structured Hybrid Hydrogels for Cyclic Mechanical Loading-Enhanced Tissue Engineering. *Chem. Mater.* **2017**, *29*, 8425–8432.

(153) Gattás-Asfura, K. M.; Stabler, C. L. Chemoselective Cross-Linking and Functionalization of Alginate via Staudinger Ligation. *Biomacromolecules* **2009**, *10*, 3122–3129.

(154) Kristina K. H.; Kerim M. G.-A.; Cherie L. S. Microencapsulation of Islets within Alginate/Poly(Ethyleneglycol) Gels Cross-Linked via Staudinger Ligation. *Acta Biomater.* **2011**, *7*, 614–624.

(155) Mahou, R.; Borcard, F.; Crivelli, V.; Montanari, E.; Passemard, S.; Noverraz, F.; Gerber-Lemaire, S.; Bühler, L.; Wandrey, C. Tuning the Properties of Hydrogel Microspheres by Adding Chemical Cross-Linking Functionality to Sodium Alginate. *Chem. Mater.* **2015**, *27*, 4380–4389.

(156) Drury, J. L.; Dennis, R. G.; Mooney, D. J. The Tensile Properties of Alginate Hydrogels. *Biomaterials* **2004**, *25*, 3187–3199.

(157) Moya, M. L.; Morley, M.; Khanna, O.; Opara, E. C.; Brey, E. M. Stability of Alginate Microbead Properties in Vitro. *J. Mater. Sci. Mater. Med.* **2012**, *23*, 903–912.

(158) Sminsrød, O.; Skjåk-Bræk, G. Alginate as Immobilization Matrix for Cells. *Trends Biotechnol.* **1990**, *8*, 71–78.

(159) de Vos, P.; De Haan, B.; Pater, J.; Van Schilfgaarde, R. Association between Capsule Diameter, Adequacy of Encapsulation, and Survival of Microencapsulated Rat Islet Allografts. *Transplantation* **1996**, *62*, 893–899.

(160) Kokufuta, E.; Yukishige, M.; Nakamura, I. Coimmobilization of Nitrosomonas Europaea and Paracoccus Denitrificans Cells Using Polyelectrolyte Complex- Stabilized Calcium Alginate Gel *J. Ferment. Technol.* **1987**, *65*, 659–664.

(161) Hertzberg, S.; Moen, E.; Vogelsang, C.; Østgaard, K. Mixed Photo-Cross-Linked Polyvinyl Alcohol and Calcium-Alginate Gels for Cell Entrapment. *Appl. Microbiol. Biotechnol.* **1995**, *43*, 10–17.

(162) Gupte, A.; D'Souza, S. F. Stabilization of Alginate Beads Using Radiation Polymerized Polyacrylamide. *J. Biochem. Biophys. Methods* **1999**, *40*, 39–44.

(163) Lim, F.; Sun, A. M. Microencapsulated Islets as Bioartificial Endocrine Pancreas. *Science* **1980**, *210*, 908–910.

(164) Köllmer, M.; Appel, A. A.; Somo, S. I.; Brey, E. M. Long-Term Function of Alginate-Encapsulated Islets. *Tissue Eng. Part B Rev.* **2016**, *22*, 34–46.

(165) Calafiore, R.; Basta, G.; Luca, G.; Lemmi, A.; Montanucci, M. P.; Calabrese, G.; Racanicchi, L.; Mancuso, F.; Brunetti, P. Microencapsulated Pancreatic Islet Allografts into Nonimmunosuppressed Patients with Type 1 Diabetes. *Diabetes Care* **2006**, *29*, 137–138.

(166) Basta, G.; Montanucci, P.; Luca, G.; Boselli, C.; Noya, G.; Barbaro, B.; Qi, M.; Kinzer, K. P.; Oberholzer, J.; Calafiore, R. Long-Term Metabolic and Immunological Follow-up of Nonimmunosuppressed Patients with Type 1 Diabetes Treated with Microencapsulated Islet Allografts: Four Cases. *Diabetes Care* **2011**, *34*, 2406–2409.

(167) Elliott, R. B.; Escobar, L.; Tan, P. L. J.; Muzina, M.; Zwain, S.; Buchanan, C. Live Encapsulated Porcine Islets from a Type 1 Diabetic Patient 9.5 Yr after Xenotransplantation. *Xenotransplantation* **2007**, *14*, 157–161.

(168) Van Hoogmoed, C. G.; Busscher, H. J.; De Vos, P. Fourier Transform Infrared Spectroscopy Studies of Alginate-PLL Capsules with Varying Compositions. *J. Biomed. Mater. Res. A* **2003**, *67*, 172–178.

(169) Tam, S. K.; Dusseault, J.; Polizu, S.; Ménard, M.; Hallé, J. P.; Yahia, L. Physicochemical Model of Alginate-Poly-l-Lysine Microcapsules Defined at the Micrometric/Nanometric Scale Using ATR-FTIR, XPS, and ToF-SIMS. *Biomaterials* **2005**, *26*, 6950–6961.

(170) Ponce, S.; Orive, G.; Hernández, R.; Gascón, A. R.; Pedraz, J. L.; de Haan, B. J.; Faas, M. M.; Mathieu, H. J.; de Vos, P. Chemistry and the Biological Response against Immunoisolating Alginate-Polycation Capsules of Different Composition. *Biomaterials* **2006**, *27*, 4831–4839.

(171) Tam, S. K.; Bilodeau, S.; Dusseault, J.; Langlois, G.; Hallé, J. P.; Yahia, L. H. Biocompatibility and Physicochemical Characteristics of Alginate-Polycation Microcapsules. *Acta Biomater.* **2011**, *7*, 1683–1692.

(172) Jeon, O.; Bouhadir, K. H.; Mansour, J. M.; Alsberg, E. Photocrosslinked Alginate Hydrogels with Tunable Biodegradation Rates and Mechanical Properties. *Biomaterials* **2009**, *30*, 2724–2734.

(173) Hillberg, A. L.; Oudshoorn, M.; Lam, J. B. B.; Kathirgamanathan, K. Encapsulation of Porcine Pancreatic Islets within an Immunoprotective Capsule Comprising Methacrylated Glycol Chitosan and Alginate. *J. Biomed. Mater. Res. B Appl. Biomater.* **2015**, *103*, 503–518.

(174) Wang, S.; Jeon, O.; Shankles, P. G.; Liu, Y.; Alsberg, E.; Retterer, S. T.; Lee, B. P.; Choi, C. K. In-Situ Photopolymerization of Monodisperse and Discoid Oxidized Methacrylated Alginate Microgels in a Microfluidic Channel. *Biomicrofluidics* **2016**, *10*, 3–6.

(175) Somo, S. I.; Langert, K.; Yang, C. Y.; Vaicik, M. K.; Ibarra, V.; Appel, A. A.; Akar, B.; Cheng, M. H.; Brey, E. M. Synthesis and Evaluation of Dual Crosslinked Alginate Microbeads. *Acta Biomater.* **2018**, *65*, 53–65.

(176) García-Astrain, C.; Avérous, L. Synthesis and Evaluation of Functional Alginate Hydrogels Based on Click Chemistry for Drug Delivery Applications. *Carbohydr. Polym.* **2018**, *190*, 271–280.

(177) Ghanian, M. H.; Mirzadeh, H.; Baharvand, H. In Situ Forming, Cytocompatible, and Self-Recoverable Tough Hydrogels Based on Dual Ionic and Click Cross-Linked Alginate. *Biomacromolecules* **2018**, *19*, 1646–1662.

(178) Desai, R. M.; Koshy, S. T.; Hilderbrand, S. A.; Mooney, D. J.; Joshi, N. S. Versatile Click Alginate Hydrogels Crosslinked via Tetrazine-Norbornene Chemistry. *Biomaterials* **2015**, *50*, 30–37.

(179) Mahou, R.; Tran, M.; Dufresne, M.; Legallais, C.; Wandrey, C. Encapsulation of Huh-7 Cells within Alginate-Poly(Ethylene Glycol) Hybrid Microspheres. *J. Mater. Sci. Mater. Med.* **2012**, *23*, 171–179.

(180) Dolgin, E. Encapsulate This. *Nat. Med.* **2014**, *20*, 9–11.

(181) Scharp, D. W.; Marchetti, P. Encapsulated Islets for Diabetes Therapy: History, Current Progress, and Critical Issues Requiring Solution. *Adv. Drug Deliv. Rev.* **2014**, *67–68*, 35–73.

(182) Rokstad, A. M. A.; Lacík, I.; de Vos, P.; Strand, B. L. Advances in Biocompatibility and Physico-Chemical Characterization of Microspheres for Cell Encapsulation. *Adv. Drug Deliv. Rev.* **2014**, *67–68*, 111–130.

(183) Ratner, B. D. The Biocompatibility Manifesto: Biocompatibility for the Twenty-First Century. *J. Cardiovasc. Transl. Res.* **2011**, *4*, 523–527.

(184) Anderson, J. M.; Rodriguez, A.; Chang, D. T. Foreign Body Reaction to Biomaterials. *Semin. Immunol.* **2008**, *20*, 86–100.

(185) Papas, K. K.; Bellin, M. D.; Sutherland, D. E. R.; Suszynski, T. M.; Kitzmann, J. P.; Avgoustiniatos, E. S.; Gruessner, A. C.; Mueller, K. R.; Beilman, G. J.; Balamurugan, A. N.; et al. Islet Oxygen Consumption Rate (OCR) Dose Predicts Insulin Independence in Clinical Islet Autotransplantation. *PLoS One* **2015**, *10*, 1–11.

(186) Komatsu, H.; Cook, C.; Wang, C. H.; Medrano, L.; Lin, H.; Kandeel, F.; Tai, Y. C.; Mullen, Y. Oxygen Environment and Islet Size Are the Primary Limiting Factors of Isolated

Pancreatic Islet Survival. *PLoS One* **2017**, *12*, 1–17.

(187) Yang, H. K.; Ham, D. S.; Park, H. S.; Rhee, M.; You, Y. H.; Kim, M. J.; Shin, J.; Kim, O. Y.; Khang, G.; Hong, T. H.; et al. Long-Term Efficacy and Biocompatibility of Encapsulated Islet Transplantation with Chitosan-Coated Alginate Capsules in Mice and Canine Models of Diabetes. *Transplantation* **2016**, *100*, 334–343.

(188) Sawhney, A. S.; Hubbell, J. A. Poly(Ethylene Oxide)-Graft-Poly(L-Lysine) Copolymers to Enhance the Biocompatibility of Poly(L-Lysine)-Alginate Microcapsule Membranes. *Biomaterials* **1992**, *13*, 863–870.

(189) Zheng, J. N.; Xie, H. G.; Yu, W. T.; Liu, X. D.; Xie, W. Y.; Zhu, J.; Ma, X. J. Chitosan-g-MPEG-Modified Alginate/Chitosan Hydrogel Microcapsules: A Quantitative Study of the Effect of Polymer Architecture on the Resistance to Protein Adsorption. *Langmuir* **2010**, *26*, 17156–17164.

(190) Vegas, A. J.; Veiseh, O.; Doloff, J. C.; Ma, M.; Tam, H. H.; Bratlie, K.; Li, J.; Bader, A. R.; Langan, E.; Olejnik, K.; et al. Combinatorial Hydrogel Library Enables Identification of Materials That Mitigate the Foreign Body Response in Primates. *Nat. Biotechnol.* **2016**, *34*, 345–352.

(191) Jiang, H.; Xu, F. J. Biomolecule-Functionalized Polymer Brushes. *Chem. Soc. Rev.* **2013**, *42*, 3394–3426.

(192) Moroni, L.; Klein Gunnewiek, M.; Benetti, E. M. Polymer Brush Coatings Regulating Cell Behavior: Passive Interfaces Turn into Active. *Acta Biomater.* **2014**, *10*, 2367–2378.

(193) Spasojevic, M.; Bhujbal, S.; Paredes, G.; De Haan, B. J.; Schouten, A. J.; De Vos, P. Considerations in Binding Diblock Copolymers on Hydrophilic Alginate Beads for Providing an Immunoprotective Membrane. *J. Biomed. Mater. Res. A* **2014**, *102*, 1887–1896.

(194) de Vos, P.; Bučko, M.; Gemeiner, P.; Navrátil, M.; Švitel, J.; Faas, M.; Strand, B. L.; Skjak-Braek, G.; Morch, Y. A.; Vikartovská, A.; et al. Multiscale Requirements for Bioencapsulation in Medicine and Biotechnology. *Biomaterials* **2009**, *30*, 2559–2570.

(195) Paredes-Juarez, G. A.; De Haan, B. J.; Faas, M. M.; De Vos, P. The Role of Pathogen-Associated Molecular Patterns in Inflammatory Responses against Alginate Based Microcapsules. *J. Control. Release* **2013**, *172*, 983–992.

(196) Veiseh, O.; Doloff, J. C.; Ma, M.; Vegas, A. J.; Tam, H. H.; Bader, A. R.; Li, J.; Langan, E.; Wyckoff, J.; Loo, W. S.; et al. Size- and Shape-Dependent Foreign Body Immune Response to Materials Implanted in Rodents and Non-Human Primates. *Nat. Mater.* **2015**, *14*, 643–651.

(197) Paredes-Juarez, G. A.; de Haan, B. J.; Faas, M. M.; de Vos, P. A Technology Platform to Test the Efficacy of Purification of Alginate. *Materials (Basel)* **2014**, *7*, 2087–2103.

(198) Dusseault, J.; Tam, S. K.; Ménard, M.; Polizu, S.; Jourdan, G.; Yahia, L.; Hallé, J. P. Evaluation of Alginate Purification Methods: Effect on Polyphenol, Endotoxin, and Protein Contamination. *J. Biomed. Mater. Res. A* **2006**, *76*, 243–251.

(199) Hu, S.; de Vos, P. Polymeric Approaches to Reduce Tissue Responses against Devices Applied for Islet-Cell Encapsulation. *Front. Bioeng. Biotechnol.* **2019**, *7*, 134.

(200) Paredes-Juarez, G. A.; Sahasrabudhe, N. M.; Tjoelker, R. S.; De Haan, B. J.; Engelse, M. A.;

De Koning, E. J. P.; Faas, M. M.; De Vos, P. DAMP Production by Human Islets under Low Oxygen and Nutrients in the Presence or Absence of an Immunoisolating-Capsule and Necrostatin-1. *Sci. Rep.* **2015**, *5*, 1–12.

(201) Unsal, I. O.; Ginis, Z.; Pinarli, F. A.; Albayrak, A.; Cakal, E.; Sahin, M.; Delibasi, T. Comparison of Therapeutic Characteristics of Islet Cell Transplantation Simultaneous with Pancreatic Mesenchymal Stem Cell Transplantation in Rats with Type 1 Diabetes Mellitus. *Stem Cell Rev. Reports* **2015**, *11*, 526–532.

(202) Vaithilingam, V.; Evans, M. D. M.; Rowe, A.; Bean, P. A.; Tuch, B. E. Coencapsulation of Target Effector Cells with Mesenchymal Stem Cells Reduces Pericapsular Fibrosis and Improves Graft Survival in a Xenotransplanted Animal Model. *Cell Transplant.* **2016**, *25*, 1299–1317.

(203) Vaithilingam, V.; Evans, M. D. M.; Lewy, D. M.; Bean, P. A.; Bal, S.; Tuch, B. E. Co-Encapsulation and Co-Transplantation of Mesenchymal Stem Cells Reduces Pericapsular Fibrosis and Improves Encapsulated Islet Survival and Function When Allografted. *Sci. Rep.* **2017**, *7*, 1–13.

(204) Laporte, C.; Tubbs, E.; Cristante, J.; Gauchez, A. S.; Pesenti, S.; Lamarche, F.; Cottet-Rousselle, C.; Garrel, C.; Moisan, A.; Moulis, J. M.; et al. Human Mesenchymal Stem Cells Improve Rat Islet Functionality under Cytokine Stress with Combined Upregulation of Heme Oxygenase-1 and Ferritin. *Stem Cell Res. Ther.* **2019**, *10*, 1–12.

(205) Vågesjö, E.; Christoffersson, G.; Waldén, T. B.; Carlsson, P. O.; Essand, M.; Korsgren, O.; Phillipson, M. Immunological Shielding by Induced Recruitment of Regulatory T-Lymphocytes Delays Rejection of Islets Transplanted in Muscle. *Cell Transplant.* **2015**, *24*, 263–276.

(206) Gliwiński, M.; Iwaszkiewicz-Grześ, D.; Trzonkowski, P. Cell-Based Therapies with T Regulatory Cells. *BioDrugs* **2017**, *31*, 335–347.

(207) Dang, T. T.; Thai, A. V.; Cohen, J.; Slosberg, J. E.; Siniakowicz, K.; Doloff, J. C.; Ma, M.; Hollister-Lock, J.; Tang, K. M.; Gu, Z.; et al. Enhanced Function of Immuno-Isolated Islets in Diabetes Therapy Byco-Encapsulation with an Anti-Inflammatory Drug. *Biomaterials* **2013**, *34*, 5792–5801.

(208) Azadi, S. A.; Vasheghani-Farahani, E.; Hashemi-Najafbabadi, S.; Godini, A. Co-Encapsulation of Pancreatic Islets and Pentoxifylline in Alginate-Based Microcapsules with Enhanced Immunosuppressive Effects. *Prog. Biomater.* **2016**, *5*, 101–109.

(209) Park, H. S.; Kim, J. W.; Lee, S. H.; Yang, H. K.; Ham, D. S.; Sun, C. L.; Hong, T. H.; Khang, G.; Park, C. G.; Yoon, K. H. Antifibrotic Effect of Rapamycin Containing Polyethylene Glycol-Coated Alginate Microcapsule in Islet Xenotransplantation. *J. Tissue Eng. Regen. Med.* **2017**, *11*, 1274–1284.

(210) Ricci, M.; Blasi, P.; Giovagnoli, S.; Rossi, C.; Macchiarulo, G.; Luca, G.; Basta, G.; Calafiore, R. Ketoprofen Controlled Release from Composite Microcapsules for Cell Encapsulation: Effect on Post-Transplant Acute Inflammation. *J. Control. Release* **2005**, *107*, 395–407.

(211) Schulz, A.; Gepp, M. M.; Stracke, F.; von Briesen, H.; Neubauer, J. C.; Zimmermann, H. Tyramine-Conjugated Alginate Hydrogels as a Platform for Bioactive Scaffolds. *J. Biomed. Mater. Res. A* **2019**, *107*, 114–121.

(212) Gattás-Asfura, K. M.; Fraker, C. A.; Stabler, C. L. Perfluorinated Alginate for Cellular Encapsulation. *J. Biomed. Mater. Res. A* **2012**, *100*, 1963–1971.

(213) Kim, Y. S.; Cho, S. W.; Ko, B.; Shin, J.; Ahn, C. W. Alginate-Catechol Cross-Linking Interferes with Insulin Secretion Capacity in Isolated Murine Islet Cells. *Diabetes Metab. J.* **2018**, *42*, 164–168.

(214) Albert, W. Alginic Acid-Acetate. *Nature* **1946**, *158*, 271.

(215) Albert, W. Alginic Acid Acetate. *J. Chem. Soc.* **1948**, *48*, 197–198.

(216) Chamberlain, N. C.; Cunningham, G. E.; Speakman, J. B. Alginic Acid Diacetate. *Nature* **1946**, *158*, 553.

(217) Schweiger, R. G. Acetylation of Alginic Acid. I. Preparation and Viscosities of Algin Acetates. *J. Org. Chem.* **1962**, *27*, 1786–1789.

(218) Schweiger, R. G. Acetylation of Alginic Acid. II. Reaction of Algin Acetates with Calcium and Other Divalent Ions. *J. Org. Chem.* **1962**, *27*, 1789–1791.

(219) Skjak-Break, G. Selective Acetylation of Mannuronic Acid Residues in Calcium Alginate Gels. *Carbohydr. Res.* **1989**, *185*, 119–129.

(220) Skjåk-Braek, G.; Paoletti, S.; Gianferrara, T. Effect of Acetylation on Some Solution and Gelling Properties of Alginates. *Carbohydr. Res.* **1989**, *185*, 131–138.

(221) Li, Q.; Liu, C. G.; Huang, Z. H.; Xue, F. F. Preparation and Characterization of Nanoparticles Based on Hydrophobic Alginate Derivative as Carriers for Sustained Release of Vitamin D3. *J. Agric. Food Chem.* **2011**, *59*, 1962–1967.

(222) Matsumoto, Y.; Ishii, D.; Iwata, T. Synthesis and Characterization of Alginic Acid Ester Derivatives. *Carbohydr. Polym.* **2017**, *171*, 229–235.

(223) Fernandes, C.; Acharya, P. C.; Bhatt, S. Preparation of Lauroyl Grafted Alginate-Psyllium Husk Gel Composite Film with Enhanced Physicochemical, Mechanical and Antimicrobial Properties. *Sci. Rep.* **2018**, *8*, 1–9.

(224) Le-Tien, C.; Mateescu, M.-A.; Millette, M.; Lacroix, M. Modified Alginate and Chitosan for Lactic Acid Bacteria Immobilization. *Biotechnol. Appl. Biochem.* **2004**, *39*, 347–354.

(225) Ronghua, H.; Yumin, D.; Jianhong, Y. Preparation and in Vitro Anticoagulant Activities of Alginate Sulfate. *Carbohydr. Polym.* **2003**, *52*, 19–24.

(226) Zhao, X.; Yu, G.; Guan, H.; Yue, N.; Zhang, Z.; Li, H. Preparation of Low-Molecular-Weight Polyguluronate Sulfate and Its Anticoagulant and Anti-Inflammatory Activities. *Carbohydr. Polym.* **2007**, *69*, 272–279.

(227) Øystein, A.; Finn, L. A.; Anders, S.; Terje, E.; Skjǎk-Bræk, G. Heparin-Like Properties of Sulfated Alginates with Defined Sequences and Sulfation Degrees. *Biomacromolecules* **2014**, 2744–2750.

(228) Öztürk, E.; Arlov, Ø.; Aksel, S.; Ling, L.; Ornitz, D. M.; Skjåk-Bræk, G.; Zenobi-Wong, M. Sulfated Hydrogel Matrices Direct Mitogenicity and Maintenance of Chondrocyte Phenotype through Activation of FGF Signaling. *Adv. Funct. Mater.* **2016**, *26*, 3649–3662.

(229) Ma, H.; Qiu, P.; Xin, M.; Xu, X.; Wang, Z.; Xu, H.; Yu, R.; Xu, X.; Zhao, C.; Wang, X.; et al. Structure-Activity Relationship of Propylene Glycol Alginate Sodium Sulfate Derivatives for Blockade of Selectins Binding to Tumor Cells. *Carbohydr. Polym.* **2019**, *210*, 225–233.

(230) Fan, L.; Jiang, L.; Xu, Y.; Zhou, Y.; Shen, Y.; Xie, W.; Long, Z.; Zhou, J. Synthesis and

Anticoagulant Activity of Sodium Alginate Sulfates. *Carbohydr. Polym.* **2011**, *83*, 1797–1803.

(231) Zeng, Y.; Yang, D.; Qiu, P.; Han, Z.; Zeng, P.; He, Y.; Guo, Z.; Xu, L.; Cui, Y.; Zhou, Z.; et al. Efficacy of Heparinoid PSS in Treating Cardiovascular Diseases and beyond - A Review of 27 Years Clinical Experiences in China. *Clin. Appl. Thromb.* **2016**, *22*, 222–229.

(232) Coleman, R. J.; Lawrie, G.; Lambert, L. K.; Whittaker, M.; Jack, K. S.; Grndahl, L. Phosphorylation of Alginate: Synthesis, Characterization, and Evaluation of in Vitro Mineralization Capacity. *Biomacromolecules* **2011**, *12*, 889–897.

(233) Kim, H. S.; Song, M.; Lee, E. J.; Shin, U. S. Injectable Hydrogels Derived from Phosphorylated Alginic Acid Calcium Complexes. *Mater. Sci. Eng. C* **2015**, *51*, 139–147.

(234) Yueqin, Y.; Caifeng, L.; Zhe, L.; Fengjun, J.; Yi, Z.; Kunshan, Y.; Shaopeng, Y. Preparation and Characterization of Biosurfactant Based on Hydrophobically Modified Alginate. *Colloid J.* **2014**, *76*, 622–627.

(235) Meng, Y.; Zhang, J.; Cao, Q.; Liu, Q.; Yu, Y.; Wu, C. Amphiphilic Alginate as a Drug Release Vehicle for Water-Insoluble Drugs. *Colloid J.* **2015**, *77*, 754–760.

(236) Wu, J.; Wu, Z.; Zhang, R.; Yuan, S.; Lu, Q.; Yu, Y. Synthesis and Micelle Properties of the Hydrophobic Modified Alginate. *Int. J. Polym. Mater. Polym. Biomater.* **2017**, *66*, 742–747.

(237) Panão, C. O.; Campos, E. L. S.; Lima, H. H. C.; Rinaldi, A. W.; Lima-Tenório, M. K.; Tenório-Neto, E. T.; Guilherme, M. R.; Asefa, T.; Rubira, A. F. Ultra-Absorbent Hybrid Hydrogel Based on Alginate and SiO_2 Microspheres: A High-Water-Content System for Removal of Methylene Blue. *J. Mol. Liq.* **2019**, *276*, 204–213.

(238) Mooney, D. J.; Damm, K. L.; Bouhadir, K. H.; Anderson, K. W.; Alsberg, E.; Lee, K. Y. Degradation of Partially Oxidized Alginate and Its Potential Application for Tissue Engineering. *Biotechnol. Prog.* **2001**, *17*, 945–950.

(239) Kong, H. J.; Kaigler, D.; Kim, K.; Mooney, D. J. Controlling Rigidity and Degradation of Alginate Hydrogels via Molecular Weight Distribution. *Biomacromolecules* **2004**, *5*, 1720–1727.

(240) Boontheekul, T.; Kong, H. J.; Mooney, D. J. Controlling Alginate Gel Degradation Utilizing Partial Oxidation and Bimodal Molecular Weight Distribution. *Biomaterials* **2005**, *26*, 2455–2465.

(241) Gomez, C. G.; Rinaudo, M.; Villar, M. A. Oxidation of Sodium Alginate and Characterization of the Oxidized Derivatives. *Carbohydr. Polym.* **2007**, *67*, 296–304.

(242) Yang, Z.; Peng, H.; Wang, W.; Liu, T. Study on Partially Oxidized Sodium Alginate with Potassium Permanganate as the Oxidant. *J. Appl. Polym. Sci.* **2009**, *113*, 3585–3589.

(243) Smidsrød, O.; Painter, T. Effect of Periodate Oxidation upon the Stiffness of the Alginate Molecule in Solution. *Carbohydr. Res.* **1973**, *26*, 125–132.

(244) Scott, J. E.; Tigwell, M. J. Periodate-Induced Viscosity Decreases in Aqueous Solutions of Acetal- and Ether-Linked Polymers. *Carbohydr. Res.* **1973**, *28*, 53–59.

(245) Scott, J. E.; Tigwell, M. J. On the Mechanism of Scission of Alginate Chains by Periodate. *Carbohydr. Res.* **1976**, *47*, 105–117.

(246) Andresen, I. L.; Painter, T.; Smidsrød, O. Concerning the Effect of Periodate Oxidation upon the Intrinsic Viscosity of Alginate. *Carbohydr. Res.* **1977**, *59*, 563–566.

(247) Marie-Christiane, C.; Christine, D.; Patrick, H.; Edith, D. Covalent Coupling of a Short Polyether on Sodium Alginate: Synthesis and Characterization of the Resulting Amphiphilic Derivative. *Carbohydr. Polym.* **1991**, *16*, 367–379.

(248) Hyun-Ah, K.; Moon Sik, S.; Ji-Won, Y. Preparation and Characterization of Hydrophobically Modified Alginate. *Polym. Bull.* **2002**, *47*, 429–435.

(249) Dahlmann, J.; Krause, A.; Möller, L.; Kensah, G.; Möwes, M.; Diekmann, A.; Martin, U.; Kirschning, A.; Gruh, I.; Dräger, G. Fully Defined in Situ Cross-Linkable Alginate and Hyaluronic Acid Hydrogels for Myocardial Tissue Engineering. *Biomaterials* **2013**, *34*, 940–951.

(250) Hauptstein, S.; Dezorzi, S.; Prüfert, F.; Matuszczak, B.; Bernkop-Schnürch, A. Synthesis and in Vitro Characterization of a Novel S-Protected Thiolated Alginate. *Carbohydr. Polym.* **2015**, *124*, 1–7.

(251) Córdova, B. M.; Jacinto, C. R.; Alarcón, H.; Mejía, I. M.; López, R. C.; de Oliveira Silva, D.; Cavalheiro, E.; Venâncio, T.; Dávalos, J. Z.; Valderrama, A. C. Chemical Modification of Sodium Alginate with Thiosemicarbazide for the Removal of Pb(II) and Cd(II) from Aqueous Solutions. *Int. J. Biol. Macromol.* **2018**, *120*, 2259–2270.

(252) Huamani-Palomino, R. G.; Jacinto, C. R.; Alarcón, H.; Mejía, I. M.; López, R. C.; Silva, D. de O.; Cavalheiro, E. T. G.; Venâncio, T.; Dávalos, J. Z.; Valderrama, A. C. Chemical Modification of Alginate with Cysteine and Its Application for the Removal of Pb(II) from Aqueous Solutions. *Int. J. Biol. Macromol.* **2019**, *129*, 1056–1068.

(253) Balakrishnan, B.; Jayakrishnan, A. Self-Cross-Linking Biopolymers as Injectable in Situ Forming Biodegradable Scaffolds. *Biomaterials* **2005**, *26*, 3941–3951.

(254) Sarker, B.; Papageorgiou, D. G.; Silva, R.; Zehnder, T.; Gul-E-Noor, F.; Bertmer, M.; Kaschta, J.; Chrissafis, K.; Detsch, R.; Boccaccini, A. R. Fabrication of Alginate-Gelatin Crosslinked Hydrogel Microcapsules and Evaluation of the Microstructure and Physico-Chemical Properties. *J. Mater. Chem. B* **2014**, *2*, 1470–1482.

(255) Grigore, A.; Sarker, B.; Fabry, B.; Boccaccini, A. R.; Detsch, R. Behavior of Encapsulated MG-63 Cells in RGD and Gelatine-Modified Alginate Hydrogels. *Tissue Eng. Part A* **2014**, *20*, 2140–2150.

(256) Sarker, B.; Rompf, J.; Silva, R.; Lang, N.; Detsch, R.; Kaschta, J.; Fabry, B.; Boccaccini, A. R. International Journal of Biological Macromolecules Alginate-Based Hydrogels with Improved Adhesive Properties for Cell Encapsulation. *Int. J. Biol. Macromol.* **2015**, *78*, 72–78.

(257) Zehnder, T.; Sarker, B.; Boccaccini, A. R.; Detsch, R. Evaluation of an Alginate-Gelatine Crosslinked Hydrogel for Bioplotting. *Biofabrication* **2015**, *7*, 025001.

(258) Bouhadir, K. H.; Hausman, D. S.; Mooney, D. J. Synthesis of Cross-Linked Poly (Aldehyde Guluronate) Hydrogels (Alginate Oxidised). *Polymer* **1999**, *40*, 3575–3584.

(259) Hafeez, S.; Ooi, H.; Morgan, F.; Mota, C.; Dettin, M.; van Blitterswijk, C.; Moroni, L.; Baker, M. Viscoelastic Oxidized Alginates with Reversible Imine Type Crosslinks: Self-Healing, Injectable, and Bioprintable Hydrogels. *Gels* **2018**, *4*, 85.

(260) Sawhney, A. S.; Pathak, C. P.; Hubbell, J. A. Interfacial Photopolymerization of Poly(Ethylene Glycol)-Based Hydrogels upon Alginate-Poly(l-Lysine) Microcapsules for Enhanced Biocompatibility. *Biomaterials* **1993**, *14*, 1008–1016.

(261) Chandy, T.; Mooradian, D. L.; Rao, G. H. R. Evaluation of Modified Alginate-Chitosan-Polyethylene Glycol Microcapsules for Cell Encapsulation. *Artif. Organs* **1999**, *23*, 894–903.

(262) Babak, V. G.; Skotnikova, E. a.; Lukina, I. G.; Pelletier, S.; Hubert, P.; Dellacherie, E. Hydrophobically Associating Alginate Derivatives: Surface Tension Properties of Their Mixed Aqueous Solutions with Oppositely Charged Surfactants. *J. Colloid Interface Sci.* **2000**, *225*, 505–510.

(263) Pelletier, S.; Hubert, P.; Lapicque, F.; Payan, E.; Dellacherie, E. Amphiphilic Derivatives of Sodium Alginate and Hyaluronate: Synthesis and Physico-Chemical Properties of Aqueous Dilute Solutions. *Carbohydr. Polym.* **2000**, *43*, 343–349.

(264) De Boisseson, M. R.; Leonard, M.; Hubert, P.; Marchal, P.; Stequert, A.; Castel, C.; Favre, E.; Dellacherie, E. Physical Alginate Hydrogels Based on Hydrophobic or Dual Hydrophobic/Ionic Interactions: Bead Formation, Structure, and Stability. *J. Colloid Interface Sci.* **2004**, *273*, 131–139.

(265) Schleeh, T.; Madau, M.; Roessner, D. Synthesis Enhancements for Generating Highly Soluble Tetrabutylammonium Alginates in Organic Solvents. *Carbohydr. Polym.* **2014**, *114*, 493–499.

(266) Jones, K. H.; Senft, J. A. An Improved Method to Determine Cell Viability by Simultaneous Staining with Fluorescein Diacetate-Propidium Iodide. *J. Histochem. Cytochem.* **1985**, *33*, 77–79.

(267) First Drug for Idiopathic Pulmonary Fibrosis Approved in Japan. *Nat. Rev. Drug Discov.* **2008**, *7*, 967.

(268) Cho, M. E.; Kopp, J. B. Pirfenidone: An Anti-Fibrotic Therapy for Progressive Kidney Disease. *Expert Opin. Investig. Drugs* **2010**, *19*, 275–283.

(269) Chen, J.; Lu, M. M.; Liu, B.; Chen, Z.; Li, Q. Bin; Tao, L. J.; Hu, G. Y. Synthesis and Structure-Activity Relationship of 5-Substituent-2(1H)-Pyridone Derivatives as Anti-Fibrosis Agents. *Bioorganic Med. Chem. Lett.* **2012**, *22*, 2300–2302.

(270) Ma, Z.; Pan, Y.; Huang, W.; Yang, Y.; Wang, Z.; Li, Q.; Zhao, Y.; Zhang, X.; Shen, Z. Synthesis and Biological Evaluation of the Pirfenidone Derivatives as Antifibrotic Agents. *Bioorganic Med. Chem. Lett.* **2014**, *24*, 220–223.

(271) Tan, Y.-C.; Christini, V.; P. Lee, A. Monodispersed Microfluidic Droplet Generation by Shear Focusing Microfluidic Device. *Sensors Actuators B* **2006**, *114*, 350–356.

(272) Zhang, H.; Tumarkin, E.; Sullan, R. M. A.; Walker, G. C.; Kumacheva, E. Exploring Microfluidic Routes to Microgels of Biological Polymers. *Macromol. Rapid Commun.* **2007**, *28*, 527–538.

(273) Wysocki, J.; Schlepphorst, C.; Glorius, F. Asymmetric Homogeneous Hydrogenation of 2-Pyridones. *Synlett* **2015**, *26*, 1557–1562.

(274) Wen, K.; Zhao, X.-L.; Hu, W.-J.; Mi, X.-Q.; Jiang, B.; Guo, F.; Ma, M.-L. Synthesis, Structure and Conformation of Terphenylene-Derived Oxacalixaromatics. *European J.*

Org. Chem. **2012**, *2012*, 1448–1454.

(275) Heller, K.; Ochtrop, P.; Albers, M. F.; Zauner, F. B.; Itzen, A.; Hedberg, C. Covalent Protein Labeling by Enzymatic Phosphocholination. *Angew. Chem. Int. Ed.* **2015**, *54*, 10327–10330.

Luca Szabó

Education

Swiss Federal Institute of Technology at Lausanne (EPFL), Switzerland
2016-2020
PhD study in organic chemistry and polymer functionalization

Budapest University of Technology and Economics, Hungary
2014-2016
Master in Pharmaceutical Engineering

Budapest University of Technology and Economics, Hungary
2010-2014
Bachelor in Chemistry and Chemical Engineering

Mihály Fazekas High School, Debrecen, Hungary
2005-2010
High School diploma, spanish bilingual diploma

Professional Experience

Swiss Federal Institute of Technology at Lausanne (EPFL), Switzerland
PhD Student, Group for Functionalized Biomaterials, Prof. Sandrine Gerber
February, 2016-February, 2020
- Functionalization of alginate; preparation and characterization of hydrogel microspheres with optimal properties for cell immobilization
- Design and implementation of cell microencapsulation experiments in close collaboration with biologists and engineers
- Practical laboratory assistant for undergraduate chemistry and chemical engineering students. Supervision of Masters Projects. Assistant of Bachelor course "Organic Functions and reactions I", Organic chemistry (for BIO, PHA). *Winner of the Teaching Excellence Award in 2019.*

The University of Manchester, United Kingdom
Master Project, Group of Dr. György Székely
September, 2014-March, 2015
- Organocatalyst syntheses for asymmetric synthesis, and catalyst recovery with organic solvent nanofiltration

Budapest University of Technology and Economics, Hungary
Research work, Group for Supramolecular Chemistry, Dr. Péter Huszthy
September, 2012-2015
- Organic preparative chemistry

Egis Pharmaceutical PLC., Hungary
Internship
June, 2013-July 2013
- IPC laboratory experience, synthesis of several active pharmaceutical ingredients

Computer Programs

Chemistry	Office	Other
ChemDraw, MestRenova, ImageJ	Suite MS-Office	Adobe Illustrator, Origin

Personal

Date of birth	1990. 05. 21.
Nationality	Hungary

Contact

Phone	+41 79 6579914
Email	szaboluca1990@gmail.com
Address	Avenue de France 64 1004 Lausanne Switzerland

Languages

English	Proficient	●●●●●
Spanish	Intermediate	●●●○○
French	Beginner	●○○○○
Hungarian	Native	●●●●●

Literature contribution

Strategies to functionalize the anionic biopolymer Na-alginate without restricting its polyelectrolyte properties *(review paper)*
Luca Szabó, Sandrine Gerber-Lemaire, Christine Wandrey. *Submitted in Polymers, 2020.*

Cross-Reactive Alginate Derivatives for the Production of Dual Ionic-Covalent Hydrogel Microspheres Presenting Tunable Properties for Cell Microencapsulation
Luca Szabó, Carmen Gonelle-Gispert, Elisa Montanari, François Noverraz, Aurélien Bornet, Léo H. Bühler, Sandrine Gerber-Lemaire
ACS Appl. Polym. Mater. **2019**, *1*, 1326-1333.

Antifibrotic Effect of Ketoprofen-Grafted Alginate Microcapsules in the Transplantation of Insulin Producing Cells
François Noverraz, Elisa Montanari, Joel Pimenta, **Luca Szabó**, Daniel Ortiz, Carmen Gonelle-Gispert, Léo H. Bühler, Sandrine Gerber-Lemaire
Bioconjugate Chem. **2018**, *29*, 1932-1941.

Beneficial Effects of Human Mesenchymal Stromal Cells on Porcine Hepatocyte Viability and Albumin Secretion
Elisa Montanari, Joel Pimenta, **Luca Szabó,** François Noverraz, Soléne Passemard, Raphael P. H. Meier, Jeremy Meyer, Jonathan Sidibe, Aurelien Thomas, Henk-Jan Schuurman, Sandrine Gerber-Lemaire, Carmen Gonelle-Gispert, Léo H. Bühler
Journal of Immunology Research, **2018**, *2018,* 1078547.

Synthesis Strategies to Extend the Variety of Alginate-based Hybrid Hydrogels for Cell Microencapsulation
Soléne Passemard, **Luca Szabó,** François Noverraz, Elisa Montanari, Carmen Gonelle-Gispert, Léo H. Bühler, Christine Wandrey, Sandrine Gerber-Lemaire
Biomacromolecules **2017**, *18*, 2747-2755.

Conferences

Swiss Summer School 2016 in Chemical Biology, Villars, Switzerland, August 21-25, 2016.
Development of Alginate-Based Hydrogels for Cell Encapsulation. *Talk and poster*

SCS (Swiss Chemical Society) Fall Meeting, Bern, Switzerland, August 21-22, 2017.
Functionalization of Sodium Alginate Hydrogels for Cell Encapsulation. *Poster*

ESB (European Society for Biomaterials) Maastricht, The Netherlands, September 9-13, 2018.
Functionalized alginate-based hybrid hydrogels with enhanced mechanical properties and potential for cell transplantation. *Poster*

SCS (Swiss Chemical Society) Fall Meeting, Lausanne, Switzerland, September 7, 2018.
Engineering of multifunctional alginate-based hydrogels to enhance mechanical properties and immunoprotection in the transplantation of microencapsulated cells. *Poster*

26th International Conference on Bioencapsulation, Strasbourg, France, August 27-29, 2019.
Multicomponent cross-linked alginate-based hydrogels for cell transplantation. *Talk. **Prize for the best oral presentation.***

SCS (Swiss Chemical Society) Fall Meeting, Zürich, Switzerland, September 6, 2019.
Multicomponent alginate-based hydrogels for improving the outcomes of cell microencapsulation as a potential treatment for type I diabetes. *Poster*